# Air Pollution at the Single-Particle Level: Integrating Atmospheric Measurements with Mathematical Models

Thesis by

Prakash Viththal Bhave

In Partial Fulfillment of the Requirements

for the Degree of

Doctor of Philosophy

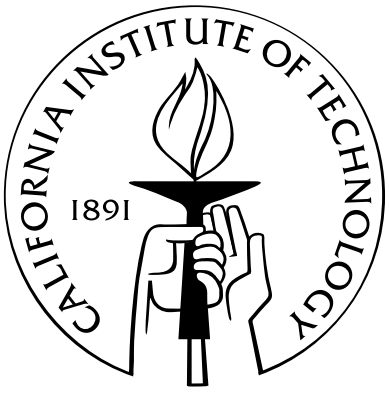


California Institute of Technology

Pasadena, California

2003

(Defended March 25, 2003)

In Loving Memory of

Professor Glen R. Cass

# Acknowledgements

The past four and a half years have been a quite an adventure, including marriage, two cross-country moves, the loss of my primary research advisor, and at last, the completion of this thesis. Along the way, a number of people made my research work possible, enjoyable, and thoroughly rewarding.

First, I would like to thank my wife, Nita, and my parents, Viththal and Charu. They provided moral support during the times I needed it most. Without them, this work would have never reached completion.

Dr. Glen Cass, my primary research advisor, motivated me to study air pollution at the single-particle level and to tackle the problems addressed in this thesis. The work described herein is my best attempt at meeting his standard of high-quality research. He continues to provide me with a rich source of optimism and enthusiasm in all aspects of life.

After Glen expired, a number of faculty members showered me with guidance and support. Michael Kleeman and Kimberly Prather shared their expertise in aerosol modeling and single-particle measurements, respectively, and provided tremendous moral support. John Seinfeld graciously served as my official advisor, and gave me full freedom to complete the work I had started under Glen's supervision. Richard Flagan challenged my knowledge of aerosol measurements, and prodded me to ask questions, rather than to be content with my own level of understanding. Ted Russell gave me opportunities to develop my teaching skills and provided valuable career counseling.

Thanks are due to Jonathan Allen, David Fergenson, Lara Gertler, and Bradley Morrical, who collaborated with me on various portions of this research. In addition,

numerous past and present members of the Prather research group at UC Riverside and UC San Diego have helped me to understand and interpret the aerosol time-of-flight mass spectrometry (ATOFMS) measurements. Among them, Don-Yuan Liu, Keith Coffee, and David Sodeman deserve special mention for being so generous with their time.

I thank the various graduate students and postdocs, whom I have shared offices with, for fostering pleasant and productive work environments. I thank Chris Worrell for troubleshooting a number of my computer-related problems and Fran Matzen for stretching my funding as long as possible. During my first couple years at Caltech, I was able to participate in much needed extra-curricular activities thanks to OASIS, Out of Context, and the Orienteering club.

I spent my third and fourth years doing research in the School of Earth and Atmospheric Sciences, at Georgia Tech. Those two years gave me a fresh perspective on aerosol science, raising my awareness of air pollution problems and air pollution research outside of southern California. I thank Michael Bergin, Rita Bryan, Carolyn Ruppel, Susan Ryan, and Martial Taillefert, for making me feel welcome at Georgia Tech, especially during the year following Glen's death. I also thank Trupti, Niranjan, Ashish, Prerana, Anjaneya, Apurva, Sunil, and Minu, for being like family, during my time in Atlanta.

Robert Harley, James Hunt, and William Nazaroff, raised my interest in environmental engineering, through intriguing courses they taught me as an undergraduate at UC Berkeley. Alison Pollack encouraged me to pursue this doctoral degree.

Lastly, I am grateful for financial support from the U.S. Environmental Protection Agency, and I look forward to a challenging and rewarding career in the Agency's Atmospheric Sciences Modeling Division.

# Abstract

Particulate air pollution is of growing concern in the United States and around the world. Elevated concentrations of aerosols (solid particles and liquid droplets suspended in air) are correlated with increased cases of lung cancer, cardiopulmonary disorders, and human mortality. A detailed understanding of the size, chemical composition, and concentration of atmospheric particles is needed to assess their effects on human health, as well as on regional visibility and global climate. One can acquire such knowledge through direct measurements, or by utilizing mathematical air quality models. New and innovative instruments allow us to measure the size and composition of individual particles, rather than to infer aerosol chemical properties from bulk particulate matter samples. Concurrently, air quality models have been developed to numerically simulate the emissions of discrete particles, and their transport and chemical evolution in the atmosphere. This thesis focuses on how to integrate and compare measurements taken by state-of-the-science single-particle instruments with the air pollutant properties calculated using state-of-the-science mathematical models. A 1996 field experiment conducted in the Los Angeles air basin serves as the case study for this thesis research.

Comparisons of model calculations against single-particle observations identify specific areas where model improvements are needed, and also identify important areas for future instrumental development. These comparisons contribute to our understanding of atmospheric pollution at the single-particle level, and ultimately, may provide tremendous value to policy makers who are seeking least-cost solutions to urban and regional air quality problems. After presenting initial comparisons of single-particle measurements and model results, efforts to quantify and catego-

rize the single-particle chemical composition data are described. The quantitatively reconstructed single-particle measurements are compared with mathematical model calculations of the atmospheric aerosol mixing characteristics. Finally, an example is presented of how the model and measurement combination enhance our ability to reduce particulate pollution in the air we breathe.

# Contents

**Acknowledgements** **iv**

**Abstract** **vi**

**List of Acronyms** **xv**

**1 Introduction** **1**

1.1 Motivation . . . . . 1

1.2 Background . . . . . 2

1.2.1 Mathematical Models of Ambient Particulate Matter . . . . . 2

1.2.2 Single-Particle Measurements of Atmospheric Aerosols . . . . 4

1.2.3 1996 Los Angeles Basin Trajectory Study . . . . . 8

1.3 Research Objectives . . . . . 10

1.4 Approach . . . . . 10

**2 Evaluation of a Source-Oriented Air Quality Model Using Semi-Quantitative ATOFMS Measurements** **13**

2.1 Introduction . . . . . 13

2.2 Methods . . . . . 15

2.2.1 Description of the Source-Oriented Air Quality Model . . . . . 15

2.2.2 Description of Single-Particle Aerosol Measurements . . . . . 20

2.2.3 Model Evaluation Procedure . . . . . 21

2.3 Results and Discussion . . . . . 28

2.3.1 Single-Component Model Evaluation . . . . . 29

2.3.2 Multi-Component Model Evaluation . . . . . 34
2.3.3 Evolution of the Aerosol Mixture . . . . . 40
2.4 Conclusions . . . . . 42

**3 A Field-Based Approach for Determining ATOFMS Instrument Sensitivities to Ammonium and Nitrate 43**
3.1 Introduction . . . . . 43
3.2 Related Studies . . . . . 46
3.3 Methods . . . . . 48
3.3.1 Aerosol Measurements . . . . . 48
3.3.2 ATOFMS Data Treatment . . . . . 51
3.3.2.1 ATOFMS Response Functions . . . . . 51
3.3.2.2 Dynamic Range Exceedances of the Data Acquisition Board . . . . . 53
3.3.2.3 Corrections for Particle Detection Efficiency . . . . . 54
3.3.3 ATOFMS-Impactor Data Comparison . . . . . 57
3.4 Results . . . . . 59
3.4.1 Size-Dependent Parameterization of Instrument Sensitivity . . 61
3.4.2 Scaled ATOFMS Measurements of $NH_4^+$ and $NO_3^-$ . . . . . 64
3.4.3 Residual Analysis . . . . . 68
3.4.3.1 Influence of Particle Detection Efficiency Corrections 69
3.4.3.2 Influence of Gas-Phase Properties . . . . . 70
3.4.3.3 Influence of Bulk Aerosol Composition . . . . . 73
3.4.3.4 Influence of Single-Particle Composition . . . . . 74
3.4.3.5 Summary of Residual Analysis . . . . . 75
3.5 Discussion . . . . . 75
3.6 Conclusions . . . . . 78

**4 A Method for Categorizing Atmospheric Single-Particle Spectra 80**
4.1 Introduction . . . . . 80
4.2 Background . . . . . 82

4.2.1 Single-Component Analysis . . . . . 82
4.2.2 Multivariate Spectral Categorization . . . . . 83
4.2.2.1 Unsupervised Categorization Methods . . . . . 85
4.2.2.2 Supervised Categorization Methods . . . . . 86
4.3 Methods . . . . . 87
4.4 Results . . . . . 89
4.4.1 Category Selection . . . . . 89
4.4.2 Seed Simplification . . . . . 94
4.4.3 Spectral Categorization . . . . . 96
4.5 Discussion . . . . . 98
4.6 Conclusions . . . . . 100

**5 Quantitative Evaluation of a Source-Oriented Air Quality Model Using ATOFMS Measurements 101**

5.1 Introduction . . . . . 101
5.2 Methods . . . . . 104
5.2.1 Description of the Air Quality Model . . . . . 104
5.2.2 Description of the Atmospheric Aerosol Data . . . . . 105
5.2.2.1 Reconstruction of Atmospheric Aerosol Concentrations 106
5.2.2.2 Mixing Characteristics Measurements . . . . . 107
5.3 Results and Discussion . . . . . 107
5.3.1 Temporal Resolution . . . . . 108
5.3.2 Particle Size Resolution . . . . . 112
5.3.3 Aerosol Mixing State . . . . . 115
5.4 Conclusions . . . . . 117

**6 Source Apportionment of Fine Particulate Matter by Clustering Single-Particle Data: Tests of Receptor Model Accuracy 119**

6.1 Introduction . . . . . 119
6.2 Methods . . . . . 122
6.2.1 Generation of Synthetic Single-Particle Data . . . . . 122

6.2.2 Simulation of ATOFMS Data . . . . . 125
6.2.2.1 Quantitative ATOFMS Particle Descriptions . . . . . 127
6.2.2.2 Qualitative ATOFMS Particle Descriptions . . . . . 129
6.2.3 Adaptive Resonance Theory-Based Neural Network . . . . . 130
6.2.4 Receptor Modeling Procedure . . . . . 132
6.3 Results and Discussion . . . . . 133
6.3.1 Source-Oriented Air Quality Model Results . . . . . 133
6.3.2 Source Apportionment Accuracy Given Maximum Compositional Detail . . . . . 136
6.3.3 Source Apportionment Accuracy Based on Simulated ATOFMS Data . . . . . 142
6.4 Conclusions . . . . . 145

**7 Conclusions** **148**
7.1 Summary . . . . . 148
7.2 Recommendations for Future Research . . . . . 151
7.2.1 Model Evaluations . . . . . 151
7.2.2 ATOFMS Sampling Biases . . . . . 152
7.2.3 Single-Particle Source Apportionment . . . . . 154
7.2.4 Model Developments . . . . . 155

**A Cass Research Group** **157**
A.1 Introduction . . . . . 157
A.2 Group Members . . . . . 157
A.2.1 Ph.D. Students . . . . . 157
A.2.2 Postdoctoral Researchers . . . . . 166
A.2.3 Research Staff . . . . . 169
A.2.4 Other Contributors . . . . . 170
A.3 Miscellaneous Notes . . . . . 171
A.4 Conclusion . . . . . 175

**References** **177**

# List of Figures


1.1 Model representation of a source-oriented externally mixed aerosol . . 5

1.2 Field sampling locations for the 1996 Los Angeles Basin Trajectory Study. 9

2.1 Schematic illustration of the model evaluation procedure. . . . . 18

2.2 Air parcel trajectory path. . . . . 19

2.3 Single-component comparisons of model results and ATOFMS measurements . . . . . 30

2.4 Multi-component comparisons of model results and ATOFMS measurements . . . . . 35

3.1 First-order ATOFMS-impactor comparison of $NH_4^+$ and $NO_3^-$ measurements . . . . . 60

3.2 Comparison of scaled ATOFMS measurements of $NH_4^+$ and $NO_3^-$ with corresponding impactor measurements. . . . . 65

3.3 Comparison of residual species concentrations with residual mass concentrations. . . . . 71

3.4 Size and temporally resolved $NH_4^+$ mass distributions at Riverside . . . 76

3.5 Size and temporally resolved $NO_3^-$ mass distributions at Riverside . . . 77

4.1 Flowchart of the iterative seed selection procedure. . . . . 93

4.2 Effects of seed simplification on classification accuracy. . . . . 95

5.1 Model calculations versus ambient measurements of hourly resolved and size-segregated mass, $NO_3^-$, and $NH_4^+$ concentrations at Riverside on September 25, 1996. . . . . 109

5.2 Model calculations versus ambient measurements of finely resolved particle size distributions of aerosol mass, $NO_3^-$, and $NH_4^+$ concentrations at Riverside, on September 25, 1996, 1500–1900 PDT. . . . . 113

5.3 Model results versus ambient measurements of size-resolved aerosol mixing characteristics at Riverside, on September 25, 1996, 1500–1900 PDT. 116

6.1 Chemical composition of fine particle emissions from major sources in southern California. . . . . 124

6.2 ART-2a classification results when supplied complete chemical composition data for each particle. . . . . 135

6.3 Chemical composition of ART-2a particle classes generated from source-oriented model results with maximum speciation. . . . . 138

6.4 ART-2a particle classification based on test cases simulating qualitative particle composition data detected in three ATOFMS operating modes. 143

6.5 ART-2a particle classification based on test cases simulating quantitative particle composition data obtained in three ATOFMS operating modes. 146

A.1 Temporal distribution of the size of the Cass research group. . . . . 172

A.2 Frequency distribution of time required to complete a Ph.D. degree in the Cass research group. . . . . 173

A.3 Careers pursued by former Ph.D. students in the Cass research group. 174

A.4 Ph.D. "descendants" of Dr. Cass. . . . . 176

# List of Tables


2.1 Description of source-oriented air quality model: Lagrangian formulation. 16

2.2 Mineral dust search criteria. . . . . 24

2.3 Exceptions to mineral dust search criteria #6–8. . . . . 25

2.4 Relative sensitivity factor estimates for species detected by ATOFMS in positive ion mode. . . . . 26

2.5 Numerical representation of Figure 2.4. . . . . 37

3.1 Intensive operating periods at Riverside, California. . . . . 50

3.2 Parameter values and 95% confidence intervals fit to the ATOFMS particle detection efficiency function $\Phi = \alpha \, \mathrm{D}_a{}^{\beta}$ . . . . . 58

3.3 Parameter values and 95% confidence intervals fit to the ATOFMS instrument sensitivity function $\Psi = \gamma \, \mathrm{D_a}{}^{\delta}$. . . . . 63

4.1 Initial evaluation of the spectral categorization method against first tier classifications. . . . . 94

4.2 Final description of the selected seed vectors. . . . . 97

4.3 Final evaluation of the spectral categorization method against first tier classifications. . . . . 98

5.1 Dimensions of ambient air quality data . . . . . 102

6.1 Relative sensitivity factor estimates for species detected by ATOFMS instruments. . . . . 128

A.1 Ph.D. dissertations published under the supervision of Dr. Glen Cass. . 158

# List of Acronyms

| | |
|---|---|
| ADAMS | algorithm for discriminant analysis of mass spectra |
| AIM | aerosol inorganic module |
| ART | adaptive resonance theory |
| ATOFMS | aerosol time-of-flight mass spectrometry |
| AUSPEX | atmospheric utility signatures, predictions, and experiments |
| CCSEM | computer-controlled scanning electron microscopy |
| CIT | California Institute of Technology |
| CMAQ | community multiscale air quality |
| CMB | chemical mass balance |
| DA | data acquisition |
| DAQM | Denver air quality model |
| EPA | environmental protection agency |
| EPXMA | electron probe X-ray microanalysis |
| EURAD | European air pollution dispersion |
| FCA | fuzzy cluster analysis |
| GATOR | gas, aerosol, transport, and radiation |
| HCA | hierarchical cluster analysis |
| IOP | intensive operating period |
| LAMPAS | laser mass analysis of particles in the airborne state |
| LMMS | laser microprobe mass spectrometry |
| PALMS | particle analysis by laser mass spectrometry |
| PDT | Pacific daylight time |
| PM | particulate matter |

| | |
|---|---|
| PST | Pacific standard time |
| RFA | rapid flow analyzer |
| RH | relative humidity |
| RSF | relative sensitivity factor |
| RSMS | rapid single-particle mass spectrometer |
| SAPRC | statewide air pollution research center |
| SAQM | SARMAP air quality model |
| SARMAP | SJVAQS/AUSPEX regional modeling adaption project |
| SCAQS | southern California air quality study |
| SCOS | southern California ozone study |
| SD | standard deviation |
| SJVAQS | San Joaquin Valley air quality study |
| UAM | urban airshed model |
| YAADA | yet another ATOFMS data analysis |
| YAG | yttrium aluminum garnet |

# Chapter 1

# Introduction

## 1.1 Motivation

The size and composition of atmospheric particles determine their deposition efficiency in different regions of the human lung [1], their toxicity [2], their degradation of visibility [3], and their effects on regional and global climate [4]. For these reasons, particulate air pollution has received increasing attention over the past decade from scientists, regulatory agencies, and in the public media. On July 17, 1997, in response to mounting epidemiological evidence correlating atmospheric fine particulate matter concentrations with elevated human mortality rates [5], the United States Environmental Protection Agency (EPA) announced new standards to regulate ambient concentrations of particles with diameter less than 2.5 micrometers ($PM_{2.5}$). The EPA set an annual average $PM_{2.5}$ standard at 15 micrograms per cubic meter ($\mu$g $m^{-3}$) and a 24-hour average $PM_{2.5}$ standard at 65 $\mu$g $m^{-3}$. During the 1999–2001 time period, over 65 million Americans lived in counties with $PM_{2.5}$ concentrations exceeding the annual standard. During the same period, the 24-hour standard was exceeded at more than a dozen $PM_{2.5}$ monitoring sites, all located in either southern or central California (www.epa.gov).

In order to reduce atmospheric particulate matter concentrations to a level that meets the federal standards intended to protect public health, it is important to understand the processes that influence particle concentrations. The atmosphere is an extremely complex system in which numerous physical and chemical processes occur

simultaneously. Mathematical models provide the necessary framework to integrate our understanding of the complex processes governing air pollutant formation, transport, and removal. Increased confidence in our understanding of the ensemble of these processes can only be achieved through extensive model evaluations against atmospheric measurements. The comparison of state-of-the-science measurements with state-of-the-science model calculations offers the most promising approach for expanding our knowledge about particulate air pollution, and such comparisons are the focus of this thesis.

## 1.2 Background

### 1.2.1 Mathematical Models of Ambient Particulate Matter

Mathematical models for the prediction of ambient particulate matter concentrations have been under development for roughly three quarters of a century. Early work in the field produced expressions known as Gaussian plume and Gaussian puff equations, for predicting the spatial density distribution of particulate matter resulting from continuous (plume) and instantaneous (puff) point and line sources [6, 7]. These single-source models were developed from observations of the dispersion of smoke trails from smoke stacks and anti-aircraft shell bursts. A quantitative relationship between the emissions from multiple sources and air pollutant concentrations over a large area was first reported by Meetham, using measurements of smoke and gas-phase $SO_2$ taken by local authorities in Britain over the course of many years [8]. Meetham was puzzled by the observation that ambient $SO_2$ concentrations were less than ambient smoke concentrations, even during periods when $SO_2$ emissions were approximately two times greater than smoke emissions. Because early Gaussian models only accounted for the advection, dispersion, and deposition of bulk primary particulate mass, and assumed that gases and particles do not interact with each other, Meetham could not explain the atmospheric losses of $SO_2$.

Since that time, numerous studies have investigated the interactions of ambient

particulate matter with the surrounding gas phase. Most of the early models of these "gas-to-particle conversion" processes were limited to calculations of a single chemical component in bulk particulate matter, such as sulfate [9], ammonium nitrate [10, 11], and organic carbon [12]. Meanwhile, mathematical models for calculating atmospheric particle size distributions were developed separately, using continuous [13], discrete [14], and lognormally-parameterized representations [15]. The first multicomponent, size-resolved particulate matter model was described by Pilinis et al. in 1987, and applied to the Los Angeles area [16, 17]. That model included a discrete representation of the particle size distribution (using nine size sections) and a treatment of six inorganic particle-phase components ($NH_4^+$, $NO_3^-$, $SO_4^=$, $Na^+$, $Cl^-$, and $H_2O$).

During the 1990's, several more mathematical models were developed to describe the size distribution and chemical composition of atmospheric particles [18–27]. In all of these models, it was assumed that the atmospheric particulate matter is *internally mixed*, meaning the chemical compositions of all like-sized particles are identical. Kleeman et al. demonstrated that this internal mixture assumption can result in a misrepresentation of the aerosol size distribution [28]. Internally mixed aerosol representations have the additional disadvantage of masking the individual contributions made by distinct emission sources, because the particle source identity is lost when all particles are averaged into a common aerosol distribution, upon emission to the atmosphere. Furthermore, global-scale model calculations reveal that inaccurate assumptions about the mixing state of ambient aerosols can introduce significant error in the calculations of radiative forcing and climate change [29]. Before proceeding, it is helpful to clarify that the term "aerosol" refers to a metastable suspension of solid or liquid particles in a gas. The terms "aerosol" and "particulate matter" are used interchangeably throughout this thesis, as is the case in much of the air pollution literature.

In the late 1990's, Kleeman and Cass developed mathematical air quality models in which the ambient aerosol is represented as an ensemble of compositionally distinct particle classes, rather than as an internally mixed distribution [28, 30]. In these

models, all particles interact with the same gas-phase conditions, but differences in the chemical compositions of particles emitted at different initial sizes and from different emission sources are retained. This aerosol representation is referred to as a *source-oriented external mixture* [28]. Models which employ this representation have the capability of simulating the particle-to-particle differences within a given size range, as illustrated in Figure 1.1. The accuracy of such model results could not be readily evaluated until recently, due to the dearth of observational data on particle-to-particle differences in the atmosphere. The advent of real-time single-particle measurement techniques provides sufficient data to test the detailed model calculations against atmospheric observations.

### 1.2.2 Single-Particle Measurements of Atmospheric Aerosols

Traditional methods for analyzing the chemical composition of atmospheric aerosols require the collection of large numbers of particles ($10^7 - 10^{15}$) on a substrate, followed by bulk chemical analyses of the entire sample. Using these methods, the chemical composition of particle ensembles can be assessed, but particle-to-particle differences are lost during the analysis procedure. If the ambient aerosol is size-segregated prior to collection, as is the case when cascade impactors are employed, the size-resolved chemical composition of an aerosol can be determined. Even with such information, the analyst can only approximate the aerosol distribution as an internal mixture or make other simplifying assumptions regarding the aerosol mixing state.

During the 1980's and 1990's, a variety of single-particle techniques were used to assess the compositional heterogeneity of atmospheric particles collected on substrates. These techniques include computer controlled scanning electron microscopy (CCSEM) [31], laser microprobe mass spectrometry(LMMS) [32], and electron probe X-ray microanalysis (EPXMA) [33]. Although these techniques made it possible to probe the particle-to-particle differences in atmospheric aerosols, they are all relatively slow, requiring several seconds to a minute for the analysis of each particle. Consequently, few particles can be analyzed in a reasonable span of time. For example,

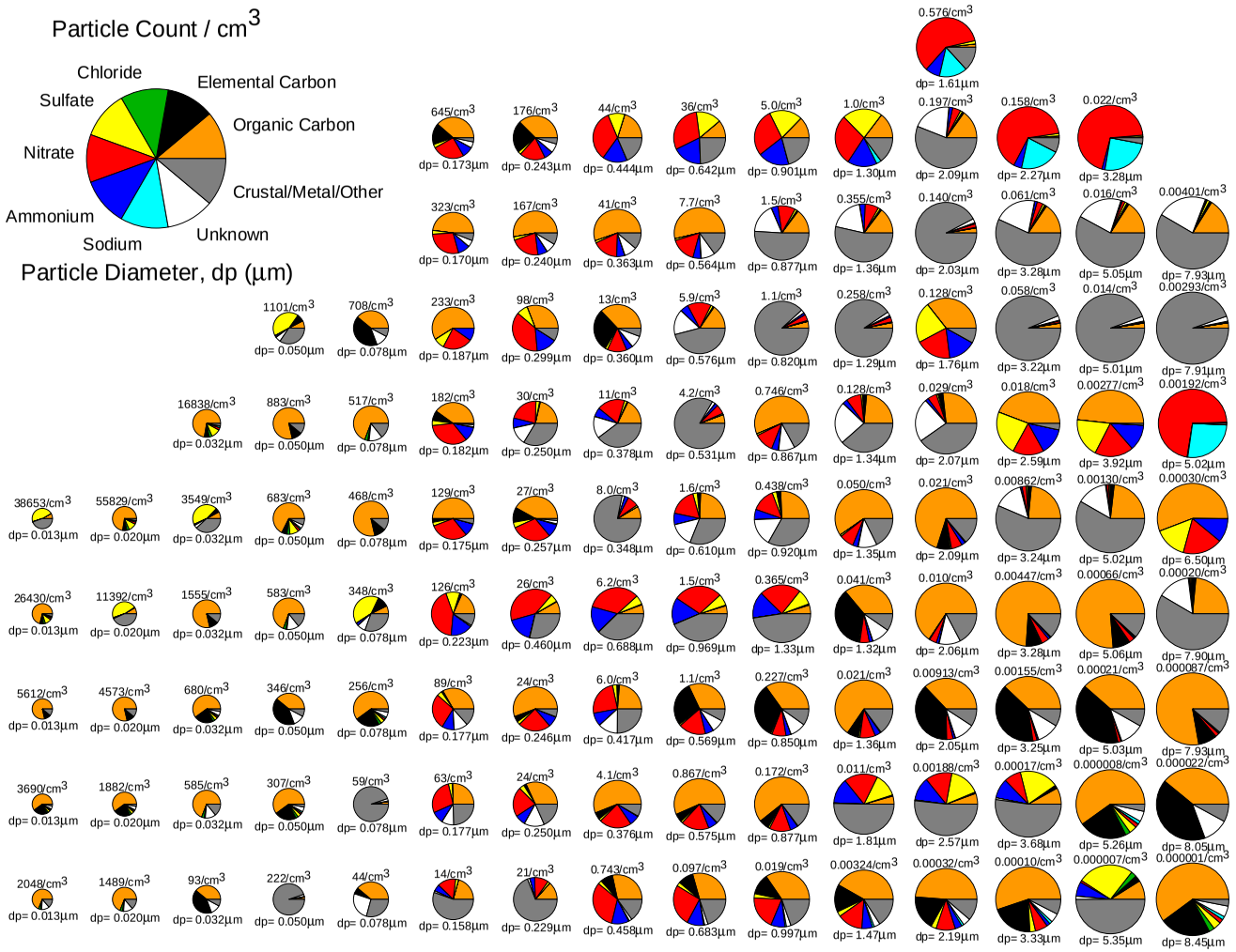


Figure 1.1: Model representation of a source-oriented externally mixed aerosol. The concentration, size, and chemical composition of each particle class tracked in the model are shown. Reproduced from "Modeling the airborne particle complex as a source-oriented external mixture," by M. J. Kleeman, G. R. Cass, and A. Eldering; *Journal of Geophysical Research*, 102: 21355–21372, 1997.

EPXMA applications typically involve the analysis of only 400 particles per atmospheric sample [33, 34], which is insufficient to fully characterize a complex ambient aerosol. Another drawback of these techniques is that they are performed "off-line." Particle ensembles are first collected on a filter or impaction substrate, and then subjected to analysis. This limits the temporal resolution of the atmospheric observations to periods of several hours. In addition, the chemical properties of collected particles can change between sample collection and analysis. For example, semivolatile species can volatilize from the substrates, water droplets collected can crystallize or evaporate depending on temperature and humidity conditions after collection, and particle-particle, gas-particle, and particle-substrate reactions can modify the aerosol composition prior to analysis.

To bypass the problems associated with sample collection and to increase the speed of analysis, "on-line" methods were developed, that allow the determination of individual particle composition within a fraction of a second after they are sampled from the atmosphere. These instruments combine aerosol beam spectrometry [35] with a variety of mass spectral techniques, including magnetic sector, quadrupole, time-of-flight, and quadrupole ion trap mass spectrometry (see [36, 37] for reviews). Among these, time-of-flight mass spectrometry has a very fast analysis time ($\sim 10^{-5}$ s) and the ability to collect the entire mass spectrum of individual particles, thus permitting the on-line analysis of highly concentrated and chemically complex aerosols, such as those found in polluted urban atmospheres. During the last decade, several different particle sizing techniques have been coupled with time-of-flight mass spectrometry, including light scattering intensity measurement [38–40], single-laser aerodynamic particle sizing [38], dual-laser aerodynamic particle sizing [41], split-laser aerodynamic particle sizing [42], and dynamic source-pressure alteration [43]. These coupled devices allow simultaneous measurements of the size and chemical composition of individual atmospheric particles to be made on-line. Furthermore, the single-particle data acquisition rates of certain on-line techniques are nearly two orders of magnitude faster than the off-line methods described earlier, thus permitting a reasonably thorough characterization of an ambient aerosol to be made within

sampling intervals of twenty minutes to an hour.

To date, four distinct on-line techniques for measuring the size and chemical composition of individual particles have been developed and applied in multi-day field campaigns. The first on-line chemical analysis of individual atmospheric particles was conducted by Murphy and Thomson at Idaho Hill, Colorado, in September 1993 [44, 45]. Using the particle analysis by laser mass spectrometry (PALMS) technique, particle size is coarsely estimated from the single-particle light scattering intensity and particle composition is determined from either a positive or negative ion mass spectrum obtained by laser ablation and ionization. The next field applications of on-line single-particle mass spectrometry instruments were conducted by Prather and co-workers at Riverside, California, in 1995 [46, 47]. Their sampling method, aerosol time-of-flight mass spectrometry (ATOFMS), uses a dual-laser technique to obtain precise measurements of the aerodynamic particle size [48], prior to laser ablation and ionization. One research group has documented their development of an instrument based on the ATOFMS design, and already used it for atmospheric sampling in Toronto, Canada, in December 2000 [49]. To date, ATOFMS has been utilized in more field experiments than any other single-particle technique, and is the only commercially available on-line single-particle mass spectrometry instrument. Hinz and co-workers were the third group to deploy an on-line single-particle instrument in a major field campaign, during the 1998 Lindenberger Aerosol Characterization Experiment, near Berlin, Germany [50]. Their instrument, the laser mass analyzer for particles in the airborne state (LAMPAS), uses a single-laser aerodynamic sizing technique that permits the sampling of particles in one narrow size fraction at a time. The distance between the detection and ablation lasers is periodically adjusted to sample particles of different size. The fourth on-line single-particle technique to be used in major field experiments was developed by Johnston and Wexler [51], and deployed during some of the recent EPA Supersite experiments [52, 53]. This instrument, referred to as a rapid single particle mass spectrometer (RSMS), is uniquely capable of measuring the size and composition of individual ultrafine particles, which have aerodynamic diameters ($D_a$) smaller than 0.1 $\mu$m. In contrast, the PALMS, ATOFMS,

and LAMPAS are configured to sample particles in the $D_a > 0.2$ $\mu$m range only.

Size and chemical composition measurements at the single-particle level open the possibility of evaluating air quality models that mathematically calculate the compositional heterogeneity among like-sized particles. State-of-the-science models and state-of-the-science instruments have been developed for assessing single-particle size and composition of atmospheric aerosols, yet the question remains: "How well can the aerosol models represent atmospheric single-particle characteristics?"

### 1.2.3 1996 Los Angeles Basin Trajectory Study

In late September and early October, 1996, a collaborative field experiment was conducted between the Cass research group from Caltech and the Prather research group from UC Riverside [54]. The primary goal of the field campaign was to collect atmospheric single-particle size and chemical composition measurements that could be used later to evaluate air quality model calculations of the compositional heterogeneity among like-sized particles. Aerosol instruments were stationed at three sites in the Los Angeles, California area: Long Beach, Fullerton, and Riverside. In addition, the size and chemical composition distribution of airborne particles and the concentrations of gas-phase pollutants were measured upwind of the study area at Santa Catalina Island on September 21–22, 1996, for the purpose of specifying initial conditions to the mathematical air quality model. Figure 1.2 displays each field sampling location on a map of the study region.

Members of the Prather research group collected single-particle measurements at Long Beach, Fullerton, and Riverside, using ATOFMS. This was the first major field experiment when ATOFMS instruments were deployed, therefore, significant resources were invested to determine how best to interpret the single-particle data. Alongside the ATOFMS instruments, members of the Cass research group operated cascade impactors, laser optical particle counters, and a number of other conventional aerosol sampling devices. The reasons for operating these instruments were to verify that the ATOFMS instruments were analyzing a random sample of the ambient par-

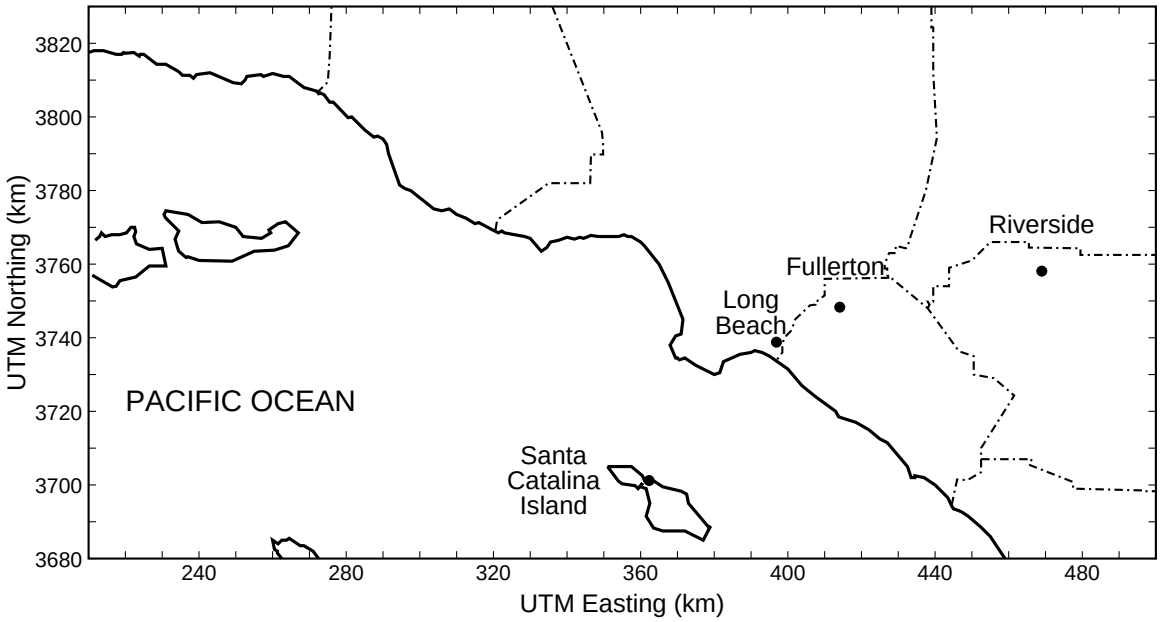


Figure 1.2: Field sampling locations for the 1996 Los Angeles Basin Trajectory Study.

ticles, and to ensure that useful model evaluation data could later be quantitatively reconstructed from the ATOFMS measurements.

A source-oriented externally mixed aerosol model was used to calculate the size distribution and chemical composition of the atmospheric aerosol at Long Beach, Fullerton, and Riverside. Comparison of air quality model calculations to both filter-based and cascade impactor-based measurements of the particle size distribution and bulk chemical composition show good agreement at all three air monitoring sites, as described by Kleeman et al. [55]. Air quality model calculations of fine particulate ($D_a < 1.8\ \mu$m) mass, sulfate, ammonium, and nitrate concentrations, as well as total particulate sodium concentrations, agree within 35% of filter-based measurements at all three monitoring sites during the episodes studied [55, Figure 3]. Furthermore, the shapes of the size distributions of fine particulate mass, ammonium, nitrate, and sulfate, as measured by cascade impactors at all three monitoring sites, were accurately calculated using the air quality model [55, Figure 4]. Having established confidence in the air quality model calculations of the aerosol size distribution as well as the bulk and size-segregated aerosol chemical composition at all three monitoring sites, the groundwork was laid to evaluate the air quality model results against single-

particle ATOFMS measurements.

## 1.3 Research Objectives

The primary objective of this thesis is to evaluate source-oriented air quality model calculations of aerosol size and chemical composition against atmospheric single-particle ATOFMS measurements. Within the scope of this research are assessments of the ATOFMS particle detection efficiencies and the ATOFMS instrument sensitivities to specific chemical components in atmospheric aerosols. Rendering the ATOFMS data and model results into comparable formats, such that model evaluations can be conducted, constitutes a major portion of this work.

Accomplishment of the primary research objective will identify specific areas where model improvements are needed, and may also identify important areas for instrumental development. The comparisons will contribute substantially to our understanding of atmospheric pollution at the single-particle level.

The secondary objective of this thesis is to use the detailed particle descriptions, obtained through mathematical model calculations, to evaluate the accuracy of a receptor-oriented method for identifying the sources of individual atmospheric particles. Source apportionment of atmospheric particulate matter has been attempted by various researchers using a number of different techniques, but no methodology has been established for testing the accuracy of source apportionment calculations.

## 1.4 Approach

The first objective of this work is to evaluate air quality model results by comparison with single-particle ATOFMS measurements. To begin with, methods must be developed for arranging model results and ATOFMS measurements in a manner such that a side-by-side comparison of the multi-dimensional data sets is possible. Either the model results must be interpreted similar to the way that the ATOFMS instruments sample and describe ambient particles, or the ATOFMS data must be quantitatively

reconstructed to match the actual distribution of particles in the atmosphere. Both of these approaches are taken in the present work.

Chapter 2 describes a method for transforming model results in a manner comparable to the ATOFMS measurements. This transformation involves simulating the losses of information incurred due to (1) the limited size range of particles detectable by the dual-laser aerodynamic particle sizing apparatus in ATOFMS instruments, (2) the non-uniform transmission efficiency of the ATOFMS instruments, (3) the varying sensitivities of ATOFMS instruments to different chemical components in atmospheric particles, and (4) the interference of ATOFMS instrumental noise with real ion signals in the single-particle mass spectra. Model calculations of the aerosols at Long Beach and Riverside during the 1996 Los Angeles Basin Trajectory Study are transformed by this method and compared against ATOFMS measurements collected at the corresponding times and locations. These comparisons focus on the percentage of particles within size-segregated aerosol populations at each site, that contain sodium, nitrate, ammonium, carbon, or mineral dust. Two methods of comparison are devised and presented in Section 2.3.

One limitation of the model-ATOFMS comparisons presented in Chapter 2 is that particle information had to be reduced to a level of the presence or absence (i.e., not the quantitative abundance) of selected chemical components in each individual particle. This reduction was necessary because the ATOFMS instrument sensitivities to specific aerosol components were not known under ambient sampling conditions. In Chapter 3, a method is described for determining the ATOFMS instrument sensitivities to ammonium ($NH_4^+$) and nitrate ($NO_3^-$) under atmospheric sampling conditions. These two chemical components are chosen primarily because $NH_4NO_3$ constitutes a very large fraction of the $PM_{2.5}$ concentrations in the eastern portion of the Los Angeles area [54, 56], a region where $PM_{2.5}$ standards are exceeded most frequently. The instrument sensitivity factors, derived from comparisons with collocated impactor measurements, are used to quantitatively reconstruct size-resolved mass distributions of $NH_4^+$ and $NO_3^-$ from the ATOFMS data collected at Riverside.

Another limitation of the model-ATOFMS comparisons presented in Chapter 2 is

that particles were categorized according to the presence of a few selected ion signals in the mass spectra, rather than the most prominent spectral patterns. In Chapter 4, an alternative method is devised for chemically categorizing ATOFMS data, that focuses on the entire particle spectrum while also mitigating the need to distinguish between instrumental noise and real ion signals. Broadly defined particle classes selected for this analysis are sea salt, mineral dust, carbonaceous particles, and miscellaneous particle types. These classes are further subdivided into 35 compositionally distinct particle categories, in a manner that can be conveyed in the literature, such that particle categorization results can be reproduced by other investigators. The spectral categorization method is applied to ATOFMS data collected during a five day sampling period at Riverside, as part of the 1996 Los Angeles Basin Trajectory Study.

In Chapter 5, the ATOFMS measurements are transformed into a format similar to the air quality model results, permitting a direct quantitative comparison of the model calculations and atmospheric single-particle measurements to be made. Model evaluations presented in this chapter are performed at finer temporal and particle size resolution than in any previous study. In addition, model calculations of the absolute contributions of sea salt, mineral dust, and carbonaceous particles, to the size-resolved aerosol mass distribution, are compared with corresponding ATOFMS measurements. This is the first quantitative comparison of air quality model calculations with atmospheric measurements of the aerosol mixing state.

The secondary objective of this thesis is addressed in Chapter 6. The source apportionment accuracy of a receptor-oriented method is tested based on its application to synthetic single-particle data generated using the source-oriented air quality model. Effects of particle "aging," caused by gas-to-particle conversion processes, on the receptor model accuracy are investigated. This methodology for evaluating the accuracy of a source apportionment technique may be applied in the future to test other receptor-oriented methods that are currently in use.

Finally in Chapter 7, the major results of this research are summarized. Important accomplishments are highlighted and areas for future research are identified.

# Chapter 2

# Evaluation of a Source-Oriented Air Quality Model Using Semi-Quantitative ATOFMS Measurements

## 2.1 Introduction

As discussed in Section 1.2.1, the vast majority of aerosol processes air quality models do not track the size and composition of individual atmospheric particles, but rather, they calculate the average chemical composition of particles falling within certain size intervals. These models include the California Institute of Technology model (CIT) [25], the European Air Pollution Dispersion model (EURAD) [26], the Urban Airshed Model-IV with aerosols (UAM-AERO) [18, 21], the Urban Airshed Model-IV with the Aerosol Inorganics Model (UAM-AIM) [24, 57], the Denver Air Quality Model (DAQM) [22], the Gas, Aerosol, Transport, and Radiation model (GATOR) [23], the SARMAP Air Quality Model with aerosols (SAQM-AERO) [27], and the Community Multiscale Air Quality model (CMAQ) [58]. Of these, the CMAQ and EURAD models parameterize the aerosol size distribution as the sum of two or three overlapping lognormal modes and the remaining models approximate the aerosol

*This chapter is reproduced with permission from "Evaluation of an Air Quality Model for the Size and Composition of Source-Oriented Particle Classes," by P. V. Bhave, M. J. Kleeman, J. O. Allen, L. S. Hughes, K. A. Prather, and G. R. Cass; *Environmental Science and Technology*, 36: 2154–2163, 2002. 

size distribution using a sectional representation. All of the models listed above treat the ambient aerosol as an internally mixture, in which all particles in a given size interval or lognormal mode have identical chemical compositions. Several investigators have shown that this internal mixture assumption is inaccurate by observing and reporting significant compositional heterogeneity among ambient particles of the same size [46, 59, 60]. Furthermore, the use of internally mixed aerosol representations in air quality models creates a number of problems, as described in Section 1.2.1.

Recently, an air quality model has been developed to overcome the internal mixture assumption, by separately tracking the evolution of source-oriented particle classes as they undergo atmospheric chemical reactions during transport across a polluted air basin. This model has been used to identify the effect of individual emission sources on ambient air quality [30, 61], and to evaluate the effectiveness of numerous proposed air pollution control strategies on particulate matter concentrations [62] and visibility [63] in the southern California region. Model calculations of the overall aerosol size distribution and chemical composition have undergone extensive evaluation and agree favorably with measurements taken during the 1987 Southern California Air Quality Study [28, 64] and the 1996 Los Angeles Basin Trajectory Study [55]. Aerosol time-of-flight mass spectrometry (ATOFMS) measurements that describe ambient single-particle size and composition are available from the 1996 Los Angeles Basin Trajectory Study [54], but model comparison against ambient single-particle measurements has yet to be attempted. The purpose of this chapter is to determine how well an air quality model that tracks source-oriented particle classes can account for single-particle characteristics observed in the atmosphere. This is the first comparison of aerosol mathematical air quality model results with atmospheric single-particle measurements.

## 2.2 Methods

### 2.2.1 Description of the Source-Oriented Air Quality Model

The air quality model used in this study simulates the most important processes that affect the size and composition distribution of the ambient aerosol. These processes are listed in Table 2.1. Detailed descriptions of the model structure and formulation can be found in the published literature [28, 30, 55, 64]. In the model, the ambient aerosol is represented as a source-oriented mixture of particle classes that are released to the atmosphere as primary emissions at 15 discrete particle sizes spanning the 0.01–10 $\mu$m particle diameter range. Primary particles are separated into 10 emission source categories: paved road dust, crustal material, diesel engine exhaust, food cooking, catalyst-equipped gasoline-powered engine exhaust, non-catalyst gasoline engine exhaust, sulfur-bearing fuel combustion and industrial sources, sea salt, non-sea salt background particles, and other miscellaneous sources [28]. The chemical composition of particles emitted from each source category is obtained from the results of emission source sampling experiments. Primary particles emitted from the most important sources in southern California are represented using chemical composition data that vary by particle size, based on impactor measurements of those emission sources [65, 66]. Particles emitted at each discrete size, from each source category, and during each hour along the air parcel trajectory, are tracked separately from all other particle classes in the model. In this manner, a source-oriented mixture of atmospheric particles is created in which all particle classes interact with the same gas-phase conditions, but differences in the size and composition of particles emitted from different sources are retained. Coagulation processes are not included in the present model formulation, because it has been determined that they do not significantly affect the aerosol mass distribution during the air pollution episode under investigation [30].

Table 2.1: Description of source-oriented air quality model: Lagrangian formulation.

| Feature | Treatment | Ref. |
|---|---|---|
| **Spatial and Temporal Dimensions** | | |
| Spatial Scale | Urban-scale applications, 5km × 5km horizontal grid resolution, 5 vertical cells | |
| Temporal Scale | Episodic applications, 1 day – 1 week | |
| **Aerosol Representation** | | |
| Chemical Species | Distinct chemical species in each particle class (EC, OC, $NH_4^+$, $NO_3^-$, $Na^+$, $Cl^-$, $SO_4^=$, and 30 minor species) | [67] |
| Particle Size Distribution | Discrete source-oriented particle classes: 15 initial sizes ranging from 0.01–10 $\mu$m, from each of 10 emission source categories, emitted during each hour of air parcel transport | |
| Particle Size Evolution | Discrete particles change size as material condenses/evaporates | |
| Particle Aging | Source-oriented particle classes are segregated by hour of emission | [64] |
| **Emissions** | | |
| Aerosol Phase | Size-resolved chemical composition from all major emission sources | [55, 67] |
| Gas Phase | $SO_2$, NO, $NO_2$, $NH_3$, CO, and over 400 specific organic compounds | [20] |
| **Transport** | | |
| Advection | Horizontal only, using interpolated wind fields | [10, 68] |
| Diffusion | Vertical only | [10] |
| Vertical Wind Shear | not included[a] | |
| **Chemical Mechanisms** | | |
| Gas Phase Chemistry | SAPRC mechanism with extensions: 100 species ($O_3$, $NO_2$, NO, $N_2O_5$, etc.) and 195 reactions | [12] |

*continued on next page*

Table 2.1: Description of source-oriented air quality model (*continued*).

| Feature | Treatment | Ref. |
|---|---|---|
| Inorganic Aerosol Thermodynamics | Aerosol Inorganics Module (AIM) with extensions: condensation, evaporation, dissolution, crystallization | [28, 69] |
| Organic Aerosol Thermodynamics | Absorption of semi-volatile organics into aerosol organic phase | [62, 70, 71] |
| Fog Kinetic Reactions | 58 species, 177 irreversible reactions | [28, 72, 73] |
| Fog Equilibrium Reactions | 29 acid-base reversible reactions | [28, 72, 73] |
| **Physical Mechanisms** | | |
| Dry Deposition | Surface resistant model with land use specific parameters | [10] |
| Wet Deposition | not included[a] | |
| Nucleation | not included[a] | |
| Coagulation | not included[a] | |

[a] Process shown to be negligible during current episode [30]

Figure 2.1a displays an example of the air quality model results. The pie chart quantitatively illustrates the chemical composition of an atmospheric particle class tracked in the air quality model. This particle class contains 15 of the 37 different aerosol phase chemical species that are tracked in the current model formulation. The atmospheric concentration, physical diameter ($D_p$), and density ($\rho$) of particles in this class, are also calculated in the model. Furthermore, each particle class tracked in the model is labeled according to the source category from which the particle core was initially emitted and the hour at which the particle was injected into the air parcel. Based on model calculations, the particle class shown in Figure 2.1a was emitted from a diesel-powered vehicle, 16 hours before reaching the receptor site.

In late September and early October, 1996, field measurements of the aerosol size distribution and chemical composition were collected to evaluate results of the air

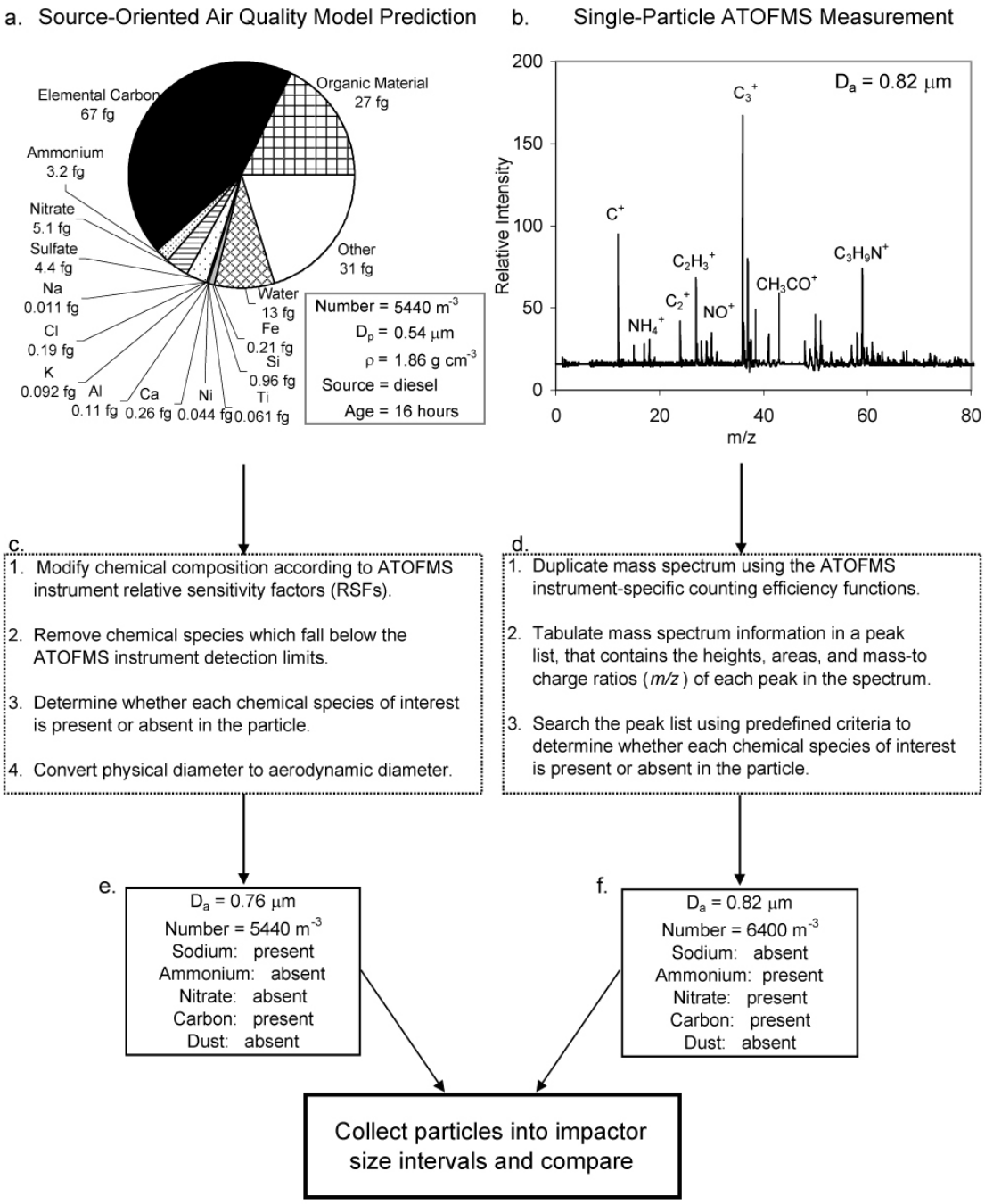


Figure 2.1: Schematic illustration of the model evaluation procedure. a) Air quality model calculation of a source-oriented particle class arriving at Long Beach on September 24, 1996 (1 fg = $10^{-15}$g). b) Mass spectrum of an ambient particle sampled by ATOFMS at Long Beach, on September 24 (peak intensities are indicated in arbitrary units on the vertical axis). c-d) Procedures to transform model calculations and single-particle mass spectra into a common format. e) Transformed description of the particle class shown in (a). f) Transformed particle description of the mass spectrum shown in (b).

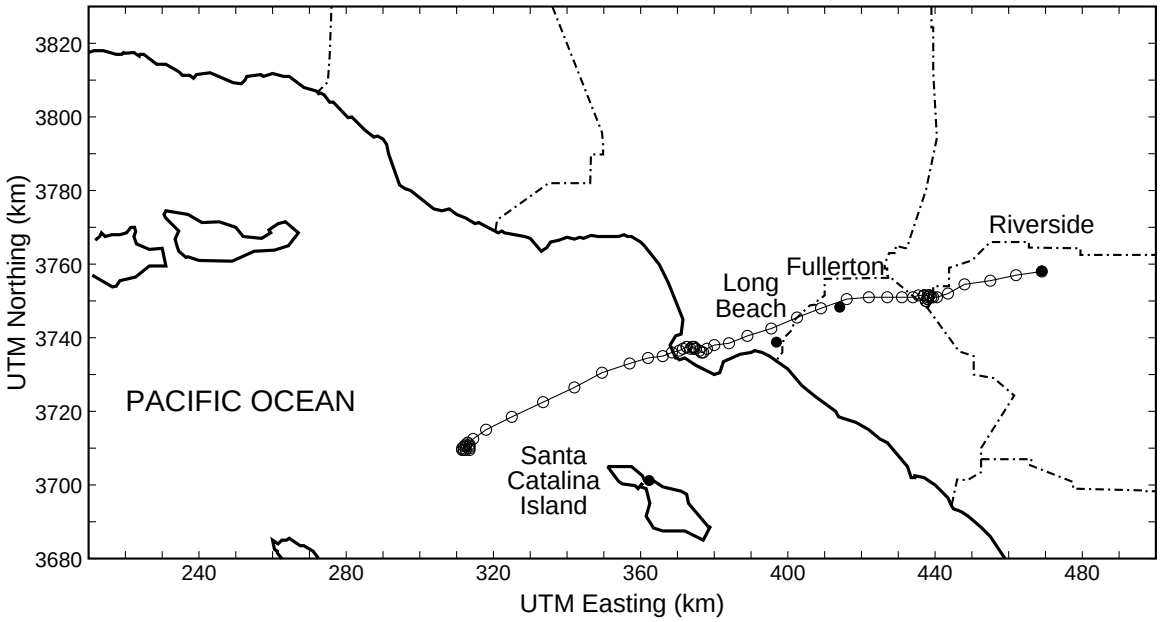


Figure 2.2: Three-day air parcel trajectory path terminating over Riverside, at 1700 PDT on September 25, 1996. Each circle represents the position of the air mass during a different hour.

quality model just described (see Section 1.2.3) [54]. Instruments were stationed at three sites in the Los Angeles, California area: Long Beach, Fullerton, and Riverside. These monitoring locations were chosen because they lie along a seasonally typical air parcel pathway crossing the Los Angeles Basin. The size and composition distribution of airborne particles and gas-phase pollutant concentrations were measured upwind of the study area at Santa Catalina Island on September 21–22, 1996, for the purpose of specifying initial conditions to the air quality model. Air parcel trajectories that passed over the Riverside site during the study period were calculated by backward integration through wind fields that were interpolated from wind observations at 29 locations in southern California [68, 74]. Trajectory calculations indicate that the air mass arriving at Riverside during the 1500–1900 PDT intensive sampling period on September 25, passed over Fullerton between 1430–1900 PDT on September 24, and stagnated near the Long Beach monitoring site during the 0700–1100 PDT intensive sampling period and throughout the morning of September 24 (see Figure 2.2).

The source-oriented air quality model described above was used to calculate the size distribution and chemical composition of the airborne particle mixture observed

at Long Beach and Fullerton on September 24, and at Riverside on September 25, 1996. Comparison of air quality model results against both filter-based and cascade impactor-based measurements of the particle size distribution and bulk chemical composition show good agreement at all three air monitoring sites (see Section 1.2.3 [55]). Having established confidence in the air quality model calculations of the aerosol size distribution as well as the bulk and size-segregated aerosol chemical composition at all three monitoring sites along the air parcel trajectory, model results now can be tested against atmospheric single-particle measurements.

### 2.2.2 Description of Single-Particle Aerosol Measurements

On September 24–25, 1996, ATOFMS instruments operated continuously at the Long Beach and Riverside sites. The Long Beach site was equipped with a field-transportable ATOFMS instrument [75], and a laboratory-bound ATOFMS instrument [46] was stationed at the Riverside site. A third ATOFMS instrument located at the Fullerton site was not operated during the September 24–25 time period. Consequently, model calculations of the Fullerton aerosol cannot be evaluated against ATOFMS measurements, and is not discussed in this chapter.

A thorough description of the ATOFMS instrument operating principles is provided elsewhere [46]. Briefly, ambient air is drawn into the ATOFMS instruments and particles are focused into a narrow beam and accelerated to a terminal velocity that is a function of their aerodynamic size. The velocity, hence aerodynamic size, of each particle is measured by detecting scattered light from two continuous wave timing lasers, positioned a fixed distance apart, orthogonal to the particle beam and to each other. The arrival time of the sized particle is predicted based on the particle velocity measurement, and a third laser is fired to intercept the sized particle. This third laser ablates and ionizes the contents of the particle and a time-of-flight mass spectrometer analyzes the generated ions, producing a mass spectrum. In this manner, ATOFMS instruments simultaneously measure the chemical composition and size of individual particles. Figure 2.1b shows the mass spectrum and aerodynamic diameter ($D_a$)

measurement of an individual atmospheric particle sampled using the transportable ATOFMS instrument at Long Beach.

At the time of the 1996 field study, the ATOFMS instruments could obtain either a positive ion or a negative ion mass spectrum for each particle hit by the ablation/ionization laser. Positive ion mass spectra were collected throughout the intensive sampling periods described in this study. As a result, negative ion markers for certain species, including sulfate, silicon, and chloride, are not available for use in this model evaluation study. Modifications to the transportable ATOFMS instrument design following the 1996 study have added dual ion detection capability, so both positive and negative ion mass spectra are obtained from individual particles in more recent field studies [76–81].

### 2.2.3 Model Evaluation Procedure

In order to evaluate the air quality model calculations, several steps are required to render the ATOFMS measurements and model results into a common format that permits a direct comparison to be made. The procedure used to transform ATOFMS measurements into such a format is outlined in Figure 2.1d. ATOFMS instruments are known to undercount ambient particles by a factor, $\phi$, that increases with decreasing aerodynamic particle diameter, $D_a$ [82].

$$\phi = \alpha \, {D_a}^{\beta} \tag{2.1}$$

where parameters $\alpha$ and $\beta$ are determined by comparing ATOFMS data with collocated reference measurements. For ATOFMS data collected during the 1996 field experiment, parameter values of $\alpha$ and $\beta$ are 2133 and -5.527, respectively, for the ATOFMS instrument stationed at Long Beach, and 4999 and -3.236, respectively, for the Riverside-based ATOFMS instrument [82]. These "counting efficiency" functions were derived for particles smaller than 1.8 $\mu$m diameter, because reference measurements at larger particle sizes were not available. In order to maximize the particle size range over which model results can be evaluated in the present study, the ATOFMS

counting efficiency functions are extrapolated upward to 3.5 $\mu$m. Each particle in the 0.32–3.5 $\mu$m aerodynamic diameter range for which a mass spectrum was obtained, is "duplicated" in proportion to the degree to which particles of that size were undercounted by the ATOFMS instruments; each particle is assumed to have the same chemical composition as the particle from which it was duplicated. This calculation accounts for the tendency of ATOFMS instruments to preferentially detect large particles rather than smaller ones, and results in a particle number distribution matching that of the atmosphere as measured by collocated laser optical particle counters and cascade impactors during the time of sampling [82].

Because manual classification of the ATOFMS data is slow, labor intensive, and subject to operator bias [83], automated computer software is used to generate a *peak list* that contains the areas, heights, and mass-to-charge (m/z) ratios of all peaks in a particle spectrum. A variety of data analysis programs use these peak lists along with the corresponding $D_a$ measurements, to group individual particles into meaningful classes. At the time of this study, chemical sensitivities of the ATOFMS instruments were not known with sufficient accuracy to quantitatively reconstruct the chemical composition of individual particles. Therefore, in this chapter, particle spectra obtained by ATOFMS are used to indicate only the presence or absence of selected chemical species in each particle rather than the quantitative amounts of each chemical component in the particle. The presence or absence of chemical species in each particle can be used to separate the ambient aerosol into compositionally distinct particle classes. Evaluations presented in this chapter compare the presence or absence of selected species in source-oriented model particle classes to the presence or absence of these species in the ATOFMS measurements.

The presence of sodium, ammonium, nitrate, carbon, or mineral dust, in each individual particle is determined by searching for certain indicator peaks in the peak list corresponding to that particle. All searches of the ATOFMS data are performed using the YAADA data analysis system [84]. The search criteria used to determine whether or not a particle contains sodium, ammonium, nitrate, and/or carbon, are described by Hughes et al. [85]. Search criteria for detecting mineral dust in ambient

particles are updated for the present model evaluation, based on recent findings from an ATOFMS single-particle source characterization study of suspended soil samples commonly found in the southern California region [86]. Eight mineral dust search criteria are defined precisely in Table 2.2. A particle spectrum that meets at least one of these criteria is classified as a dust-containing particle in the present study. Ninety percent of the positive ion mass spectra obtained from suspended soil samples in the source characterization study satisfy these search criteria. This represents a marked improvement in the source classification of southern California ambient particles, in comparison to previous studies [85]. Because these search criteria were developed by visual inspection of single-particle spectra from southern California soil and ambient samples, they should not be used to categorize ambient ATOFMS data collected in other regions.

By following the procedure outlined in Figure 2.1d, each mass spectrum acquired by ATOFMS is rendered into the format shown in Figure 2.1f. Aerodynamic particle diameters are obtained directly from the ATOFMS measurements, whereas the atmospheric number concentration of particles having the same size and composition as the sampled particle is determined using the counting efficiency function in Equation 2.1. The peak list search criteria are used to determine whether the five chemical species of interest were present or absent in each sampled particle. For example, the mass spectrum shown in Figure 2.1b contains peaks that indicate the presence of ammonium, nitrate, and carbon.

Figure 2.1c outlines the procedure followed to transform the quantitative air quality model results into the semi-quantitative ATOFMS data format. The sensitivity of ATOFMS instruments for detecting individual chemical components present in the mixed ambient aerosol varies dramatically from one chemical component to another. For example, recent laboratory work demonstrated that ATOFMS instruments detect $K^+$ in individual particles with 360 times greater sensitivity than $NH_4^+$ [87]. In order to make an accurate comparison between the air quality model results and the single-particle characteristics measured by ATOFMS, the chemical sensitivities and chemical detection limits of the ATOFMS instruments must be accounted for. For

Table 2.2: Criteria for identifying the presence of mineral dust in ATOFMS positive ion spectra collected in southern California.

| | Ion | m/z range[a] | Peak List Search Criteria[b] |
|---|---|---|---|
| 1 | $Al^+$ | [27] | Height $\geq$ 200 AND |
| | $Fe^+/CaOH^+$ | [54,58] | Height $\geq$ 200 |
| 2 | $H^+$ | [0.5,2.5] | Height $\geq$ 100 AND |
| | $C^+$ | [12] | Height $<$ 100 |
| 3 | Metals | [40,50] | Area $\geq$ 50000 |
| 4 | $Ti^+$ | [47,49] | Height $\geq$ 200 AND |
| | $TiO^+$ | [63,65] | Height $\geq$ 200 |
| 5 | $Na^+$ | [22,24] | (Height $\geq$ 100 OR Relative Area[c] $\geq$ 0.5) AND |
| | $K^+$ | [38,39.5] | Height $<$ 50 AND |
| | $Na_2Cl^+$ | [81] | Height $<$ 10 AND |
| | $Na_2NO_3^+$ | [107,109] | Height $<$ 10 AND |
| | $Na_3SO_4^+$ | [164,166] | Height $<$ 10 AND |
| | $C^+$ | [12] | Height $<$ 50 AND |
| | $C_3^+$ | [36] | Height $<$ 50 AND |
| | $C_2H_3O^+$ | [43] | Height $<$ 50 |
| 6 | $K^+$ | [38,39.5] | (Height $\geq$ 100 OR Relative Area[c] $\geq$ 0.5) AND |
| | $C^+$ | [12] | Height $<$ 50 AND |
| | $C_3^+$ | [36] | Height $<$ 50 AND |
| | $C_2H_3O^+$ | [43] | Height $<$ 50 AND |
| | | | not sea salt[d] |
| 7 | $Ca^+$ | [40] | Height $\geq$ 200 AND |
| | $CaO^+/CaOH^+$ | [55,58] | Height $\geq$ 20 AND |
| | $Ca_2O^+$ | [95,97] | Height $\geq$ 20 AND |
| | $C^+$ | [12] | Height $<$ 50 AND |
| | $C_3^+$ | [36] | Height $<$ 50 AND |
| | | | not sea salt[d] |
| 8 | $Al^+$ | [27] | Height $\geq$ 20 AND |
| | $Fe^+/CaOH^+$ | [54,58] | Height $\geq$ 100 AND |
| | $V^+$ | [51] | Height $<$ 50 AND |
| | | | not sea salt[d] |

[a]Unless otherwise specified, m/z range is ±0.5 Daltons

[b]Height and area thresholds are listed in arbitrary units

[c]Relative area is the ratio of the area of a given peak to the total area under the mass spectrum

[d]Sea salt particle spectra contain a peak in the m/z range [22,24] with Height $\geq$ 50 arbitrary units (indicative of $Na^+$) and meet at least one of the four criteria listed in Table 2.3.

Table 2.3: Exceptions to mineral dust search criteria #6–8.

| | Ion | m/z range[a] | Peak List Search Criteria[b] |
|---|---|---|---|
| 1 | $Na_2Cl^+$ | [81] | Height $\geq$ 30 |
| 2 | $Na_2NO_3^+$ | [107,109] | Height $\geq$ 30 |
| 3 | $Na_3SO_4^+$ | [164,166] | Height $\geq$ 10 AND |
| | $Na_2Cl^+$ | [81] | Height $\geq$ 10 |
| 4 | $Na_3SO_4^+$ | [164,166] | Height $\geq$ 10 AND |
| | $Na_2NO_3^+$ | [107,109] | Height $\geq$ 10 |

[a]Unless otherwise specified, m/z range is $\pm$0.5 Daltons
[b]Height and area thresholds are listed in arbitrary units

the present evaluation, the air quality model calculations of the chemical composition of each source-oriented particle class are transformed to simulate the ATOFMS instrument sensitivity to different chemical substances. Mass concentrations of the chemical components within each particle are scaled to reflect the fact that some substances stand out clearly in an ATOFMS single-particle spectrum even when present at very small concentrations within the particle. ATOFMS relative sensitivity factors (RSF's) are defined as the sensitivity of ATOFMS instruments to a species of interest divided by the ATOFMS sensitivity to sodium [87]. Estimated and experimentally determined RSF's for all chemical species tracked by the air quality model appear in Table 2.4. Conversion of the mass concentrations, calculated in the air quality model, to molar concentrations, and then multiplying by the positive ion mode RSF's, results in a collection of particles with increased apparent concentrations of chemical species whose RSF's are greater than unity and decreased apparent concentrations of species whose RSF's are less than unity.

After applying the RSF's, the air quality model results are further modified to simulate the chemical detection limits of the ATOFMS instruments. In ATOFMS data, species present at very low levels in a particle may not be detectable due to interference from noise in the mass spectrum. In one ATOFMS study, a 2% relative peak area threshold was applied to distinguish real mass spectral peaks from mass spectrometer noise [90], where the relative peak area is defined as the ratio of the area of a given peak to the total area under the mass spectrum. In an analogous manner,

Table 2.4: Relative sensitivity factor estimates for species detected by ATOFMS in positive ion mode.

| **Species** | **RSF** |
|---|---|
| Aluminum | 0.5[a] |
| Ammonium | 0.014[b] |
| Barium | 4.0[a] |
| Calcium | 3.0[a] |
| Carbon | 0.05[a] |
| Cesium | 7.9[b] |
| Chloride | 0[c] |
| Copper | 0.3[a] |
| Iron | 3.5[a] |
| Lead | 0.5[a] |
| Magnesium | 0.8[a] |
| Manganese | 0.5[a] |
| Molybdenum | 0.5[a] |
| Nitrate | 0.018[d] |
| Phosphorus | 0[c] |
| Potassium | 5.1[b] |
| Rubidium | 6.0[b] |
| Silicon | 0[c] |
| Silver | 0.09[a] |
| Sodium | 1.0[b] |
| Strontium | 20.0[a] |
| Sulfate | 0[c] |
| Tin | 0.5[a] |
| Titanium | 0.35[a] |
| Vanadium | 0.13[a] |
| Zinc | 0.05[a] |

[a]Estimates based on ionization potential and laboratory experience [88]
[b]Determined from laboratory experiments [87]
[c]Zero entry indicates chemical species is not commonly detected in positive ion mode
[d]Determined from field experiments based on comparison with impactor measurements [89]

the interference from mass spectrometer noise is approximated by discarding model calculations of chemical species whose RSF-adjusted apparent concentrations in an individual particle are less than 2% of the total apparent concentrations of all species in the particle. The 2% chemical detection limit is applied to model results in order to determine whether each particle class contains ammonium, nitrate, and/or carbon, in quantities large enough to be detected by the ATOFMS instruments. No detection threshold is applied to categorize modeled particle classes as sodium-containing because the ATOFMS instruments are thought to be capable of detecting particulate sodium at a level far below the detection limits of the instruments used to dictate sodium emission inputs to the air quality model. In the model results, dust-containing particles are identified as such if they originated from the suspension of either crustal material or paved road dust, taking advantage of the air quality model's ability to track the original source of each particle class. In this manner, each particle class tracked in the air quality model is categorized according to whether or not it contains sodium, ammonium, nitrate, carbon, and/or mineral dust.

As illustrated on the left-hand side of Figure 2.1, the detailed, quantitative particle description, calculated using the air quality model, is reduced to an abbreviated particle description shown in Figure 2.1e, for the purposes of comparison with the semi-quantitative ATOFMS data. The physical particle diameter tracked by the air quality model is converted to aerodynamic diameter using the particle density calculated in the model and assuming that all particles are spherical, whereas the particle number concentration is obtained directly from model calculations. The presence or absence of the five chemical species of interest in each particle is determined after scaling the chemical composition according to ATOFMS instrument RSF's, and removing species that fall below the simulated ATOFMS detection limits. In the example shown in Figure 2.1a, model calculations reveal that the particle contains small amounts of ammonium and nitrate. While simulating the ATOFMS instrument chemical sensitivities and detection limits, however, the particle is "stripped" of its ammonium and nitrate, resulting in the particle description shown in Figure 2.1e.

After the ATOFMS measurements and air quality model results are transformed

into a comparable format, the particles are separated into aerodynamic diameter intervals corresponding to those of the cascade impactors ($D_a$ = 0.32–0.56 $\mu$m, 0.56–1.0 $\mu$m, 1.0–1.8 $\mu$m, and 1.8–3.5 $\mu$m). Size-segregated and chemically-categorized air quality model calculations and ATOFMS measurements can then be directly compared with one another.

## 2.3 Results and Discussion

The remainder of this chapter focuses on two 4-hour air pollution episodes: (1) 0700–1100 PDT on September 24 at Long Beach; and (2) 1500–1900 PDT on September 25 at Riverside. As discussed earlier, model calculations of the aerosol size distribution and chemical composition agree favorably with the filter and impactor-based measurements taken at both sites during the indicated time periods [55]. Moreover, air parcel trajectory calculations reveal that the same air mass passed over both Long Beach and Riverside monitoring sites in succession, during the 4-hour time periods listed above. Selection of these two sampling periods permits an evaluation of air quality model calculations of the evolution of a source-oriented particle mixture within a single air parcel, as it is transported across the Los Angeles area. For these reasons, the current model evaluation study focuses on the two indicated time periods.

In this section, air quality model results and ATOFMS measurements during the two time periods of interest are compared. ATOFMS instruments acquired positive ion mass spectra from 4780 particles with $D_a$ = 0.56–3.5 $\mu$m during the 4-hour intensive sampling period at Long Beach, and 3517 particles with $D_a$ = 0.32–3.5 $\mu$m during the intensive sampling period at Riverside. Model results are obtained by computing the pollutant evolution along trajectories terminating hourly at each monitoring site during the 4-hour intensive sampling periods. The air quality model tracked the evolution of 2388 source-oriented particle classes reaching the Long Beach site with $D_a$ = 0.56–3.5 $\mu$m during the time period of interest, and 8872 particle classes with $D_a$ = 0.32–3.5 $\mu$m reaching the Riverside site. In this section, model calculations are compared with ATOFMS measurements in two steps. First, the fractions of particles

in each size interval that contain one or more of the five chemical species of interest are compared. These are referred to as *single-component* comparisons, because the model results are compared with ATOFMS measurements one chemical component at a time. Next, the compositional heterogeneity of size-segregated particle populations calculated using the air quality model are compared with the ATOFMS measurements at both sites. These are referred to as *multi-component* comparisons, because model calculations of the fractions of particles consisting of unique combinations of multiple chemical species are compared with ATOFMS measurements.

### 2.3.1 Single-Component Model Evaluation

Figure 2.3 displays the fraction of particles in each size interval containing any one of the five chemical species of interest. Air quality model results are plotted as black stars and ATOFMS measurements are plotted as solid lines. The left column of Figure 2.3 depicts single-component comparisons at the Long Beach monitoring site. Trajectory calculations indicate that the air parcels studied here spent between thirteen and seventeen hours over land before reaching the Long Beach site during the time period of interest. The aerosol sampled at Long Beach had therefore undergone significant atmospheric processing in the polluted region upwind of Long Beach, and this degree of atmospheric processing is simulated accurately in the air quality model. The model calculations accurately reveal the abundance of sodium-containing and nitrate-containing particles with $D_a$ = 1.8–3.5 $\mu$m, and the abundance of ammonium-containing, nitrate-containing, and carbon-containing particles in the 1.0–1.8 $\mu$m and 0.56–1.0 $\mu$m size ranges. Also, the air quality model calculations accurately reveal that mineral dust is present in a relatively small fraction of the ambient particles in all three size ranges studied. Overall, air quality model results and ATOFMS measurements are in excellent agreement with one another for all five chemical species of interest, across the entire particle size range measured using the transportable ATOFMS instrument, at Long Beach.

The right-hand column of Figure 2.3 depicts single-component comparisons be-

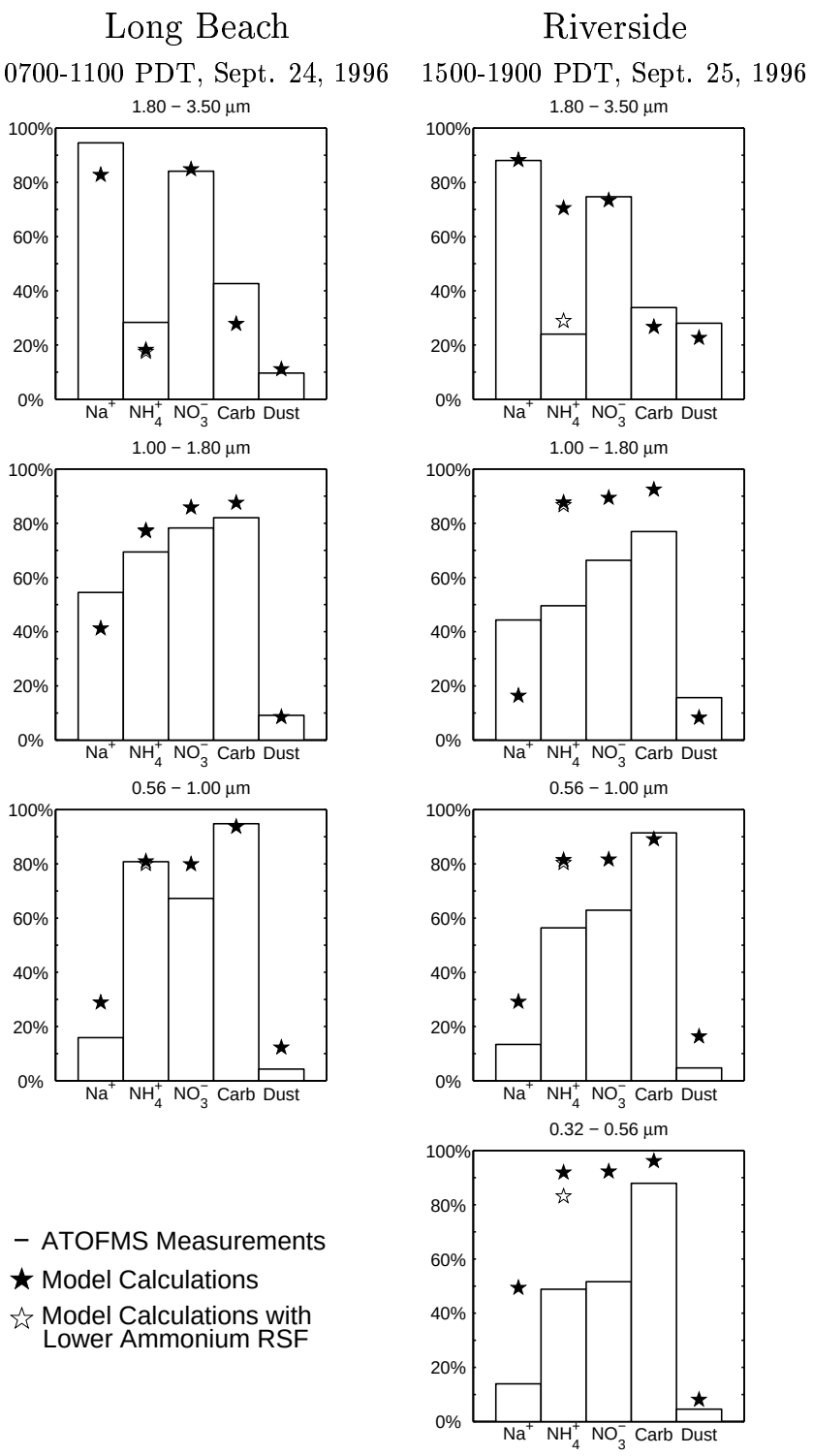


Figure 2.3: Single-component comparisons of model results and ATOFMS measurements. Vertical axes indicate the fraction of particles in the given size interval that contain the chemical component of interest. The transportable ATOFMS instrument stationed at Long Beach did not sample a sufficient number of particles smaller than 0.56 $\mu$m to warrant a comparison in the 0.32–0.56 $\mu$m size range.

tween the air quality model results and ATOFMS measurements at the Riverside monitoring site. Overall, model calculations are in good agreement with ATOFMS measurements in the largest particle size range measured at Riverside, but there is less agreement at smaller particle diameters.

In the 1.8–3.5 $\mu$m size range, the air quality model calculations match the percentage of atmospheric particles that contain sodium, nitrate, carbon, and mineral dust, as shown in the upper right-hand subplot of Figure 2.3. The ammonium-containing particle fraction calculated using the air quality model in the 1.8–3.5 $\mu$m size range is almost three times as large as that measured by the ATOFMS instrument at Riverside. The high ammonium-containing particle fraction calculated in the air quality model results primarily from a large ammonia source located in the Chino dairy area upwind of the Riverside site, as well as many smaller ammonia sources located throughout the Los Angeles region. Filter and impactor measurements of the particulate ammonium mass concentration at Riverside during the sampling period reinforce confidence in the air quality model calculations [55]. One possible explanation for the difference between the model results and ATOFMS measurements is that the ATOFMS instrument may be less sensitive to detecting ammonium ions in atmospheric particles than was previously assumed. The ammonium ion RSF applied to model results in the current study is based on laboratory measurements of an aerosol generated from equimolar solutions of NaCl and $NH_4Cl$ [87]. Ammonium in the 1.8–3.5 $\mu$m range at Riverside is present primarily in the form of $NH_4NO_3$, not $NH_4Cl$, raising the possibility that the ammonium ion RSF may be inapplicable to the ambient aerosol studied here. We can simulate a reduced sensitivity to ammonium by lowering the ammonium ion RSF applied to the model results by a factor of two. Model calculations of the ammonium-containing particle fraction, modified by this lower ammonium ion RSF, are displayed as white stars in Figure 2.3. This RSF reduction brings model results into agreement with ATOFMS measurements of the ammonium-containing particle fraction in the 1.8–3.5 $\mu$m size range at Riverside, and slightly improves agreement in the 0.32–0.56 $\mu$m size range. Furthermore, the reduced ammonium ion RSF does not significantly affect model performance at the Long Beach site across all of the size ranges stud-

ied. This lends credence to the hypothesis that ATOFMS sensitivity to ammonium is lower in the ambient aerosol studied here, than in the laboratory-generated aerosol from which the ammonium ion RSF was determined. The sensitivities of ATOFMS instruments to $NH_4^+$ and $NO_3^-$ are assessed in Chapter 3 [91]. Use of those sensitivity factors will allow more refined comparisons of ATOFMS measurements and air quality model calculations in Chapter 5.

In the three smallest size ranges examined at the Riverside site, model results show less agreement with the single-particle ATOFMS measurements. The most noticeable difference is that the model results show larger ammonium-containing and nitrate-containing particle fractions in the fine particle size intervals ($D_a < 1.8$ $\mu$m), as compared to the the ATOFMS measurements. Some of this difference is mitigated by reducing the ammonium ion RSF as discussed above. However, this still leaves air quality model calculations of both ammonium and nitrate in excess of the ATOFMS measurements in the fine particle size range. Analysis of the single-particle ATOFMS measurements at the Riverside site reveal a large class of fine carbonaceous particles that contain neither ammonium nor nitrate. This particle class appears to be composed of fresh combustion source emissions that did not have time to accumulate ammonium nitrate before being sampled by the ATOFMS instrument. The laboratory-based ATOFMS instrument was stationed on the second floor of Pierce Hall at the University of California, Riverside, which unfortunately was located near the loading docks for the campus cafeteria and bookstore. At the time of sampling, the bookstore was receiving more deliveries than usual, due to the start of the fall academic term. In addition, a strong food cooking smell was noted at the sampling site during the study period, possibly due to cafeteria operations upwind of the sampling equipment. The number of purely carbonaceous particles measured by ATOFMS dropped off by a factor of two after 1700 PDT on September 25, possibly corresponding with the end of the business day for the campus cafeteria and bookstore. The largest difference between the model calculations and ATOFMS measurements of the ammonium-containing and nitrate-containing particle fractions at Riverside is noted in the smallest measured size range ($D_a = 0.32$–$0.56$ $\mu$m), which corresponds with

the peak in the aerosol size distributions of freshly emitted motor vehicle exhaust and emissions from meat cooking operations [65, 66]. For the reasons listed above, vehicle exhaust from the loading docks and food cooking particles from the cafeteria are both likely sources of the purely carbonaceous aerosol measured by ATOFMS at Riverside. The air quality model operates using a horizontal spatial resolution of 5km $\times$ 5km, and therefore, is unable to resolve emissions from sources located very near a monitoring site. However, large quantities of gas phase ammonia and nitric acid measured at the Riverside site during the sampling period [85] support air quality model calculations that show most of the aged particles in the fine particle size range having accumulated ammonium nitrate before reaching the Riverside monitoring site.

The fractions of dust-containing particles in the air quality model results between 0.32–1.0 $\mu$m $D_a$ at Riverside and between 0.56–1.0 $\mu$m $D_a$ at Long Beach are slightly larger than the corresponding dust-containing particle fractions measured by ATOFMS. Air quality model calculations of the sodium-containing particle fractions in these size ranges are also larger than the corresponding ATOFMS measurements. Chemical composition profiles of both crustal material and paved road dust contain sodium [92], suggesting that these two differences may be associated with one another. Due to the unavailability of size-distributed measurements of suspended crustal material and paved road dust, the submicron size distributions of these two aerosol emission sources used in the air quality model are obtained from ambient impactor measurements of the non-hygroscopic particle fraction collected at Claremont, California [60]. In order to improve air quality model calculations of the dust-containing and sodium-containing particle fractions in the submicron size range, a detailed characterization of the size and composition distribution of both crustal material and paved road dust is warranted. The presence of near-field sources of fresh carbonaceous particles at the Riverside site, discussed above, reduce the dust-containing and sodium-containing particle fractions measured by ATOFMS, further contributing to the differences between ATOFMS measurements and air quality model results in the fine particle size range.

### 2.3.2 Multi-Component Model Evaluation

After noting the general agreement between model results and ATOFMS measurements in the single-component comparisons, the air quality model calculations are subjected to an even more stringent evaluation. All particles in the air quality model results and in the ATOFMS data set which contain the same combination of chemical species are grouped together and compared against one another. Figure 2.4 shows the results of this multi-component comparison as a color-coded display, illustrating the chemical heterogeneity among size-segregated particles in both model results and ATOFMS measurements at the Long Beach and Riverside sites. Each of the 100 dots within a square plot in Figure 2.4 represents one percent of the particle population at the time and location indicated, within the specified $D_a$ range. Each dot is striped with colors that correspond to the chemical components found in one percent of the size-segregated particle population. The exception to this rule is the dust particle category; all mineral dust-containing particles are represented as solid gray dots because the ATOFMS ion peaks associated with dust often have areas so large that they exceed the instrument's dynamic range and produce noise in the rest of the mass spectrum, making the detection of other peaks less reliable. Therefore, any or all of the other chemical species may be present within the mineral dust-containing particles represented by a solid gray dot. As a result, the gray dots in Figure 2.4 relay the same information depicted by the corresponding stars and solid lines in Figure 2.3. In Figure 2.4, a colored stripe only qualitatively indicates the presence of the corresponding chemical species; no conclusions should be drawn about the relative amounts of each chemical substance in a particle. The "many types" category, shown in green, is the sum of those particle types which each encompass less than approximately 0.5% of the particle population, which therefore, would not warrant representation by an entire dot.

Table 2.5 provides a numerical representation of the color-coded display shown in Figure 2.4. The values listed in Table 2.5 correspond to the number of dots in Figure 2.4, that represent particles in the corresponding chemical class. For example,

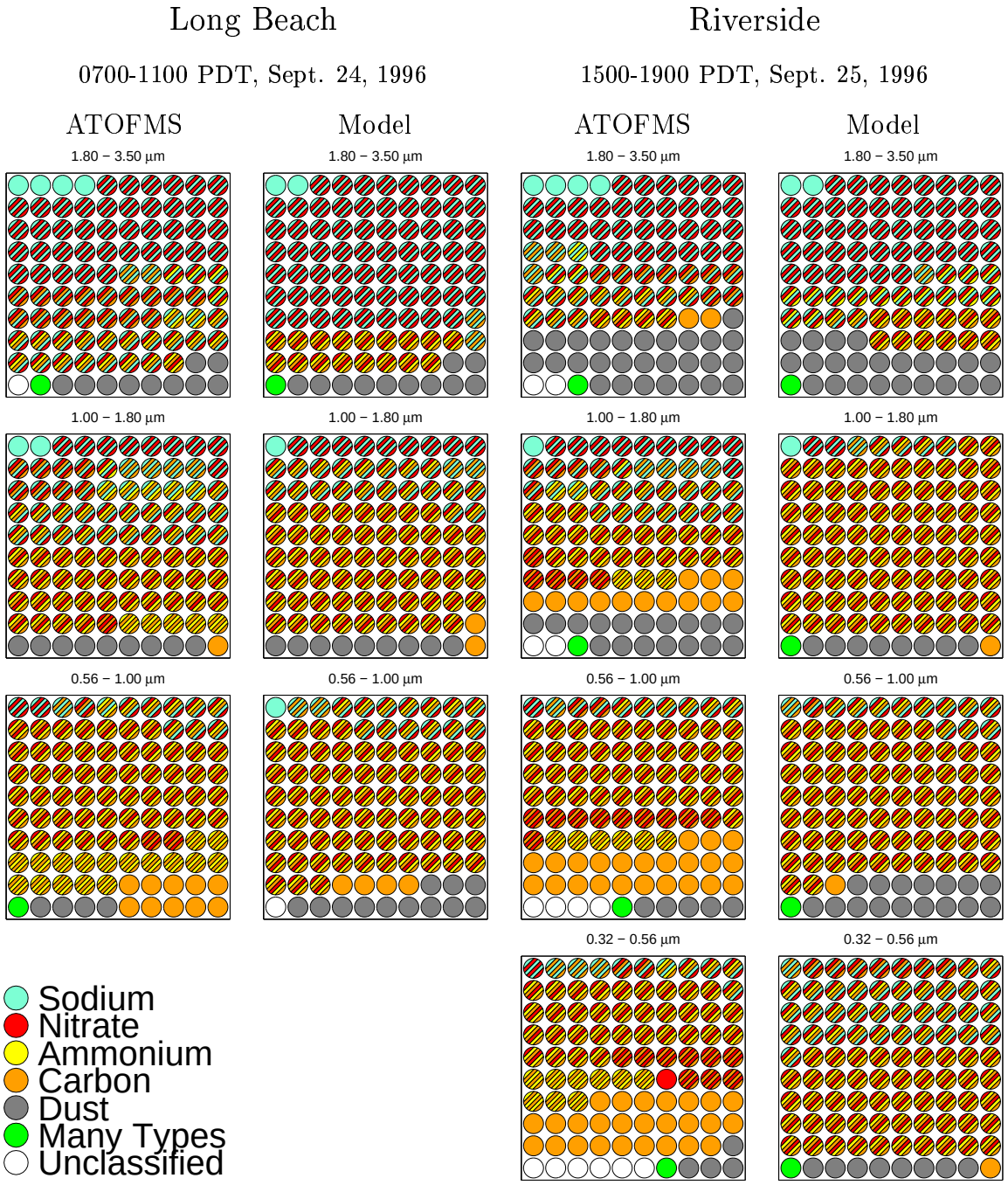


Figure 2.4: Multi-component comparisons of model results and ATOFMS measurements. Each dot represents 1% of the particle population within the indicated aerodynamic particle diameter range. The transportable ATOFMS instrument stationed at Long Beach did not sample a sufficient number of particles smaller than 0.56 $\mu$m to warrant a comparison in the 0.32–0.56 $\mu$m size range.

Table 2.5 indicates that 34% of the counting efficiency corrected ATOFMS measurements in the 1.00 - 1.80 $\mu$m particle size range at Long Beach contain nitrate, ammonium, and carbon. The corresponding subplot of Figure 2.4 includes 34 dots with red, yellow, and orange stripes.

The ATOFMS measurements displayed in Figure 2.4 are identical to those that appear in [85, Figure 8 h-n], with the exception that the mineral dust search criteria updated for the present study result in a larger fraction of particles being classified as "dust" across all size ranges and at both monitoring sites. The model results shown in Figure 2.4 are obtained by following the procedures described above, and the RSF applied to model calculations of ammonium ions at both sites and all particle size ranges is reduced by a factor of two. This adjustment is made to simulate a lower ATOFMS instrument sensitivity to ammonium ions in ambient particles, as inferred from the single-component analyses presented in the previous section.

The left half of Figure 2.4 displays multi-component comparisons between air quality model results and ATOFMS measurements at the Long Beach site. In the 1.8–3.5 $\mu$m size range, the model calculations accurately reveal the presence of sodium and nitrate (represented by blue and red stripes) in the vast majority of particles. Model calculations indicate that these particles originated as sea spray. Likewise, ATOFMS spectra associated with the sodium and nitrate-containing particle class in the 1.8–3.5 $\mu$m size range contain indicator peaks that commonly result from the ablation/ionization of sea salt particles. This suggests that the model accurately calculates the relative contribution of sea spray aerosols to the particle number concentration in this size range. The air quality model results also accurately reveal a small fraction of particles containing sodium and carbon, that have not accumulated ammonium nitrate. These particles are represented by blue and orange striped dots. Model calculations suggest that these particles were emitted from motor vehicles near the Long Beach site during the morning rush hour traffic period. Model calculations of the dust-containing particle fraction (solid gray dots) are in excellent agreement with the ATOFMS measurements in the 1.8–3.5 $\mu$m size range. This agreement lends credence to the emission inventories of paved road dust and crustal material, used as

Table 2.5: Numerical representation of Figure 2.4.

| | Long Beach 0700–1100 PDT, Sept. 24, 1996 | | Riverside 1500–1900 PDT, Sept. 25, 1996 | |
|---|---|---|---|---|
| | ATOFMS | Model | ATOFMS | Model |
| | 1.80–3.50 $\mu$m | | 1.80–3.50 $\mu$m | |
| Sodium | 4% | 2% | 4% | 2% |
| Sodium & Nitrate | 41% | 67% | 33% | 44% |
| Sodium & Ammonium | | | 1% | |
| Sodium & Carbon | 2% | 2% | 3% | 1% |
| Sodium, Nitrate, & Ammonium | 4% | | 2% | 15% |
| Sodium, Nitrate, & Carbon | 16% | | 9% | |
| Sodium, Ammonium, & Carbon | 2% | | | |
| Sodium, Nitrate, Ammonium, & Carbon | 18% | | 11% | 2% |
| Nitrate, Ammonium, & Carbon | 1% | 17% | 4% | 12% |
| Carbon | | | 2% | |
| Dust | 10% | 11% | 28% | 23% |
| Many Types | 1% | 1% | 1% | 1% |
| Unclassified | 1% | | 2% | |
| | 1.00–1.80 $\mu$m | | 1.00–1.80 $\mu$m | |
| Sodium | 2% | 1% | 1% | 1% |
| Sodium & Nitrate | 9% | 9% | 10% | 2% |
| Sodium & Carbon | 4% | 2% | 4% | 1% |
| Sodium, Nitrate, & Ammonium | 1% | | 1% | |
| Sodium, Nitrate, & Carbon | 8% | | 5% | |
| Sodium, Ammonium, & Carbon | 5% | | 2% | |
| Sodium, Nitrate, Ammonium, & Carbon | 21% | 20% | 14% | 4% |
| Nitrate, Ammonium, & Carbon | 34% | 57% | 22% | 82% |
| Nitrate & Carbon | 1% | | 5% | |
| Ammonium & Carbon | 5% | | 3% | |
| Carbon | 1% | 2% | 13% | 1% |
| Dust | 9% | 9% | 17% | 8% |
| Many Types | | | 1% | 1% |
| Unclassified | | | 2% | |
| | 0.56–1.00 $\mu$m | | 0.56–1.00 $\mu$m | |
| Sodium | | 1% | | |
| Sodium & Nitrate | 2% | | 1% | |
| Sodium & Carbon | 1% | 2% | 1% | 1% |
| Sodium, Nitrate, & Carbon | 1% | | 2% | 1% |
| Sodium, Ammonium, & Carbon | 1% | | | |
| Sodium, Nitrate, Ammonium, & Carbon | 8% | 13% | 6% | 11% |
| Nitrate, Ammonium, & Carbon | 53% | 67% | 41% | 69% |
| Nitrate & Carbon | 2% | | 10% | |
| Ammonium & Carbon | 17% | | 6% | |
| Carbon | 10% | 4% | 23% | 1% |
| Dust | 4% | 12% | 5% | 16% |
| Many Types | 1% | | 1% | 1% |
| Unclassified | | 1% | 4% | |
| | | | 0.32–0.56 $\mu$m | |
| Sodium & Nitrate | | | 1% | |
| Sodium & Carbon | | | 3% | 1% |
| Sodium, Nitrate, & Carbon | | | 2% | 7% |
| Sodium, Ammonium, & Carbon | | | 1% | |
| Sodium, Nitrate, Ammonium, & Carbon | | | 4% | 33% |
| Nitrate, Ammonium, & Carbon | | | 33% | 49% |
| Nitrate & Carbon | | | 9% | |
| Nitrate | | | 1% | |
| Ammonium & Carbon | | | 9% | |
| Carbon | | | 26% | 1% |
| Dust | | | 4% | 8% |
| Many Types | | | 1% | 1% |
| Unclassified | | | 6% | |

input to the air quality model.

ATOFMS measurements reveal that 16% of the particles in the 1.8–3.5 $\mu$m size range at Long Beach contain carbon, sodium, and nitrate (orange, blue, and red striped dots), whereas air quality model calculations in the same size range at Long Beach do not contain this particle type. Analyses of the associated single-particle measurements indicate that this class of particles originated as sea spray. In the air quality model calculations, sea spray aerosols are initialized as an internal mixture of sodium, chloride, and nitrate [55], and these particles do not accumulate sufficient amounts of secondary organic material during transport between the coastline and Long Beach to exceed the simulated ATOFMS detection threshold for carbon. This suggests that the carbon detected by ATOFMS in these particles may be primary in nature. Although it is not possible to discern from the Long Beach ATOFMS data whether this sea salt-associated carbon is primary or secondary, recent single-particle measurements of clean marine air indicate that a large fraction of sea salt particles contain primary organic carbon [93]. In the future, it may be possible to seed the air quality model with multiple classes of sea spray aerosol, each having a distinct chemical composition. This will very likely improve the agreement between model results and ATOFMS measurements of the coarse mode carbon-containing particle fraction. The air quality model results show that 17% of particles in the 1.8–3.5 $\mu$m size range contain ammonium, nitrate, and carbon (red, orange, and yellow striped dots), but they lack sodium. This particle type composes only 1% of the ATOFMS data. Instead the ATOFMS data show 18% of particles in the coarse size range containing sodium, nitrate, ammonium, and carbon (blue, red, yellow, and orange striped dots). The likely cause of this difference is that ATOFMS instruments are extremely sensitive to the sodium ion, and therefore detect sodium in particles that originated from emission sources for which the model's emission source profiles contain no sodium.

In the 1.0–1.8 $\mu$m size range at Long Beach, the model results continue to meet the stringent multi-component evaluation. Model calculations of particles containing sodium only (solid blue dots), sodium and nitrate (blue and red striped dots), sodium

and nitrate and ammonium and carbon (blue, red, yellow, and orange striped dots), carbon only (solid orange dots), and mineral dust (solid gray dots), all match the ATOFMS measurements within 1%. The close agreement between model calculations and ATOFMS measurements of the particle class containing sodium, nitrate, ammonium, and carbon, suggests that ammonium nitrate formation and partitioning processes within the model are relatively accurate. The only noteworthy difference between model results and ATOFMS measurements in the 1.0–1.8 $\mu$m size range at Long Beach is the excess fraction of particles containing ammonium, nitrate, and carbon in the model results (red, orange, and yellow striped dots). This difference is to be expected based on the single-component comparisons, which showed that the model results slightly overestimates the ammonium-containing, nitrate-containing, and carbon-containing particle fractions, in the 1.0–1.8 $\mu$m $D_a$ range (see Figure 2.3).

The air quality model results accurately reveal that the most common particle type present in the 0.56–1.0 $\mu$m size range at Long Beach contains ammonium, nitrate, and carbon (red, orange, and yellow striped dots). The air quality model results also contain three compositionally distinct sodium-containing particle types, agreeing fairly well with the chemical heterogeneity of sodium-containing particles measured by ATOFMS. The model overestimation of dust-containing particles (solid gray dots) in the 0.56–1.0 $\mu$m size range at Long Beach was discussed in conjunction with the single-component comparison. The only other apparent difference between the model results and ATOFMS measurements at Long Beach in the 0.56–1.0 $\mu$m size range is the lack of a particle type containing only carbon and ammonium (orange and yellow striped dots) in the model calculations. Instead, the model results show an excess of particles containing ammonium, nitrate, and carbon (red, orange, and yellow striped dots). The absence of nitrate in the ATOFMS measurements of the particle type containing only carbon and ammonium may be due to the fact that only positive ion mass spectra were collected during the 1996 field experiment. ATOFMS instruments are known to be more sensitive to nitrate when operating in the negative ion mode than when operating in the positive ion mode. The availability of dual polarity ATOFMS data in more recent field experiments may yield better agreement between

model results and ATOFMS measurements of the nitrate-containing particle fraction.

The right half of Figure 2.4 documents the multi-component comparisons between model results and ATOFMS measurements at the Riverside site. In the 1.8–3.5 $\mu$m size range, the air quality model results accurately show that the most common particle types at Riverside contain either sodium and nitrate (blue and red striped dots) or mineral dust (solid gray dots). The air quality model results show seven compositionally distinct particle types in quantities greater than 0.5% of the particle population in the 1.8–3.5 $\mu$m size range at Riverside. ATOFMS measurements in the same particle size range display 10 compositionally distinct particle types at the Riverside site. Comparing the number of distinct particle types serves as yet another measure of the model's ability to represent the complex mixtures present in the polluted ambient aerosol. The multi-component comparisons in the fine particle size range ($D_a < 1.8$ $\mu$m) studied at Riverside are very likely affected by the presence of combustion sources located near the ATOFMS instrument during the sampling period, and therefore, are not discussed in detail.

### 2.3.3 Evolution of the Aerosol Mixture

Taken as a whole, Figure 2.4 displays the ability of the air quality model to represent the urban aerosol as an ensemble of source-oriented particle classes, and to calculate how that particle population evolves due to emissions of new particles, dry deposition, and atmospheric reactions, as it is transported across the Los Angeles area. Most coarse particles ($D_a > 1.8$ $\mu$m) in the air parcel studied here contain sodium and nitrate at Long Beach. As the air parcel traverses the Los Angeles urban area, it picks up significant quantities of mineral dust material. The particles which originally contained sodium and nitrate (blue and red striped dots) accumulate ammonium, nitrate, and carbon, due to gas-to-particle conversion processes. At first glance, the smaller particles studied here ($D_a < 1.8$ $\mu$m) appear to undergo a less pronounced evolution than their coarse mode counterparts, based on the color-coded display shown in Figure 2.4. However, Figure 2.4 does not display the relative amounts of the various

chemical species present in the atmospheric particles. The air quality model results reveal substantial increases in the amounts of ammonium, nitrate, and organic carbon on fine particles over time. As the quantification ability of single-particle instruments is improved, it may be possible in the future to quantitatively evaluate model calculations of the relative amounts of various chemical substances present in source-oriented particle classes.

While the results of the multi-component comparisons presented in this study are promising, it appears that the air quality model results somewhat underestimate the number of compositionally distinct particle types present in the urban aerosol, as compared to the number of distinct particle types measured by the ATOFMS instruments. One possible explanation for this underestimation is that some of the particle types measured by ATOFMS are coagulation products of two or more particles that were emitted from different source types. Coagulation processes are not included in the current model formulation, but they may be necessary to improve the accuracy of model calculations in future applications. A second possible explanation is that the method by which ATOFMS data are categorized is highly dependent on the analyst-defined peak list search criteria, which can lead to significant uncertainties if the thresholds are within the range of detection limits (see Section 4.2). An alternative method for spectral categorization is presented in Chapter 4. A third possible explanation for the underestimation of ambient particle heterogeneity is that the emissions inputs to the air quality model are represented as source-specific internal mixtures, where all particles emitted from a certain source type at a given initial size are assumed to have identical chemical compositions. Recent ATOFMS studies reveal that primary particles emitted at the same size from the same emission source actually exhibit different chemical compositions [86, 94–97]. In future work, emissions inputs to the air quality model may be represented as source-specific mixtures of compositionally distinct particle types, by incorporating the results of single-particle emission source characterization studies that are currently underway (see Section 7.2.3).

## 2.4 Conclusions

Air quality model calculations of the size and composition of atmospheric particle classes have been evaluated by comparison with ATOFMS single-particle measurements at Long Beach and Riverside, during September 1996. The air quality model tracks the physical diameter, chemical composition, and atmospheric concentration of thousands of particle classes as they are transported from sources to receptors while undergoing atmospheric chemical reactions. In the model, each particle class interacts with a common gas phase, but otherwise evolves separately from all other particle classes. The model calculations yield an aerosol representation, in which particles of a given size may exhibit different chemical compositions. Model results were transformed to simulate the chemical sensitivities and compositional detection limits of the ATOFMS instruments, and ATOFMS data were adjusted for instrument-specific particle detection efficiencies. This permitted direct, semi-quantitative comparisons between the air quality model results and single-particle ATOFMS measurements to be made. The fractions of atmospheric particles containing sodium, ammonium, nitrate, carbon, and mineral dust, across all particle sizes measured by ATOFMS at the Long Beach site, and in the coarse particle size range at the Riverside site, are accurately simulated in the air quality model. Given that this model evaluation is very likely the most stringent test of any aerosol air quality model to date, the model calculations show impressive agreement with the single-particle ATOFMS measurements.

# Chapter 3

# A Field-Based Approach for Determining ATOFMS Instrument Sensitivities to Ammonium and Nitrate

## 3.1 Introduction

The development of on-line single-particle mass spectrometry techniques has been identified as the most significant advance in aerosol instrumentation during recent years [98]. Although single-particle mass spectrometry instruments differ from one another in their particle sizing techniques (see Section 1.2.2), the vast majority obtain chemical composition information by laser ablation/ionization of individual particles, time-of-flight mass spectrometry, and subsequent analysis of the ion mass spectra. A commonly cited limitation of laser ablation/ionization techniques is that the chemical composition measurements are not quantitative [37, 99]. There are two main obstacles to quantitation. First, the ion signal intensities produced by laser ablation/ionization of nominally identical particles vary greatly from shot-to-shot [100], primarily because of inhomogeneities in the laser beam [101]. Second, instrument sensitivities to different aerosol-phase chemical species are largely unknown. In the

*This chapter is reproduced with permission from "A Field-Based Approach for Determining ATOFMS Instrument Sensitivities to Ammonium and Nitrate," by P. V. Bhave, J. O. Allen, B. D. Morrical, D. P. Fergenson, G. R. Cass, and K. A. Prather; *Environmental Science and Technology*, 36: 4868–4879, 2002. Copyright 2002 American Chemical Society.

present work, *instrument sensitivity* is defined as the ion signal intensity per unit mass of a chemical species, averaged over a particle ensemble.

It has been reported that shot-to-shot variations in the ion signal intensities can be mitigated by using very high laser irradiances, but molecular information is lost due to fragmentation of polyatomic ions [102]. For example, laser irradiances $> 2 \times 10^{10}$ W cm$^{-2}$ have been shown to fragment pure ammonium sulfate particles into monatomic N, H, S, and O [102]. To retain molecular information, most single-particle mass spectrometry techniques use moderate laser irradiances ($\sim 10^{7}$–$10^{9}$ W cm$^{-2}$). Operating at moderate irradiances, it is not yet possible to quantify the chemical composition of individual particles due to the shot-to-shot variations in ion signal intensities described above. However, it may be possible to quantify the chemical composition of small ensembles of single particles if the mass spectra from a collection of nominally identical particles are obtained and averaged [100, 103].

Quantifying aerosol chemical composition from an ensemble of single-particle spectra requires a knowledge of instrument sensitivities to each chemical species in the particle ensemble. Instrument sensitivities can vary dramatically from one chemical species to another [87, 103], due to chemically specific differences in ionization efficiency. To date, all efforts to determine instrument sensitivities have been based on particles generated in laboratory environments [87, 100, 102–104]. These laboratory-generated particles are typically monodisperse, spherical, and have nominally identical chemical compositions. By comparing the average ion signal intensities obtained from 20 or more identical particles to the known chemical composition of the particle ensemble, investigators have been able to determine instrument sensitivities to a few chemical species under controlled laboratory conditions [100, 103]. Recent studies revealed that instrument sensitivities can be affected substantially by the size of the individual particle being sampled [103, 105], trace impurities in the particle matrix [106], and relative humidity of the background gas [107]. Due to an incomplete understanding of these effects, extrapolation of the instrument sensitivities derived from simple laboratory-generated particles to the more complex atmospheric particles has not been successfully demonstrated.

In contrast to the laboratory-based approach described above, a *field-based approach* for determining instrument sensitivities would rely entirely on atmospheric particle measurements. Instrument sensitivities determined from a field-based approach would be directly applicable to ambient aerosol data. Moreover, a field-based approach can potentially elucidate the relative influences of particle size, particle composition, and meteorology, on instrument sensitivities under ambient sampling conditions. Ideally, the instrument sensitivities deduced from a field-based approach may be verified and further tested in laboratory experiments. Although a field-based approach for determining instrument sensitivity is appealing, it is subject to three limitations which are not encountered in a laboratory-based approach. First, a field-based approach requires quantitative reference measurements of the chemical species of interest to be taken in parallel with the single-particle measurements, because the chemical composition of an atmospheric aerosol is unknown at the time of sampling. Consequently, the accuracy of instrument sensitivities determined from a field-based approach is limited by the precision of the reference measurements. Second, a field-based approach requires the collection of a much larger number of single-particle spectra than are needed for most laboratory-based approaches, in order to obtain a statistically significant number of nominally identical particles from the complex mixture of particle types in the atmosphere. Third, particle detection efficiencies of the single-particle instrument must be well characterized to ensure the success of a field-based approach. Unlike the laboratory-generated particles, atmospheric aerosols are distributed by size, chemical composition, density, and morphology, all of which can influence the particle detection efficiency of a single-particle instrument [82, 108].

In the present study, we describe a field-based approach for determining single-particle instrument sensitivities that addresses the three limitations listed above. Our approach uses parallel measurements of atmospheric particles taken by an aerosol time-of-flight mass spectrometry (ATOFMS) instrument and a cascade impactor. ATOFMS is a rapidly developing and increasingly accepted single-particle mass spectrometry technique (see Section 1.2.2). ATOFMS instruments have been deployed in numerous field campaigns, yielding very large data sets ($\sim 10^4$–$10^6$ spectra) of

ambient single-particle size and chemical composition [76–81, 85]. Recently, Allen et al. developed a procedure for determining ATOFMS particle detection efficiencies under ambient sampling conditions [82]. After the single-particle spectra are duplicated to correct for particle undercounting, ATOFMS ion signal intensities can be compared quantitatively with collocated cascade impactor measurements of aerosol chemical composition, yielding instrument sensitivity factors that can be used to quantify the chemical composition of size-segregated atmospheric particle ensembles.

The procedure is developed using ATOFMS and impactor measurements of ammonium and nitrate, taken at Riverside, California, in September 1996, August 1997, and October 1997. ATOFMS instrument sensitivities, determined from the ATOFMS-impactor comparisons, are used to reconstruct continuous time series of quantitative, size-segregated $NH_4^+$ and $NO_3^-$ measurements over the 0.32–1.8 $\mu$m aerodynamic diameter ($D_a$) range. The applicability of the instrument sensitivity factors derived in this study to other aerosol data sets, collected at locations where different ATOFMS instrument designs are used and different particle types are abundant, remains to be tested. However, application of the ATOFMS-impactor comparison methodology described herein to other atmospheric data sets will be straightforward. In the future, it may be possible to extend the field-based approach to single-particle mass spectrometry instruments other than ATOFMS, and to aerosol species other than $NH_4^+$ and $NO_3^-$. The purposes of this chapter are to develop a field-based approach for determining ATOFMS instrument sensitivities, and to illustrate some applications of the $NH_4^+$ and $NO_3^-$ sensitivity factors.

## 3.2 Related Studies

Prior to this work, two quantitative comparisons of ATOFMS data with collocated measurements of atmospheric aerosol chemical composition have been reported in the literature. Liu et al. [90] compared the number of nitrate-containing particles detected by an ATOFMS instrument (defined as those particles which yielded an ion signal at mass-to-charge ratio 30 ($NO^+$) with relative intensity greater than 2%) with

collocated $NO_3^-$ mass concentration measurements taken by an automated nitrate monitor [109], at 10-minute sampling intervals. The numbers of nitrate-containing particles detected by ATOFMS exhibited a linear correlation ($R^2 = 0.73$) with the automated nitrate monitor measurements throughout the 53-hour sampling event at Riverside, demonstrating the ability of an ATOFMS instrument to track atmospheric $NO_3^-$ concentrations based on the presence of a specific chemical marker ($NO^+$) in the single-particle mass spectra [90].

Fergenson et al. [89] applied a multivariate calibration technique to compare ATOFMS data with collocated impactor measurements of 44 different aerosol-phase chemical species taken at Riverside, California, on September 23–26, 1996. In that study, ATOFMS data were grouped into a large number ($\sim$ 600–700) of clusters based on similar features of the single-particle mass spectra. The masses of each particle cluster were compared with collocated impactor measurements by the partial least-squares algorithm, yielding multivariate linear regression coefficients that relate the cluster masses with the atmospheric concentrations of 44 different aerosol-phase chemical species. Using eleven data cohorts as calibrants and one as a predictor, it was possible to evaluate the predictive value of the multivariate calibrations. The good overall agreement ($R^2 = 0.83$) between impactor measurements and the multivariate calibrated ATOFMS data presented in that study provides further evidence that ATOFMS data can potentially yield quantitative measurements of atmospheric aerosol chemical composition [89].

Both of the previous studies compared quantitative, bulk measurements of atmospheric aerosol chemical composition with the presence and abundance of specific *particle types* detected by ATOFMS. This work differs from previous studies because it presents the first comparison of *ion signal intensities* measured by a single-particle mass spectrometry instrument with quantitative, bulk measurements of atmospheric aerosol chemical composition. A unique advantage of the present approach is that instrument sensitivities can be deduced from atmospheric aerosol data. In the future, these sensitivity factors can be verified and further tested under controlled laboratory conditions. As such, the results of the present study can assist in the design of

laboratory experiments aimed at quantifying the chemical composition of aerosols by single-particle mass spectrometry.

## 3.3 Methods

The data presented in this chapter were collected as part of four multi-site field experiments that are described in detail elsewhere [54, 56, 79, 85, 110, 111]. During each of these experiments, individual atmospheric particles were sampled continuously by an ATOFMS instrument stationed at Riverside, California. In addition, a collocated micro-orifice impactor collected size-segregated samples of the fine ambient aerosol ($D_a < 1.8$ $\mu$m) during selected time periods. The periods of tandem ATOFMS-impactor sampling are referred to hereafter as intensive operating periods (IOPs). Data from 11 IOPs are analyzed in this work (see Table 3.1).

### 3.3.1 Aerosol Measurements

Operating principles of the ATOFMS instrument stationed at Riverside during the IOPs are described in detail elsewhere [41, 46, 112], so only the details relevant to the present study are given here. Ambient particles are drawn into the ATOFMS instrument through a converging nozzle where they are accelerated to terminal velocities that are a function of their aerodynamic diameters. Next, each particle enters a sizing region where it passes through and scatters light from two continuous wave lasers separated by a known distance. The time difference between the scattering pulses indicates the velocity of the particle, which is recorded and later used to determine the particle aerodynamic diameter. The time difference between scattering pulses is also used to actuate the firing of a high power pulse from a Nd:YAG laser, operating at 266 nm wavelength and $2 \times 10^7$–$4 \times 10^8$ W cm$^{-2}$ irradiance, upon the particle's arrival in the source region of a time-of-flight mass spectrometer. The ion signals resulting from ablation/ionization of a single particle by the Nd:YAG laser are detected by a dual microchannel plate and digitized using an 8-bit data acquisition board (Signatec, Model DA500), interfaced to a personal computer. The digitized

mass spectrum is later analyzed to determine the chemical composition of the particle. Although field-transportable ATOFMS instruments are capable of dual ion acquisition [75], the ATOFMS instrument stationed at Riverside [46] was configured to analyze only positive ions during the IOPs. The number of positive ion mass spectra collected by ATOFMS during each IOP, as a function of $D_a$, are listed in Table 3.1.

A summary of impactor operations and sample analyses relevant to the present work is presented here; detailed descriptions can be found elsewhere [54, 110, 111]. Size-segregated particles were collected on Teflon impaction substrates loaded in a 10-stage micro-orifice impactor (MSP Corporation, Model 110) [113]. Fine particles ($D_a < 1.8$ $\mu$m) in the Los Angeles atmosphere are generally sticky enough to avoid particle bounce problems within the impactor [114]. Coarse particles ($D_a >$ 1.8 $\mu$m), which are more likely to bounce off their intended impactor stage, were removed by Teflon-coated AHIL-design cyclone separators positioned upstream of the impactor inlets. No coatings were applied to the impaction substrates. After each IOP, the substrates were removed immediately and refrigerated until analysis, to prevent volatilization losses. The size-segregated particle ensembles on each impaction substrate were analyzed by ion chromatography (Dionex Corp, Model 2020i) for $NO_3^-$ [115], and by an indophenol colorimetric procedure for $NH_4^+$ [116] using an Alpkem rapid flow analyzer (Model RFA-300). Impactor measurements of $NH_4^+$ and $NO_3^-$ in three aerodynamic diameter ranges, 0.32–0.56 $\mu$m, 0.56–1.0 $\mu$m, and 1.0–1.8 $\mu$m, are selected for the present analysis because particles collected on these three impactor stages span the overlapping aerodynamic size range of the ATOFMS instrument and the impactor. Data collected from the chemical analyses of 33 impaction substrates (11 IOPs $\times$ 3 $D_a$ ranges) are used in this work.

Table 3.1: Intensive operating periods at Riverside, California.

| Field Experiment | IOP Code | Date | Time | Temp[a] (°C) | RH[a] (%) | Number of Spectra Acquired 0.32–0.56 | 0.56–1.0 | 1.0–1.8 |
|---|---|---|---|---|---|---|---|---|
| 1996 Trajectory Study | T96-a | 23 Sep 96 | 1500–1900 PDT | 25.1 | 43.1 | 219 | 372 | 889 |
| 1996 Trajectory Study | T96-b | 24 Sep 96 | 1500–1900 PDT | 30.2 | 42.6 | 601 | 1462 | 1275 |
| 1996 Trajectory Study | T96-c | 25 Sep 96 | 1500–1900 PDT | 27.4 | 48.4 | 504 | 1547 | 1130 |
| 1996 Trajectory Study | T96-d | 26 Sep 96 | 1500–1900 PDT | 27.6 | 68.6 | 644 | 1643 | 843 |
| SCOS97[b] First Vehicle Experiment | V1-a | 21 Aug 97 | 1400–1800 PDT | 34.2 | 27.6 | 472 | 679 | 650 |
| SCOS97 First Vehicle Experiment | V1-b | 22 Aug 97 | 1400–1800 PDT | 35.0 | 27.5 | 574 | 675 | 571 |
| SCOS97 Second Vehicle Experiment | V2-a | 27 Aug 97 | 1400–1800 PDT | 32.3 | 28.5 | 125 | 74 | 678 |
| SCOS97 Second Vehicle Experiment | V2-b | 28 Aug 97 | 0600–1000 PDT | 22.9 | 57.1 | 311 | 273 | 747 |
| SCOS97 Second Vehicle Experiment | V2-c | 28 Aug 97 | 1355–1800 PDT | 30.9 | 33.7 | 351 | 322 | 649 |
| SCOS97 Third Nitrate Experiment | N3-a | 31 Oct 97 | 0955–1353 PST | 28.1 | 21.2 | 263 | 1009 | 1499 |
| SCOS97 Third Nitrate Experiment | N3-b | 31 Oct 97 | 1450–1810 PST | 26.5 | 29.9 | 291 | 1253 | 1907 |

[a] Average met conditions during IOP

[b] 1997 Southern California Ozone Study

The masses of $NH_4^+$ measured on three of the impaction substrates was found to be less than that measured on "blank" substrates which were unexposed to ambient aerosols, due to a combination of analytical error and low atmospheric $NH_4^+$ concentrations, yielding "negative" impactor measurements after blank subtraction. In ATOFMS measurements, ion signal intensities are nonnegative by definition, and there is no data analysis procedure analogous to blank subtraction. To avoid introducing a positive bias in the ATOFMS-impactor comparisons, $NH_4^+$ measurements from the 3 affected impactor samples are excluded from the present analysis. These samples contained (1) 1.0–1.8 $\mu$m particles collected at 1400–1800 PDT on August 22, 1997, (2) 0.56–1.0 $\mu$m particles collected at 1400–1800 PDT on August 27, 1997, and (3) 1.0–1.8 $\mu$m particles collected at 1400–1800 PDT on August 27, 1997. In total, 30 impactor measurements of $NH_4^+$and 33 impactor measurements of $NO_3^-$ are compared with the corresponding ATOFMS data.

### 3.3.2 ATOFMS Data Treatment

Before ATOFMS and impactor measurements can be compared with each other, the measurements which best represent ATOFMS instrument responses to $NH_4^+$ and $NO_3^-$ must be selected, and the ATOFMS data must be corrected for certain sampling biases.

#### 3.3.2.1 ATOFMS Response Functions

To compare ATOFMS data with quantitative measurements of $NH_4^+$ and $NO_3^-$, a measure of the ATOFMS instrument's response to $NH_4^+$ and $NO_3^-$ must be precisely defined. Ion signals indicating the presence of $NH_4^+$ in an individual particle are detected most often at mass-to-charge (m/z) ratio 18, when sampling Riverside aerosols by ATOFMS [46]. The ion signal at m/z 30 ($NO^+$) is an established measure of aerosol nitrate at Riverside [90]. Ion signals at other m/z ratios (e.g., m/z 35 ($NH_4NH_3^+$), m/z 46 ($NO_2^+$), and m/z 108 ($Na_2NO_3^+$)) also indicate the presence of $NH_4^+$ and $NO_3^-$ in atmospheric particles [90]. As a first approximation, only the ion signals at m/z 18

and 30 are considered because they are the most common and pronounced indicators of $NH_4^+$ and $NO_3^-$ in positive ion ATOFMS measurements of Riverside aerosols. The validity of this approximation is discussed in Section 3.4.3.4. In ATOFMS positive ion spectra, the presence of particulate $H_2O$ is typically indicated by a peak at m/z 19 ($H_3O^+$) [46], and therefore does not augment the $NH_4^+$ signal at m/z 18.

Ion signals at m/z 18 and 30 are also detected when the ablation/ionization laser fragments certain nitrogen-containing organic compounds [96, 117, 118]. However, $NH_4NO_3$ typically comprises the largest fraction of fine particle mass sampled at Riverside [54, 56, 110], so we expect the contributions of fragmented nitrogen-containing organic compounds to the ion signals at m/z 18 and 30 to be negligible relative to the contributions from $NH_4^+$ and $NO_3^-$. The validity of this assumption is discussed in Section 3.4.3.4.

Although there are several possible measures of ion signal intensity, absolute area and relative area are the most appropriate for quantification of mass spectrometry data. In laboratory ATOFMS studies of nominally identical particles, shot-to-shot variations caused the absolute areas of specific ion signals to vary by an average of 59%. During the same studies, relative areas, defined as the absolute area of the ion signal of interest divided by the total area of the mass spectrum, varied by an average of only 16% [87]. This evidence suggests that relative areas should be used for quantification of ATOFMS data. However, when sampling a polydisperse multi-component aerosol, such as that found in an urban atmosphere, relative area measurements can be affected greatly by the presence of additional chemical species in the particle. For example, the relative area of an ion signal at m/z 18 produced from ablation/ionization of a pure $NH_4NO_3$ particle will likely be larger than the relative area at m/z 18 measured from an identical particle that also contains a trace amount of potassium, because potassium is efficiently ionized [87] and will therefore increase the total area of the mass spectrum. Hence, relative area is not a stable measure of ion signal intensity when determining instrument sensitivities by a field-based approach. Instead, absolute area is selected as the measure of ion signal intensity in the present work. For the remainder of this chapter, we define the ATOFMS instrument response

to $NH_4^+$, $Resp_{NH_4^+}$, as the absolute area of the ion signal at m/z 18 ± 0.5 Daltons, and the ATOFMS response to $NO_3^-$, $Resp_{NO_3^-}$, as the absolute area of the ion signal at m/z 30 ± 0.5 Daltons.

#### 3.3.2.2 Dynamic Range Exceedances of the Data Acquisition Board

Ion signal intensities produced by laser ablation/ionization can vary dramatically from shot-to-shot, due to inhomogeneities in the laser beam [101], and due to differing ionization efficiencies among the chemical species of interest [87]. As a result, laser ablation/ionization of a single particle can produce a very large quantity of ions in a narrow m/z interval, occasionally exceeding the dynamic range of the 8-bit data acquisition board that was used to digitize the mass spectra collected at Riverside in 1996 and 1997. While conducting the present analysis, a peculiar feature was observed among a small class of particles that yielded ion signals at $m/z < 3$, which were large enough to exceed the dynamic range of the data acquisition board. Mass spectra of this type have been reported in ATOFMS data from ambient and emission source testing experiments [85, 86], and are believed to result when ATOFMS instruments encounter certain types of dust-containing particles. The peculiar feature observed in mass spectra of this type is a substantially elevated noise level in the $0 < m/z < 60$ Dalton range. The elevated noise levels at m/z 18 and 30 make it impossible to estimate the quantities of $NH_4^+$ and $NO_3^-$ that were initially present in these particles. Therefore, $Resp_{NH_4^+}$ and $Resp_{NO_3^-}$ from particles of this type are assumed to be zero in the present analysis. Only 3.3% of the single-particle spectra analyzed in the present work (802 out of 24502) are affected by this assumption. The affected spectra are believed to result from ablation/ionization of resuspended dust particles, which are hydrophobic and hence unlikely to accumulate significant amounts of $NH_4^+$ and $NO_3^-$. Therefore, disregarding the ion signals at m/z 18 and 30 in this small class of spectra should not have a significant effect on results of the present study. However, when attempting to determine ATOFMS instrument sensitivities to chemical species that are known to be abundant in dust aerosols (e.g., Si, Fe, Al), it may be necessary to estimate and subtract the mass spectrometer noise level from the total mass spectrum

generated by ablation/ionization of each particle in this specific class.

When an ion signal exceeds the dynamic range of the 8-bit data acquisition board, the signal height reaches a maximum recordable value of $2^8$ arbitrary units while the width continues to increase nonlinearly. This hinders our ability to reliably measure the areas of very large ion signals. Fortunately, dynamic range exceedances at m/z 18 and 30 were relatively infrequent among the single-particle spectra analyzed in the present work. Ion signals at m/z 18 and 30 exceeded the dynamic range in only 763 (3.2%) and 668 (2.8%) of the 23700 spectra, respectively, that were unaffected by the elevated noise levels described above ($24502 - 802 = 23700$). At these low levels, dynamic range limitations of the data acquisition board should not have a significant effect on the results of the present study.

#### 3.3.2.3 Corrections for Particle Detection Efficiency

Allen et al. determined that ATOFMS instruments undercount particles by a factor, $\phi$, that follows a power law dependence on aerodynamic particle diameter [82],

$$\phi = \alpha \, \mathrm{D}_a{}^{\beta} \tag{3.1}$$

where parameters $\alpha$ and $\beta$ are determined by nonlinear regression of impactor mass concentrations on the number of particles detected by ATOFMS [82]. In the present work, the procedure of Allen et al. is modified slightly such that the nonlinear regression parameters, $\alpha$ and $\beta$, are determined from the ATOFMS single-particle measurements of $\mathrm{D_a}$, rather than assuming an average diameter for all particles within each narrow size interval.

In the procedure described by Allen et al., each impactor size interval is subdivided into 10 narrower size intervals, $j$. Individual particle spectra acquired by ATOFMS are aggregated into these narrow size intervals based upon their measured aerodynamic diameters. Once aggregated, all particles within a given size interval are assumed to be of identical aerodynamic diameter, $\overline{\mathrm{D}_{a,j}}$, calculated as the logarithmic mean of the upper and lower limits of size interval $j$. The physical diameter of particles

in each size interval, $\overline{\mathrm{D}_{p,j}}$, is calculated by assuming all particles in size interval $j$ are spherical with density, $\rho_p = 1.3$ g cm$^{-3}$, and aerodynamic diameter, $\mathrm{D_a} = \overline{\mathrm{D}_{a,j}}$. Aggregated ATOFMS data collected during each intensive operating period (IOP) are then compared with impactor measurements collected over the corresponding time period and size interval, using the following model:

$$m_i = \sum_{j \subset i} \frac{N_j \, \alpha \, \overline{\mathrm{D}_{a,j}}^{\beta} \, \frac{\pi}{6} \rho_p \overline{\mathrm{D}_{p,j}}^3}{\mathrm{V}_i} + \epsilon_i \tag{3.2}$$

where subscript $i$ represents the particle ensemble within a specified aerodynamic diameter interval, sampled during a given IOP. In Equation 3.2, $m_i$ is the impactor mass concentration measurement of particle ensemble $i$, $N_j$ is the number of particle spectra recorded by ATOFMS in size interval $j$, $\mathrm{V}_i$ is defined in Equation 3.4 below, and the parameters $\alpha$ and $\beta$ are determined by minimizing the sum of squared residual aerosol mass concentrations, $\sum_i {\epsilon_i}^2$, by nonlinear regression. For brevity, the procedure outlined above uses slightly different notation than that used by Allen et al. [82].

In the present work, the procedure of Allen et al. [82] is modified slightly to eliminate the aggregation of ATOFMS data into narrow size intervals. The modified regression model is

$$m_i = \sum_{j \subset i} \frac{\alpha \, {\mathrm{D}_{a,j}}^{\beta} \, \frac{\pi}{6} \rho_p {\mathrm{D}_{p,j}}^3}{\mathrm{V}_i} + \epsilon_i \tag{3.3}$$

where the subscript $j$ now represents an individual particle spectrum acquired by ATOFMS, rather than an aggregation of particle spectra in a narrow size interval. In Equation 3.3, $\mathrm{D}_{a,j}$ is the single-particle aerodynamic diameter measured by ATOFMS, rather than an assumed mean aerodynamic diameter, and $\mathrm{D}_{p,j}$ is calculated from $\mathrm{D}_{a,j}$ for each individual particle. As in the procedure of Allen et al. [82], all particles are assumed to be spherical with $\rho_p = 1.3$ g cm$^{-3}$.

In Equations 3.2 and 3.3, $\mathrm{V}_i$ refers to the volume of air sampled by ATOFMS (m$^3$) during the IOP when particle ensemble $i$ was sampled. These sample volumes

are calculated as

$$V_i = Q_{\text{ATOFMS}} \times (t_{\text{IOP},i} - t_{\text{off},i} - t_{\text{busy},i}) \tag{3.4}$$

where $Q_{\text{ATOFMS}}$ is the volumetric flow rate of ambient air through the ATOFMS instrument ($20 \times 10^{-6}$ $m^3$ $s^{-1}$) [46, 48], $t_{\text{IOP},i}$ is the duration of the IOP (s) when particle ensemble $i$ was sampled, $t_{\text{off},i}$ is the amount of time (s) that the ATOFMS instrument was off-line during the IOP, and $t_{\text{busy},i}$ is the amount of time (s) the ATOFMS electronic data acquisition system was busy recording particle data [82].

To calculate $t_{\text{off},i}$, ATOFMS data collected during the given IOP are searched for gaps of two minutes or longer when no particle data were recorded. These data gaps are presumed to be periods when the ATOFMS instrument was off-line. The sum of all such data gaps within the IOP when particle ensemble $i$ was sampled, is designated $t_{\text{off},i}$.

The amount of time during each IOP that the ATOFMS electronic data acquisition system was busy recording particle data is calculated by

$$t_{\text{busy},i} = A_1 \times \text{Sized}_i + A_2 \times \text{Hit}_i + A_3 \times (\text{AvgHitPos}_i \times \text{Hit}_i) \tag{3.5}$$

where $\text{Sized}_i$ is the number of $D_a$ measurements that the ATOFMS instrument recorded during the IOP when particle ensemble $i$ was sampled, $\text{Hit}_i$ is the number of particle spectra that the ATOFMS instrument recorded, and $\text{AvgHitPos}_i$ is the average folder position each particle spectrum was stored in. $A_1$ is the time required to record a particle velocity measurement by the data acquisition system, $A_2$ is the time required to record a particle velocity and spectrum, and $A_3$ is the amount of additional time required to record each spectrum depending on the number of spectra that are already stored in the given folder. The parameters $A_1$, $A_2$, and $A_3$, were measured as 130 ms, 504 ms, and 0.167 ms, respectively, for the data acquisition system used at Riverside in 1996, and 100 ms, 450 ms, and 0.244 ms, for the system used at Riverside in 1997.

ATOFMS particle detection efficiencies varied gradually from one field experiment to the next, as a result of a routine instrument cleaning procedure that inadvertently modified the inlet nozzle dimensions. To account for the inlet modifications, best-fit

values of the nonlinear regression parameters in Equation 3.1 are calculated separately for each field study (see Table 3.2). Note that the first two field studies in 1997 (V1 and V2) were spaced one week apart from each other, whereas the second and third studies (V2 and N3) were conducted three months apart (see Table 3.1). During the interim periods, the instrument inlet was routinely cleaned. The larger change in parameter values between V2 and N3, relative to the modest change between V1 and V2 (see Table 3.2), reflects the cumulative effect of the inlet cleaning procedure on ATOFMS transmission efficiencies over the three month interim period. The slight differences between the 1996 parameter values shown in Table 3.2 and those reported previously [82, Table 2], result from the regression model revision described above. Using the parameter values listed in Table 3.2, each single-particle mass spectrum obtained by ATOFMS is duplicated by a dimensionless factor, $\phi$ (see Equation 3.1), which accounts for the degree to which particles of a given size were undercounted by ATOFMS during the given experiment. Allen et al. demonstrated that ATOFMS particle detection efficiencies during the 1996 Los Angeles Basin Trajectory Study were not significantly affected by chemical composition, when averaged over the size-segregated ambient aerosol [82]. By a similar analysis, no clear evidence could be found to indicate that chemical composition affected ATOFMS particle detection efficiencies during the 1997 field experiments. Therefore in the present work, ATOFMS data corrected for particle detection efficiencies are assumed to have the same chemical composition as the particle spectra from which they were duplicated.

### 3.3.3 ATOFMS-Impactor Data Comparison

Having corrected the ATOFMS measurements for detection biases, a quantitative comparison of the ATOFMS and impactor data can be made. The purpose of this comparison is to determine ATOFMS instrument sensitivities to $NH_4^+$ and $NO_3^-$ in size-segregated atmospheric particles under the sampling conditions encountered during the IOPs at Riverside. Recall that instrument sensitivity is defined as the ion signal intensity per unit mass of a chemical species, averaged over a particle ensemble.

Table 3.2: Parameter values and 95% confidence intervals fit to the ATOFMS particle detection efficiency function $\Phi = \alpha \, \mathrm{D}_a{}^{\beta}$

| **Field Experiment** | $\alpha$ | $\beta$ | **Number of Samples for Comparison** |
|---|---|---|---|
| T96[a] | 5040 ± 1190[b] | -3.13 ± 0.64[b] | 12 |
| SCOS97-V1[c] | 1450 ± 434 | -3.90 ± 0.52 | 6 |
| SCOS97-V2[d] | 2050 ± 624 | -4.46 ± 0.46 | 9 |
| SCOS97-N3[e] | 5130 ± 2140 | -4.68 ± 1.04 | 6 |

[a]1996 Los Angeles Basin Trajectory Study
[b]In reference [82, Table 2], $\alpha = 4999 \pm 998$ and $\beta = -3.236 \pm 0.520$
[c]1997 Southern California Ozone Study - First Vehicle Experiment
[d]1997 Southern California Ozone Study - Second Vehicle Experiment
[e]1997 Southern California Ozone Study - Third Nitrate Experiment

In the present study, we compare large ensembles of single-particle ATOFMS data with collocated impactor measurements of $NH_4^+$ and $NO_3^-$. The ATOFMS spectra recorded during each IOP are segregated into three aerodynamic diameter intervals: 0.32–0.56 $\mu$m, 0.56–1.0 $\mu$m, and 1.0–1.8 $\mu$m. This size-segregation yields 33 ensembles of ATOFMS spectra (11 IOPs $\times$ 3 $\mathrm{D_a}$ ranges) which can be compared with corresponding impactor measurements, using a regression model of the form

$$m_{ik} = \frac{\sum_{j \subset i} \phi_j \, \mathrm{Resp}_{jk} \, \psi_{jk}}{\mathrm{V}_i} + \epsilon_{ik} \tag{3.6}$$

In Equation 3.6, the subscript $i$ represents the particle ensemble within a specified aerodynamic diameter interval, sampled during a given IOP. The subscript $j$ represents an ATOFMS single-particle measurement, and $k$ represents the chemical species of interest. The mass concentration of species $k$ ($\mu$g m$^{-3}$), from the impactor measurement of ensemble $i$, is designated as $m_{ik}$. The dimensionless factor $\phi_j$, is used to correct for the undercounting of particles by ATOFMS. For each particle $j$ detected by ATOFMS, $\phi_j$ is calculated from the corresponding ATOFMS measurement of aerodynamic diameter, $\mathrm{D}_{a,j}$, using Equation 3.1. The ATOFMS instrument response (ion signal area units) to species $k$ in particle spectrum $j$, defined earlier, is designated as

$\mathrm{Resp}_{jk}$. The variable $\psi_{jk}$ represents the reciprocal of the ATOFMS instrument sensitivity ($\mu$g/ion signal area) to species $k$ in particle $j$. The volume of air ($\mathrm{m}^3$) sampled by ATOFMS, during the IOP when particle ensemble $i$ was analyzed, is designated $\mathrm{V}_i$ and defined in Equation 3.4. The residual mass concentration ($\mu\mathrm{g\ m}^{-3}$) of species $k$ in ensemble $i$, unexplained by the regression model, is denoted as $\epsilon_{ik}$. In the following section, we seek a physically meaningful parameterization of $\psi_{jk}$ that minimizes the sum of squared residuals, $\sum_i {\epsilon_{ik}}^2$, in Equation 3.6. All calculations are performed using the Matlab statistics package (The MathWorks, Natick, MA), and facilitated by the YAADA data analysis system [84].

## 3.4 Results

Figure 3.1 illustrates a first-order comparison of the ATOFMS and impactor measurements of $\mathrm{NH}_4^+$ and $\mathrm{NO}_3^-$. The vertical coordinates of each data point represent ATOFMS measurements, $\frac{\sum_{j \subset i} \phi_j \mathrm{Resp}_{jk}}{\mathrm{V}_i}$, after correcting for particle detection efficiencies. The horizontal coordinates of each data point represent the impactor measurement, $m_{ik}$, with horizontal error bars spanning $\pm$ 2 standard deviations, as determined from the repeated analysis of a fraction of the impactor samples and from consistency in the repeated analyses of a set of standards. It is important to emphasize that the horizontal coordinates of each data point represent the ATOFMS measurements of a size-segregated ensemble of individual particles sampled during the indicated IOP. The number of single-particle measurements represented by each data point is listed in Table 3.1. Data points are plotted with different symbols and shading patterns, to represent data collected during different IOPs and in different particle size intervals, respectively.

Without any prior knowledge of the numerous factors that can affect ATOFMS instrument sensitivities, one might hypothesize that ion signal intensities are linearly correlated with the mass of a chemical species of interest (i.e., $\psi_{jk}$ = constant). If this were the case, all of the data points in Figures 3.1a and 3.1b would lie along a straight line ($R^2 = 1.0$). Instead, the data points appear to be clustered along

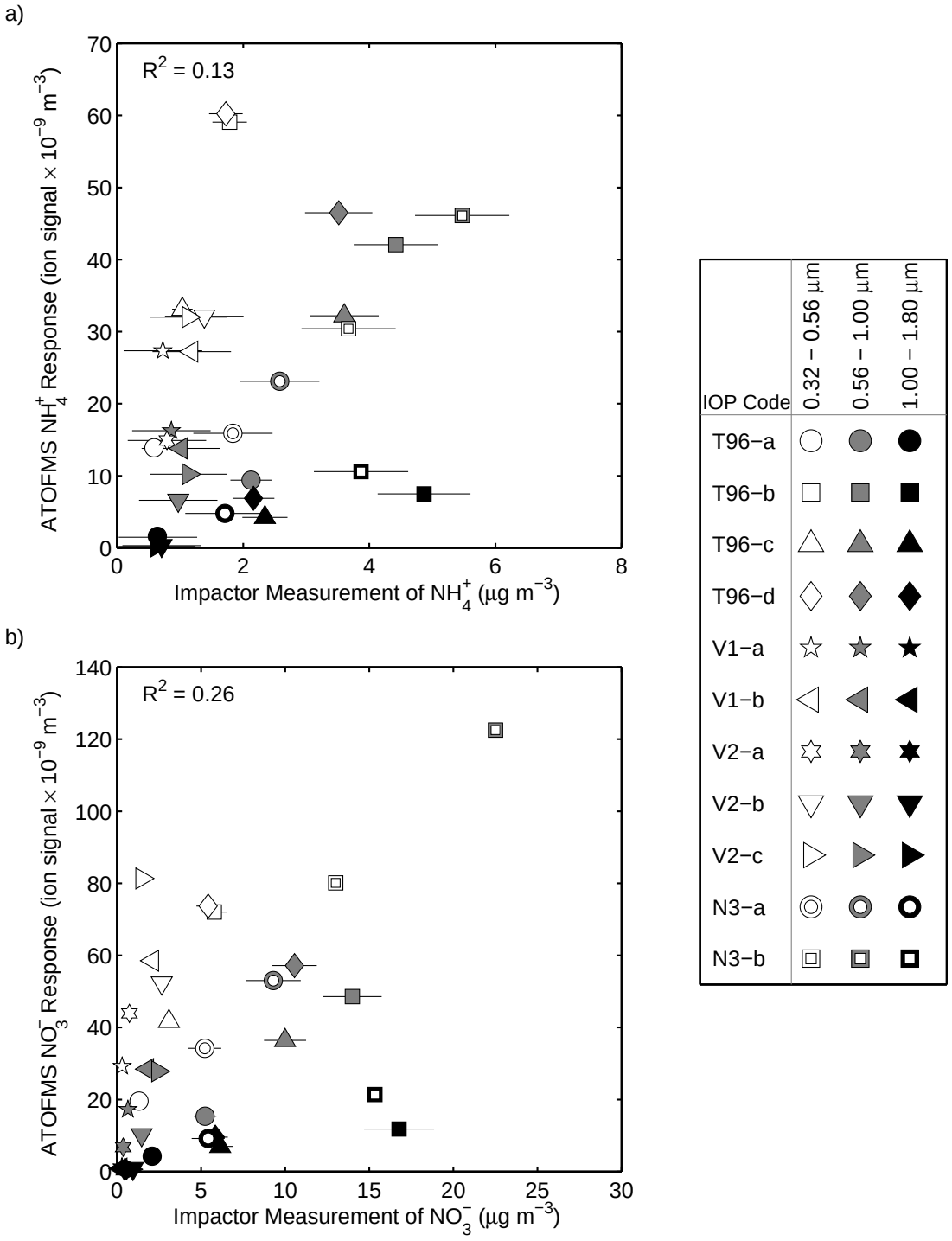


Figure 3.1: First-order comparison of impactor measurements with corresponding ATOFMS measurements, duplicated to correct for particle detection efficiencies. Horizontal error bars indicate ± 2 standard deviations in the impactor measurements. In cases where ± 2 SD is small relative to the horizontal axis scale, the error bars may be covered entirely by the plotting symbol, and therefore, not visible. IOP codes are defined in Table 3.1.

separate lines as a function of particle size range, indicating that $\psi_{jk}$ is strongly influenced by the size of the particle sampled. The ratio of a data point's vertical coordinate to its horizontal coordinate is generally largest for particle ensembles in the 1.0–1.8 $\mu$m $D_a$ range, and smallest for ensembles in the 0.32–0.56 $\mu$m range, for both $NH_4^+$ and $NO_3^-$ (see Figure 3.1). This suggests that the ion signal intensity produced by laser ablation/ionization of a unit mass of either species ($NH_4^+$ or $NO_3^-$) decreases as particle aerodynamic diameter increases over the 0.32–1.8 $\mu$m range. In other words, ATOFMS instruments are more sensitive to $NH_4^+$ and $NO_3^-$ when sampling particles of smaller size. The increased instrument sensitivity to chemical species in smaller particles is presumed to be due to (1) a greater volume fraction of small particles being vaporized by the ablation/ionization laser relative to larger particles, and (2) a lower probability of positive-negative charge recombination in the ablation plume of small particles relative to larger ones [105]. Similar trends have been reported in single-particle mass spectrometry analyses of pure, laboratory-generated $RbNO_3$, $(NH_4)_2SO_4$, NaCl, and KCl particles [103, 105, 119], but this is the first such observation in atmospheric aerosol measurements.

### 3.4.1 Size-Dependent Parameterization of Instrument Sensitivity

Further analyses of the trends in Figure 3.1 indicate that instrument sensitivity can be parameterized by a power law relationship in aerodynamic diameter,

$$\psi_{jk} = \gamma_k \, {D_{a,j}}^{\delta_k} \tag{3.7}$$

where $\psi_{jk}$ represents the inverse ATOFMS sensitivity ($\mu$g/ion signal area) to species $k$ in particle $j$, $D_{a,j}$ is the single-particle aerodynamic diameter ($\mu$m) measured by ATOFMS, and $\gamma_k$ and $\delta_k$ are nonlinear regression parameters, specific to chemical species $k$ but independent of particle size, that can be determined using the regression model in Equation 3.6. No major changes were made to the instrument's

ablation/ionization configuration between the IOPs, so $\gamma_k$ and $\delta_k$ are assumed to be constant across all four field experiments. Pooling data from all four experiments permits an evaluation of the stability of instrument sensitivities to $NH_4^+$ and $NO_3^-$ during eleven IOPs spaced over a 1-year time period.

The power law form of Equation 3.7 can be related to the physical and chemical factors that influence ATOFMS instrument sensitivities to $NH_4^+$ and $NO_3^-$ under ambient sampling conditions. In Equation 3.7, $\gamma_k$ can be treated as a surrogate measure of the ionization efficiency of chemical species $k$. In general, chemical species which are efficiently ionized should have a smaller $\gamma$ value than species which are more difficult to ionize. Therefore, best-fit values of $\gamma_{NH_4^+}$ and $\gamma_{NO_3^-}$ are expected to be different.

In Equation 3.7, $\delta_k$ can be considered a surrogate measure of the volumetric fraction of an individual particle that is vaporized by the ablation/ionization laser, assuming that the increased probability of positive-negative charge recombination in the ablation plume of small particles has only a secondary effect. If $\delta_k \simeq 0$, instrument sensitivity is independent of particle size, implying that the ATOFMS ablation/ionization laser vaporizes either the entire particle volume or a constant volumetric fraction of each particle in the 0.32–1.8 $\mu$m $D_a$ range. If $\delta_k \simeq 3$, the instrument sensitivity is proportional to particle volume, implying that the laser vaporizes a constant volume of each particle in the 0.32–1.8 $\mu$m range. A result of $0 < \delta_k < 3$ might suggest that small particles are completely vaporized while particles at the upper end of the 0.32–1.8 $\mu$m $D_a$ range are only partially vaporized. Laboratory studies of ATOFMS instrument behavior indicate that laser irradiances similar to those used during the IOPs vaporize the entire volume of submicron particles, but only partially vaporize particles that are larger than approximately 1.0 $\mu$m $D_a$ [120]. Hence, we expect best-fit values of $\delta_{NH_4^+}$ and $\delta_{NO_3^-}$ to fall in the intermediate range ($0 < \delta_k < 3$).

When a particle is partially vaporized by the ablation/ionization laser, the ATOFMS instrument is more likely to detect material near the particle surface than material in the particle core [121]. $NH_4^+$ and $NO_3^-$ are believed to have similar spatial distributions within the individual particle matrices studied here, because the origin

of these two species in Riverside aerosols is largely attributed to the condensation of gas-phase ammonia and nitric acid molecules on the surface of pre-existing particles [55]. Therefore in the present work, it is reasonable to assume that neither $NH_4^+$ nor $NO_3^-$ will be preferentially vaporized in the event of partial vaporization. For this reason, the best-fit values of $\delta_{NH_4^+}$ and $\delta_{NO_3^-}$ deduced in the present work are expected to be similar.

Table 3.3 shows the best-fit values of $\gamma_k$ and $\delta_k$, along with 95% confidence intervals for each, as calculated by nonlinear regression using Equations 3.6 and 3.7. Note that the best-fit values of $\delta_{NH_4^+}$ and $\delta_{NO_3^-}$ are identical within two significant figures (2.4 $\pm$ 0.4), even though they were calculated independently using two different sets of measurements. Moreover, both $\delta$ values are in the 0–3 range, as expected from the above discussion. These two observations support the physical explanation of the particle size-dependent instrument sensitivity parameterization (Equation 3.7), and imply that $NH_4^+$ and $NO_3^-$ do indeed have similar spatial distributions within the matrices of the larger particles studied here.

Table 3.3: Parameter values and 95% confidence intervals fit to the ATOFMS instrument sensitivity function $\Psi = \gamma \, D_a{}^{\delta}$.

| **Species** | $\gamma$ | $\delta$ | **Number of Samples for Comparison** |
|---|---|---|---|
| $NH_4^+$ | $2.5 \times 10^{-10} \pm 0.4 \times 10^{-10}$ | $2.4 \pm 0.4$ | 30 |
| $NO_3^-$ | $4.7 \times 10^{-10} \pm 0.7 \times 10^{-10}$ | $2.4 \pm 0.4$ | 33 |

Best-fit values of $\gamma_{NH_4^+}$ and $\gamma_{NO_3^-}$ are statistically different from one another with 95% confidence (see Table 3.3), as we had expected from the discussion above. The ratio of these two values can be used to determine the relative sensitivity of ATOFMS instruments to $NH_4^+$ versus $NO_3^-$, as follows

$$\mathrm{RSF}\left(\frac{NH_4{}^+}{NO_3{}^-}\right) = \frac{18}{62} \cdot \frac{\gamma_{NO_3^-}}{\gamma_{NH_4^+}} \tag{3.8}$$

where 18 and 62 are the molar masses of $NH_4^+$ and $NO_3^-$, respectively. Relative sen-

sitivity factors (RSFs) are typically defined on a molar basis, and are often used to correct for differences between the instrument sensitivities to two chemical species of interest, when analyzing the composition of a multi-component sample [87, 122]. Prior to this study, all ATOFMS RSFs have been deduced from laboratory-generated aerosols [87, 96], and their applicability to ambient aerosol data has not been tested. Using Equation 3.8 and the best-fit $\gamma_k$ values listed in Table 3.3, the RSF of $NH_4^+$ versus $NO_3^-$ under the Riverside IOP sampling conditions is 0.5, and lies in the 0.4–0.7 range with 95% confidence. This implies that ATOFMS measurements of particles containing equimolar concentrations of $NH_4^+$ and $NO_3^-$, should yield larger ion signals at m/z 30 than at m/z 18, by a factor of approximately two. The RSF derived above should be verified in laboratory experiments so that ultimately, it may be used to determine the relative abundances of $NH_4^+$ and $NO_3^-$ in individual atmospheric particles.

### 3.4.2 Scaled ATOFMS Measurements of $NH_4^+$ and $NO_3^-$

Using raw ATOFMS data and the best-fit parameter values listed in Tables 3.2 and 3.3, we can reconstruct quantitative measurements of $NH_4^+$ and $NO_3^-$, $\hat{m_{ik}}$, in size-segregated atmospheric particle ensembles.

$$\hat{m_{ik}} = \frac{\sum_{j \subset i} \phi_j \, \mathrm{Resp}_{jk} \, \psi_{jk}}{\mathrm{V}_i} \tag{3.9}$$

All terms in Equation 3.9 are defined in Equations 3.6 and 3.7. Scaled ATOFMS measurements are compared with the corresponding impactor measurements of atmospheric $NH_4^+$ and $NO_3^-$ concentrations in Figure 3.2. The horizontal coordinate of each data point in Figure 3.2 represents an impactor measurement, $m_{ik}$, with error bars spanning $\pm$ 2 standard deviations. The vertical coordinate of each data point represents a scaled ATOFMS measurement, $\hat{m_{ik}}$, with error bounds calculated by propagating 95% confidence intervals on the best-fit values of $\gamma_k$ and $\delta_k$. Vertical error bars do not account for uncertainties in the ATOFMS particle detection efficiency parameters, $\alpha$ and $\beta$, but those uncertainties are discussed below in detail.

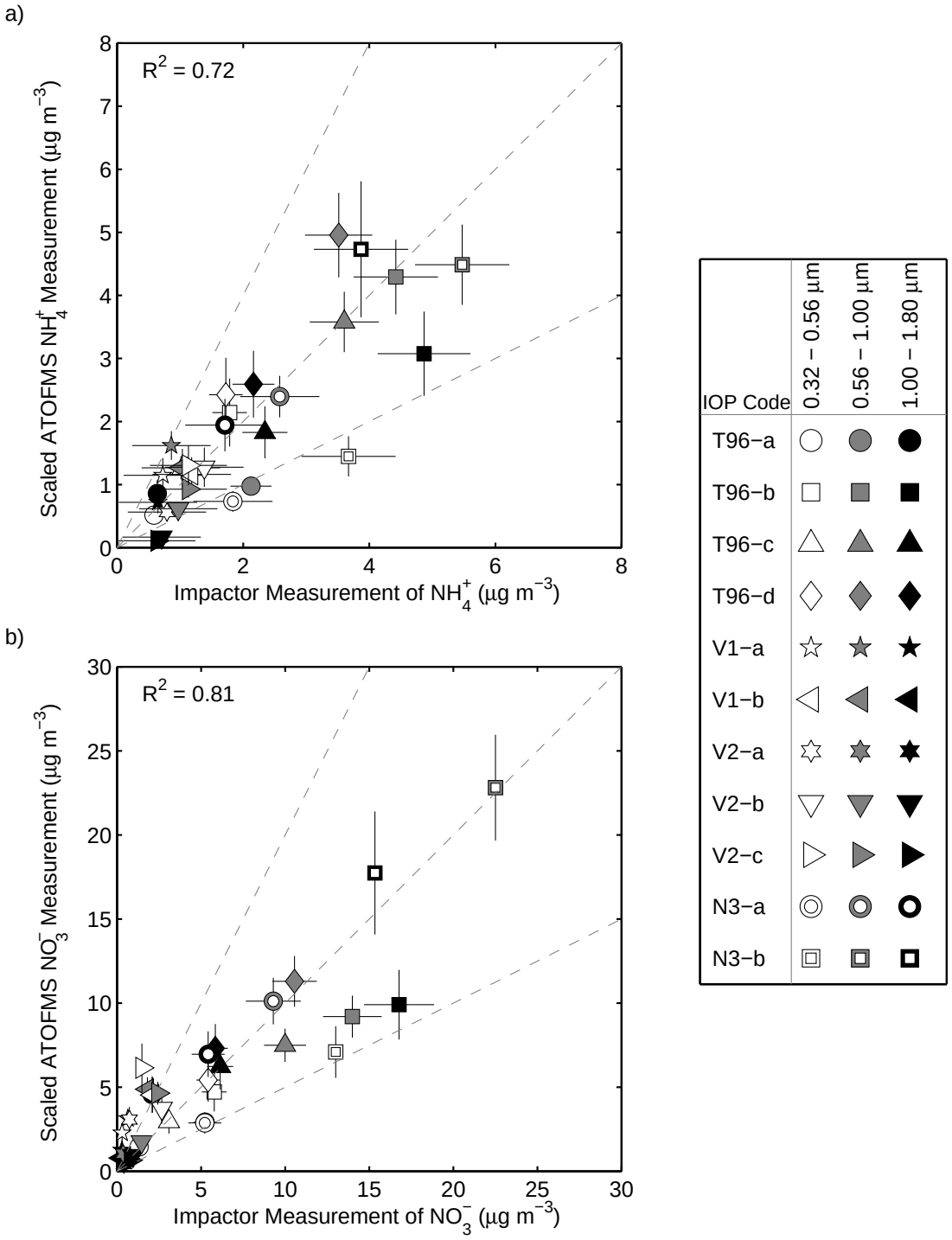


Figure 3.2: Comparison of scaled ATOFMS measurements with the corresponding impactor measurements. Diagonal dashed lines represent the 1:2, 1:1, and 2:1 lines of correspondence. Vertical error bars indicate 95% confidence intervals of the scaled ATOFMS measurements. Horizontal error bars indicate ± 2 standard deviations in the impactor measurements. In cases where an error bar length is small relative to the scale of the coordinate axes, it may be covered entirely by the plotting symbol, and therefore, not visible. IOP codes are defined in Table 3.1.

When evaluating the accuracy of the ATOFMS instrument sensitivity parameterization (Equation 3.7), impactor data are used as the reference because impactors currently provide the most reliable data on size-segregated aerosol composition. However, impactor measurements of $NH_4^+$ and $NO_3^-$ are subject to certain biases. Volatilization of $NH_4NO_3$ from impaction substrates during sampling is favored at high temperatures and low relative humidities [123], and has been shown to result in 7–8% losses of fine particulate nitrate under hot (35 °C) and dry (18% relative humidity) conditions [114]. Volatilization losses can be even greater ($\sim$ 10–20%) when aerosol loadings are low, because the exposed surface area of particle deposits is large relative to the aerosol mass collected on the impaction substrates [124]. The possible effects of $NH_4NO_3$ volatilization on results of the present study are discussed in Section 3.4.3.2. Future applications of the tandem ATOFMS-impactor sampling procedure to less volatile chemical species (e.g., $SO_4^{2-}$) might permit a more accurate determination of ATOFMS instrument sensitivities.

One simple set of criteria for judging whether the ATOFMS scaling functions yield accurate measurements of atmospheric $NH_4^+$ and $NO_3^-$ concentrations is as follows. If a scaled ATOFMS measurement falls within $\pm$ 2 standard deviations of the corresponding impactor measurement, it is judged to be "excellent." If the 95% confidence interval of an ATOFMS measurement overlaps within $\pm$ 2 standard deviations of the corresponding impactor measurement, the ATOFMS measurement is considered to be "good." If neither of the above conditions are met but the scaled ATOFMS measurement falls within a factor of 2 of the impactor measurement, it is judged as "fair." If none of these conditions are met, the ATOFMS measurement is "poor." The advantages of these evaluation criteria are that they account for the analytical error inherent in the impactor data, and the scaled ATOFMS measurements can be evaluated easily by visual inspection of Figure 3.2.

Using these criteria, 16 of the 30 scaled ATOFMS $NH_4^+$ measurements are excellent, 9 are good, 2 are fair, and only 3 are poor (see Figure 3.2a). The large fraction (90%) of "excellent," "good," and "fair" ATOFMS measurements indicate that the particle size-dependent parameterization of instrument sensitivity to $NH_4^+$ is stable

over the range of fine particle concentrations encountered at Riverside ($PM_{1.8}$ = $17.58 \pm 2.02$ – $127.8 \pm 1.76$ $\mu$g m$^{-3}$). All three of the "poor" ATOFMS $NH_4^+$ measurements are smaller than the corresponding impactor measurements, and one of these is largely due to inaccuracies in the ATOFMS particle detection efficiency, as discussed below. Of the 33 scaled ATOFMS $NO_3^-$ measurements, 10 are excellent, 6 are good, 7 are fair, and 10 are poor (see Figure 3.2b). All ten of the "poor" ATOFMS $NO_3^-$ measurements are greater than the corresponding impactor measurement, and in all 10 cases, the impactor $NO_3^-$ measurements are less than 2.1 $\mu$g m$^{-3}$ (see lower-left corner of Figure 3.2b). Moreover, 9 of the 10 poor measurements correspond to data collected during IOPs when the highest ambient temperatures were encountered (T > 30°C), suggesting that the impactor measurements during these periods may have been subject to volatilization losses. This issue will be explored in 3.4.3.2. The "excellent," "good," and "fair" $NO_3^-$ measurements further increase our confidence in the selected parameterization of ATOFMS instrument sensitivity (Equation 3.7). Recall that the data plotted in Figure 3.2 were collected during four field experiments spaced over a year, and the ATOFMS instrument's inlet design was modified between experiments. The lack of observable biases in the scaled ATOFMS measurements, obtained from data collected during different field experiments (compare positions of the experiment-specific plotting symbols relative to the 1:1 line), suggests that the instrument sensitivities to $NH_4^+$ and $NO_3^-$ are unaffected by modifications to the instrument's inlet design.

A second set of criteria for evaluating the ATOFMS scaling functions employs statistical correlations of the impactor measurements with corresponding scaled ATOFMS measurements, irrespective of the error bounds on each. The advantage of using statistical correlations is that they may be used to estimate the relative influence of different parameters on ATOFMS instrument sensitivities. For example, scaled ATOFMS $NH_4^+$ measurements and corresponding impactor measurements exhibit a squared correlation coefficient ($R^2$) of 0.72. This indicates that approximately 72% of the variance in $\psi_{j,NH_4^+}$ is explained by the size-dependent instrument sensitivity parameterization shown in Equation 3.7. By an analogous calculation, 81% of the

variance in $\psi_{j,NO_3^-}$ is explained by the size-dependent sensitivity parameterization. These high correlation coefficients indicate that the most influential factor governing ATOFMS instrument sensitivities to $NH_4^+$ and $NO_3^-$ is particle aerodynamic diameter, under the sampling conditions encountered at Riverside. Note that the $R^2$ values of 0.72 and 0.81 are significantly higher than those calculated under the assumption that instrument sensitivity is independent of particle size ($R^2 = 0.13$ in Figure 3.1a and $R^2 = 0.26$ in Figure 3.1b).

Attaining perfect correlations ($R^2 = 1.00$) is infeasible due to analytical error inherent in the impactor measurements, but it may be possible to reduce the sum of squared residuals further (i.e., increase $R^2$) by identifying measurable factors other than particle size which significantly influence ATOFMS instrument sensitivities. In the following section, we assess the relative influence of other factors on ATOFMS instrument sensitivities to $NH_4^+$ and $NO_3^-$, under the Riverside ambient sampling conditions.

### 3.4.3 Residual Analysis

Aside from particle size, the measurable factors which might also affect instrument sensitivities include (1) accuracy of the ATOFMS particle detection efficiency corrections; (2) properties of the background gas; (3) size-segregated aerosol chemical composition, as determined from chemical analyses of the impactor samples; and (4) single-particle chemical composition, as determined from ATOFMS ion signals measured at m/z ratios other than 18 and 30. To identify which of these factors significantly influenced ATOFMS sensitivities to $NH_4^+$ and $NO_3^-$ during the IOPs, we examine the $R^2$ values of each factor with the residual concentrations, denoted as $\epsilon_{ik}$ in Equation 3.6. For brevity, we discuss only those factors which show "strong evidence" of an influence on ATOFMS instrument sensitivities. In the present work, strong evidence requires that $R^2$ values exceed a critical value, defined as follows.

$$R^2 > \frac{(t_{df,x})^2}{df + (t_{df,x})^2} \tag{3.10}$$

where $R^2$ is the correlation coefficient squared and $t_{df,x}$ is the critical value associated with Student's $t$-distribution at a confidence level of $1 - 2x$, given $df$ degrees of freedom [125]. In the present work, we seek $R^2$ values which are greater than zero with 95% confidence (i.e., $x = 0.025$ in Equation 3.10). The number of degrees of freedom is defined as two less than the number of data points used to calculate $R^2$. The critical $R^2$ values required to satisfy Equation 3.10 with 95% confidence decrease as the number of data points increases.

In some cases, an $R^2$ value satisfies Equation 3.10 with 95% confidence, but removal of a single data point renders the $R^2$ value statistically insignificant at the 95% confidence level. This indicates that the apparent correlation is largely due to the presence of only one data point, and is not sufficient evidence that the correlation is physically meaningful. Therefore, $R^2$ values in this regime are not discussed in this section.

#### 3.4.3.1 Influence of Particle Detection Efficiency Corrections

As stated earlier, one of the three main limitations of a field-based approach is that it requires an accurate characterization of the ATOFMS instrument's particle detection efficiency. In other words, each single-particle spectrum $j$ must be duplicated by a precise particle detection efficiency factor, $\phi_j$, in order to reconstruct accurate $NH_4^+$ and $NO_3^-$ measurements from raw ATOFMS data (see Equation 3.9). For a variety of reasons, it is not yet possible to determine precise values of $\phi_j$ under ambient sampling conditions [82, 108]. Instead, particle detection efficiencies are approximated as a function of $D_a$ (see Equation 3.1), and these approximations are somewhat uncertain.

To assess the influence of particle detection efficiency uncertainties on the scaled $NH_4^+$ and $NO_3^-$ measurements, we define a residual aerosol mass concentration ($\mu$g m$^{-3}$), $\epsilon_i$, as

$$\epsilon_i = m_i - \sum_{j \subset i} \frac{\phi_j}{V_i} \rho_p \frac{\pi}{6} {D_{p,j}}^3 \tag{3.11}$$

where $m_i$ is the mass concentration ($\mu$g m$^{-3}$) of particle ensemble $i$ determined from gravimetric analysis of the impactor samples, and $\rho_p \frac{\pi}{6} {D_{p,j}}^3$ is the estimated mass of

an individual particle detected by ATOFMS, assuming particles are spherical with density, $\rho_p = 1.3$ g cm$^{-3}$, and physical diameter, $D_p$. Note that $m_i$ and $\epsilon_i$ refer to total aerosol mass concentrations, whereas $m_{ik}$ and $\epsilon_{ik}$ are specific to a chemical component (compare Equations 3.6 and 3.11). In short, $\epsilon_i < 0$ indicates that the particle detection efficiency correction factors applied to ATOFMS data collected from ensemble $i$ are too large on average, whereas $\epsilon_i > 0$ indicates the correction factors are too small.

In cases where the particle detection efficiency correction factors applied to ATOFMS data are too large (i.e., $\epsilon_i < 0$), one would expect the scaled ATOFMS measurements of $NH_4^+$ and $NO_3^-$ concentrations to exceed the corresponding impactor measurements ($\hat{m_{ik}} > m_{ik}$), and vice versa. This hypothesis is confirmed by examining the correlation of $NH_4^+$ and $NO_3^-$ residuals with aerosol mass concentration residuals, as illustrated in Figure 3.3. Both subplots show statistically significant positive correlations ($R^2 = 0.35$ for $NH_4^+$ and $R^2 = 0.36$ for $NO_3^-$), indicating that approximately 35% of the variance in $\epsilon_{ik}$ can be explained by a linear relationship with $\epsilon_i$. In other words, approximately one third of the error in the instrument sensitivities to $NH_4^+$ and $NO_3^-$ is attributable to uncertainty in the ATOFMS particle detection efficiencies. This demonstrates a need to precisely characterize ATOFMS particle detection efficiencies, perhaps by comparing ATOFMS data with collocated particle number concentration data, which can be obtained continuously at very fine particle size and temporal resolutions.

#### 3.4.3.2 Influence of Gas-Phase Properties

Neubauer et al. reported that relative humidity of the background gas can exert a strong influence on single-particle mass spectra [107], motivating the present analysis. Although our data set provided no clear evidence that instrument sensitivities to $NH_4^+$ nor $NO_3^-$ are affected by ambient relative humidity over the 21–69 % range, statistically significant negative correlations of $\epsilon_{ik}$ with ambient temperature ($R^2 = 0.14$ for $NH_4^+$ and $R^2 = 0.39$ for $NO_3^-$) indicate that scaled ATOFMS measurements of $NH_4^+$ and $NO_3^-$ tend to exceed the corresponding impactor measurements when

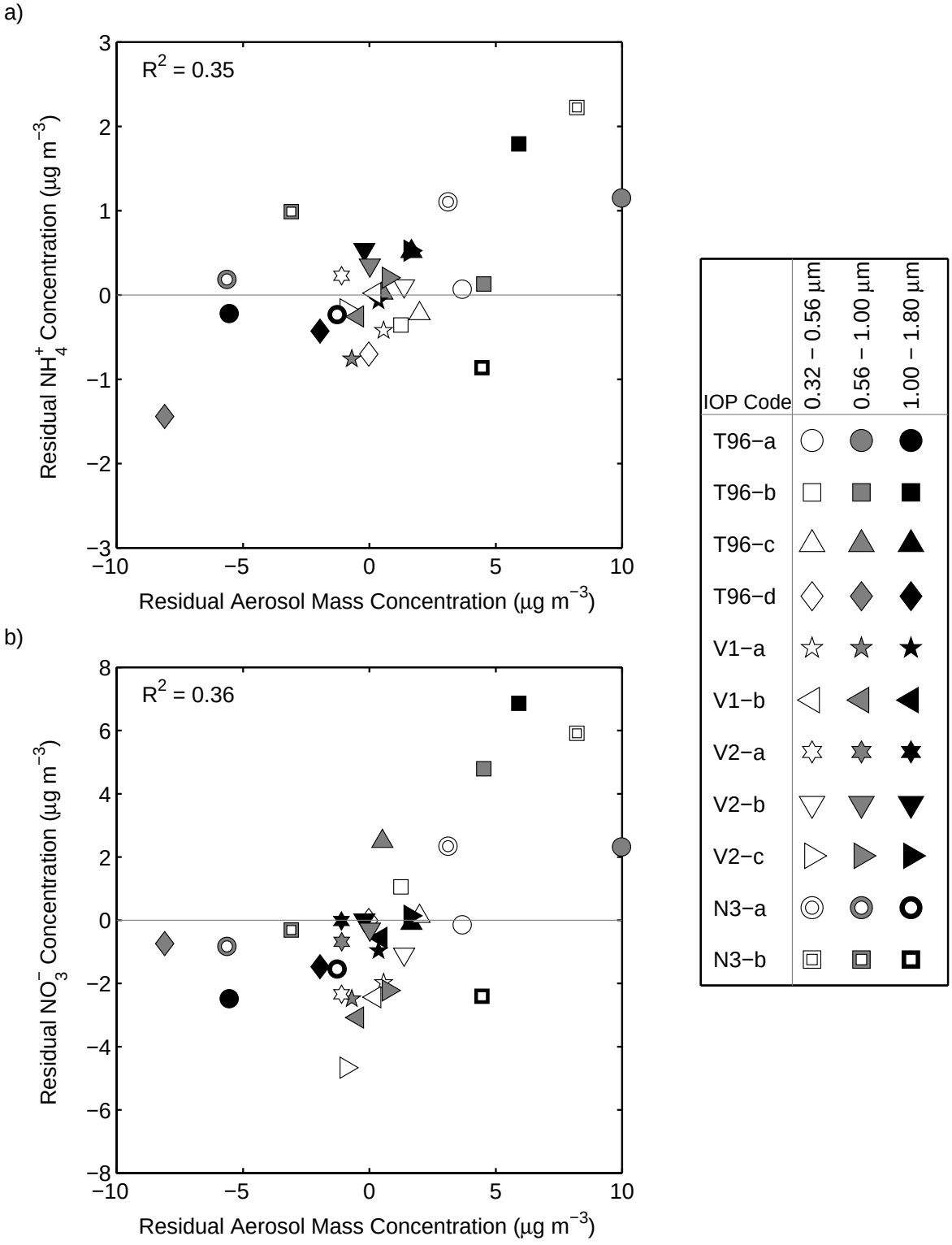


Figure 3.3: Comparison of residual species concentrations, $\epsilon_{ik}$, with residual mass concentrations, $\epsilon_i$. IOP codes are defined in Table 3.1.

sampling at high temperatures. The highest ambient temperatures were encountered during the afternoon IOPs of August 1997 (V1-a, V1-b, V2-a, V2-c). This apparent temperature effect is most likely due to the condensation of gas-phase $NH_3$ and $HNO_3$ upstream of the ATOFMS instrument, which was stationed in an air conditioned laboratory (T $\simeq$ 22–25°C) and drawing ambient air through a $\sim$ 5 m long sampling line at a relatively low flowrate. When the warmest temperatures were encountered (T $\geq$ 30.5°C), high ambient concentrations of gas-phase $NH_3$ ($23.8 \pm 1.6 - 45.4 \pm 1.5$ $\mu$g m$^{-3}$) and $HNO_3$ ($5.6 \pm 0.6 - 9.3 \pm 0.6$ $\mu$g m$^{-3}$) were present [110]. The apparent ATOFMS overestimates during the high-temperature IOPs, which include 90% of the "poor" ATOFMS $NO_3^-$ measurements, might be entirely explained by $NH_4NO_3$ and $HNO_3$ condensation in the ATOFMS sampling line. In addition, volatilization of $NH_4NO_3$ from the impaction substrates during sampling may have decreased the impactor measurements of $NH_4^+$ and $NO_3^-$ during the high-temperature IOPs by 10–20%, as discussed in Section 3.4.2.

Residual correlations indicate that the high-temperature sampling artifacts contribute 39% of the variance in $\epsilon_{i,NO_3^-}$. To assess the effect of high-temperature sampling artifacts on the results of the present study, sensitivity parameters can be recalculated using the 21 data points corresponding to low-temperature IOPs (T $<$ 30.5°C). This recalculation does not affect the $\gamma_{NO_3^-}$ value shown in Table 3.3, but the best-fit $\delta_{NO_3^-}$ value is reduced from $2.4 \pm 0.4$ to $2.2 \pm 0.4$. In contrast with $NO_3^-$, only 14% of the variance in $\epsilon_{i,NH_4^+}$ can be explained by the high-temperature sampling artifacts. The effect on ATOFMS $NH_4^+$ measurements is less pronounced than on $NO_3^-$ measurements because three of the $NH_4^+$ measurements taken during high-temperature IOPs were excluded from the entire analysis, for reasons given above. Recalculation of the $NH_4^+$ regression coefficients using only the 21 low-temperature data points does not change the best-fit values of $\gamma_{NH_4^+}$ and $\delta_{NH_4^+}$ listed in Table 3.3. This suggests that the instrument sensitivity parameterization (Equation 3.7) for $NH_4^+$ is stable over the 23–35 °C temperature range. Average temperatures and relative humidities during each IOP are listed in Table 3.1.

#### 3.4.3.3 Influence of Bulk Aerosol Composition

Laboratory studies of single-particle mass spectrometry instruments reveal that the presence of certain chemical species in a particle can dramatically affect the instrument response to other species present in the same particle [106]. These phenomena, commonly referred to as *matrix effects*, have not yet been assessed under ambient sampling conditions. Extensive bulk aerosol composition data are available from chemical analyses of the impactor samples [54, 56, 85, 110], allowing an assessment of whether chemical composition significantly affects ATOFMS instrument sensitivities to $NH_4^+$ and $NO_3^-$, when averaged over the size-segregated ambient aerosols studied here. Correlation coefficients of $\epsilon_{i,NH_4^+}$ and $\epsilon_{i,NO_3^-}$ with all analyte measurements that are greater than two standard errors above zero in at least half of the impaction substrates (mass, organic carbon, $NH_4^+$, $NO_3^-$, $SO_4^{2-}$, $Na^+$, La, and Sb), were calculated. No evidence of bulk compositional effects on ATOFMS instrument sensitivity to $NH_4^+$ was found. However, impactor measurements of aerosol mass, organic carbon, $NH_4^+$, $NO_3^-$, and $SO_4^{2-}$, all exhibit statistically significant negative correlations with $\epsilon_{i,NO_3^-}$ ($R^2$ = 0.26–0.34). These correlations are largely due to the ATOFMS-impactor measurement discrepancies during high-temperature IOPs. Without the high-temperature data points, none of the impactor measurements are correlated with $\epsilon_{i,NO_3^-}$.

Based on these calculations, one may conclude that aerosol chemical composition had an insignificant influence on the sensitivity of ATOFMS instruments to $NH_4^+$ and $NO_3^-$, when averaged over the size-segregated particle ensembles sampled at Riverside. It is important to note that $NH_4^+$ and $NO_3^-$ comprise a large fraction of the aerosols studied in this work, so the ATOFMS instrument response to $NH_4^+$ and $NO_3^-$ may be less influenced by matrix effects than the instrument response to other species. In addition, the aerosol mixtures during different IOPs may have been too similar to one another to reveal bulk compositional biases in the instrument sensitivities. In the future, it may be possible to elucidate such biases by comparing ATOFMS-impactor data sets collected at two geographic locations with very different aerosol

compositions, or by analyzing an ATOFMS-impactor data set collected at a single location over an extended study period that spans a significant change in bulk aerosol composition (see Section 7.2.2).

#### 3.4.3.4 Influence of Single-Particle Composition

In Equation 3.6, $\text{Resp}_{j,\text{NH}_4^+}$ and $\text{Resp}_{j,\text{NO}_3^-}$ are defined as the ion signals at m/z 18 and 30, respectively. To examine the influence of other ion signals on the scaled ATOFMS $\text{NH}_4^+$ and $\text{NO}_3^-$ measurements, the correlations of $\epsilon_{i,\text{NH}_4^+}$ and $\epsilon_{i,\text{NO}_3^-}$ with all ion signal intensities in the $0 < \text{m/z} < 250$ Dalton range that appear in at least one particle spectrum in each size-segregated sample, are calculated. In this analysis, ion signals are duplicated to account for ATOFMS particle detection efficiencies, and ion signals in the $0 < \text{m/z} < 60$ Dalton range are discarded from single-particle spectra in which an elevated noise level was observed, for reasons described in Section 3.3.2.2.

Ion signals at 27 different m/z ratios exhibit statistically significant negative correlations with $\epsilon_{i,\text{NH}_4^+}$ ($0.14 \leq R^2 \leq 0.23$), indicating that $\text{NH}_4^+$ concentrations are overestimated when ion signals at these m/z ratios are abundant. Negative correlations may imply that (1) some fraction of the ion signals at m/z 18 resulted from aerosol species other than $\text{NH}_4^+$; and (2) the presence of other species in the aerosols increased the ionization efficiency of $\text{NH}_4^+$ (i.e., a matrix effect). Determining the most probable explanation for all 27 observed correlations is beyond the scope of this study. Moreover, many of these correlations are likely to be interrelated.

In laboratory-based ATOFMS studies, Angelino et al. discovered that ion signals at m/z 18 are commonly detected when sampling individual particles that contain organic amines [118]. In ATOFMS data, the most common indicators of organic amines appear at m/z 58 and 86 [118]. Ion signals at m/z 58 and 86 are among the 27 m/z ratios which are significantly correlated with residual $\text{NH}_4^+$ concentrations ($R^2$ = 0.19 and 0.16, respectively). Laboratory experiments are necessary to quantify and subtract the relative contribution of organic amine fragmentation from the total ion signal at m/z 18. If this approach proves to be feasible, it may be possible in the future to determine causes of the observed correlations with other ion signals.

Ion signals at each m/z ratio are uncorrelated with $\epsilon_{i,NO_3^-}$, indicating that ions at m/z ratios other than 30 do not significantly influence scaled ATOFMS $NO_3^-$ measurements in the Riverside aerosols. When sampling larger particle sizes ($D_a > 1.8$ $\mu$m) and/or marine aerosols, a significant fraction of the aerosol nitrate may be present in the form of $NaNO_3$. In these cases, it may be necessary to incorporate the ion signal at m/z 108 ($Na_2NO_3^+$) into the definition of $Resp_{NO_3^-}$.

#### 3.4.3.5 Summary of Residual Analysis

The analyses described in section 3.4.3 indicate the relative influences of various measurable factors on ATOFMS instrument sensitivities to $NH_4^+$ and $NO_3^-$, under the Riverside sampling conditions. Aside from particle aerodynamic diameter, few factors significantly influenced the instrument sensitivities to $NH_4^+$ and $NO_3^-$. The second most pronounced influence is attributed to uncertainties in the ATOFMS particle detection efficiency. Sampling artifacts at high ambient temperatures contributed a significant fraction of the variance in $\epsilon_{i,NO_3^-}$. Finally, a small fraction of the variance in $\epsilon_{i,NH_4^+}$ may be attributed to interfering ion signals at m/z 18 resulting from the fragmentation of organic amines, and to matrix effects that enhance the ionization efficiency of $NH_4^+$.

## 3.5 Discussion

The instrument sensitivity factors derived from tandem ATOFMS-impactor sampling can be used to reconstruct continuous ATOFMS measurements of size-segregated $NH_4^+$ and $NO_3^-$ concentrations throughout the 1996 and 1997 field experiments, with very fine size resolution. For example, Figure 3.4a shows $NH_4^+$ measurements at Riverside, binned into 15 particle size intervals spanning the 0.32–1.80 $\mu$m $D_a$ range, and twenty-four 4 h time intervals spanning four days of the 1996 Los Angeles Basin Trajectory Study. Each row in Figure 3.4a can be translated into a conventional plot of $NH_4^+$ concentration as a function of particle size, during the specified 4 h sampling period. To illustrate this, Figures 3.4b and 3.4c show size-resolved ATOFMS measure-

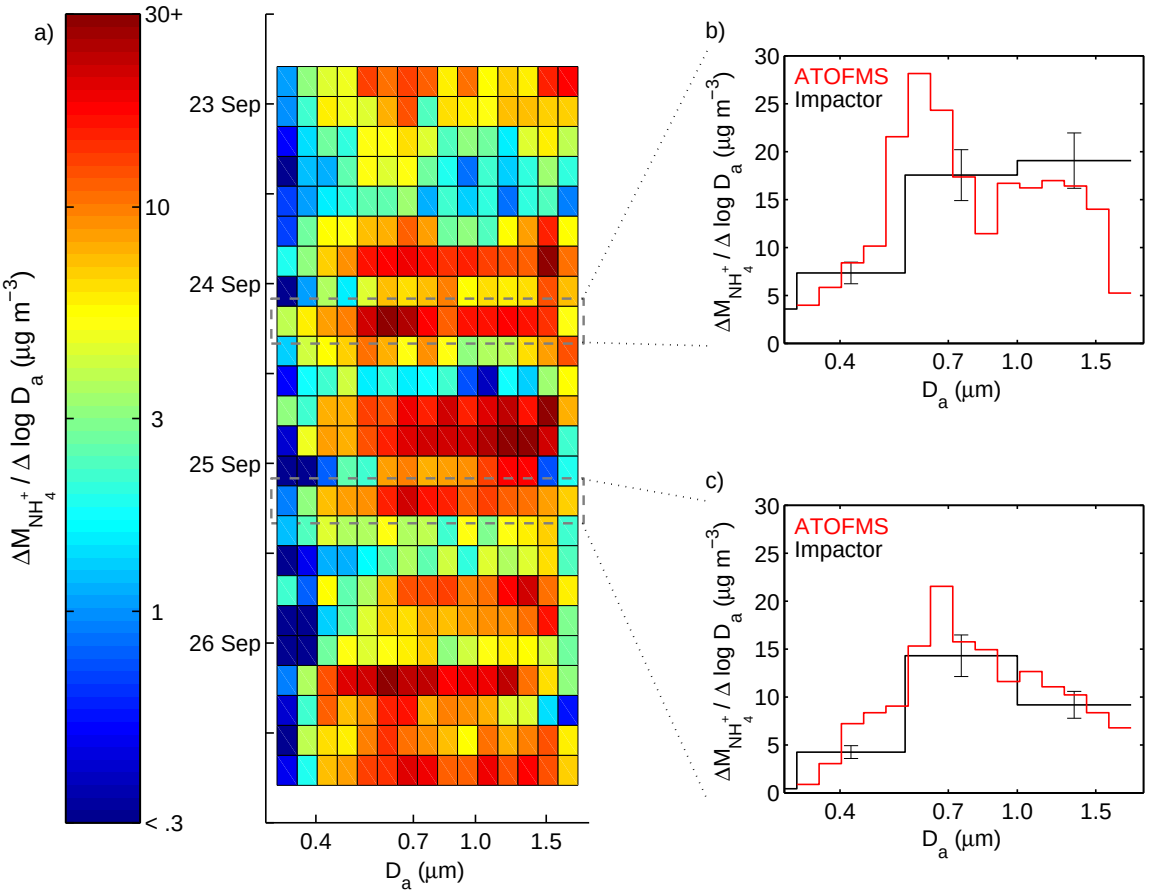


Figure 3.4: Ammonium mass distributions at Riverside. (a) Time series based on scaled ATOFMS measurements for 4-hour intervals from September 23 through 27, 1996, with divisions at 0300, 0700, 1100, 1500, 1900, and 2300 PDT. (b) Scaled ATOFMS data and impactor data at 1500–1900 PDT on September 24, 1996. (c) Scaled ATOFMS data and impactor data at 1500–1900 PDT on September 25, 1996.

ments of $NH_4^+$ concentration corresponding to the two highlighted rows of Figure 3.4a. Also, impactor measurements taken during the same time periods are plotted in Figures 3.4b and 3.4c, for the purpose of comparison. Similarly, Figure 3.5 illustrates the tandem ATOFMS-impactor $NO_3^-$ measurements. High-resolution chemical composition measurements capture many of the detailed characteristics of the Riverside aerosol, which cannot be detected using impactors alone. For example, measurements taken during the September 25, 1996 IOP show sharp peaks at ca. 0.7 $\mu$m in the $NH_4^+$ and $NO_3^-$ size distributions (see Figures 3.4c and 3.5c).

The applicability of the instrument sensitivity factors derived in this study to

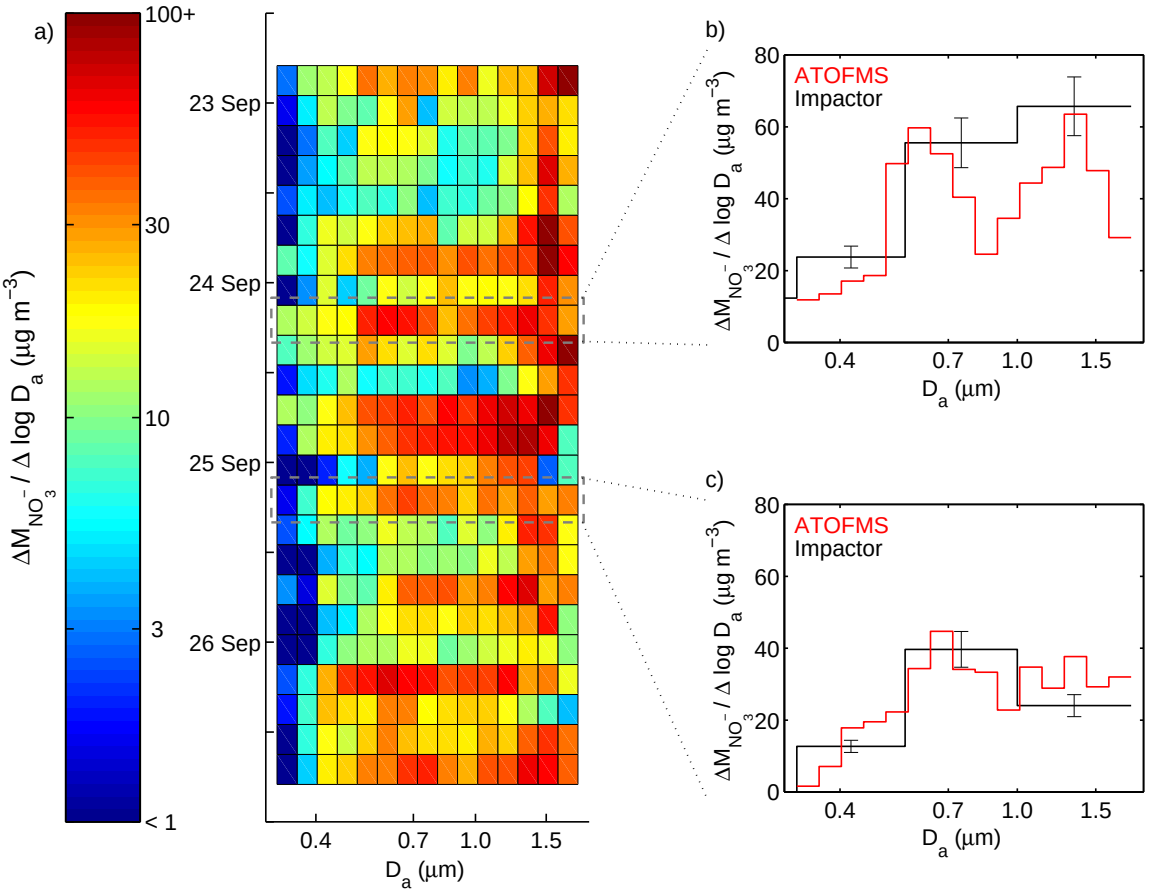


Figure 3.5: Nitrate mass distributions at Riverside. (a) Time series based on scaled ATOFMS measurements for 4-hour intervals from September 23 through 27, 1996, with divisions at 0300, 0700, 1100, 1500, 1900, and 2300 PDT. (b) Scaled ATOFMS data and impactor data at 1500–1900 PDT on September 24, 1996. (c) Scaled ATOFMS data and impactor data at 1500–1900 PDT on September 25, 1996.

other data sets, collected at locations where different ATOFMS instrument designs are used and different particle types are abundant, remains to be tested. However, application of the *methodology* described herein to other tandem ATOFMS-impactor data sets will be straightforward. In future field experiments, collocated reference measurements of aerodynamic particle size distributions may yield more accurate determinations of the ATOFMS particle detection efficiencies, which in turn will improve the precision of the instrument sensitivity factors calculated using the field-based approach. In addition, laboratory experiments can be designed to test and verify the instrument sensitivities calculated in the present work. In the future, it may be possible to extend the field-based approach to single-particle mass spectrometry instruments other than ATOFMS, and to aerosol species other than $NH_4^+$ and $NO_3^-$. Such applications remain to be tested. The strong influence of particle size on instrument sensitivities is an important conclusion of the present work. This size-dependence demonstrates a necessity for accurate particle sizing by single-particle instruments [48], if the field-based approach is to be successfully applied and further developed. In addition, collocated reference instruments must provide size-resolved chemical composition data, if they are to be used for the purpose of determining the sensitivities of laser ablation/ionization instruments to aerosol-phase species.

## 3.6 Conclusions

ATOFMS chemical composition measurements are difficult to quantify, largely because the instrument sensitivities to different chemical species in mixed ambient aerosols are unknown. In this chapter, a field-based approach is described for determining ATOFMS instrument sensitivities to ammonium and nitrate in size-segregated atmospheric aerosols, using tandem ATOFMS-impactor sampling. ATOFMS measurements were compared with collocated impactor measurements taken at Riverside, California, in September 1996, August 1997, and October 1997. This is the first comparison of ion signal intensities from a single-particle instrument with quantitative measurements of atmospheric aerosol chemical composition. The compari-

son reveals that ATOFMS instrument sensitivities to both $NH_4^+$ and $NO_3^-$ decline with increasing particle aerodynamic diameter over a 0.32–1.8 $\mu$m calibration range. The stability of this particle size dependence is tested over the broad range of fine particle concentrations ($PM_{1.8} = 17.6 \pm 2.0$ – $127.8 \pm 1.8$ $\mu$g $m^{-3}$), ambient temperatures (23–35 °C), and relative humidity conditions (21–69%), encountered during the field experiments. This chapter describes a potentially generalizable methodology for increasing the temporal and size resolution of atmospheric aerosol chemical composition measurements, using tandem ATOFMS-impactor sampling. Continuous measurements of size-resolved $NH_4^+$ and $NO_3^-$ will substantially augment the amount of experimental data currently available for air quality model evaluations.

# Chapter 4

# A Method for Categorizing Atmospheric Single-Particle Spectra

## 4.1 Introduction

Several mass spectrometry instruments have been deployed in field experiments to measure the size and chemical composition of individual atmospheric particles on-line (see Section 1.2.2). To help render the massive single-particle data sets into condensed and usable formats, particles can be size-segregated based on the optical or aerodynamic diameter measurements. However, no standardized method exists for segregating the single-particle spectra into compositional categories. Chemical categorization of single-particle spectra has a variety of potential applications. A commonly cited application of spectral categorization is the source apportionment of atmospheric particles. If individual particles can be categorized according to the primary emissions source from which they originated, the contributions that different emitting sources make to an ambient aerosol can be quantified readily. Another application, tied closely to the work described in this thesis, is that the compositionally segregated single-particle data can be compared with air quality model calculations of the aerosol mixing characteristics, and thereby used for model evaluation purposes. Spectral categorization is also a necessary prerequisite for improving our understanding of matrix effects on the particle detection efficiencies [108] and chemical sensi-

tivities [106] of single-particle instruments, because the atmospheric single-particle matrices must be precisely defined before their effects on instrument performance can be assessed quantitatively (see Section 7.2.2). Finally, spectral categorization may be applied in epidemiological studies, to determine statistical correlations between adverse human health effects and the atmospheric concentrations of compositionally distinct particle types.

The complexities of atmospheric single-particle mass spectral analysis have recently begun receiving attention in the literature [126–130]. The most common analysis methods currently in use focus on data reduction, typically by clustering single-particle spectra into similar groups. However, none of the available methods address the need for reproducibility and communicability of particle categorization results. As single-particle mass spectrometry measurements become increasingly common, a standard format for describing the compositional heterogeneity among individual particles must be established. Absent such a standard, the single-particle results will be difficult to use and interpret by investigators who are outside the community of mass spectral analysts. As a result, the important applications of single-particle observational data to a variety of fields, ranging from urban air quality management, to epidemiology, to global climate change, will be delayed significantly.

The purpose of this chapter is to describe an efficient method for the chemical categorization of atmospheric single-particle spectra, that can be communicated in a condensed format, and that will yield reproducible results. The condensed format is a list of particle categories along with quantitative criteria that each particle must satisfy, in order to be placed into one of those categories. The method is described and then used to group 82,261 single-particle spectra into 35 compositionally distinct categories and one miscellaneous category. This is the first presentation of chemically categorized single-particle data along with the complete details required to reproduce the categorization results.

## 4.2 Background

This section reviews the methods used for analyzing atmospheric aerosol spectra collected by on-line single-particle mass spectrometry instruments.

### 4.2.1 Single-Component Analysis

In field applications of the PALMS instrument [44, 45, 93, 131–135] and some early applications of ATOFMS [54, 80, 85, 90], mass spectra were analyzed primarily to determine the presence or absence of selected chemical species in atmospheric particles. These *single-component* analyses can provide general information on the fraction of a particle population that contains an individual chemical species. By combining single-component analysis results from more than one chemical species, the degree of internal versus external mixing in ambient aerosols has been estimated [85, 131–134] and also used to conduct the air quality model evaluations described in Chapter 2 [136].

There are three major shortcomings associated with single-component analyses. First, the results are strongly dependent on analyst-defined thresholds for delineating the presence or absence of selected ion signals in each particle spectrum. The shot-to-shot variability in the interaction of individual particles with the ablation/ionization laser causes the absolute detection limits for individual ions to vary significantly from one particle to the next, in an unknown and unpredictable manner [100, 101]. Analyst-defined thresholds that are set within this broad range of detection limits can lead to large uncertainties in the single-component analysis results, whereas thresholds set at conservatively high levels tend to underestimate the fractions of a particle population that actually contain the species of interest.

Second, the results of single-component analyses can be hindered by multiple interfering ion signals detected at a single mass-to-charge ratio (m/z). Some common examples of such interferences in positive ion atmospheric particle spectra include $C_2^+$ and $Mg^+$ at m/z 24, $C_2H_3^+$ and $Al^+$ at m/z 27, $C_3H_3^+$ and $K^+$ at m/z 39, $Na_2^+$ and $NO_2^+$ at m/z 46, $C_4^+$ and $Ti^+$ at m/z 48, $C_4H_3^+$ and $V^+$ at m/z 51, $C_6^+$ and $FeO^+$ at m/z 72, and $C_9^+$ and $Na_2NO_3^+$ at m/z 108. To account for interfering ion

signals in single-component analyses, one must define additional thresholds and mass spectral search criteria. For example, Murphy and Thomson designated ion signals at m/z 39 as $K^+$ indicators only when their intensities exceeded those of neighboring spectral peaks at m/z 37, 38, or 41 [44]. Such criteria substantially increase the complexity of single-component analysis procedures, and can potentially increase the uncertainty in results. In a recent single-component analysis of atmospheric particle spectra collected in Atlanta, Lee et al. reported that 20–99% of the particle population contained nitrate [134]. With such large uncertainties, the results obtained from single-component analyses are of limited value.

Third, single-component analyses "throw away" a substantial amount of spectral information, and as a result, fail to describe the overall character of each particle. For example, the combination of two single-component analyses may designate a particle as "carbon and sulfate containing," however, it is not clear whether these are the dominant components of the particle or whether they are trace constituents that marginally exceed the analyst-defined detection thresholds. Some investigators have addressed this problem by displaying frequency histograms of the ion signal intensities corresponding to a specific chemical component within a particle population [93, 131–133]. These chemical histograms provide semi-quantitative information on the distribution of a single component within an aerosol population, but one would have to extend the displays to two dimensions in order to convey any information on the mixing characteristics of a multi-component aerosol. Numerous two-dimensional histograms would be required to convey the many important mixing characteristics in an atmospheric aerosol. This would be a very inefficient method of presenting aerosol mixing characteristics measurements.

### 4.2.2 Multivariate Spectral Categorization

Due to the complexities and uncertainties associated with single-component analyses, investigators more commonly are categorizing single-particle data based on patterns and combinations of predominant ion signals in individual spectra. These *spectral cat-*

*egorization* approaches effectively bypass all of the shortcomings of single-component analyses listed in the previous section. First, arbitrary detection thresholds need not be set by analysts, because ion signals that marginally exceed the spectral noise level are essentially ignored. Second, the complex procedures to mitigate the effects of interfering ion signals are unnecessary because the entire mass spectrum is considered as a whole, rather than focusing on any individual spectral peak. In many cases of atmospheric importance, multivariate spectral categorization obviates the need to consider interferences. For example, if the spectra acquired from sea salt and soot particles are first separated into distinct categories, the chemical identity of the ion signals at m/z 108 ($C_9^+$ or $Na_2NO_3^+$) becomes unambiguous. Third, spectral categorizations are based on the overall character of each particle spectrum, thereby preserving important information on the relative intensities of multiple ion signals.

In the first field applications of ATOFMS, single-particle mass spectra were manually categorized by visual inspection [46, 47]. Particle categories were named according to predominant characteristics of the individual spectra. For example, most of the atmospheric particle spectra collected at Riverside in April and May 1995, were categorized as either marine particles, organic/nitrate mixtures, inorganic/organic mixtures, and inorganic oxides [46]. The drawbacks of visual inspection as a categorization method are that it is slow, labor intensive, and the results are not reproducible, because they are subject to operator bias [83]. Moreover, many atmospheric single-particle data sets collected during recent years consist of $10^5 - -10^6$ mass spectra [77–81, 134], rendering visual inspection an impractical and obsolete approach for spectral categorization.

In more recent ATOFMS applications, single-particle mass spectra have been exported to custom-built databases in either Microsoft Access [137, Chapter 3] or the Matlab programming environment [84], where various automated searches can be performed on single-particle data. Analysts have developed complex search criteria to group spectra into distinct compositional categories, such as sea salt, mineral dust, and carbonaceous [76–78, 86, 95, 136, 138]. An example of such search criteria is shown in Table 2.2. In most cases, the search algorithms used for these studies were

too complex for mass spectral analysts to succinctly communicate them in the literature. As a result, the spectral categorizations reported in those studies cannot be replicated readily.

#### 4.2.2.1 Unsupervised Categorization Methods

The first application of an automated spectral categorization method to on-line single-particle mass spectrometry data was reported by Song et al. in 1999 [127]. They used an adaptive resonance theory-based neural network algorithm (ART-2a) [139] to cluster approximately 43,000 single-particle spectra collected at Long Beach, California, during the 1996 Los Angeles Basin Trajectory Study. The ART-2a algorithm has several advantages over the methods discussed above. Most importantly, the algorithm is fully automated and requires no prior knowledge of the particle characteristics. Therefore, it can be used to cluster the members of a particle population with unknown chemical composition, with minimum analyst intervention, and without the need to define any mass spectral search criteria. For these reasons, the algorithm has received widespread use in numerous field applications of ATOFMS [79, 81, 89, 127] and RSMS [52, 53]. The ART-2a algorithm is described in more detail in Section 6.2.3. Recently, Murphy and co-workers described the application of a hierarchical cluster analysis method (HCA) to spectra acquired using their PALMS instrument [130]. The categorization method is referred to hereafter as HCA-PALMS. The method is reported to have certain advantages over ART-2a algorithm [130]. For example, results from both strict and loose classifications can be saved in a single run. In contrast, the ART-2a algorithm must be rerun using different vigilance parameters to yield strict and loose classifications.

The ART-2a and HCA-PALMS algorithms are referred to as *unsupervised* categorization approaches, those which do not require predefined groups. Both are excellent tools for quickly assessing the compositional heterogeneity among atmospheric aerosols sampled by single-particle mass spectrometry. Although these algorithms result in groups of similar particle spectra, they do not provide quantitative criteria for the determination of the membership of a given particle spectrum.

#### 4.2.2.2 Supervised Categorization Methods

In contrast to the algorithms described above, supervised methods categorize members of a population into predefined groups. Supervised approaches that have been applied to atmospheric single-particle data include fuzzy cluster analysis (FCA) [126] and the algorithm for discriminant analysis of mass spectra (ADAMS) [129]. It is important to emphasize that these methods do not replace the need for unsupervised methods. In fact, applications of FCA and the ADAMS to atmospheric aerosol data use some combination of ART-2a, HCA, and manual categorization, to construct the predefined particle categories.

The unique feature of FCA is that each particle may be classified into more than one category, with varying degrees of membership [126]. An example where this feature would be advantageous is for the categorization of a coagulation product of soot and sea salt. In "hard" classification algorithms, such spectra would likely be categorized as either soot or sea salt, or otherwise, remain unclassified. In atmospheric applications, the "fuzzy" classification feature is not particularly advantageous, because most particles tend to be classified into a single category with a much greater degree of membership than in any other category, provided the categories are broadly defined [50, Figure 5].

In the ADAMS, "discriminant" mass spectral markers are selected for each predefined particle category, that discriminate the category from all others. Then, the mass spectral peaks in each individual particle that are neither discriminant markers nor statistically associated with those discriminant markers ("associated non-markers"), are summed to obtain a "remainder" value. For each predefined category, a linear combination of the discriminant markers and the remainder value of a particle spectrum is calculated to determine which category the particle should be placed in [129]. Advantages of the ADAMS are that the categorization procedure consistently yields the same result for any given spectrum, all particle spectra in a data set are categorized, and the discriminant markers can be selected such that the dominant peaks in single-particle spectra do not govern the categorization results. One disadvantage of

the ADAMS is that in order to communicate the categorization methodology with sufficient detail to allow reproduction of the results, a significant amount of information must be provided. For example, to convey the exact procedure for grouping 12,790 positive ion mass spectra collected at Toronto into nineteen compositionally distinct particle categories [129], one must provide nineteen lists of discriminant markers, nineteen lists of associated non-markers, and nineteen "association matrices" that contain weight values for each pair of discriminant marker and associated non-marker. In the Toronto application of the ADAMS, individual association matrices contained as many as 200 weight values [129].

Each of the spectral categorization methods discussed thus far have certain advantages and drawbacks. In the present chapter, a principle common to both ART-2a and HCA-PALMS, namely the use of dot products as the measure of spectral similarity, is exploited to devise a spectral categorization procedure that will consistently yield identical results for a given set or subset of spectra. The final categorization procedure is communicated in a condensed format, allowing other investigators to easily reproduce, further improve, and quantitatively assess the resulting particle categorization results.

## 4.3 Methods

Aerodynamic diameter measurements and positive ion mass spectra were collected using a laboratory-based ATOFMS instrument [46] stationed at the University of California, Riverside, as part of the 1996 Los Angeles Basin Trajectory Study [54, 85, 89]. A total of 82,261 individual particles in the 0.32–1.8 $\mu$m aerodynamic diameter ($D_a$) range were sized and chemically analyzed by the ATOFMS instrument, between September 23 07:00 PDT and September 28 08:30 PDT. All of these particle data are used in the present study.

After field measurements are collected, automated computer software is used to generate a *peak list* that contains the areas, heights, and mass-to-charge (m/z) ratios of all peaks in each particle spectrum that exceed the spectral noise level by at

least five arbitrary height units and ten area units. These peak lists, along with the associated particle size measurements, are exported to the Matlab programming environment (The MathWorks, Natick, MA). The data exporting and all subsequent calculations are facilitated by the YAADA data analysis system [84]. Particle spectra are processed into the form of a two dimensional data matrix, with rows corresponding to each particle spectrum and columns corresponding to each integer unit of m/z. Each row of this matrix is referred to as a "particle vector." The $j$th element of a particle vector contains the total area under all peaks within 0.5 Da of m/z $j$, in that particle spectrum.

The spectral categorization procedure described in the present chapter consists of three steps. The first step involves selecting categories that are considered to be representative of the entire particle population. Any combination of unsupervised approaches supplemented with visual inspection may be used in this step. Second, the category descriptions are simplified to the extent that they can be conveyed succinctly. Third, the simplified category descriptions are used to compositionally segregate the entire set of atmospheric particle spectra. The method is designed in such a way that the steps which are complicated and subject to operator bias are isolated from the final categorization step. Given a set of simple particle category descriptions, one needs to perform only the third step the procedure, in order to replicate the particle categorization results.

To efficiently complete the first two steps, a random selection of 5000 spectra was drawn from the full particle data set. The first 350 Da of each mass spectrum are considered, because ion signals at higher m/z ratios are infrequently detected in typical ambient ATOFMS data. Therefore, the data matrix used in the first two steps consists of 5000 rows and 350 columns. It should be noted that the spectral categorization method is described here in the context of unipolar mass spectra, however, application to dual ion mass spectra would require only a trivial modification.

## 4.4 Results

### 4.4.1 Category Selection

As is the case in many supervised spectral categorization techniques, the most labor-intensive step of the present method involves the selection of particle categories that are representative of a large fraction of the particle population. There are a number of available tools to help with this step, including the ART-2a and HCA-PALMS algorithms. The method that one chooses to select particle categories is not the focus of the present work, however a method is provided here for completeness, and may be regarded as an example of how one might use the ART-2a algorithm to select atmospherically relevant particle categories, and test their representativeness of the entire population. It is important to emphasize that any category selection method may be substituted for the one described in the following paragraphs.

For the present analysis, a two-tiered approach was taken, where particles are first broadly classified as either sea salt, dust, carbonaceous, or miscellaneous, and then subdivided into compositionally distinct particle categories. To help conduct the first tier classification, the ART-2a algorithm was applied to the $5000 \times 350$ element data matrix, using a vigilance parameter of 0.7, a learning rate of 0.05, and twenty iterations. This particular ART-2a run produced 417 clusters, of which 153 contained more than one member. The average mass spectrum of each non-singleton cluster (obtained by columnwise averaging of the particle vectors corresponding to members of that cluster) was visually inspected, and classified as either sea salt, dust, carbonaceous, or miscellaneous, based on prominent spectral features. For example, average spectra containing intense ion signals at m/z 12 ($C^+$), 24 ($C_2^+$), 36 ($C_3^+$), and 37 ($C_3H^+$), were classified as carbonaceous [46]. Sea salt particle spectra typically contain intense ion signals at m/z 23 ($Na^+$) and 39 ($K^+$), as well as less prominent ion signals at m/z 46 ($Na_2^+$), 81 ($Na_2Cl^+$), 108 ($Na_2NO_3^+$), and 165 ($Na_3SO_4^+$) [138]. Mass spectra from the ablation/ionization of dust typically contain some combination of ion signals at m/z 23 ($Na^+$), 24 ($Mg^+$), 27 ($Al^+$), 39 ($K^+$), 40 ($Ca^+$), and 56 ($Fe^+$) [86, 136]. Clusters in which the average spectrum did not contain a recognizable

combination of peaks were classified as miscellaneous.

When the most appropriate class could not be determined by visual inspection of the average mass spectrum, a histogram of the $D_a$ measurements for members of that cluster was examined. Average mass spectra that appeared similar to both carbonaceous and sea salt particle spectra were categorized as sea salt if the size histogram revealed an absolute maximum in the $D_a > 1$ $\mu$m range, as carbonaceous if the maximum was in the $D_a < 1$ $\mu$m range, and as miscellaneous otherwise (e.g., size histogram exhibited no absolute maximum). An analogous criterion was used to classify the average spectra that appeared similar to both dust and carbonaceous particle spectra. These criteria are based on well-established evidence that atmospheric carbonaceous particles are generated at very small sizes by combustion processes or result from the condensation of secondary organic compounds onto the surfaces of accumulation mode particles, whereas dust and sea salt particles are mechanically generated and therefore, larger in size. In cases where it was not clear whether an average spectrum was indicative of dust or sea salt, the cluster was classified as miscellaneous. The average spectrum of one minor cluster, containing 11 members, appeared to be representative of coagulation products of carbonaceous particles with either sea salt or dust particles. This cluster was classified as miscellaneous. In this manner, 4 clusters were classified as sea salt, 22 as dust, 75 as carbonaceous, and 52 as miscellaneous. In total, the sea salt clusters contained 1027 members, the dust clusters contained 288 members, and the carbonaceous clusters contained 3222 members. The combination of all miscellaneous and singleton clusters contained 463 members. This set of intermediate results is referred to hereafter as the "first tier" particle classification.

The four particle classes described above were chosen because, in most cases, they can be identified readily by visual inspection of the mass spectra. However, these classes are rather broadly defined, and hence, do not provide a very detailed representation of the aerosol heterogeneity. Therefore, compositionally distinctive particle "categories" were sought within the sea salt, dust, and carbonaceous "classes," to better represent the particle-to-particle heterogeneity among members of each class. This is the second part of the two-tier category selection process. Distinguishing

subtle spectral patterns by visual inspection is challenging and labor intensive, so the ART-2a algorithm was applied separately to the members of each class, using a 0.05 learning rate and five iterations. The algorithm was run twice on each particle class, at vigilance parameters of 0.5 and 0.7. The 0.5 vigilance parameter run yielded 3 sea salt clusters, 9 dust clusters, and 21 carbonaceous clusters. The 0.7 vigilance run yielded 4 sea salt clusters, 25 dust clusters, and 79 carbonaceous clusters. These results indicate that the carbonaceous particle class included the most diverse set of particle spectra, and the sea salt spectra were the most homogeneous. The particle spectra belonging to each ART-2a cluster were averaged together, to create two sets of "seed vectors" (one set obtained using each vigilance parameter). The seed vectors were then evaluated in an iterative manner until those which are "most representative" of the entire particle population were identified.

A flowchart of the iterative seed selection procedure is shown in Figure 4.1. Initially, only the set of 0.5 vigilance parameter seed vectors was considered. Each particle vector and seed vector are normalized to unit length, and the Euclidean angle between each particle vector and seed vector is calculated using the dot product. Particle vectors are each assigned to the seed vector that they form the maximum dot product with, provided that it exceeds a threshold of 0.7. Particle vectors that do not satisfy this criterion with any seed vector are assigned to a miscellaneous group. This association procedure is similar to applying the ART-2a algorithm with a vigilance parameter of 0.7, one iteration, zero learning rate, and predefined weight vectors, such that reproducibility of the cluster memberships is ensured. Seed vectors that are associated with fewer than 0.1% of the 5000 particle vectors are removed from the seed matrix, and particle associations with the remaining seed vectors are recalculated. Next, all particle vectors that assigned to a sea salt seed are grouped together, those assigned to a dust seed are grouped, and those assigned to a carbonaceous seed are grouped. These three groups of particle vectors along with the miscellaneous group assembled earlier, are then compared against results of the first tier classification. Cases where this comparison reveals large differences are analyzed in detail. Seed vectors from the 0.7 vigilance parameter ART-2a results are manually selected based

on their potential to improve agreement between the dot product particle associations and the first tier class memberships. The new seed vectors are added to the seed matrix and particle associations with the revised set of seed vectors are recalculated. The entire procedure was repeated until all seed vectors were associated with at least 0.1% of the particle population, and the dot product associations matched the first tier classifications with at least 95% accuracy. In this manner, a total of 35 seed vectors (3 sea salt, 12 dust, and 20 carbonaceous) were selected to represent the particle population.

A comparison of the supervised dot product associations with the first tier classifications is presented in Table 4.1. Summing all values along the main diagonal indicates that 4811 of the 5000 spectra (96.22%) are "accurately" categorized using the supervised approach with the 35 seed vectors selected above. Many of the miscellaneous particle spectra appear to be "misclassified" as either sea salt, dust, or carbon. Closer inspection of these particle vectors reveals that almost 10% of them were among the singleton clusters in the initial ART-2a results, and were therefore assigned to the miscellaneous class by default. In these specific cases, the dot product associations likely yield better results than the ART-2a algorithm. In the supervised approach, 75 of the carbonaceous spectra are assigned to the miscellaneous class. This is indicative of the diversity among carbonaceous particle spectra, which can be largely attributed to complex fragmentation patterns of organic aerosol species when analyzed by laser ablation/ionization [117]. Even so, over 97% of the carbonaceous spectra are accurately classified as such using the supervised approach, with only twenty carbonaceous seed vectors. Overall, spectral categorization by the supervised approach yields results of comparable accuracy to those obtained from the unsupervised, manual classification of ART-2a clusters. Furthermore, the particle categories obtained using the supervised approach are more narrowly defined than the first tier classes, and will potentially yield a more detailed and accurate representation of the ambient aerosol heterogeneity.

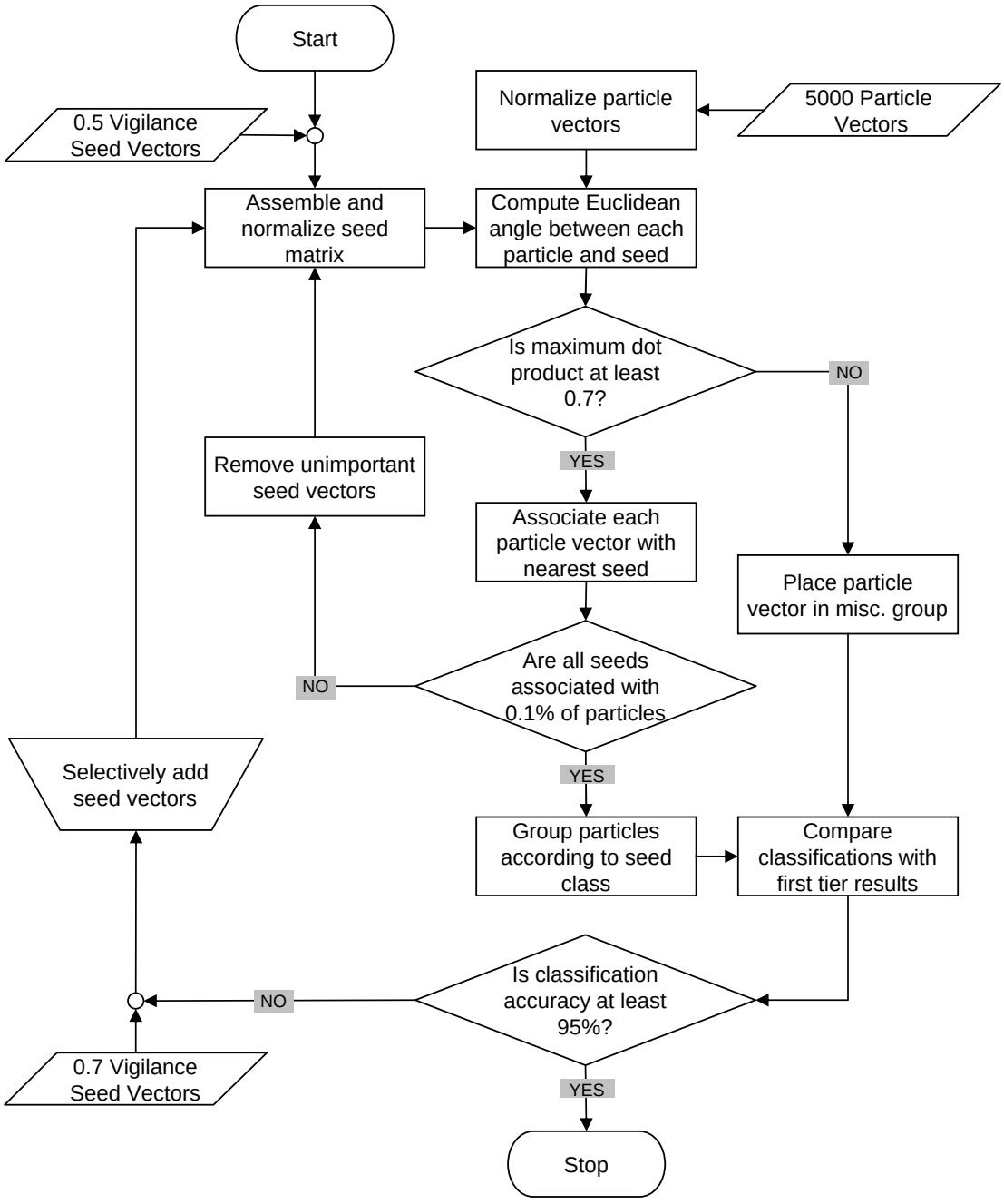


Figure 4.1: Flowchart of the iterative seed selection procedure.

Table 4.1: Comparison of the unsupervised first tier classification with the supervised classification, using the entire 35 × 350 seed matrix.

| | Supervised Classification | | | |
|---|---|---|---|---|
| **First Tier Class** | **Sea Salt** | **Dust** | **Carb.** | **Misc.** |
| Sea Salt | 1018 | 0 | 7 | 2 |
| Dust | 6 | 270 | 3 | 9 |
| Carbonaceous | 3 | 5 | 3139 | 75 |
| Misc. | 26 | 13 | 40 | 384 |

### 4.4.2 Seed Simplification

The second step of the spectral categorization method is intended to increase the communicability of the categorization procedure. Complete representation of the seed vectors selected above would require displaying a 35 × 350 matrix of values. These are too many values to convey in the published literature, however, simplification of the seed matrix can reduce this number by over one and a half orders of magnitude without a significant loss of accuracy in the final particle categorizations. This step of the method distinguishes it from other spectral categorization methods.

During the seed selection process and in previous experiences using the ART-2a algorithm, it was observed that the dot product between a particle and seed vector is influenced primarily by the largest values in the particle and seed vectors, whereas the smaller values have minimal effects on the categorization results. This indicates that the seed matrix may be simplified by nullifying minor components of each seed vector, without greatly influencing the final particle categorizations. To explore this in detail, a series of numerical experiments were conducted. The seed matrix was simplified by converting minor elements of each seed vector to zeros, where minor elements are defined as those which individually contribute less than a fixed fraction of the sum of all elements in the seed vector. This fixed fraction, or "relative intensity threshold," was varied between 0.1% and 10%. At each threshold, the dot product associations were calculated for all 5000 particle vectors, and the spectra were aggregated into one of the four major particle classes. Figure 4.2 provides a summary of the results.

As the relative intensity threshold is increased, the average number of nonzero

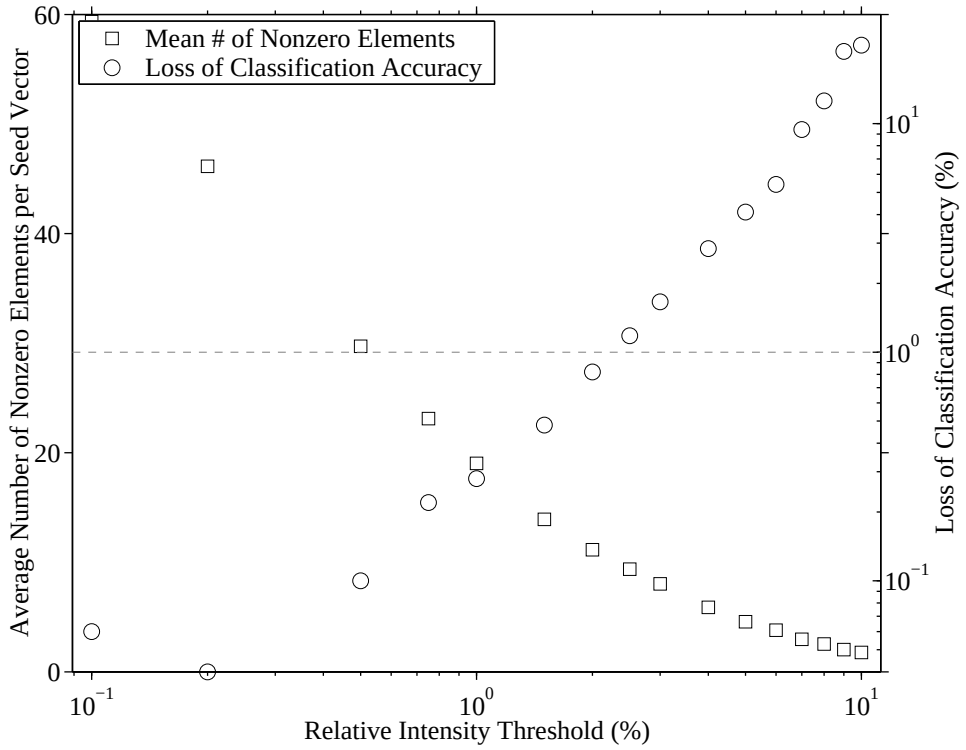


Figure 4.2: Effects of seed simplification on classification accuracy. The maximum allowable loss of accuracy selected for the present study is shown by the dashed gray line.

elements in each seed vector decreases and the classification results become less accurate. The loss of classification accuracy is calculated by comparing the classification results obtained when using the complete seed descriptions (as shown in Table 4.1) with those obtained using the simplified seed descriptions. By selecting a maximum allowable loss of classification accuracy, one can determine the largest relative intensity threshold to apply to the seed vectors, such that the seed matrix contains the fewest possible number of nonzero elements. In the present study, the maximum allowable loss of classification accuracy is set at 1%, shown by the gray dashed line in Figure 4.2. This level can be attained with optimum seed simplification by applying a 2% relative intensity threshold to the seed vectors.

The seed descriptions are further simplified by linearly scaling each row of the seed matrix, such that the maximum value in each row is 1000, and then rounding each element of the seed matrix to the nearest integer. This is similar to reporting each seed vector value with four significant digits, except by scaling each seed vector to a common maximum value, one can more easily assess the differences between seed vectors with similar combinations of peaks. The scaling and rounding operations were found to have no effect on the classifications of the 5000 particle spectra. Table 4.2. lists all of the nonzero elements in the simplified seed matrix. Classification results obtained by applying the supervised approach with 35 simplified seed vectors are compared against the first tier classification in Table 4.3. These results are almost identical to those shown in Table 4.1, illustrating the negligible effect of the seed simplification procedure on classification results.

### 4.4.3 Spectral Categorization

After selecting and simplifying seed vectors that adequately represent the particle population, the entire set of particle spectra can be compositionally segregated. Particle vectors are categorized according to the seed vector in Table 4.2 that they form a maximum dot product with, and all particle vectors that do not yield a dot product greater than 0.7 with at least one of the seed vectors are placed into a 36th mis-

Table 4.2: Final description of the selected seed vectors.

| ID | m/z (Intensity) |
|---|---|
| **Sea Salt Seed Vectors** | |
| S1 | 23(1000) 24(262) 39(164) 40(139) 25(91) 26(72) 41(57) 30(53) 27(48) |
| S2 | 24(1000) 23(820) 40(334) 39(326) 25(261) 26(155) 41(124) 30(99) |
| S3 | 23(1000) 36(641) 37(417) 12(392) 24(362) 39(292) 27(261) 43(234) 30(215) 18(163) 38(112) |
| **Dust Seed Vectors** | |
| D1 | 39(1000) 40(619) 41(499) 23(486) 42(274) 24(206) 57(153) 27(143) 56(123) 30(115) |
| D2 | 40(1000) 41(590) 23(496) 24(480) 42(409) 57(408) 56(277) 39(254) 43(179) 44(165) 25(141) 28(132) 27(132) |
| D3 | 56(1000) 39(812) 27(761) 24(624) 40(600) 23(475) 41(446) 57(407) 28(359) 30(313) 25(264) 54(209) |
| D4 | 27(1000) 24(949) 2(690) 25(501) 28(494) 40(460) 23(422) 39(366) 16(301) 29(245) 26(237) 41(227) 57(182) |
| D5 | 27(1000) 23(525) 29(521) 28(511) 24(257) 30(223) 1(218) 40(197) 48(189) 39(185) 25(181) |
| D6 | 2(1000) 17(813) 28(719) 24(398) 25(369) 41(199) 27(197) 23(178) 48(138) 40(127) |
| D7 | 64(1000) 48(738) 27(567) 49(315) 47(284) 46(282) 50(201) 66(189) 28(179) 65(176) 51(137) 23(130) 63(123) 62(123) |
| D8 | 40(1000) 36(898) 37(383) 12(270) 56(225) 18(225) 27(208) 57(201) 43(179) 51(176) 30(169) 24(166) 39(137) |
| D9 | 39(1000) 23(980) 40(411) 24(388) 41(315) 42(201) 36(125) 27(125) 25(112) |
| D10 | 24(1000) 56(983) 25(635) 27(565) 23(487) 26(415) 39(376) 57(344) 28(294) 54(269) 41(241) 30(210) 58(203) 40(192) |
| D11 | 56(1000) 39(814) 64(407) 48(331) 27(316) 23(301) 55(241) 57(220) 40(111) |
| D12 | 56(1000) 40(677) 57(362) 24(143) 54(130) 27(119) 48(95) |
| **Carbonaceous Seed Vectors** | |
| C1 | 36(1000) 37(183) 12(182) 24(117) 48(61) 39(56) 43(53) 27(49) |
| C2 | 36(1000) 37(576) 12(352) 27(227) 43(226) 24(185) 39(151) 38(123) 30(100) 18(90) 29(87) |
| C3 | 36(1000) 12(913) 24(639) 37(510) 27(271) 30(244) 18(214) 43(201) 39(157) 25(135) 17(131) 13(119) |
| C4 | 36(1000) 37(909) 27(756) 12(697) 43(556) 24(436) 39(434) 30(377) 18(376) 29(264) 38(260) 19(200) |
| C5 | 30(1000) 12(937) 18(901) 36(758) 24(669) 37(652) 27(620) 43(484) 39(453) 19(424) 29(284) 17(234) |
| C6 | 39(1000) 36(344) 12(215) 37(153) 41(147) 24(134) 30(110) 18(100) 40(98) 23(76) 27(63) |
| C7 | 36(1000) 60(389) 48(380) 37(262) 12(115) 39(114) 43(92) 61(82) |
| C8 | 30(1000) 18(639) 19(372) 31(332) 12(306) 17(211) 24(198) 36(192) 39(188) 46(180) 27(173) 35(171) 32(165) 43(145) 37(132) |
| C9 | 37(1000) 36(476) 27(292) 43(199) 39(185) 38(142) 18(133) 86(121) 30(119) 12(108) 29(96) 24(80) |
| C10 | 56(1000) 57(426) 54(277) 55(246) 58(203) 27(139) 39(135) 30(135) 73(120) 23(104) |
| C11 | 86(1000) 30(360) 18(238) 58(216) 87(202) 27(196) 36(183) 12(162) 37(161) 67(156) 43(129) 29(122) |
| C12 | 51(1000) 56(568) 67(312) 12(229) 36(226) 27(179) 37(164) 58(156) 30(153) 24(151) 39(129) 18(129) 43(127) |
| C13 | 18(1000) 39(758) 30(595) 37(463) 36(416) 27(371) 43(366) 12(294) 19(279) 86(200) 29(172) |
| C14 | 43(1000) 37(804) 36(779) 27(360) 30(243) 39(238) 18(224) 29(162) 12(156) 19(151) 86(142) 38(134) |
| C15 | 27(1000) 36(482) 37(335) 12(291) 30(260) 18(240) 43(175) 24(113) 29(87) 28(87) |
| C16 | 39(1000) 43(723) 27(659) 41(584) 37(442) 40(423) 29(405) 57(400) 55(319) 38(291) 63(280) 51(278) 36(272) |
| C17 | 60(1000) 48(349) 36(312) 84(193) 132(117) 120(91) 72(75) 37(74) 144(66) 39(64) |
| C18 | 60(1000) 36(960) 61(858) 132(838) 84(755) 37(742) 48(654) 120(596) 85(476) 108(454) 72(411) 39(367) |
| C19 | 37(1000) 50(646) 86(414) 27(379) 38(357) 43(306) 36(281) 61(186) 49(167) 39(137) 26(112) |
| C20 | 132(1000) 72(430) 36(309) 120(226) 180(184) 84(156) 168(130) 37(109) 108(100) 60(93) 61(86) 144(79) |

Table 4.3: Classification of 5000 spectra using the simplified seed matrix, compared with first tier classifications.

| | Supervised Classification | | | |
|---|---|---|---|---|
| **First Tier Class** | **Sea Salt** | **Dust** | **Carb.** | **Misc.** |
| Sea Salt | 1020 | 0 | 5 | 2 |
| Dust | 6 | 263 | 5 | 14 |
| Carbonaceous | 2 | 7 | 3127 | 86 |
| Misc. | 26 | 12 | 36 | 389 |

cellaneous category. This is a computationally efficient process, requiring only ten minutes to categorize 82,261 spectra on a 700 MHz personal computer.

## 4.5 Discussion

Table 4.2 contains all of the information necessary to compositionally segregate any subset of the 82,261 ATOFMS single-particle spectra considered in the present study. By following the procedure described here, any particle in the data set can be grouped into one of the 35 compositionally distinct categories, or into a 36th miscellaneous category. Most importantly, the final categorization of each particle is reproducible. At first glance, the amount of data contained in Table 4.2 may appear overwhelming, but this is far easier to handle than a set of complex peak list search criteria. The other currently available method for precisely conveying particle categorizations is to explicitly list each particle in a data set along with its category number. However, that approach inhibits users of the single-particle data from further improving or quantitatively assessing the chemical categorization results. Providing the full list of category descriptions as shown in Table 4.2 can facilitate multiple applications of the same single-particle data set. For example, investigators may assign different physical or descriptive properties to each particle category (e.g., density, refractive index, source origin) without having to explain the contents of that particle category. This may be useful in air quality management applications, radiative forcing calculations, and in the analysis of matrix effects on single-particle instrument sensitivities.

Application of the present method to any single-particle data set is fairly straight-

forward. The most difficult step involves defining particle categories that are representative of the sampled aerosol population. However, most single-particle data analyses entail some form of data reduction using unsupervised clustering algorithms. In the present study, a two-tiered approach based on the ART-2a algorithm was used to select particle categories. The advantage of a two-tiered approach relative to standard ART-2a clustering is that if the first tier classifications are carefully determined, compositionally distinct particles that yield spectra containing the same dominant ion signal can be distinguished from one another. For example, the ART-2a algorithm often confuses positive ion spectra from potassium-rich soil dust with the spectra from potassium-rich biomass combustion particles, because potassium is efficiently ionized and therefore tends to dominate the resulting mass spectra. By applying the present method to the seed vectors listed in Table 4.2, particles of the former type would fall under Category D1, and the latter type would fall under Category C6. Another example of atmospheric particle types commonly grouped by the ART-2a algorithm are iron-rich soil dust (Categories D3, D11, D12) and iron-rich combustion products (Category C10). The second and third steps of the procedure can be viewed as an extension of unsupervised categorization algorithms, that will yield reproducible results in a communicable format.

An important application of an the present method is for categorization of single-particle emissions source data. If the source characterization data can be expressed in a format comparable to that shown in Table 4.2, they will provide information on the compositional heterogeneity among individual particles from the same source, that can be interpreted with relative ease. Such information can then be used to construct particulate matter emissions inventories with single-particle level detail, and subsequently used as inputs to mathematical air quality models. This application is discussed further in Section 7.2.3.

## 4.6 Conclusions

A method has been described for the efficient categorization of single-particle data into compositionally distinct categories, based on the dot products between single-particle data vectors. The methodology is conveyed in a condensed format, as a list of particle categories along with quantitative criteria that each particle must satisfy, in order to be placed into one of those categories. The unique feature of the method is that the categorization of each particle is unambiguous and therefore, reproducible. After describing the method, it was used to group 82,261 single-particle spectra into 35 compositionally distinct categories and one miscellaneous category. This was the first presentation of chemically categorized single-particle data along with the complete details required to reproduce the categorization results. It is important to stress that the chemical categorizations should not be viewed as a data analysis endpoint, but rather, as a tool for more extensive analyses of single-particle data. For example in Chapter 5, ATOFMS data are chemically categorized by the present method and used to quantitatively reconstruct size-resolved measurements of the atmospheric aerosol mixing characteristics.

# Chapter 5

# Quantitative Evaluation of a Source-Oriented Air Quality Model Using ATOFMS Measurements

## 5.1 Introduction

Mathematical air quality models provide the necessary framework to integrate our understanding of the complex processes governing air pollutant formation, transport, and removal. Increased confidence in our understanding of the ensemble of these processes can only be achieved through extensive model evaluations against atmospheric measurements. The evaluation of atmospheric aerosol models is complicated by the multidimensional nature of particulate matter (PM) data. Table 5.1 contrasts the degree of complexity associated with atmospheric ozone data versus PM data. Whereas the ozone concentration or that of any gas-phase pollutant at a particular time and location can be represented by a single number, a multidimensional matrix is required to accurately describe the PM concentration at any point and time. The sizes of airborne particles vary over several orders of magnitude, and to a large extent, determine the effects of PM on human health, visibility degradation, and climate forcing. Thus, the particle size distribution must be specified when characterizing atmospheric PM concentrations. In addition, PM consists of numerous chemical components, which may be present in a variety of phases, and the PM chemical composition typically varies with particle size. Finally, atmospheric particles of the same size, present at a

given time and location, may exhibit differing chemical compositions. In the present work, distributions of chemical constituents among particles of a given size are referred to as the aerosol *mixing characteristics*. These may be viewed as an additional dimension of PM data.

Table 5.1: Dimensions of ambient air quality data

| **Dimension** | **$O_3$ Data** | **PM Data** |
|---|---|---|
| Spatial | √ | √ |
| Temporal | √ | √ |
| Particle Size | | √ |
| Chemical Composition | | √ |
| Mixing Characteristics | | √ |

The first models to account for the size and composition distribution of atmospheric PM were evaluated against bulk filter-based measurements of inorganic aerosol components, taken in southern California in August 1982 [16, 140]. The 1987 Southern California Air Quality Study (SCAQS) provided a more comprehensive data set for testing mechanistic air quality models [141]. Several aerosol models were developed thereafter, and evaluated against filter-based chemical composition measurements of fine and coarse particulate matter taken during the SCAQS [21, 27, 142]. Other models were tested more rigorously, by comparison with the SCAQS size-resolved aerosol chemical composition measurements [20, 24, 25, 28]. More recently, mechanistic air quality models describing the size and composition distribution of aerosols have been developed and applied to regions outside of southern California [22, 143–145]. These model calculations have been evaluated against bulk aerosol and fine particle chemical composition measurements only, due to the dearth of more detailed aerosol data at these geographic locations.

To take advantage of real-time aerosol measurement techniques developed after the SCAQS, a comprehensive field campaign was undertaken in the Los Angeles Basin in September 1996 (see Section 1.2.3). This campaign included the collection of aerosol measurements at one offshore and three inland receptor sites, using electronic parti-

cle size distribution monitors, filter-based samplers, cascade impactors, and aerosol time-of-flight mass spectrometry (ATOFMS) instruments [54, 85, 89]. Comparisons of the collocated ATOFMS and impactor data elucidated methods to quantitatively reconstruct continuous, size-resolved measurements of aerosol mass, nitrate, and ammonium concentrations, at the Riverside monitoring site (see Chapter 3) [82, 91]. The resulting aerosol data are enriched in three dimensions, relative to the most comprehensive data sets used for previous aerosol model evaluations. First, the data are available with greater temporal resolution than traditional filter or impactor data alone, owing to the continuous sampling capabilities of the ATOFMS instrument. Second, the particle size resolution of the reconstructed aerosol data is greater than that obtained from traditional impactor sampling [82, 91]. Third, the single-particle measurements can be disaggregated according to the relative abundance of compositionally distinct single-particle types detected by ATOFMS, to yield quantitative measurements of the ambient aerosol mixing characteristics.

Investigations of ambient aerosol mixing characteristics have been limited to date, due to the inability to quantitatively measure the mixing characteristics and due to the simplifying "internal mixture" assumption made in the vast majority of mechanistic aerosol models. In the present study, model results are obtained using a source-oriented air quality model that simulates the ambient aerosol as an ensemble of discrete particle types, that are transported from different emission sources to a downwind receptor site (see Section 2.2.1) [28, 55]. Model calculations of the aerosol size and chemical composition distribution agree favorably with measurements taken during the SCAQS [28, 64], as well as with filter and impactor-based measurements taken during the 1996 Los Angeles Basin Trajectory Study [55]. In Chapter 2, the model results were shown to agree favorably with semi-quantitative aerosol mixing characteristics measurements taken at Long Beach and Riverside in September 1996 [136]. The primary purpose of this chapter is to illustrate quantitative comparisons that now can be made between air quality model results and aerosol measurements, given the improved temporal resolution, the improved particle size resolution, and the new aerosol mixing characteristics information, that have recently

become available. In addition, this study serves to further evaluate the calculations of a state-of-the-science atmospheric aerosol model, including the first model evaluation against quantitative measurements of atmospheric aerosol mixing characteristics.

## 5.2 Methods

### 5.2.1 Description of the Air Quality Model

Detailed descriptions of the air quality model appear in the published literature [28, 30, 55, 64, 136] and in Section 2.2.1, so only the aspects most relevant to this chapter are highlighted here. The distinguishing feature of the model is that the ambient aerosol is represented as an ensemble of compositionally distinct particle classes, rather than as an internally mixed distribution in which the chemical composition of all like-sized particles are assumed to be identical. This model formulation permits detailed calculations of the aerosol mixing characteristics to be made. The chemical evolutions of primary particles emitted at 15 discrete sizes (spanning the 0.01–10 $\mu$m particle diameter range) and from 10 source categories (paved road dust, crustal material, diesel engine exhaust, food cooking, catalyst-equipped gasoline-powered engine exhaust, non-catalyst gasoline engine exhaust, sulfur-bearing fuel combustion and industrial sources, sea salt, non-sea salt background particles, and other miscellaneous sources) are tracked separately in the model. All particle classes interact with the same gas-phase conditions, but differences in the size and composition of particles emitted at different sizes and from different sources are retained. In addition, particles emitted during different hours are tracked separately, to simulate differences in the size and composition distributions of freshly emitted particles compared to those of aged particles originating from the same source category [64].

The model used in the current study is based in a Lagrangian framework, in which the atmospheric processes within an individual air parcel are followed in a coordinate system that moves with the average wind velocity. Although a version of this model has been developed recently within a 3-D Eulerian framework [30], hence capturing

the effects of vertical wind shear and horizontal turbulent diffusion, the Lagrangian model formulation is used in the present study for three reasons. First, model results are to be evaluated at a single receptor site, so calculating the spatial distribution of pollutants over the entire study region is unnecessary. Second, vertical wind shear and horizontal turbulent diffusion were found to have a negligible effect on the aerosol mass distribution during the episode studied here [30], so both versions of the model yield similar results at the receptor of interest. Third, the computational burden currently associated with tracking the compositions and concentrations of discrete particle types virtually prohibits calculations of the physiochemical differences between freshly emitted and aged particles to be made in an Eulerian framework. Thus, the Lagrangian formulation yields an accurate set of model results at the target receptor during the period of interest, with more detailed aerosol mixing characteristics than are provided by the current formulation of the Eulerian model.

Air parcel trajectories are calculated by backward integration through wind fields interpolated from wind observations taken at 29 locations in southern California [55]. A time series of model results with hourly temporal resolution is obtained by computing pollutant evolution along 24 trajectories, terminating hourly at the Riverside monitoring site on September 25, 1996.

### 5.2.2 Description of the Atmospheric Aerosol Data

The aerosol measurements presented in this study were collected as part of the Los Angeles Basin Trajectory Study described in Section 1.2.3 [54, 85]. For the entire duration of September 25, individual atmospheric particles were sampled continuously at Riverside, using an ATOFMS instrument. In addition, size-segregated aerosol samples were collected from 1500–1900 Pacific Daylight Time (PDT), using two collocated micro-orifice impactors (MSP Corp., models 100 and 110), and later analyzed for particulate mass, nitrate, ammonium, and numerous other chemical species.

#### 5.2.2.1 Reconstruction of Atmospheric Aerosol Concentrations

Methods to quantitatively reconstruct size-resolved particulate mass, nitrate, and ammonium concentrations, from raw ATOFMS data have been described thoroughly in Chapter 3 [82, 91], and can be summarized as follows

$$\hat{m}_i = \frac{\sum_{j \subset i} \phi_j \frac{\pi}{6} \rho_p {\mathrm{D}_{p,j}}^3}{\mathrm{V}_i} \tag{5.1}$$

$$\hat{m_{ik}} = \frac{\sum_{j \subset i} \phi_j \, \mathrm{Resp}_{jk} \, \psi_{jk}}{\mathrm{V}_i} \tag{5.2}$$

$$\phi_j = \alpha \, {\mathrm{D}_{a1,j}}^{\beta} \tag{5.3}$$

$$\psi_{jk} = \gamma_k \, {\mathrm{D}_{a1,j}}^{\delta_k} \times \frac{1 \, \mu\mathrm{g}}{\text{unit of ion signal intensity}} \tag{5.4}$$

where the subscript $i$ represents an arbitrary ensemble of single-particle ATOFMS measurements, subscript $j$ represents an individual particle measurement, subscript $k$ represents a chemical species of interest, $\hat{m}$ is an atmospheric aerosol concentration ($\mu$g m$^{-3}$) reconstructed from raw ATOFMS data, $\phi$ is a particle size-dependent, dimensionless factor by which the ATOFMS instrument undercounted particles during the field study, $\rho_p \frac{\pi}{6} {\mathrm{D}_{p,j}}^3$ is the estimated mass ($\mu$g) of an individual particle detected by ATOFMS (assuming particles are spherical with density, $\rho_p$ = 1.3 g cm$^{-3}$, and physical diameter, $\mathrm{D}_p$ ($\mu$m)), $\mathrm{V}_i$ is the volume of air sampled by ATOFMS (m$^3$) during the time period when particle ensemble $i$ was encountered (Equation 3.4), $\mathrm{Resp}_{jk}$ is the ATOFMS instrument response to species $k$ in particle $j$ (ion signal area units), $\psi$ relates ATOFMS ion signal intensities to the mass of a species of interest ($\mu$g/ion signal area), $\mathrm{D}_{a1}$ is a dimensionless aerodynamic particle diameter (measured $\mathrm{D_a} \div$ 1 $\mu$m), and $\alpha$, $\beta$, $\gamma$, and $\delta$ are dimensionless parameters whose values and 95% confidence intervals during the study period are determined to be $\alpha = 5040 \pm 1190$, $\beta = -3.13 \pm 0.64$, $\gamma_{\mathrm{NO_3^-}} = 4.7 \pm 0.7 \times 10^{-10}$, $\delta_{\mathrm{NO_3^-}} = 2.4 \pm 0.4$, $\gamma_{\mathrm{NH_4^+}} = 2.5 \pm 0.4 \times 10^{-10}$, and $\delta_{\mathrm{NH_4^+}} = 2.4 \pm 0.4$ [91]. Equations 5.1–5.4 are valid in the 0.32–1.8 $\mu$m $\mathrm{D_a}$ range only, thereby limiting the model evaluations described in the present study to this range of aerodynamic particle diameters.

#### 5.2.2.2 Mixing Characteristics Measurements

The present analysis of aerosol mixing characteristics is focused on the 1500–1900 PDT period, on September 25, 1996. During these four hours, the ATOFMS instrument acquired single-particle spectra from 3181 particles in the 0.32–1.8 $\mu$m aerodynamic diameter range. These particles are separated into three compositional classes (sea salt, dust, and carbonaceous), using the spectral described in Chapter 4. Particles which fall in categories S1–S3 in Table 4.2 are combined into the sea salt class, D1–D12 into the dust class, and C1–C20 into the carbonaceous class. Particles which do not fit into any of these 35 compositional categories are placed into a miscellaneous particle class.

After compositional classification, the particles in each class are size-segregated according to their measured aerodynamic diameters. The mass concentrations of each size and compositionally segregated particle ensemble are then determined using Equations 5.1 and 5.3. In this manner, a quantitative measure of the atmospheric aerosol mixing characteristics is obtained.

## 5.3 Results and Discussion

In this section, air quality model results are compared with aerosol measurements taken at Riverside, on September 25, 1996. First, model results at each hour of the day are compared with hourly, size-segregated measurements of aerosol mass, nitrate, and ammonium concentrations. Next, model results during 1500–1900 PDT are aggregated into very narrow particle size intervals, and compared with fine resolution measurements of aerosol mass, nitrate, and ammonium concentrations. Finally, model calculations of the absolute contributions of sea salt, dust, and carbonaceous particles to the size-resolved aerosol mass distribution are compared with corresponding measurements of the aerosol mixing characteristics at 1500–1900 PDT. The latter two comparisons are restricted to a 4-hour afternoon sampling period, because the ATOFMS measurements collected during that time period have been validated

against collocated impactor measurements, and thus, have greater absolute certainty than the ATOFMS measurements taken during other times of the day.

### 5.3.1 Temporal Resolution

Time series of size-segregated mass, nitrate, and ammonium concentrations are shown in Figure 5.1. Model results are compared with measurements in three aerodynamic particle diameter intervals ($D_a$ = 0.32–0.56 $\mu$m, 0.56–1.0 $\mu$m, and 1.0–1.8 $\mu$m), which correspond to the size intervals of aerosol samples collected with micro-orifice impactors during the field study. For reference, impactor measurements are plotted as horizontal gray bars, spanning the 4-hour time period when the size-segregated samples were collected. Atmospheric concentrations of the size-segregated particle ensembles analyzed by ATOFMS during each hour are quantitatively reconstructed using Equations 5.1–5.4, and plotted as solid lines in Figure 5.1, with error bars representing 95% confidence intervals. Model calculations of the atmospheric aerosol concentrations at Riverside are plotted as circles.

During the field study, the ATOFMS instrument was stationed inside an air conditioned laboratory, while drawing ambient air through a $\sim$ 5 m long sampling line at a 20 cubic centimeter per second flowrate. If at any time during sampling, the temperature and/or relative humidity inside the sampling line differed sufficiently from outdoor conditions, it would be possible for semivolatile molecules such as water vapor and ammonium nitrate to condense on or evaporate from the ambient particles before being analyzed by the ATOFMS instrument. The potential effects of a heated and/or dried sampling line (relative to ambient conditions) on modeled aerosol concentrations are depicted by squares in Figure 5.1. These simulations represent an extreme case in which all water is removed from the particles prior to sampling, and the aerosols are size-segregated according to their dry aerodynamic diameters. The vertical distances between the squares and circles plotted in the left column of Figure 5.1 approximately represent model calculations of the particle-bound water concentration in each size and time interval. In some cases, the reduction in particle size due to water removal

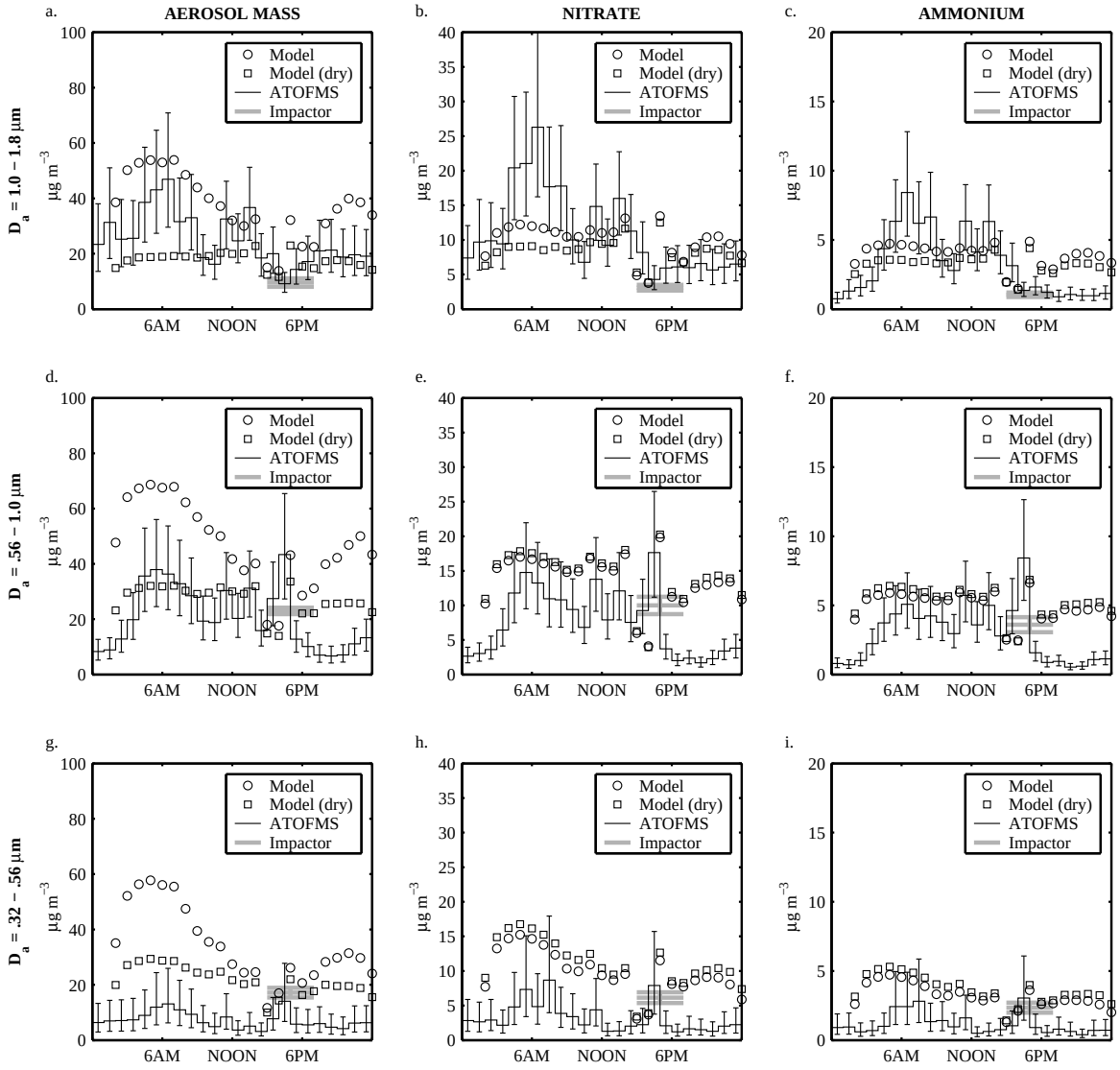


Figure 5.1: Model calculations versus ambient measurements of hourly resolved and size-segregated mass, nitrate, and ammonium concentrations at Riverside, on September 25, 1996. Error bars on the ATOFMS measurements represent 95% confidence intervals of the reconstructed aerosol data. Broad, gray error bars represent ± 2 standard deviations in the impactor measurements. Model results are plotted at both ambient (◯) and dried (□) mass concentrations.

is large enough to shift particles from one size interval to another, thereby influencing the size-segregated nitrate and ammonium concentrations as well (see second and third columns of Figure 5.1).

Figure 5.1a-5.1c displays model versus measurement comparisons in the 1.0–1.8 $\mu$m $D_a$ range. Model calculations of the ambient aerosol mass concentration in this size interval exhibit a diurnal trend very similar to the ATOFMS measurements, with peak concentrations in the morning and a concentration minimum in the late afternoon (see Figure 5.1a). Based on model calculations, this diurnal pattern is driven largely by the ambient relative humidity, which averaged 90% from 0200–1200 PDT, before dropping to 56% at 1600 PDT. In the morning hours, model results indicate that most of the 1.0–1.8 $\mu$m aerosol mass was composed of water. In the afternoon, model calculations show that the aerosol was almost devoid of water, resulting in reduced mass concentrations. ATOFMS measurements of 1.0–1.8 $\mu$m aerosol mass are in better agreement with the ambient aerosol model results than with the dried aerosol model calculations, suggesting that particles in the supermicron size interval were not significantly influenced by evaporation in the sampling line.

Model calculations of the nitrate and ammonium concentrations in 1.0–1.8 $\mu$m particles are in reasonable agreement with observations, falling within the 95% confidence intervals of the ATOFMS measurements during most of the day (see Figure 5.1b-5.1c). Notable exceptions are the morning peak in measured nitrate concentrations at 0400–0900 PDT and the nighttime decline in measured ammonium concentrations at 1800–2400 PDT, which are not displayed in the model results.

Figure 5.1d-5.1f displays comparisons in the 0.56–1.0 $\mu$m $D_a$ range. ATOFMS measurements of aerosol mass are in better agreement with dried aerosol model results than with the ambient aerosol model calculations, indicating that particles in this size interval may have been more influenced than the supermicron particles, by drying in the sampling line. This explanation is supported by the fact that smaller particles tend to equilibrate more quickly than large particles, when subjected to changing gas-phase conditions [146]. Model calculations of nitrate and ammonium concentrations in the 0.56–1.0 $\mu$m size range are in excellent agreement with ATOFMS measure-

ments throughout most of the day, exhibiting high concentrations from 0400–1400 PDT, followed by a sharp decline at 1500–1600 PDT, and a recovery at 1700 PDT. Model calculations reveal that this afternoon concentration oscillation is primarily due to changes in ambient meteorology. The maximum temperature and minimum relative humidity on September 25 ($T > 24°C$, $RH < 57\%$) were both experienced during the 1500–1600 PDT period, leading to evaporation of ammonium nitrate, water, and other semivolatile species, from the aerosol phase. By 1700 PDT, the ambient temperature began to decline and the relative humidity increased. These meteorological changes in conjunction with $N_2O_5$ production at sunset followed by hydrolysis to nitric acid, resulted in the observed increase in ammonium and nitrate concentrations at 1700 PDT. It is important to note that absent the continuous ATOFMS measurements taken during this time period, the afternoon oscillation in ammonium and nitrate concentrations would not have been observed, due to the 4-hour averaging period of the impactor measurements (see gray bars in Figure 5.1e-5.1f). After 1800 PDT, model calculations of aerosol mass, nitrate, and ammonium, exceed ATOFMS measurements by approximately a factor of three. The cause of this difference is still under investigation.

Figure 5.1g-5.1i displays comparisons in the 0.32–0.56 $\mu$m range. Once again, ATOFMS measurements of aerosol mass are in better agreement with dried aerosol model results than with the ambient aerosol model calculations, suggesting that a dried and/or heated sampling line may have biased the measurements. Model results in this size interval exceed ATOFMS measurements throughout the sampling period. During the 1996 field study, the ATOFMS instrument detected and analyzed fewer than ten out of every million ambient particles in the 0.32–0.56 $\mu$m size range [82]. Given this extremely low particle detection efficiency (which has been increased in recent years) and the resulting poor counting statistics, it is not surprising that the ATOFMS measurements in this size interval differ from model results by a factor of two or three. Ignoring the absolute difference in measured and modeled concentrations, it is interesting to note that the model calculations show an afternoon oscillation in 0.32–0.56 $\mu$m aerosol concentrations analogous to that observed in the

0.56–1.0 $\mu$m range, and this fluctuation is qualitatively matched by the corresponding ATOFMS measurements.

### 5.3.2 Particle Size Resolution

Finely resolved particle size distributions of aerosol mass, nitrate, and ammonium, during the 1500–1900 PDT intensive sampling period, are shown in Figure 5.2. Model results and ATOFMS measurements are aggregated into 15 particle size intervals spanning the 0.32–1.8 $\mu$m range. This representation illustrates that the size resolution of reconstructed ATOFMS data is roughly five times greater than that of traditional impactor measurements. If a longer sampling interval is used, the size resolution of ATOFMS measurements can be increased even further. As in Figure 5.1, model results are plotted under both ambient and dried conditions. The difference between the ambient and dry aerosol mass distributions shown in Figure 5.2a is indicative of the aerosol water content, which was fairly small, due to low relative humidities during this afternoon sampling period.

Peak concentrations in the aerosol mass, nitrate, and ammonium size distributions measured by ATOFMS, are all accurately calculated in the air quality model. Moreover, model calculations of the particle size interval that contains peak aerosol concentrations are within 0.1 $\mu$m of the ATOFMS measurements. Peaks in the ATOFMS size distributions at 0.7 $\mu$m are sharper and more pronounced than in the modeled distributions. This reflects the fact that the particle size resolution of the aerosol emissions inventories used as model inputs are coarser than the size resolution of measurements reconstructed from ATOFMS data. In the future, it may be possible to generate finer size resolution emissions inputs for model calculations, using quantitative measurements reconstructed from ATOFMS source characterization data.

Model results in the particle size range smaller than 0.5 $\mu$m exceed the corresponding measurements. The difference in modeled and measured aerosol mass concentrations in this size range is approximately equal to the sum of the excess nitrate and ammonium concentrations calculated in the model. It is possible that model results

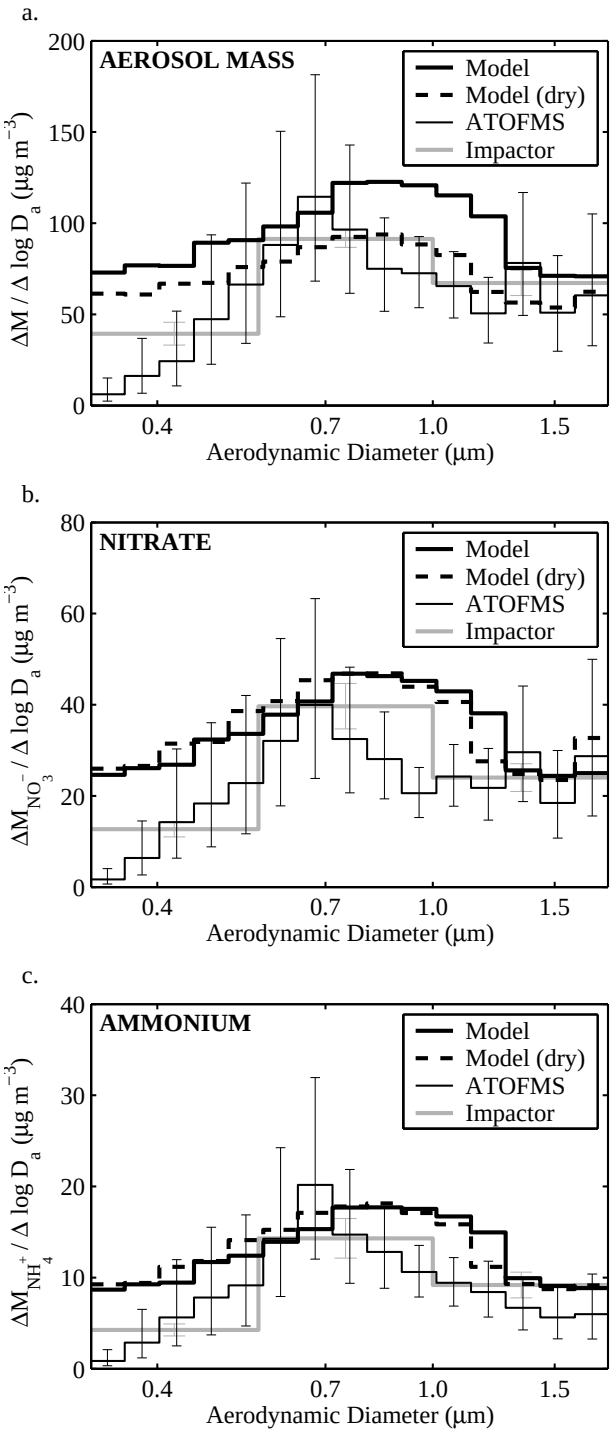


Figure 5.2: Model calculations versus ambient measurements of finely resolved particle size distributions of aerosol mass, nitrate, and ammonium concentrations at Riverside, on September 25, 1996, 1500–1900 PDT. Dark error bars on the ATOFMS measurements represent 95% confidence intervals of the reconstructed aerosol data. Gray error bars represent ± 2 standard deviations in the impactor measurements. Model results are plotted as ambient (solid line) and dried (dashed line) mass distributions.

overestimate the formation of $NH_4NO_3$ aerosol in the 0.32–0.5 $\mu$m range, or that measurements are biased low. As noted above, the quantitative ATOFMS measurements are obtained by comparing raw ATOFMS data with collocated impactor measurements, however, impactor measurements are subject to certain biases. The warm and dry atmospheric conditions encountered during the sampling period ($T > 24°C$, $RH < 57\%$) favor $NH_4NO_3$ volatilization from the impaction substrates [123]. Also, the effects of volatilization on impactor measurements are known to increase with decreasing particle size, because the lower impactor stages operate at reduced pressures [147]. Moreover, volatilization effects are enhanced on substrates with low aerosol loadings [124], such as the impaction substrate on which the 0.32–0.56 $\mu$m sample was collected. The data reconstruction procedure ensures that experimental errors which affected the impactor measurements are translated to the quantified ATOFMS measurements. Therefore, the ATOFMS data plotted in Figure 5.2 may be vicariously influenced by $NH_4NO_3$ volatilization from the impaction substrates. In the future, it may be possible to quantitatively reconstruct ATOFMS data without relying on collocated impactor (or other reference) measurements. Such an advancement, or the development of new instruments capable of quantitatively measuring size-segregated nitrate and ammonium concentrations without volatilization losses, might permit a more reliable evaluation of model results in the $D_a < 0.5$ $\mu$m range.

The maximum particle size resolution used in previous model evaluations of aerosol chemical composition was limited by the size-segregation capabilities of cascade impactors. The comparisons in Figure 5.2 exhibit five times greater size resolution than can be measured by traditional impactors, and this additional detail reveals that model calculations may not accurately capture the shape of the aerosol size distribution, particularly in the vicinity of the peak aerosol mass concentrations. Measurements taken using more recently developed aerosol mass spectrometers [148, 149] may provide an opportunity to extend the model comparisons shown in Figure 5.2 to smaller particle sizes in the future.

### 5.3.3 Aerosol Mixing State

Figure 5.3 displays a comparison of the modeled and measured aerosol mixing characteristics, during the 1500–1900 PDT intensive sampling period. The thousands of discrete particle types tracked in the air quality model are grouped into four categories, permitting a direct comparison with the size and compositionally categorized ATOFMS data to be made. Particles emitted as paved road dust or other crustal material are placed in the "dust" category. Particles that originated as sea spray droplets are placed in the "sea salt" category. Primary particles that were emitted from motor vehicle exhaust, meat cooking, or the combustion of high-sulfur fuels, are categorized as "carbonaceous." In addition, nonsea salt background particles are categorized as "carbonaceous," due to their high organic carbon content [55]. Particles emitted from other miscellaneous sources are placed in the "other types" category.

Figure 5.3b displays quantitatively reconstructed ATOFMS measurements of the aerosol mixing characteristics, in 15 size intervals spanning the 0.32–1.8 $\mu$m range. The ATOFMS measurements are compositionally segregated as described in Section 5.2.2.2. It should be noted that a mixing characteristics representation, such as that shown in Figure 5.3b, cannot be obtained using conventional bulk sampling techniques, such as filter or impactor-based measurements, because those techniques cannot differentiate the chemical compositions of individual particles collected on a substrate, and therefore cannot identify the relative contributions that different particle types make to a bulk or size-segregated aerosol sample. An aerosol representation like that shown in Figure 5.3b can only be obtained using single-particle techniques, such as ATOFMS. Figure 5.3 represents the first quantitative comparison of modeled and measured aerosol mixing characteristics.

In general, the agreement between the model results and measurements is very good. Model calculations accurately reveal that carbonaceous particles dominate the aerosol mass distribution throughout the .32–1.8 $\mu$m size range. ATOFMS measurements indicate that the mass concentration of dust particles is distributed evenly across the size range of interest, and is slightly elevated in the 1.3–1.8 $\mu$m range.

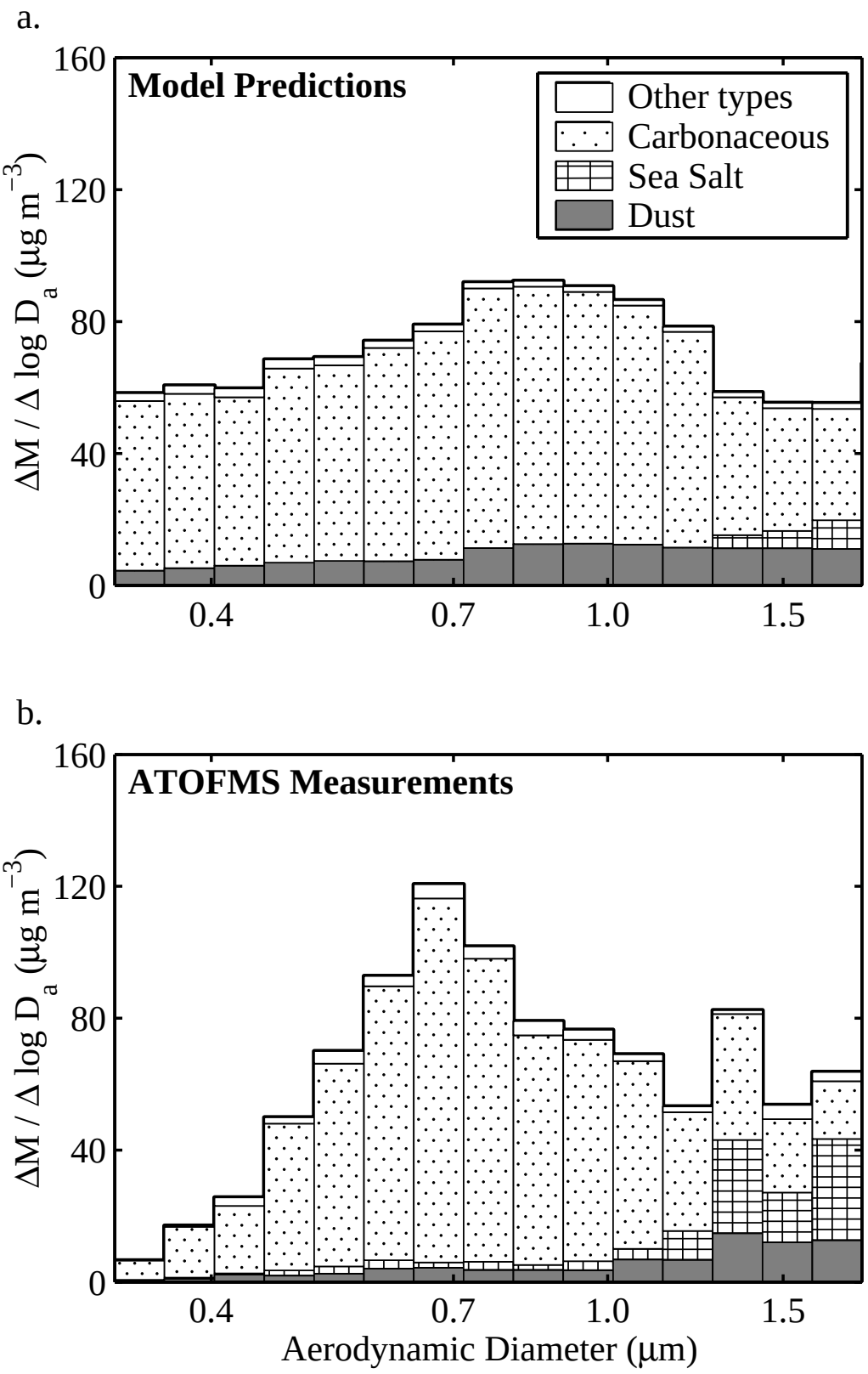


Figure 5.3: Model results versus ambient measurements of size-resolved aerosol mixing characteristics at Riverside, on September 25, 1996, 1500–1900 PDT.

Model results also show a fairly even distribution of dust particles, and the magnitude of the dust contribution matches the observed concentrations quite well. Finally, the contribution of sea salt particles to the aerosol mass distribution is observed to increase nearly monotonically with particle size, over the 0.4–1.8 $\mu$m range. Model calculations contain no sea salt in the $D_a < 1.3$ $\mu$m range, but the modeled sea salt concentration does exhibit a monotonic increase with particle size between 1.3–1.8 $\mu$m. The absence of sea salt particles in the model results below 1.3 $\mu$m is due to the assumed sea spray size distribution used as input to the model [55]. In future modeling studies, a more accurate, size-resolved representation of the sea spray source function may yield better agreement with the ATOFMS sea salt concentration measurements.

The bulk of the aerosol mass distribution shown in Figure 5.3 is made up of carbonaceous particles, which include primary particle emissions from a variety of combustion sources, as well as background particles advected into the air basin from over the Pacific Ocean. In the near future, results of single-particle source characterization studies may provide the information necessary to identify the primary emission sources of individual, atmospheric carbonaceous particles sampled by ATOFMS. Such source identifications can then be used to subdivide the carbonaceous particle class shown in Figure 5.3b, and ultimately evaluate model calculations of the absolute contributions that various emissions sources make to urban aerosols. This is discussed further in Section 7.2.3.

## 5.4 Conclusions

Calculations of a source-oriented air quality model have been evaluated against ambient aerosol measurements taken at Riverside, CA, on September 25, 1996. The aerosol data set includes continuous, quantitative, size-resolved measurements of particulate mass, nitrate, and ammonium concentrations, as well as quantitative measurements of atmospheric aerosol mixing characteristics. These measurements, reconstructed from collocated ATOFMS and impactor data, provide an opportunity to perform more detailed and stringent evaluations of aerosol air quality models than were pre-

viously possible. The hourly time series of size-segregated aerosol mass, nitrate, and ammonium concentrations, calculated using the model, exhibit diurnal trends comparable to the measurements. Measurements during a 4-hour intensive sampling period were aggregated into narrow particle size intervals to test model calculations of the detailed structure of the aerosol mass, nitrate, and ammonium distributions. Model calculations of the absolute contributions of sea salt, dust, and carbonaceous particles, to the size-resolved aerosol mass distribution were found to be in good agreement with the corresponding measurements. These model evaluations were performed at finer temporal and particle size resolution than in any previous study, and represent the first quantitative comparison of aerosol mixing characteristics measurements with source-oriented air quality model results.

# Chapter 6

# Source Apportionment of Fine Particulate Matter by Clustering Single-Particle Data: Tests of Receptor Model Accuracy

## 6.1 Introduction

The model-ATOFMS comparisons presented in Chapters 2 and 5 establish reasonable confidence that the air quality model calculations yield aerosol descriptions that are representative of atmospheric particle populations. In this chapter, the air quality model results are treated as synthetic single-particle data sets, and used to test methods for determining the sources of atmospheric particles. In order to deliberately control atmospheric fine particle concentrations, the relative influences of the various contributing sources must be known [150, 151]. Two approaches for identifying source contributions to atmospheric particle concentrations exist: source-oriented models and receptor-oriented models. While source-oriented models begin with emission rates and atmospheric transport calculations to estimate the ambient pollutant concentration increments due to each source, receptor-oriented models begin with ambient pollutant concentration data and seek to subdivide the particulate mass among

*This chapter is reproduced with permission from "Source Apportionment of Fine Particulate Matter by Clustering Single-Particle Data: Tests of Receptor Model Accuracy," by P. V. Bhave, D. P. Fergenson, K. A. Prather, and G. R. Cass; *Environmental Science and Technology*, 35: 2060–2072, 2001. Copyright 2001 American Chemical Society.

its different sources. Receptor-oriented models developed to date can be grouped into two basic categories, chemical methods and microscopic methods.

The fundamental principles of various chemical methods for receptor modeling, including chemical mass balance (CMB) and multivariate methods, have been reviewed in detail [152–157]. The first receptor modeling technique applied to ambient aerosol samples reported in the literature is a multivariate method using factor analysis [158] in which correlations between the concentration fluctuations of observed chemical species are used to determine groups of chemical elements that are transported together in nearly fixed proportions, indicating a common source. Factor analysis offers the advantage of not requiring prior knowledge of the chemical composition and size distribution of emissions from specific sources (i.e., source profiles) but has the drawback of being mathematically indeterminate, allowing a wide range of possible solutions even when applied to relatively simple simulated data sets [159]. It is uncommon to resolve contributions from more than six sources by factor analysis [156] and resolution of four primary sources is a more typical result. CMB models infer source contributions by determining the best-fit linear combination of measured source profiles needed to reconstruct the measured chemical composition of an atmospheric sample [160]. The number of resolvable sources using CMB models is strictly bound by the number of measurable chemical species in the ambient and emission source samples, although the number of sources actually resolved by CMB methods usually falls far short of that limit. Trace element-based CMB analyses seldom resolve more than six or seven sources [156] whereas organic compound-based CMB analyses have been shown to resolve up to nine or ten primary particle source types [161, 162].

Microscopic methods use the properties of individual particles and therefore have the potential to obtain a more thorough separation of the dozens of sources actually present in an urban atmosphere [156]. Initially, development of these methods was limited by the highly-skilled labor required to analyze each sample [156] and methods were difficult to standardize because source identification relied on the ability of the microscopist to recognize the source of each particle by comparison to libraries of standard particles from many sources [153]. Development of automated

single-particle analysis methods such as computer-controlled scanning electron microscopy (CCSEM) with X-ray detection have alleviated the need for highly skilled microscopists in some cases [31] and the application of neural network analyses to spectroscopy data has provided an automated method by which individual particles can be clustered into groups of similar particles [163]. Microscopic methods are still viewed as difficult and costly because many thousands of separate particles typically need to be processed following the actual field experiment, in order to characterize a single source or atmospheric sample.

Aerosol time-of-flight mass spectrometry (ATOFMS) and other on-line single-particle techniques provide a breakthrough in the level of particle description and speed of analysis which may make it possible to distinguish particles from different sources at the same time that they are measured in the atmosphere. Initially, ATOFMS presented the problem that data were acquired at a rate far exceeding the rate of data analysis by conventional methods [83]. More recently, the application of an adaptive resonance theory-based neural network algorithm (ART-2a) to ATOFMS data has been developed to rapidly cluster particles on the basis of their chemical content and apparent origin [127].

The purpose of this chapter is to determine the level of accuracy by which the ART-2a neural network algorithm can distinguish particles in the atmosphere from different sources. Source apportionment accuracy is determined by applying the neural network algorithm to a set of test cases consisting of synthetically created single-particle descriptions where each particle has a known source. These test cases range from the most realistic description of the ensemble of fine particles in an urban atmosphere that can be created given recent source test data and air quality models for the evolution of particles in the atmosphere, to test cases that mimic the way that these particles would be described if they had been sampled by an ATOFMS instrument. This method of receptor model evaluation is conceptually similar to that employed in the U.S. Environmental Protection Agency's Mathematical and Empirical Receptor Models Workshop (Quail Roost II) [164], with an added ability to create test cases consisting of single-particle descriptions that represent the effect of particle aging in

the atmosphere on particle size and composition.

## 6.2 Methods

### 6.2.1 Generation of Synthetic Single-Particle Data

A source-oriented Lagrangian trajectory model is used to generate synthetic data sets of source-segregated individual particles. The model formulation has been described in Section 2.2.1 and in the published literature [28, 30, 55, 64, 136]. The inputs to this model include discrete primary particle emissions at 15 different sizes spanning the 0.01–10 $\mu$m particle diameter range, with chemical composition that varies by particle size according to cascade impactor measurements of the most important emission sources. All like-sized particles emitted from the same source type during the same hour are tracked separately from all other particles in the model. In this manner, an external mixture of particles in the atmosphere is created in which all particles interact with the same gas-phase conditions, but differences in the size and composition of particles emitted from different sources are retained. In addition, the size and composition of aged particles differs from freshly emitted particles even though they may have been emitted from the same source [64]. Each particle tracked in the model is labeled according to the source type from which the particle core was initially emitted, thus tracking the original source of the particle at all times. The source categories tracked separately in the model include paved road dust, other crustal material, diesel engines, food cooking, catalyst-equipped gasoline-powered engines, non-catalyst gasoline engines, sulfur-bearing fuel and industrial sources, sea salt, non-sea salt background particles, and other miscellaneous sources. The model calculation yields a highly heterogeneous mixture of particle types that approximates the population of real particles encountered when an ATOFMS instrument extracts particles one at a time from the atmosphere [28].

The emission source profiles that describe particle chemical composition within the air quality model were expanded for use in the present study. Previous formulations

of the source-oriented externally mixed aerosol processes trajectory model tracked the chemical composition of individual particles in terms of the following chemical components: elemental carbon, organic compounds, sodium, chloride, ammonium, sulfite, sulfate, nitrate, iron (oxidation states II and III), manganese (oxidation states II and III), copper (oxidation states I and II), all remaining metals as a single group, and all other non-metallic species as a single group [28]. For the purposes of the present study, the model was extended to track the chemical composition of twenty-seven trace elements present to varying degrees in individual particles in addition to the chemical components mentioned above. All of the 110 source profiles used as inputs to the trajectory model were extended to include minor species measured in quantities greater than two analytical standard errors above zero during the original source tests [65, 66, 92, 165–168]. Iron, copper, and manganese remain in the model, but the lumped metallic and non-metallic species categories in previous formulations of the model are replaced by separate entries for aluminum, antimony, arsenic, barium, bromine, cadmium, calcium, chromium, cobalt, cesium, gallium, lead, magnesium, molybdenum, nickel, phosphorus, potassium, rubidium, selenium, strontium, tin, titanium, vanadium, silicon, silver, zinc, and zirconium. In previous model applications, the lumped metallic and non-metallic species were assumed to be nonreactive and this assumption is not modified in the current model extension. Figure 6.1 displays the detailed chemical composition, averaged over all fine particle sizes ($D_p \leq 2.5\mu m$), of the particles emitted from a few selected sources. The "other" material shown in Figure 6.1 is often oxygen associated with mineral elements such as aluminum and silicon.

In late September and early October, 1996, the Los Angeles Basin Trajectory Study was conducted to help evaluate results of the air quality model just described (see Section 1.2.3) [54, 85]. Instruments were stationed at Long Beach, Fullerton, and Riverside. The aerosol processes trajectory model was used to calculate the evolution of the ambient fine particle mixture along an air parcel trajectory path that passed just north of the Long Beach monitoring site at 1300 PST on September 24, 1996 and over the Fullerton monitoring site at approximately 1600 PST on September 24, 1996,

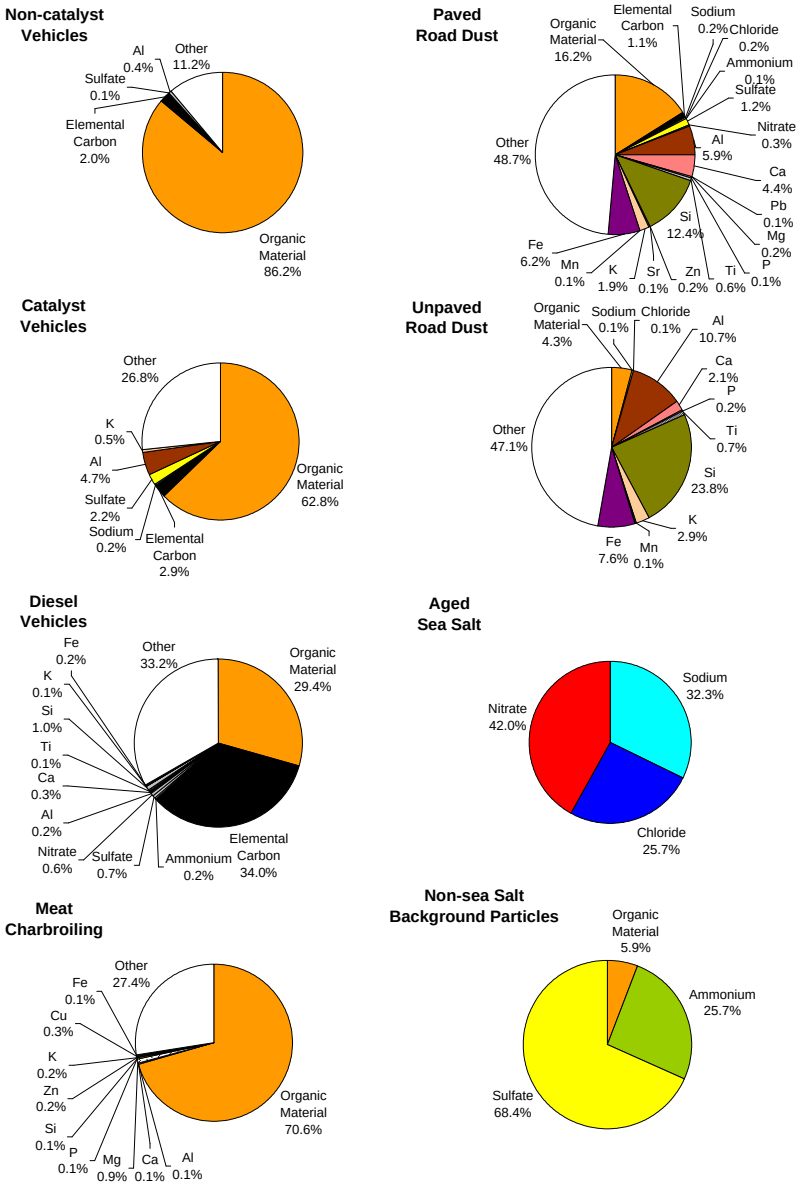


Figure 6.1: Chemical composition of fine particle emissions from major sources in southern California.

before terminating in Riverside on September 25, 1996 at 1600 PST (see Figure 2.2). Comparison of air quality model results to both filter-based and cascade impactor-based measurements of particle size distribution and bulk chemical composition show good agreement at all three air monitoring sites [55]. Furthermore, the studies described in Chapters 2 and 5 established some confidence in model calculations at the single-particle level.

Synthetic mixtures of chemically complex particles from known sources generated by the air quality model form an ideal test data set for determining the ability of neural network algorithms to identify and group particles that were originally emitted from the same source even after they have been altered by atmospheric processes. By simulating the accumulation of gas-to-particle conversion products including sulfates, nitrates, and organics, one can determine whether neural network algorithms are able to resolve the sources of the primary particle cores as the particles become coated with secondary aerosol conversion products over time. The air quality model calculations at Long Beach, Fullerton, and Riverside, provide three synthetic single-particle data sets. Each record within a data set contains the physical diameter of the particle, the mass concentrations of up to thirty-seven chemical components present in the particle, the source category from which the particle core was emitted, the age of the particle since the time of emission or entry into the study region, and the number concentration of atmospheric particles of the given size emitted during the same hour from the given emission source category. The data sets themselves are not included in this article because of their length (1791 particle descriptions at the Long Beach site, 2076 in Fullerton, and 3808 in Riverside).

### 6.2.2 Simulation of ATOFMS Data

The primary goal of the present study is to estimate the ability of the ART-2a neural network algorithm to group particles according to their original source using ATOFMS measurements of single-particle mass spectra. With the ART-2a neural network algorithm capable of chemically grouping particles at a rate that approaches the rate

of ATOFMS data acquisition [127], applying the algorithm as a receptor modeling tool potentially allows source attribution of particles in real-time as the particles are sampled from the atmosphere.

To estimate the ability of the ART-2a neural network algorithm to perform receptor modeling-based calculations using ATOFMS measurements, we first simulate how the three sets of synthetic data representing the Long Beach, Fullerton, and Riverside aerosol, would be described (both quantitatively and qualitatively) if they had been sampled by an ATOFMS instrument. ATOFMS instruments possess the ability to acquire either positive or negative ion mass spectra, as well as the ability to simultaneously analyze both positive and negative ions (dual ion mass spectra) from individual particles [75]. Depending on the instrument operating mode, certain chemical species are currently almost impossible to detect (e.g., sulfate in positive ion mode). Table 6.1 contains the intersection of the set of chemical components detectable by ATOFMS with the set of chemical components tracked in the aerosol processes trajectory model. To simulate ATOFMS measurements when operating in either unipolar or dual ion mode, the synthetic airborne particle data sets generated by the trajectory model are degraded such that they contain only the concentrations of species which are detectable in the mode of interest (designated by a non-zero entry in Table 6.1). In this manner, each of the synthetic single-particle data sets, representing the Long Beach, Fullerton, and Riverside aerosol at the indicated times of interest, are postprocessed to generate three separate receptor modeling test cases containing the molar concentrations of 22 (positive ion mode), 6 (negative ion mode), and 26 (dual ion mode) chemical components, respectively. Because the appropriate ion markers that allow one to distinguish between organic carbon and elemental carbon were not yet established at the time of this study, these separately tracked components are combined to simulate the carbonaceous peaks detected by ATOFMS. Currently, the smallest particle that is detectable by ATOFMS has a 0.2 $\mu$m aerodynamic diameter [75] and particles larger than 3.5 $\mu$m are typically lost in the instrument's inlet. Therefore, to further refine our simulation of ATOFMS measurements, synthetic particles with aerodynamic diameters smaller than 0.2 $\mu$m and greater than 3.5 $\mu$m are deleted from

the test cases.

#### 6.2.2.1 Quantitative ATOFMS Particle Descriptions

The sensitivity of ATOFMS instruments for detecting individual chemical components present in the mixed ambient aerosol varies dramatically from one chemical component to another. For example, recent laboratory work has demonstrated that ATOFMS instruments detect $Na^+$ in individual particles with 70 times greater sensitivity than $NH_4^+$ [87]. To simulate the effect of this variation in instrument sensitivity to different substances, one must rescale the mass concentrations of chemical components within each particle in the test cases to reflect the fact that some substances stand out clearly even when present at small concentrations within a single particle. Sensitivity factors for $NH_4^+$ and the Group I cations ($Li^+$, $K^+$, $Rb^+$, $Cs^+$) have been determined relative to $Na^+$ in the laboratory [87]. Sensitivity factors of $NO^+$ (an indicator ion for $NO_3^-$ during positive ion mode ATOFMS instrument operation) and $NH_4^+$ relative to $Na^+$ were estimated based on the comparison of side-by-side ATOFMS and cascade impactor measurements similar to that described in Chapter 3 [120]. Sensitivity factors for the remaining species listed in Table 6.1 relative to $Na^+$ are estimated based on the ionization potential and lattice energies of the species, along with practical laboratory experience [88]. For chemical species that are detectable in both positive and negative ion operating modes (e.g., nitrate, carbon), the greater of the two sensitivity factors is applied to the dual ion mode test cases. Converting the mass concentrations produced by the aerosol processes trajectory model to molar concentrations per particle, and then applying sensitivity factors to a test case results in a list of particles with increased apparent concentrations of chemical species whose sensitivity factors are greater than unity and decreased apparent concentrations of species whose sensitivity factors are less than unity.

After applying the estimated and experimentally determined sensitivity factors in the above manner, the synthetic particle data sets are further degraded to simulate the inability to detect species present at very low levels in particles due to interference from spectral noise. Instrument noise is simulated by discarding data for chemical

Table 6.1: Relative sensitivity factor estimates for species detected by ATOFMS instruments.

| | **Positive Ion Mode**[a] | **Negative Ion Mode**[a] | **Dual Ion Mode**[b] |
|---|---|---|---|
| Aluminum | 0.5[e] | | 0.5 |
| Ammonium | 0.014[c] | | 0.014 |
| Barium | 4.0[e] | | 4.0 |
| Calcium | 3.0[e] | | 3.0 |
| Carbon | 0.05[e] | 0.02[e] | 0.05 |
| Cesium | 7.9[c] | | 7.9 |
| Chloride | | 0.1[e] | 0.1 |
| Copper | 0.3[e] | | 0.3 |
| Iron | 3.5[e] | | 3.5 |
| Lead | 0.5[e] | | 0.5 |
| Magnesium | 0.8[e] | | 0.8 |
| Manganese | 0.5[e] | | 0.5 |
| Molybdenum | 0.5[e] | | 0.5 |
| Nitrate | 0.018[d] | 1.0[e] | 1.0 |
| Phosphorus | | 0.2[e] | 0.2 |
| Potassium | 5.1[c] | | 5.1 |
| Rubidium | 6.0[c] | | 6.0 |
| Silicon | | 0.2[e] | 0.2 |
| Silver | 0.09[e] | | 0.09 |
| Sodium | 1.0[c] | | 1.0 |
| Strontium | 20.0[e] | | 20.0 |
| Sulfate | | 0.35[e] | 0.35 |
| Tin | 0.5[e] | | 0.5 |
| Titanium | 0.35[e] | | 0.35 |
| Vanadium | 0.13[e] | | 0.13 |
| Zinc | 0.05[e] | | 0.05 |

[a]Non-zero entry indicates chemical species is commonly detected in the given single ion mode
[b]Greater of the single ion mode sensitivity factors is applied to dual ion mode test cases
[c]Determined from laboratory experiments [87]
[d]Determined from field experiments based on comparison with impactor measurements [89]
[e]Estimates based on ionization potential and laboratory experience [88]

species whose sensitivity-adjusted apparent molar concentrations are less than 2.0% of the sum of the apparent molar concentrations of all detectable species in the individual particle [90]. Discarded data which fall below the 2.0% noise level are replaced with zeros in the test cases.

The data transformation procedure just described in identical to the one used in Chapter 2 to perform the initial round of model-ATOFMS comparisons. In this manner, an approximation of how the synthetic atmospheric particles would be quantitatively described if they had been measured by an ATOFMS instrument in a format analogous to the peak lists described above. The application of relative sensitivity factors in the method described above does not account for so-called *matrix effects*. The detectability of certain chemical components is known to be dependent on the chemical composition of the given particle [106]. These matrix effects are not well quantified at this time so for the present study, sensitivity factors are applied uniformly to all particles regardless of the presence or absence of other chemical components which may affect the sensitivity of the ATOFMS instruments to the component of interest.

#### 6.2.2.2 Qualitative ATOFMS Particle Descriptions

In the absence of a current capability to quantify the exact amount of each chemical substance in individual particles, ATOFMS data often are reduced to the point where only the presence or absence of each chemical component in the particles is disclosed [85, 90, 138]. To simulate the ability of the ART-2a algorithm to cluster particles from sources when the particle contents are known only to the extent that an element is present or absent, selected test cases are produced by further degrading the quantitative approximations of ATOFMS data described above. In these selected test cases, chemical components with non-zero apparent molar concentrations are replaced with a value of "1" and the remaining components are given a value of "0." Therefore, for each of the three synthetic single-particle data sets (representing the Long Beach, Fullerton, and Riverside aerosol), a total of six test cases simulating ATOFMS measurements are created (3 operating modes: dual ion, positive ion, and

negative ion, each presented in two data formats: quantitative and qualitative).

### 6.2.3 Adaptive Resonance Theory-Based Neural Network

Adaptive resonance theory-based (ART) neural network algorithms were introduced as theoretical models describing selected aspects of the brain's classification behavior [169, 170]. They attempt to unite two contradictory behavioral features of the human brain: robust against outliers, but adaptive to slight changes and new knowledge. ART-based neural network algorithms are capable of solving complicated pattern recognition tasks by finding clusters of similar members among large populations with many variables. Most importantly, they have the ability to generate a new class in the event that a data point falls outside a preset proximity to all existing classes. ART-based neural networks have been used in a variety of practical applications [171] ranging from Chinese character classification [172] to chemical pattern recognition [173]. The most recent incarnation of the ART-based neural network is a particularly efficient algorithm called ART-2a [139]. The ART-2a neural network algorithm was previously used to identify particle classes on the basis of off-line CCSEM single-particle shape and elemental composition measurements [163, 174] as well as ATOFMS measurements of ambient aerosols sampled in real-time [127]. Recently, the ART-2a algorithm received use as a source apportionment tool for distinguishing particles from 2–3 different sources [175, 176]. The question posed by the present study is, "How accurate is the ART-2a algorithm in achieving source separation when supplied with ATOFMS measurements of ambient aerosols?"

General descriptions of the ART-2a algorithm appear elsewhere [139, 163, 174–176] so only a description focusing on its application to the synthetic single-particle data sets will be presented here. For the purposes of the present study, the ART-2a algorithm is used to identify various classes of particles based on their chemical composition. Ideally, each class of particles should represent particles from a different source or meaningfully related group of sources. To visualize a class, it is convenient to generate a "quintessential" particle which represents the class. The

set of quintessential particles is called the *weight matrix* and members of that set are referred to as *weight vectors*. *Particle vectors* are generated by normalizing the compositional description of each particle to unit length, using the Euclidean norm. Particles are selected in a random order and compared to each weight vector (by evaluating the dot product of the particle vector and the weight vector) until the weight vector with minimum Euclidean distance to the particle vector is found. If the dot product of the particle vector and the "winning" weight vector is greater than or equal to a predefined *vigilance parameter*, the particle is said to be in *resonance* with the weight vector and is assigned to the class which the winning weight vector represents. The winning weight vector is then shifted in the direction of the particle vector by a fixed amount called the *learning rate*. In this manner, the weight matrix is allowed to *adapt* in response to small changes in particle composition. If the dot product of the particle vector with the winning weight vector is less than the vigilance parameter, the neural network has discovered a *novelty* and that particle is considered to be representative of a previously unidentified class. When a novelty is encountered, the new particle vector is appended to the weight matrix. Particles are selected, one at a time, until all are classified. Maintaining the weight matrix between iterations, this process is repeated, allowing the weight vectors to nucleate classes of increasingly similar particles from one iteration to the next. After a given number of iterations or *training cycles*, the particle classification is complete.

The ART-2a algorithm can be adjusted to yield many or few particle classes, depending on the predetermined value of the vigilance parameter. A vigilance parameter of 1.0 will yield a separate class for each individual particle, whereas a vigilance parameter of 0.0 will place all particles into a single class. In a previous study, a vigilance parameter of 0.70 was found to be appropriate in classifying particles of marine origin [127] and hence is used as the baseline for this study. A perturbation analysis of the value of the vigilance parameter is conducted, as will be discussed in Section 6.3.2. All ART-2a runs in this study used 40 training cycles with a learning rate of 0.05. The ART-2a algorithm is coded in Matlab (The MathWorks, Natick, MA) and executed on an IBM-compatible microcomputer.

### 6.2.4 Receptor Modeling Procedure

To determine the utility of the ART-2a algorithm as a receptor modeling tool, the analyst applied the neural network classification algorithm to each of the test cases described. During the tests that follow, the operator of the ART-2a computer program (D. P. Fergenson) was not given any information on how the test cases were generated. He was completely blind to the knowledge of which time and geographic location was represented by a particular test case so that he could not use this knowledge to judge the quality of his answers. Further, the chemical species in the particles were concealed and presented in an unknown order that varied from data set to data set. The source of each particle core and the age of each particle since the time of emission or entry into the study region were not disclosed to the analyst. Particle size information also was omitted from the test cases provided to the analyst, because it was unclear how much weight the particle size data should be given relative to the chemical composition information in the neural network algorithm. Finally, the test cases themselves were shuffled and renamed so that the analyst could neither distinguish which monitoring site (Long Beach, Fullerton, or Riverside) a particular set of particles represented, nor whether the test case contained direct unaltered trajectory model descriptions of atmospheric particles or a simulation of ATOFMS data, nor in the latter case, which ATOFMS operating mode (positive, negative or dual ion) was being simulated. The only test case feature apparent to the analyst was whether the chemical composition information contained therein was qualitative or quantitative. At the end of the ART-2a classification process, the ART-2a class assigned to each particle was reported to the operator of the air quality trajectory model (P. V. Bhave) who then compared the ART-2a classification of each particle to the known source of the particle as documented by the trajectory model.

Preliminary testing of the ART-2a algorithm revealed that species which are present at trace quantities in the particles have minimal influence on the classification results. This feature of the algorithm hinders its ability to classify particles based on their source because many of the conservative trace elements, when present

in particles, make up a very small fraction of the particle mass (see Figure 6.1). In order to give all chemical species roughly equal weight in the classification algorithm, each chemical component concentration in a given test case was transformed to have zero mean and unit variance ($z$-transformation), and range scaled such that all values of the given chemical component lay between 0 and 1. This pretreatment method is applied to all test cases containing quantitative particle descriptions before presenting them to the analyst and has been used in previous applications of the ART-2a algorithm for the classes of individual particles [175]. Test cases containing qualitative particle descriptions are unaffected by this transformation. Application of this pretreatment method to real ATOFMS data presents the potential risk of magnifying spectral noise in the case where an occasional noise peak extends above the noise rejection threshold and therefore should be exercised with caution.

## 6.3 Results and Discussion

### 6.3.1 Source-Oriented Air Quality Model Results

The upper row of Figure 6.2 summarizes the bulk properties of the aerosol trajectory model results from which the synthetic atmospheric particle data sets were generated. The subplots of Figure 6.2 are positioned in columns, from left to right, in the order of increasing time that the air parcel spent traveling over the urban area before reaching the given monitoring site. Based on trajectory calculations using interpolated wind fields [68, 74], the air parcel studied here spent 20 hours above the urban area before reaching the Long Beach monitoring site from the west, 23 hours before reaching the Fullerton site, and 45 hours before reaching Riverside. Particle mass concentrations increase during transport across the air basin, with the highest particle concentrations present at Riverside, the furthest inland monitoring site. Changes in particle origin and mass concentration are modest between Long Beach and Fullerton, and much larger between Fullerton and Riverside. The sharp increase in mass concentration between the latter pair of monitoring sites reflects the accumulation of both primary

and secondary particulate matter in the Lagrangian air parcel during its 23 hour travel time from Fullerton to Riverside. $PM_{2.5}$ concentrations calculated using the model are 42.2 $\mu g/m^3$ in Long Beach, 52.2 $\mu g/m^3$ in Fullerton, and 131.4 $\mu g/m^3$ in Riverside. These values are slightly larger than the model results tabulated in reference [55, Table 2] because these are modeled concentrations at a single time in the afternoon rather than 24-hour average concentrations. Note that the vertical axis scale in the Riverside subplots is significantly larger than that used in the Long Beach and Fullerton subplots, for the purpose of readability.

Each bar in the upper panels of Figure 6.2 represents the ambient $PM_{2.5}$ concentration increment contributed by particles whose initial core originated from a given emission source category, as calculated using the aerosol processes trajectory model. Non-sea salt background particles, largely sulfate particles advected into the air basin from over the Pacific Ocean and transformed by gas-to-particle conversion processes occurring in the urban atmosphere, are calculated to make the largest contribution to $PM_{2.5}$ concentrations at all three sampling sites during the indicated times of interest. Much of the increase in mass associated with background sulfate particles is due to ammonium nitrate accumulation over time on these hygroscopic particle cores. Sea salt particles, which are injected into each trajectory air mass when crossing the surf zone at the coastline, once transformed by atmospheric reactions constitute the second largest source contribution to $PM_{2.5}$ concentrations at each site during the times of interest. The relative importance of particles having primary cores from other source categories to the $PM_{2.5}$ mass concentrations depends on the location of the sampling site within the air basin. Particles emitted from diesel engines and from the combustion of sulfur-bearing fuel are prominent in Long Beach and Fullerton at the indicated times. The contribution from crustal material other than paved road dust is shown to increase substantially between Fullerton and Riverside, becoming the single largest non-background source of fine particle mass in Riverside; whereas crustal material is shown as one of the smallest contributors to $PM_{2.5}$ concentrations in the Long Beach subplot. This reflects the drier and dustier soil conditions as well as the lower proportion of paved road surface in the agricultural Riverside area com-

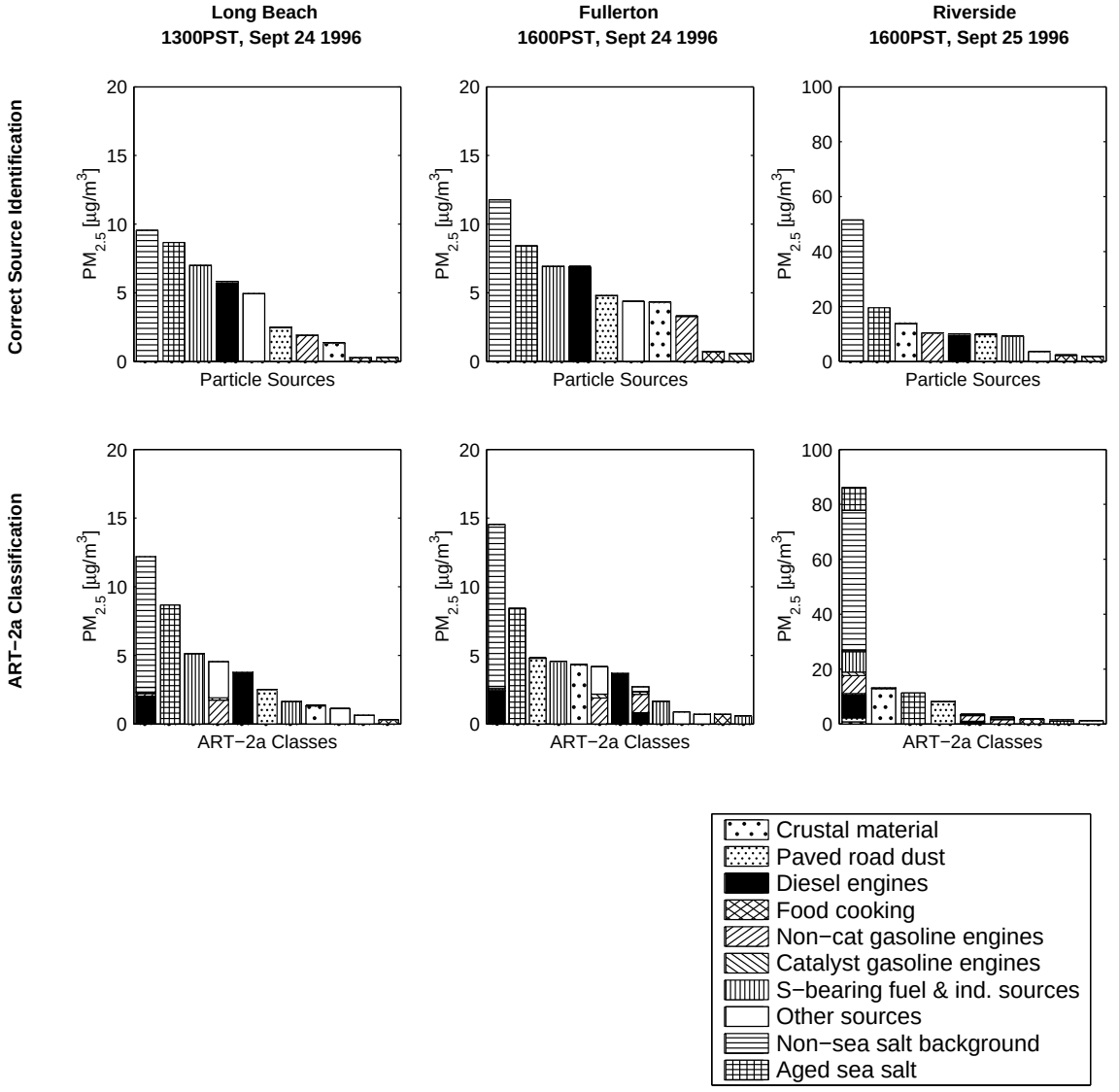


Figure 6.2: ART-2a classification when complete chemical composition data for each particle are supplied directly from the air quality trajectory model. The top panels show the mass concentration of particles within the trajectory model that have primary particle cores emitted from the specific sources shown (the "correct answer"). The lower panels show how the ART-2a algorithm assigns the same particles to separate source classes.

pared to the conditions of the near coastal plain. Particles whose cores were emitted from food cooking and catalyst-equipped gasoline-powered motor vehicles, on the other hand, make relatively small contributions to the total $PM_{2.5}$ concentration at all three monitoring sites during the times of interest.

### 6.3.2 Source Apportionment Accuracy Given Maximum Compositional Detail

The first test of the ART-2a algorithm attempts to simulate how well this source apportionment procedure could work if given essentially complete information on each atmospheric particle. The air quality trajectory model is exercised with particle emissions from 10 separate source types. The fully quantified chemical description of every particle tracked by the air quality trajectory model then is supplied to the ART-2a analyst with no rescaling or other attempt to simulate how ATOFMS instruments would measure each particle. The lower panels of Figure 6.2 display the classification results of the ART-2a algorithm based on this most complete and realistic description of the ensemble of fine particles that can be calculated using air quality models given recent source test data. Each bar within the lower panels of Figure 6.2 represents a particle class ("source") isolated by the ART-2a algorithm. The masses of individual particles in each particle class are added together such that the height of each bar corresponds to the $PM_{2.5}$ concentration in the ART-2a class. The number of bars in each subplot (11 in Long Beach, 13 in Fullerton, and 9 in Riverside) reflects the number of ART-2a classes containing at least 0.5% of the total $PM_{2.5}$ concentration at the given site. To facilitate the present discussion, the bars of each subplot will be referred to as Class 1, Class 2, Class 3, etc., in the order of decreasing $PM_{2.5}$ mass concentration. The source of the primary particle cores of those particles falling into each class are represented by different shading patterns in Figure 6.2, to illustrate how the neural network algorithm classifies particles originating from each of the 10 real source categories present. A bar shaded with more than one pattern indicates that the ART-2a algorithm is unable to distinguish particles originating from multiple

emission source categories. Appearance of the same shading pattern in more than one bar indicates that particles from a single source are being mistakenly placed into multiple classes. If the neural network algorithm were able to correctly differentiate all ambient particles according to the emission source of their primary particle cores, the lower set of subplots would appear identical to the upper row of subplots in Figure 6.2.

ART-2a classification results in Figure 6.2 illustrate that identification of the source of the primary core of individual particles becomes increasingly difficult as one moves downwind of an urban area, even when given essentially complete information on each atmospheric particle. Near the coastline, the ART-2a algorithm is able to isolate particles from the majority of the different source categories actually present. Of course, an analyst will know only the chemical composition of the particle clusters created but not the names of the source categories represented by each cluster, and therefore must be careful to interpret the source identities correctly by reference to source profile data available in the scientific literature and appropriate ion marker combinations obtained from single-particle source characterization studies. At the far inland Riverside site, particles from different sources become virtually indistinguishable from one another because they have reacted with a common gas phase over a period of 30–40 hours, thereby becoming coated with gas-to-particle conversion products that disguise the initial differences between the particles at their source. Figure 6.3 provides a detailed description of the chemical features of the particles that are grouped into each ART-2a class, along with information on the sources that contributed the primary cores of the particles in each group. The vertical axis of each subplot in Figure 6.3 is linearly scaled, ranging from zero to one, indicating the relative mass concentrations of selected chemical components present in each ART-2a particle class. The mass concentrations of trace species are summed together and represented by the bar labeled "trc."

When applied to the Long Beach data set, the ART-2a algorithm performs as a fairly accurate receptor-oriented model. The algorithm successfully isolates particles originating from sea salt (Class 2), paved road dust (Class 6), crustal material (Class

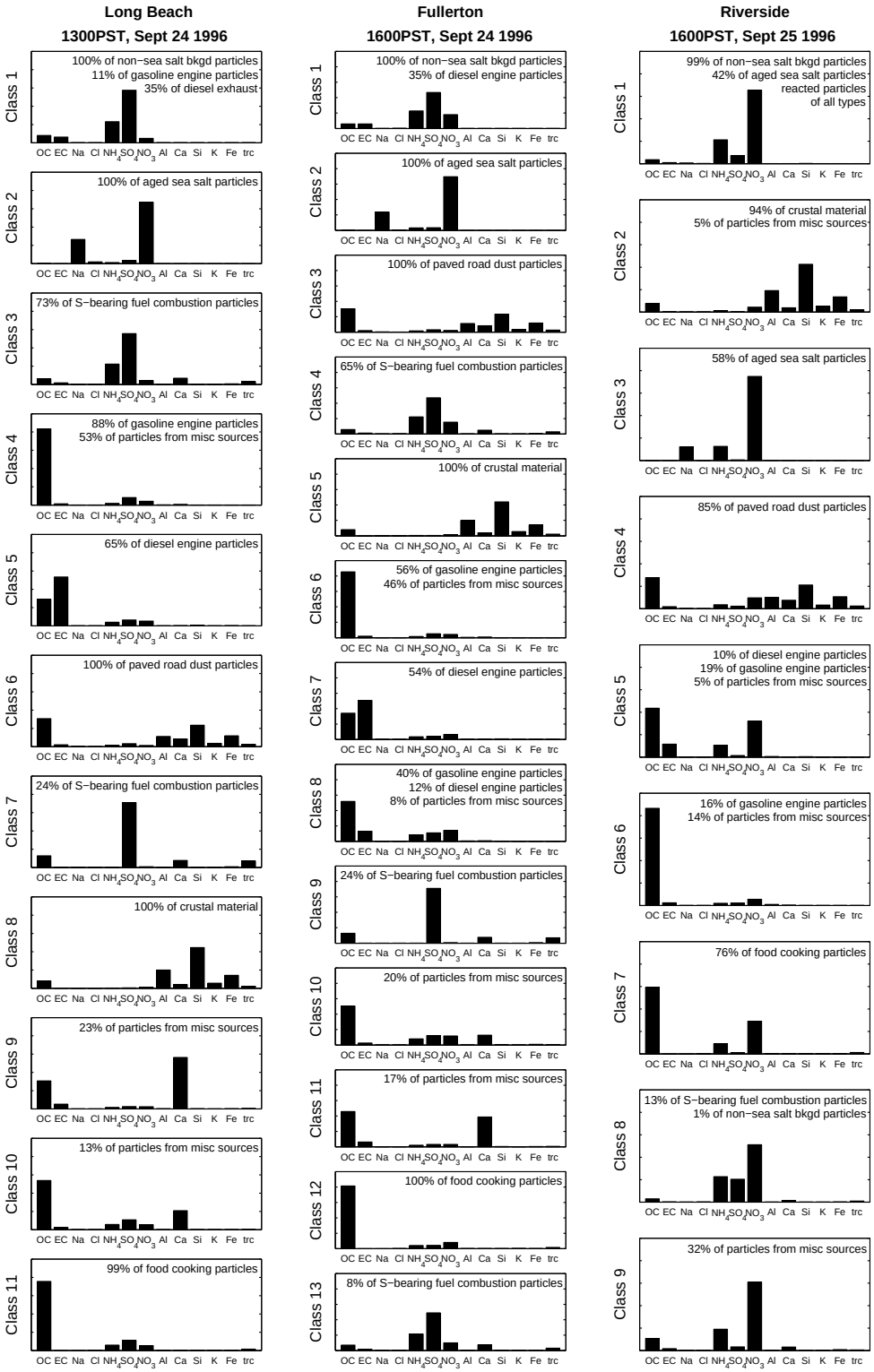


Figure 6.3: Chemical composition of ART-2a particle classes generated from source-oriented model results with maximum speciation.

8), and food cooking emissions (Class 11), into distinct particle classes. Particles emitted from the combustion of sulfur-bearing fuel and other industrial sources are also correctly isolated from all other source categories, but the ART-2a algorithm separates these particles into two classes (Classes 3 and 7). The left-hand column of Figure 6.3 reveals the reason for this separation. Class 7 particles at Long Beach primarily consist of sulfate, organic compounds, calcium, and other trace species. In addition to these chemical components, Class 3 particles at Long Beach contain significant mass contributions from ammonium and nitrate, indicating that the Class 3 particles have undergone further transformation by gas-to-particle conversion processes than the Class 7 particles. The ART-2a algorithm also separates particles emitted from diesel engines at Long Beach into two classes (Classes 1 and 5). The source-oriented air quality trajectory model results reveal that diesel particles in Class 5 at Long Beach have an average atmospheric age of 7.4 hours since emission to the atmosphere, whereas Class 1 diesel particles at that site on average have been transported through the urban atmosphere for 12.2 hours. Figure 6.3 illustrates that Class 5 diesel particles are primarily composed of organic compounds and elemental carbon. The aged diesel particles in Class 1 on the other hand, contain substantial quantities of secondary reaction products including ammonium, sulfate, and nitrate. Because particles emitted from catalyst-equipped gasoline engines and non-catalyst gasoline engines have similar chemical source profiles (see Figure 6.1), the particles emitted from all gasoline-powered motor vehicles at Long Beach are lumped together by the ART-2a algorithm. Gasoline-powered motor vehicle emissions at Long Beach are found primarily in Class 4, and contribute a small fraction of the Class 1 particle mass as well. Particles from other sources that are not separately tracked by the air quality model are found primarily in Classes 4, 9, and 10 at Long Beach. The ART-2a algorithm groups all of the non-sea salt background particles at Long Beach into Class 1. This class also contains reacted diesel particles as well as minor contributions from aged particles that were originally emitted from gasoline-powered vehicles, paved road dust, and the combustion of sulfur-bearing fuel.

When operating on the particle descriptions generated by the source-oriented air

quality trajectory model results at Fullerton, the ART-2a algorithm once again successfully separates particles originating from sea salt (Class 2), paved road dust (Class 3), crustal material (Class 5), and food cooking (Class 12). Class 1 at Fullerton contains those particles which have accumulated the largest quantities of secondary aerosol reaction products. This class includes all of the non-sea salt background particles as well as heavily transformed particles from various other sources. Particles emitted from diesel engines are found in Classes 1, 7, and 8, and have average ages since emission to the atmosphere of 12.9, 6.9, and 4.9 hours, respectively. Particles emitted from the combustion of sulfur-bearing fuel and other industrial sources also are assigned to three distinctly different particle classes (Classes 4, 9, and 13) at Fullerton. Particles emitted from gasoline-powered motor vehicle engines are primarily assigned to two classes in the Fullerton data set (Classes 6 and 8). The separation of diesel exhaust particles and sulfur-bearing fuel combustion emissions into three separate classes in the Fullerton data set (as opposed to two classes in Long Beach) and the separation of gasoline-powered motor vehicle emissions into two particle classes in the Fullerton data set (as opposed to a single class in Long Beach) illustrates an important effect of atmospheric aging on particle composition. Particles that were originally emitted from a single source category at different points along the air parcel trajectory evolve to have chemical compositions that are sufficiently different from one another such that multiple particle classes are created by the ART-2a algorithm. The effects of atmospheric aging on particle size and chemical composition are described in detail by Kleeman and Cass [64].

When supplied with the most complete particle descriptions produced by the source-oriented air quality trajectory model at Riverside, the source apportionment accuracy of the ART-2a algorithm is greatly reduced relative to the success encountered when operating on the Long Beach and Fullerton data sets (see Figure 6.2). When applied to the Riverside data set, the ART-2a algorithm places 65.5% of the $PM_{2.5}$ mass concentration into one particle class. As shown in Figure 6.3, Class 1 particles at Riverside primarily consist of ammonium and nitrate, with small amounts of sulfates and organics. The largest contributors to the Class 1 particle mass at

Riverside began as non-sea salt background particles, which originally consisted of ammonium, sulfate, and organic compounds, and which accumulated secondary organics and ammonium nitrate while being transported across the polluted air basin. In addition, Class 1 at Riverside contains 42% of the fine particle mass originating from aged sea salt particles. The remainder of the aged sea salt particles are found in Class 3, as the ART-2a algorithm easily identifies most sea salt particles based on their large sodium content (see Figure 6.3). The ART-2a algorithm is unable to identify the source of Class 1 sea salt particles because they have submicron diameters, such that their relatively low sodium content is overwhelmed by accumulation of secondary ammonium nitrate on their relatively large surfaces. Aside from the aged sea salt particles and non-sea salt background particles advected into the study region from over the Pacific Ocean, Class 1 at Riverside contains particles originating from vehicle emissions, crustal material, paved road dust, food cooking emissions, the combustion of sulfur-bearing fuel, and other sources which are not separately tracked by the model. Class 1 particles originating from these continental sources all have undergone significant chemical transformations as a result of gas-to-particle conversion processes. Among the continental particle sources, paved road dust and crustal material are the least readily transformed by gas-to-particle conversion processes because their initial particle cores are relatively large and hydrophobic (see Figure 6.1). As a result, the ART-2a algorithm correctly isolates most particles that were originally emitted from sources of crustal material (Class 2) and paved road dust (Class 4). Smaller particles such as diesel and gasoline engine exhaust particles, which dominate the aerosol surface area distribution and which in some cases (e.g., sub-micron sea salt and non-sea salt marine background particles) have hygroscopic cores, are readily transformed by gas-to-particle conversion processes and can become virtually indistinguishable from one another by the time that they reach Riverside.

A perturbation analysis of the vigilance parameter ($0.7 \pm 0.2$) provided some insight regarding the impact of vigilance parameter selection on ART-2a source apportionment accuracy. Reducing the vigilance parameter to 0.5 combined the crustal material and paved road dust particles into a single class at all three sites and resulted

in poorer classification of the particles arriving at Riverside. Increasing the vigilance parameter to 0.9 split classes of particles that originated from a single source into multiple classes, without noticeably improving the source separation obtained during the baseline experiments.

### 6.3.3 Source Apportionment Accuracy Based on Simulated ATOFMS Data

Figure 6.4 shows the ART-2a algorithm classification results obtained when operating on test cases that simulate qualitative ATOFMS data in which the particles are described by the presence or absence of a particular chemical substance without any information on the relative amount of each substance. The top panel of Figure 6.4 displays the mass concentration associated with particles having a primary core emitted from the indicated sources (the "correct" source identification) and the lower three panels display the ART-2a classification results based on the positive, negative, and dual ion mode test cases. The source-oriented trajectory model results shown in the upper panel include all particles with physical diameter less than 2.5 $\mu$m. Certain high density particles with physical diameters of circa 2.0–2.5 $\mu$m and larger are excluded from the ATOFMS data simulations if their aerodynamic diameters exceed the 3.5 $\mu$m aerodynamic diameter detection limit of the ATOFMS instruments. For this reason, summations of the fine particle mass concentrations displayed in the lower panels of Figure 6.4 are slightly smaller than the total $PM_{2.5}$ mass concentrations displayed in the top row of subplots for the corresponding locations and times.

When supplied with qualitative particle descriptions from simulated ATOFMS dual ion mode measurements, the ART-2a algorithm is fairly successful at classifying particles into the correct number of source categories at Long Beach (see lower left panel of Figure 6.4). With dual ion mode capability, diesel emissions are classified separately from the sulfur-bearing fuel combustion particles in both Long Beach and Fullerton. This separation occurs because sulfates are detectable in the dual ion mode and the sulfate content of most diesel exhaust particles falls below the 2%

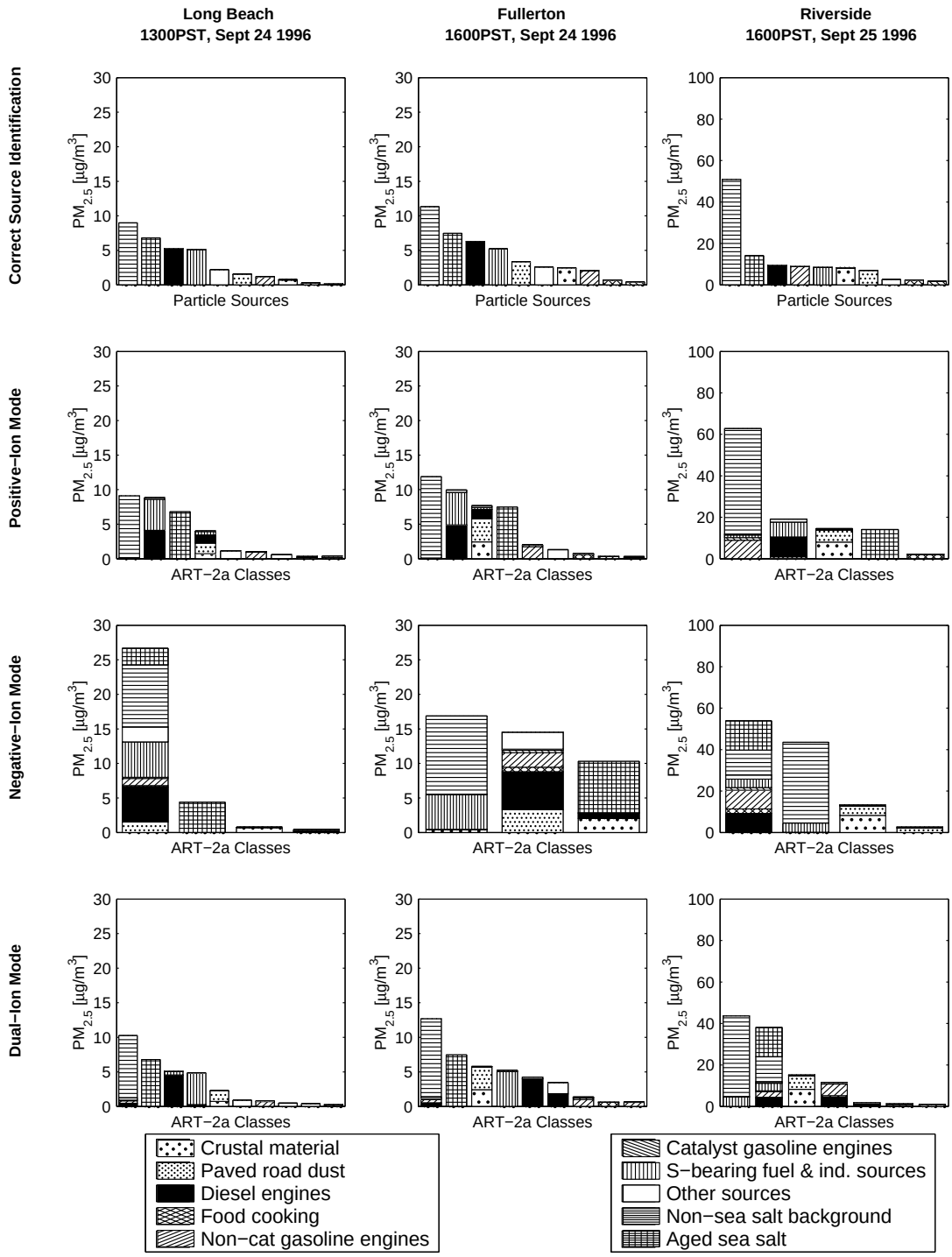


Figure 6.4: ART-2a particle classification based on test cases that simulate qualitative particle composition data showing the presence or absence of chemical substances detected in three ATOFMS operating modes. The top row describes the correct identification of the sources from which the primary core of each particle was emitted and the lower three rows show how the same particles are sorted into source categories by the ART-2a neural network algorithm.

noise threshold, whereas the sulfur-bearing fuel combustion particles contain a large quantity of sulfates. The dual ion mode capability also permits the ART-2a algorithm to separate paved road dust and crustal material particles from other particle sources at all three monitoring sites. This separation is possible because silicon is detectable in the dual ion mode, and silicon is present above the noise threshold only in paved road dust and crustal material particles. The source apportionment accuracy of the ART-2a algorithm grows progressively worse between Long Beach and Riverside for all three ATOFMS operating modes, due to the effects of aging on particle composition discussed above. Among the three ATOFMS operating modes, negative ion mode test cases yield the least amount of particle composition information (6 chemical components) and hence result in the poorest source apportionment. Operating on the qualitative negative ion mode test cases, the ART-2a algorithm is unable to isolate particles from any source category into a single class. The qualitative positive ion mode test cases yield better results. In the Long Beach and Fullerton positive ion mode data simulations, the ART-2a algorithm successfully isolates non-sea salt background particles, aged sea salt particles, particles from gasoline-powered vehicles, and food cooking particles, into separate classes.

Figure 6.5 illustrates the level of source apportionment accuracy that might be attainable if the ART-2a algorithm were applied to ATOFMS data that quantitatively conveyed the varying heights and areas of the peaks in the mass spectra of each particle rather than reducing the particle compositions to a qualitative statement of the simple presence or absence of each detectable chemical substance. Overall, these results appear to be quite similar to the results shown in Figure 6.4 when processing purely qualitative particle descriptions although a few key differences exist. For all three ATOFMS operating mode test case results shown in Figure 6.5, the ART-2a algorithm is able to consistently differentiate the grouped combination of paved road dust and crustal material from particles emitted from all other sources when given quantitative information on peak areas. Operating on the qualitative particle descriptions, this separation is only possible given dual ion mode data (see Figure 6.4). In two cases shown in Figure 6.5 (Fullerton positive ion mode and Long Beach dual ion

mode), the ART-2a algorithm is further able to distinguish paved road dust particles separately from other crustal material.

Applying the ART-2a algorithm to quantitative ATOFMS data also has drawbacks however. When the ART-2a algorithm is applied to quantitative ATOFMS data, non-sea salt background particles are no longer classified separately from sulfur-bearing fuel combustion particles (compare Figures 6.4 and 6.5). Similarly, classification of particles based on simulated ATOFMS data in which peak areas are quantified results in particles from gasoline-powered engines being lumped together with diesel engine particles, whereas the ART-2a algorithm is able to distinguish particles from these sources when provided with qualitative data. This effect results from the fact that creation of qualitative data in which only the presence or absence of each chemical substance is noted greatly increases the relative importance of trace elements while suppressing differences between particles that occur as particles of different ages accumulate differing amounts of gas-to-particle conversion products. In the future, it may be possible to combine the strengths of both qualitative and quantitative descriptions of the ATOFMS data.

## 6.4 Conclusions

The source apportionment accuracy of a neural network algorithm (ART-2a) was tested based upon its application to synthetic single-particle data generated by a source-oriented aerosol processes trajectory model that simulates particle emission, transport, and chemical reactions in the atmosphere. The ART-2a algorithm successfully groups particles from the majority of sources actually present when given complete data on ambient particle composition at monitoring sites located near the emission sources. As particles age in the atmosphere, accumulation of gas-to-particle conversion products can act to disguise the source of the primary core of the particles. When single-particle data are modified to simulate the biases in ATOFMS measurements, the source apportionment accuracy of the method is reduced. This result demonstrates a general necessity of understanding the impacts of measure-

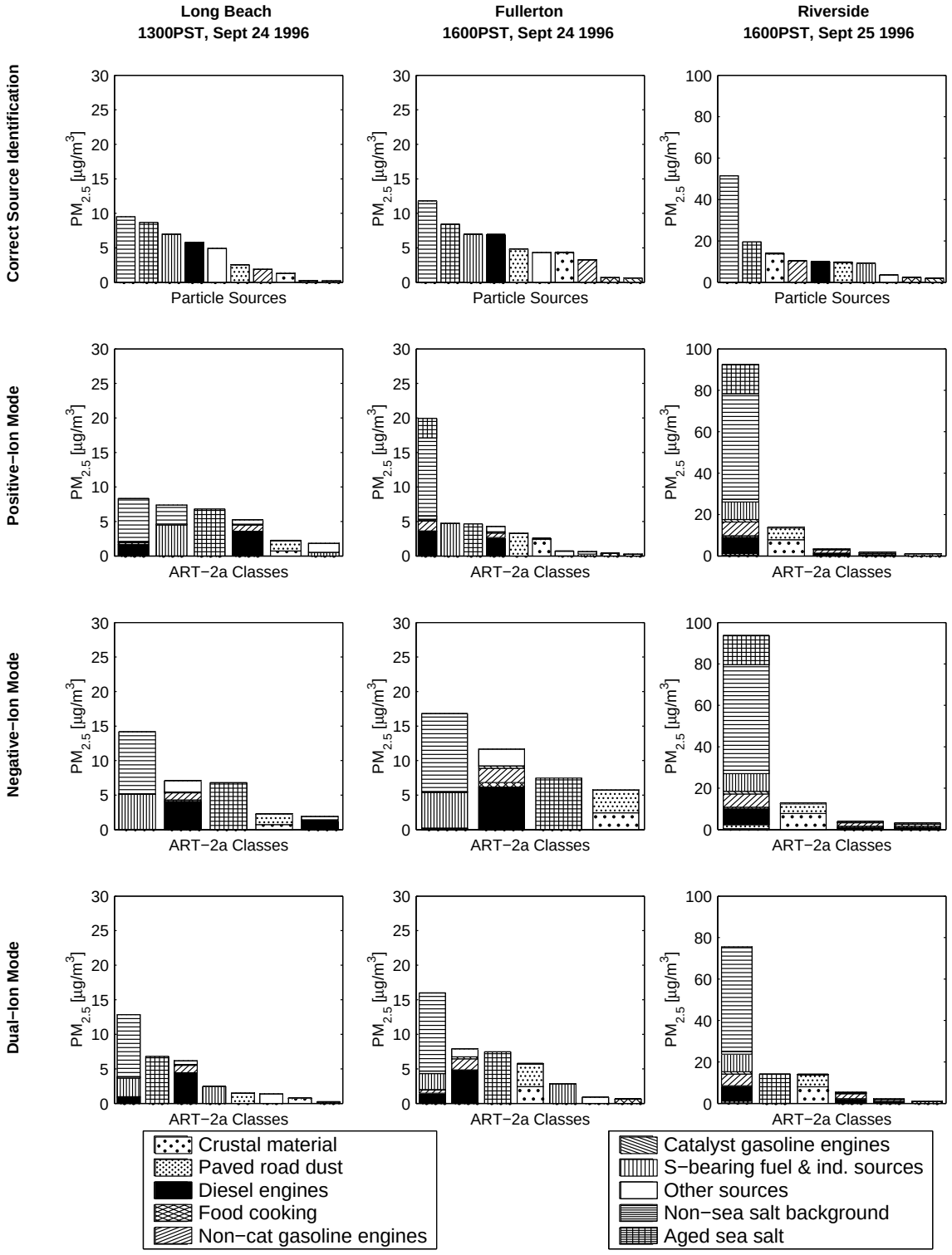


Figure 6.5: ART-2a particle classification based on test cases simulating quantitative particle composition data obtained in three ATOFMS operating modes. The top row contains correct source identification and the lower three rows are the ART-2a classification results.

ment methods on data analysis. When simulated ATOFMS data are classified by the ART-2a algorithm, the best source apportionment results are obtained for dual ion mode data. In the future, it may be possible to devise an algorithm that places greater importance on the presence or absence of specific trace species which are unique to certain emission sources or an algorithm with a built-in bias against secondary aerosol components (e.g., sulfates, nitrates) that otherwise may disguise the primary source of the particles. If properly executed, such algorithms may overcome the difficulty of identifying the original sources of individual particles that have undergone significant accumulation of gas-to-particle conversion products. In general, this study presents a novel method for testing the source apportionment accuracy of receptor-oriented methods. This procedure may be applied to test the accuracy of other receptor-oriented models in the future.

# Chapter 7

# Conclusions

## 7.1 Summary

Methods have been developed for comparing atmospheric single-particle measurements with mathematical air quality model results. These comparisons demonstrate very good agreement, indicating that a source-oriented, externally mixed aerosol representation does capture many of the particle-to-particle differences within a polluted urban aerosol. The air quality model results were compared with ATOFMS measurements collected at Long Beach and Riverside, during the 1996 Los Angeles Basin Trajectory Study.

In the first set of comparisons, model results were transformed in a manner comparable to the ATOFMS measurements, and ATOFMS data were adjusted according to the instrumental particle detection efficiencies. Both sets of aerosol information were reduced using a single-component analysis technique that determines the presence or absence of selected chemical species within individual atmospheric particles. Five chemical species were chosen for this analysis: sodium, nitrate, ammonium, carbon, and mineral dust. ATOFMS measurements of the fractions of size-segregated particle populations containing each of these components were then compared with model results. Very good agreement was found across the entire particle range measured at Long Beach for all five chemical species considered. Also, good agreement was found in the coarse particle size range ($D_a \geq 1.8$ $\mu$m) at the Riverside site. Next, results of the single-component analyses for different chemical species were combined to as-

sess air quality model calculations of the combinations of multiple chemical species within individual particles. For example, model-ATOFMS comparisons of the fraction of a particle population containing ammonium, nitrate, and carbon, were conducted. These multi-component comparisons also revealed good agreement, suggesting further that the model calculations accurately account for the compositional heterogeneity among like-sized atmospheric particles.

After conducting the first set of model comparisons, a method was developed for quantitatively determining the ATOFMS instrument sensitivities to $NH_4^+$ and $NO_3^-$ under atmospheric sampling conditions. The method involves comparing ambient aerosol measurements collected simultaneously by an ATOFMS instrument and a cascade impactor stationed at the same location. These ATOFMS-impactor comparisons revealed that the ATOFMS instrument sensitivities to both $NH_4^+$ and $NO_3^-$ are strongly dependent on the size of the particle being sampled. The ATOFMS sensitivity to both species was found to increase at decreasing particle sizes, and this size-dependence was parameterized using statistical regression analyses. The resulting parameterizations were then used to quantitatively reconstruct size-resolved mass distributions of $NH_4^+$ and $NO_3^-$ collected by the ATOFMS instrument at Riverside.

Next, a method was developed to segregate the ATOFMS single-particle spectra into compositionally distinct particle categories. This categorization method is a substantial improvement over the single-component analysis technique used for the initial set of model-ATOFMS comparisons. Rather than focusing on the presence or absence of individual chemical species in particles, the new method categorizes spectra based on multivariate spectral patterns. The unique feature of this method is that the categorization procedure can be succinctly communicated in a manner such that the particle categorizations can be reproduced, quantitatively assessed, and further improved, by other investigators. In addition, the method is very computationally efficient, requiring only ten minutes to categorize 82,261 spectra on a 700 MHz personal computer. The method was used to categorize particle spectra collected at Riverside as either sea salt, dust, carbonaceous, or miscellaneous. Then, the sea salt, dust, and carbonaceous classes were further subdivided to generate 35 categories of

compositionally distinct atmospheric particles.

The ATOFMS sensitivities to $NH_4^+$ and $NO_3^-$ and the spectral categorization method described in Chapters 3 and 4, were used to conduct a second set of model-ATOFMS comparisons. ATOFMS data collected at Riverside were quantitatively reconstructed to yield continuous, size-resolved measurements of particulate mass, nitrate, and ammonium concentrations, as well as quantitative measurements of the atmospheric aerosol mixing characteristics. These data provide an opportunity to perform more detailed and stringent evaluations of air quality model calculations than were previously possible. Using these data, model-ATOFMS comparisons were performed at finer temporal and particle size resolution than in any previous study. The hourly time series of size-segregated aerosol mass, nitrate, and ammonium concentrations, calculated using the model, exhibits diurnal trends comparable to the measurements. Measurements during a 4-hour intensive sampling period, aggregated into narrow particle size intervals, revealed certain details of the aerosol size distribution that are not captured in the model calculations. Finally, model calculations of the absolute contributions of sea salt, mineral dust, and carbonaceous particles, to the size-resolved aerosol mass distribution, were found to be in good agreement with the corresponding ATOFMS measurements. This was the first quantitative comparison of aerosol mixing characteristics measurements with source-oriented air quality model calculations, and further increased confidence in model calculations of the compositional heterogeneity among like-sized atmospheric particles.

In the process of establishing confidence in model calculations of the size and chemical composition of individual particle classes, we have increased confidence in the emissions inventories used as inputs to the model, as well as the source identifications of individual particle classes tracked within the model. Having reliable information on the size, chemical composition, and source of individual particles within an atmospheric aerosol opens up numerous opportunities for studying the source-receptor relationships that are very important for air pollution control. For example, the source-oriented model results can be used to test the ability of receptor-oriented models for calculating contributions that various emission sources make to atmo-

spheric particulate matter concentrations. In Chapter 6, the source apportionment accuracy of a neural network algorithm (ART-2a) was tested. The algorithm was found to successfully group particles from the majority of sources actually present, when given complete data on ambient particle composition at monitoring sites located near the emission sources. But as particles aged in the atmosphere, accumulation of gas-to-particle conversion products acted to disguise the source of the primary particle cores. The results suggest that the use of continuous single-particle measurements coupled with neural network algorithms can potentially improve the temporal resolution of particulate matter source apportionment.

## 7.2 Recommendations for Future Research

### 7.2.1 Model Evaluations

The 1996 Los Angeles Basin Trajectory Study was the first major field experiment where single-particle aerodynamic size and chemical composition measurements were collected in real time. Research in the past seven years has led to improvements in the detectable particle size range (ultra-fine mode), the level of compositional detail (dual-ion mass spectra and wide dynamic range), and the acquisition rate of single-particle measurements. During this time, single-particle instruments have been operated at various locations around the world. The model-ATOFMS comparison methods derived in this work should be applied to other air pollution episodes and locations where single-particle measurements have been collected. Such comparisons will further our confidence in the model calculations, elucidate shortcomings in our understanding of atmospheric aerosols, and help to identify instrumental biases which can direct the further development of single-particle measurement technology.

As part of the 1997 Southern California Ozone Study, ATOFMS instruments were stationed at selected locations in the Los Angeles basin, specifically to examine the influence of motor vehicle emissions and large local ammonia sources on the atmospheric aerosol [56, 79, 111]. The results of these studies should be used to further

evaluate mathematical model calculations, in the same manner as described in the present work. Currently, the source-oriented air quality model is being adapted for application to the Central California region. Model calculations of the single-particle characteristics in this region should be compared with ATOFMS measurements collected at Bakersfield in January 1999 [78], and at Fresno and Angiola in December 2000 through February 2001. Such comparisons will provide unique insights in the Central California region, where less is known about the relative contributions of various air pollution sources to ambient aerosol concentrations.

### 7.2.2 ATOFMS Sampling Biases

The comparisons of collocated ATOFMS and impactor measurements taken during the 1996 Los Angeles Basin Trajectory Study were the first attempts at understanding the particle detection efficiencies and chemical sensitivities of the ATOFMS instruments under ambient sampling conditions. These analyses should be repeated using the newly available atmospheric aerosol data sets, and the chemical sensitivity analyses described in Chapter 3 should be extended to species other than $NH_4^+$ and $NO_3^-$.

In the ATOFMS-impactor comparisons conducted to date, it was assumed that single-particle composition and shape did not affect the ATOFMS particle detection efficiencies [82], and very little evidence was found to indicate that single-particle composition affected the ATOFMS sensitivities to $NH_4^+$ and $NO_3^-$ (see Section 3.4.3) [91]. However, recent laboratory experiments have shown strong compositional effects on the particle detection efficiencies [108] and chemical sensitivities [106] of different laser ablation/ionization instruments. The magnitude of these sampling biases should be assessed using atmospheric ATOFMS data, such that the mixing characteristics of atmospheric aerosols can be determined with accuracy.

A detailed reanalysis of the ATOFMS data collected during various field studies can be used to determine the effects of single-particle chemical composition on ATOFMS particle detection efficiencies, under a variety of atmospheric sampling conditions. One approach for making this assessment would be to calculate the detection

probabilities, $P_i j$, for particles in each size interval, $i$, and compositional category, $j$, as follows:

$$S_i = \sum_{j \subset i} \frac{H_{ij}}{P_{ij}} \; \forall k \tag{7.1}$$

where S is the number of particles aerodynamically sized by ATOFMS, H is the number of "hit" particles from which a mass spectrum was acquired, and $k$ represents an individual sampling period when the atmospheric conditions were relatively stable ($k = 1, 2, \ldots K$). The compositional categories ($j = 1, 2, \ldots J$) can be defined using the spectral categorization method described in Chapter 4. The only unknown in Equation 7.1 is $P_{ij}$, which can be calculated by linear regression, provided that $K \geq J$. Given the quantity of ATOFMS data collected during recent years, this constraint can be satisfied with ease. Knowing the values of $P_{ij}$ for the most common atmospheric particle types will permit more accurate reconstructions of the aerosol mixing characteristics data.

The atmospheric ATOFMS measurements collected during recent years can also be used to elucidate effects of single-particle composition on the ATOFMS sensitivities to different aerosol chemical components. (i.e., matrix effects). During the sampling events studied in Chapter 3, the bulk composition of atmospheric aerosols at Riverside did not change significantly from one period to the next. As a result, the matrix effects on ATOFMS sensitivity to $NH_4^+$ and $NO_3^-$ appeared to be negligible. In contrast, the field experiment conducted at Bakersfield in January 1999 spanned periods of diverse meteorological conditions, which resulted in significant changes in the aerosol chemical composition [78]. Preliminary assessments of those data indicate that ATOFMS sensitivities to both $NO_3^-$ and $SO_4^{2-}$ were enhanced during periods of high dust loadings and suppressed during periods of high sea salt loadings, relative to the periods with heavy ammonium, nitrate, and organic carbon loadings [177]. Further analyses should be conducted on sets of collocated ATOFMS-impactor data, when aerosol compositions varied significantly between sampling periods. In the event that impactor measurements do not provide sufficient particle size and temporal resolution to quantitatively assess the matrix effects, collocated, size-resolved

measurements collected using an Aerodyne aerosol mass spectrometer [148] may be used for comparison.

Laboratory-based ATOFMS experiments should be conducted to quantitatively assess the effects of particle morphology on ATOFMS transmission efficiencies. Studies have shown that non-spherical particles diverge from the aerosol beam centerline, so they are less likely to be detected by the ATOFMS lasers, which are aligned orthogonally to the aerosol beam. The effects of particle morphology on ATOFMS detection efficiencies is evidenced by the diurnal variation in sea salt particles counted by ATOFMS at Riverside. The frequency of sea salt particle detection is highest at night, when the particles are spherical droplets, and lowest in the afternoon, when they are in crystalline form. These shape effects need to be studied in more detail so that ATOFMS measurements of non-spherical particles can be appropriately scaled to yield accurate measurements of the atmospheric aerosol mixing characteristics. Future instrumental developments should include a measurement of single-particle shape [178], in series with the size and chemical composition measurements, such that the shape-specific scaling coefficients can be used to quantitatively reconstruct atmospheric aerosol data.

### 7.2.3 Single-Particle Source Apportionment

Recently, single-particle size and chemical composition of aerosols emitted from different sources have been measured using ATOFMS [86, 94–97]. These emissions source measurements are being compared with atmospheric single-particle measurements, to identify the sources of individual particles in ambient aerosols. Currently, these source apportionment calculations rely entirely on the ART-2a algorithm, for clustering particles of similar composition. Future source apportionment efforts should apply supervised spectral categorization algorithms in addition to ART-2a, such that the results of source apportionment calculations can be reproduced, quantitatively assessed, and further improved. In addition, a simple format for conveying source-specific seed vectors, such as that shown in Table 4.2, will facilitate communication

between the numerous investigators who are addressing the problem of particulate matter source apportionment.

In the existing air quality model, all like-sized particles emitted from the same emissions source category are assumed to have identical chemical compositions. In other words, the present model formulation treats the emitted particles from each source as internal mixtures. However, the ATOFMS source characterization studies discussed above reveal substantial compositional heterogeneity among like-sized particles emitted from individual emissions sources. Once the single-particle emissions measurements are compositionally segregated, it should be possible to quantitatively construct source-specific, externally mixed emissions inputs to the mathematical air quality model. The resulting air quality model calculations would more accurately simulate the particle-to-particle differences in atmospheric aerosols, than is possible with the currently available emissions data.

With the level of detail provided in the current air quality model calculations, it is possible to test the source apportionment accuracy of receptor-oriented methods, as demonstrated in Chapter 6. A logical extension of this work would be to use the synthetic aerosol information generated by the source-oriented air quality model to test and further improve the accuracy of receptor-oriented source apportionment techniques.

### 7.2.4 Model Developments

The air quality model evaluations presented in this thesis have demonstrated the ability to accurately calculate the compositional heterogeneity among atmospheric particles, using a source-oriented, externally mixed aerosol representation. To date, all applications of this model have been restricted to urban or valleywide geographical regions. This spatial restriction is imposed by the enormous computational burden associated with performing the model calculations. In order to successfully implement this very realistic aerosol representation in continental and global-scale air quality simulations, research efforts must be directed at improving the computational effi-

ciency of the mathematical formulation. One potential solution is to approximate the particle population of each compositionally distinct particle category as a log-normally distributed aerosol mixture, rather than as a set of discrete particle classes interacting with a common gas phase. Mathematical models using lognormal aerosol representations are extremely computationally efficient, and yield relatively accurate aerosol size distributions when simulating both condensation and coagulation processes [179, 180]. These representations have already been employed to simulate internally mixed aerosol dynamics on continental-scales over North America [58] and Europe [26]. A logical future step would be to implement an externally mixed aerosol representation in such large-scale air quality model simulations.

# Appendix A

# Cass Research Group

## A.1 Introduction

This dissertation is dedicated to the memory of Dr. Glen Cass, who had the vision and provided the motivation for conducting the research work described in the preceding chapters. Glen served as my doctoral advisor for nearly three years before his death on July 30, 2001. Since that time, several articles have been written about his professional accomplishments, scientific contributions, personal integrity, and inspiring personality [181–184]. In one article, it was noted that Glen's greatest contribution may be found in the generation of researchers to whom he transmitted his enthusiasm for air pollution studies [185]. This appendix provides an account of the Cass research group members, all of whom have benefitted from Glen's supervision and leadership in one form or another.

## A.2 Group Members

### A.2.1 Ph.D. Students

A substantial fraction of the research conducted in the Cass group can be found in the Ph.D. dissertations written by Glen's former students. Table A.1 lists all of the doctoral theses published in the group. Students are listed chronologically in the order they began graduate studies at Caltech.

Table A.1: Ph.D. dissertations published under the supervision of Dr. Glen Cass.

| Name | Title | Dept[a] |
|---|---|---|
| H. Andrew Gray | Control of Atmospheric Fine Primary Carbon Particle Concentrations | ENV |
| Armistead G. Russell | Formation and Control of Atmospheric Aerosol Nitrate and Nitric Acid | ME |
| Susan E. Fuhs | Studies of Inertial Deposition of Particles onto Heat Exchanger Elements | ME |
| Susan M. Larson | A Study of Summer Midday Low-Visibility Events in the Los Angeles Area | ENV |
| Lynn M. Hildemann | A Study of the Origin of Atmospheric Organic Aerosols | ENV |
| William W. Nazaroff | Mathematical Modeling and Control of Pollutant Dynamics in Indoor Air | ENV |
| Robert A. Harley | Mathematical Modeling of Gas-Phase Organic Air Pollutants | ENV |
| Wolfgang F. Rogge | Molecular Tracers for Sources of Atmospheric Carbon Particles: Measurements and Model Predictions | ENV |
| Annmarie Eldering | Alternative Models for Air Pollutant Effects on Visibility | ENV |
| Christos Christoforou | Control of Air Exchange and Particle Deposition within the Buddhist Cave Temples of Yungang, China | ME |
| Darrell A. Winner | Long-term Modeling of Regional Ozone Concentrations and Control Strategies | ENV |
| Michael P. Hannigan | Mutagenic Particulate Matter in Air Pollutant Source Emissions and in Ambient Air | ENV |
| Matthew P. Fraser | Measuring and Modeling the Concentrations of Individual Organic Compounds in the Urban Atmosphere | ENV |
| Christopher G. Nolte | Polar Organic Compounds in Fine Particulate Matter Sources and in the Urban Atmosphere | ENV |
| James J. Schauer | Source Contributions to Atmospheric Organic Compound Concentrations: Emissions Measurements and Model Predictions | ENV |
| Michael J. Kleeman | Source Contributions to the Size and Composition Distribution of Urban Particulate Air Pollution | ENV |
| Lara S. Hughes | Evolution of Atmospheric Aerosols Along Trajectories Crossing the Los Angeles Basin | ENV |
| Phil M. Fine | The Contribution of Biomass Combustion to Ambient Fine Particle Concentrations in the United States | ENV |
| Zohir Chowdhury | Fine Particle Characterization in South Asia[b] | EAS |
| Prakash V. Bhave | Air Pollution at the Single-Particle Level: Integrating Atmospheric Measurements with Mathematical Models | ENV |

[a]Department where degree was completed. ENV = Environmental Engineering and science, Caltech. ME = Mechanical Engineering, Caltech. EAS = Earth and Atmospheric Sciences, Georgia Tech.

[b]Tentative thesis title

**H. Andrew Gray** joined the Cass group in the summer of 1979 after receiving an undergraduate degree from Carnegie Mellon University. His thesis work involved the development of an inventory of primary particulate carbon emissions in the Los Angeles basin, the measurement of carbonaceous aerosol concentrations at ten southern California sites throughout the 1982 calendar year, and the quantitative evaluation of various control strategies for reducing fine primary carbon particle concentrations in Los Angeles. After completing his thesis in November 1985, Dr. Gray worked at the South Coast Air Quality Management District where he served as the program manager for $PM_{10}$ and visibility. He later worked at Systems Applications, Inc. for eight years before starting his own consulting company in San Rafael, California. He currently manages Gray Sky Solutions, an air pollution research consulting firm specializing in particulate matter and visibility issues.

**Armistead (Ted) G. Russell** came to the Cass group in the fall of 1979 with a bachelors degree in mechanical engineering from Washington State University. His thesis work included the development of a mathematical model for the formation and transport of ammonium nitrate aerosol, the measurement of aerosol nitrate, sulfate, ammonium, and their precursors during an intensive 1982 southern California field study, and the evaluation of his model for predicting atmospheric ammonium nitrate concentrations. In January 1985, Dr. Russell became the first Ph.D. student to finish under Glen's supervision. He was appointed to an assistant professor position at Carnegie Mellon University, where he worked until 1996. Currently, he is a distinguished professor of environmental engineering at Georgia Tech. His research group studies numerous aspects of ambient air pollution, with a focus on air quality model development. To date, nine students have received Ph.D. degrees under Dr. Russell's supervision.

**Susan E. Fuhs** joined the Cass group after receiving a bachelors degree in mechanical engineering from Caltech in 1980. As a graduate student, she examined the mechanisms of particle deposition on the gas-side external surface of compact heat exchanger elements. This type of fouling is commonly found in combustion systems such as coal or oil fired boilers, gas turbines, and diesel enginers. Dr. Fuhs completed

her thesis in October 1987, and has worked for several private corporations in the southern California area. Recently, she served as the manager of new business development in the Engines and Systems group of Allied Signal, and she is currently the general manager of the Hybrid Power Generation Systems group in the General Electric Company.

**Susan M. Larson** received bachelors degrees in physics and German at Washington University before joining the Cass group in 1981. Her Ph.D. thesis involved the study of image processing based visibility models, the measurement of aerosol concentrations at five southern California sites throughout the 1984 summer, and the development and application of a modeling approach that allows the causes of regional visibility problems to be characterized quantitatively. After finishing her thesis in October 1987, Dr. Larson became an assistant professor at the University of Illinois at Urbana-Champaign (UIUC) and is a recipient of the Presidential Young Investigator award. She is currently an associate professor of environmental engineering and the director of the Women in Engineering program at UIUC. Her research group conducts laboratory-based experiments, air pollution field studies, and develops and evaluates the performance of air pollution control devices. To date, four students have received Ph.D. degrees under Dr. Larson's supervision.

**Lynn M. Hildemann** joined the Cass group in 1982, after earning a bachelors degree in biology from Caltech. Her thesis involved measuring the size distribution, inorganic chemical composition, and speciated organic composition of particulate matter emitted from seventeen different source categories. In order to simulate real-world combustion conditions, she designed a dilution stack sampler which has been replicated and used by numerous researchers around the world. Dr. Hildemann completed her thesis in September 1989, and was appointed to an assistant professor position at Stanford University. She is currently an associate professor of environmental engineering and science and an associate editor of *Environmental Science & Technology*. Dr. Hildemann is a recipient of the Presidential Young Investigator award and the American Association of Aerosol Research's Kenneth T. Whitby award. Her research group studies the sources and size distributions of indoor particulate matter

as well as the hygroscopic properties of organic aerosols. To date, six students have received Ph.D. degrees under Dr. Hildemann's supervision.

**William W. Nazaroff** had received a bachelors degree in physics and a masters degree in electrical engineering from UC Berkeley before joining the Cass group in 1984. His thesis research focused on mathematically modeling the reactivity and transport of indoor air pollutants. He also assisted in the measurement of aerosol concentrations at five southern California museums during 1987–1988, in an effort to study and control the deposition of aerosols on works of art. Dr. Nazaroff was the fastest Ph.D. student in Cass group history, finishing his thesis in four years. He became an assistant professor at UC Berkeley in 1988, and is now a distinguished professor. Dr. Nazaroff is a recipient of the Presidential Young Investigator award and an elected member of the International Academy of Indoor Air Sciences. He is an associate editor of the *Journal of Air & Waste Management Association* and a past associate editor of *Health Physics*. He recently coauthored a textbook entitled, *Environmental Engineering and Science*, with Lisa Alvarez-Cohen. Dr. Nazaroff's research group focuses on indoor air quality and exposure analysis. To date, ten students have received Ph.D. degrees under his supervision.

**Robert A. Harley** joined the Cass group in 1987 with a bachelors degree in engineering science from the University of Toronto. At Caltech, his research focused on mathematically modeling the concentrations of ozone, volatile organic compounds, and toxic organic air pollutants. He also developed a speciated organic gas emissions inventory for the Los Angeles area which was used for several subsequent air quality modeling studies. After completing his thesis in December 1992, Dr. Harley became an assistant professor at UC Berkeley and is now a full professor. He is a recipient of the National Science Foundation's CAREER development award and on the editorial advisory board of *Atmospheric Environment*. His research group researches mobile sources of air pollutant emissions and conducts air quality modeling studies. To date, four students have received Ph.D. degrees under Dr. Harley's supervision.

**Wolfgang F. Rogge** also came to the Cass group in 1987, after receiving an engineering degree from Technische Universitat Berlin. As a graduate student, he

conducted a detailed analysis of particle-phase individual organic compounds emitted from all major sources of fine organic aerosols in the urban environment. The results of these studies are reported in a series of nine papers published in *Environmental Science & Technology* between 1991 and 1998. Dr. Rogge was appointed to an assistant professor position at Florida International University after completing his thesis in May 1993. His research group studies numerous aspects of atmospheric pollutants, with an emphasis on the measurement and source apportionment of individual organic compounds in atmospheric aerosols. He is currently an associate professor.

**Annmarie Eldering** joined the Cass group in 1988 after earning a bachelors degree in chemical engineering from Cooper Union. Her thesis describes the development and application of four mathematical models for determining the effects of air pollution on visibility. The models include a Lagrangian source-oriented air quality model, an image processing based model, and a model based on satellite-generated landscape data. After completing her thesis in March 1994, Dr. Eldering became an assistant professor at the University of Iowa, where she supervised seven masters degree students. In 1997, she moved back to southern California to work at the University of California, Los Angeles (UCLA). Currently, Dr. Eldering conducts research at the Jet Propulsion Laboratory and holds an adjunct assistant professor position at UCLA. Her current research focuses on the radiative impacts of aerosols and clouds.

**Christos S. Christoforou** also joined the Cass group in 1988, after obtaining an undergraduate degree in mechanical engineering from Rice University. His graduate research was focused on the air pollutants inside Buddhist cave temples at the Yungang Grottoes in China. He conducted air pollution measurement campaigns at the Grottoes in the spring of 1991, and used mathematical models to develop strategies for controlling the air exchange and reducing particle deposition to the cave walls. After finishing his thesis in May 1995, Dr. Christoforou did two years of service in his home country of Cyprus before joining the faculty at Clemson University in South Carolina. He is currently an assistant professor of environmental engineering and science at Clemson. His research group studies various aspects of air pollution control.

**Darrell A. Winner** joined the Cass group in 1989 after earning a bachelors degree in chemical engineering from Carnegie Mellon University. His thesis describes efficient methods for mathematically modeling regional ozone concentrations over periods of a year or longer. He applied these methods to determine the effect of emission control strategies on long-term ozone concentration distributions. He left Caltech in February 1996 to fulfill service obligations in the United States Air Force and finished his thesis in June 1998. Dr. Winner currently serves as a science advisor to regulatory staff at the EPA. He is a project officer in the EPA Center for Global Change, where he plans and implements solicitations for future research in atmospheric science, air quality engineering, and global change. In addition, Dr. Winner is the program manager of the Experimental Program to Stimulate Competitive Research (EPSCoR) within the EPA's National Center for Environmental Research.

**Michael P. Hannigan** joined the group in 1990 after obtaining a bachelors degree in mechanical engineering from Southern Methodist University. As a graduate student, he determined the bacterial and human cell mutagenicity of aerosols in emissions source and atmospheric samples. He also assisted in the measurement of atmospheric aerosols at five southern California sites throughout the 1993 calendar year. After completing his thesis in May 1997, Dr. Hannigan did postdoctoral research at MIT and Colorado State University, Fort Collins. He was a member of the University of Denver faculty for a couple of years before moving to the University of Colorado, Boulder. He is currently a research associate in the mechanical engineering department at Boulder. He focuses on urban and remote air pollutant characterization and recently has begun studying air pollution sampler development and current trends in energy use.

**Matthew P. Fraser** came to the Cass group in 1991 with a bachelors degree from Carnegie Mellon University. His thesis work involved the measurement of individual atmospheric organic compounds at five southern California sites during the 1993 summer. By sampling air in the Van Nuys tunnel, he determined the motor vehicle emission rates of 221 vapor-phase, semivolatile, and particle-phase organic compounds. He used these data to evaluate a mathematical model for calculating

the concentrations of individual organic compounds in the Los Angeles atmosphere. Dr. Fraser completed his thesis in January 1998 and joined the faculty at Rice University. He is currently an assistant professor at Rice, where his research group studies organic air pollutants in source and ambient samples, as well as air pollution problems specific to the Houston metropolitan area.

**Christopher G. Nolte** joined the Cass group in 1992 after earning a bachelors degree in physics at Stanford University. His thesis research elucidated the concentrations of polar organic aerosol compounds in source and atmospheric samples. He also determined the atmospheric concentrations of numerous carboxylic acids in the Los Angeles atmosphere and helped collect samples during several field studies. After completing his thesis in February 2001, Dr. Nolte began working at Silicon Age, a small software company in San Francisco.

**James (Jamie) J. Schauer** held a bachelors degree from the Colorado School of Mines and a masters degree from UC Berkeley before joining the Cass group in 1993. At Caltech, he measured the concentrations of individual gas-phase and aerosol-phase organic compounds emitted from eight major air pollutant emission source categories. To date, the results of these studies constitute a five-paper series published in *Environmental Science & Technology* between 1999 and 2002. He also measured the atmospheric concentrations of individual organic compounds at three sites in central California during the 1995 Integrated Monitoring Study and used these data in combination with his source characterization data for receptor-oriented source apportionment calculations. Dr. Schauer joined the faculty at the University of Wisconsin, Madison after finishing his thesis in March 1998. Dr. Schauer is currently an assistant professor at Wisconsin and a recent recipient of the Health Effects Institute's Rosenblith Young Investigator Award. His research group investigates the origin of air pollutants as well as their impact on human health and the ecosystem.

**Michael J. Kleeman** also joined the group in 1993, after receiving a bachelors degree in mechanical engineering from the University of Waterloo. His thesis research involved the development and application of an air quality model in which the atmospheric aerosol is represented as a source-oriented external mixture. He measured

the size-resolved chemical composition of aerosols emitted from six major combustion source categories and used those data as input to the air quality model. After completion of his thesis in October 1998, Dr. Kleeman joined the faculty at UC Davis. His research group studies urban and regional air quality problems with an emphasis on the size and composition of atmospheric particles and gas-to-particle conversion processes.

**Lara S. Hughes** earned a bachelors degree from Washington University before joining the Cass group in 1994. As a graduate student, she conducted two major field sampling experiments in the Los Angeles area, and helped conduct an experiment in the Indian Ocean. Her southern California experiments were conducted in 1996 and 1997, and involved measurements of the pollutant mixture within single air parcels at multiple ground-based locations as the parcels were advected across the Los Angeles basin. In addition to these trajectory studies, Lara reported the first comprehensive data set on the chemical composition of ultrafine ($D_a < 0.1$ $\mu$m) particles. She got married soon after completing her thesis in September 2000 and is now Dr. Lara Gertler. She was a postdoctoral fellow at UC Riverside, and currently works for the Ashworth Leininger Group, an environmental consulting firm in Thousand Oaks, California.

**Phil M. Fine** completed a bachelors degree in mechanical engineering from UC Berkeley and worked as an environmental consultant before joining the Cass group in 1995. His doctoral work involved determining the emission rates of over 250 individual organic compounds generated from the combustion of 22 species of North American wood. He used these data to quantify the contributions of biomass combustion particles to the atmospheric aerosol in various regions of the United States. After completing his thesis in January 2002, Dr. Fine conducted postdoctoral research at the University of Southern California (USC). He is currently a research assistant professor of environmental engineering at USC.

**Zohir Chowdhury** joined the Cass group in 1997 after earning a bachelors degree from Montana Tech. As a graduate student, he measured atmospheric aerosol properties in Maldives during the 1999 intensive field phase of the Indian Ocean

Experiment and characterized aerosols emitted from a variety of combustion source categories unique to the Indian subcontinent. After receiving a masters degree from Caltech, Zohir transferred to Georgia Tech with Dr. Cass in 2000. He conducted an aerosol characterization study at four megacities in the Indian subcontinent during each season of the 2001 calendar year, with the goal of apportioning the sources of fine particles at each site. Zohir will complete his thesis under the supervision of Ted Russell at Georgia Tech by the end of 2003, and plans to pursue a career at the World Bank.

**Prakash V. Bhave** was the last graduate student to join the Cass research group, after receiving a bachelors degree in environmental engineering from UC Berkeley in 1998. His thesis compares the properties of individual atmospheric particles with the single-particle properties calculated using a source-oriented externally mixed aerosol air quality model. After completing his thesis in March 2003, Dr. Bhave was appointed as a physical scientist in the Atmospheric Modeling division of the National Oceanic and Atmospheric Administration's Air Resources Laboratory in Research Triangle Park, North Carolina. He is responsible for developing the aerosol components of EPA's CMAQ model.

### A.2.2 Postdoctoral Researchers

During his career, Dr. Cass hired eight postdoctoral researchers who each brought unique skills to the group. These individuals propelled the group into new areas of research, such as artwork degradation, organic compound speciation, and heterogenous atmospheric chemistry. Postdoctoral researchers also played instrumental roles in a number of field experiments.

**Paul M. Whitmore** worked in the Cass research group from 1984–1986 after completing a Ph.D. in chemistry from UC Berkeley and a postdoctoral research fellowship in Caltech's chemistry department. In the Cass group, Dr. Whitmore methodically studied the fading of a variety of artwork colorants due to reactions with ozone and nitrogen dioxide. After leaving Caltech, Dr. Whitmore worked in the con-

servation department of the Harvard University art museums. Since 1988, he has directed the Research Center on the Materials of the Artist and Conservator at the Carnegie Mellon Research Institute in Pittsburgh, Pennsylvania.

**Paul A. Solomon** joined the Cass group in December 1984 after finishing a Ph.D. in analytical and environmental chemistry at the University of Arizona. During the 1986 calendar year, he conducted a major field sampling program at nine southern California sites. This data set has been used by several investigators to map out the spatial and temporal distributions of $PM_{10}$, organic acid, and inorganic acid concentrations in the Los Angeles atmosphere. After leaving Caltech in 1988, Dr. Solomon worked for ten years as an environmental scientist at Pacific Gas and Electric company in San Ramon, California, before joining the U.S. EPA's National Exposure Research Laboratory. He is currently a senior research scientist at the EPA office in Las Vegas, Nevada, where he plans and implements regional field measurement and modeling programs aimed at developing cost effective control strategies for $PM_{2.5}$, $PM_{10}$, ozone, and related pollutants.

**Monica A. Mazurek** joined the Cass research group in February 1986 after completing her Ph.D. in geochemistry at UCLA. Her research at Caltech focused on interpreting gas chromatography/mass spectrometry (GC/MS) data acquired from atmospheric aerosols and emissions source samples. These studies laid much of the groundwork for future efforts aimed at quantifying the concentrations of individual organic compounds in source and ambient aerosol samples. Dr. Mazurek worked at the environmental chemistry division at Brookhaven National Laboratory from 1989 to 1995, before moving to Rutgers University. She is currently an associate research professor and the director of academic initiatives at Rutgers. Her research activities include studying the sources, distributions, and fates of carbonaceous aerosol particles. Dr. Mazurek is currently a member of the National Science Foundation advisory board, and was previously serving on the *Aerosol Science & Technology* editorial advisory board.

**Mary P. Ligocki** worked in the Cass group from March 1987 to July 1989. She coordinated sampling campaigns at five southern California museums during the

summer of 1987 and winter of 1988. She passed away in 1996.

**Jonathan O. Allen** received a Ph.D. degree in chemical engineering from MIT before joining the Cass group in 1997. During his three years at Caltech, Dr. Allen helped manage the 1997 trajectory experiments and analyzed single-particle data collected using ATOFMS instruments. As a postdoc, he developed the YAADA software toolkit for ATOFMS data analysis and continues to maintain and update it. Dr. Allen worked briefly at Aerodyne Research, Inc. before joining the faculty of Arizona State University in 2001. His research group studies the formation and evolution of atmospheric aerosols with an emphasis on organic constituents. He is currently an assistant professor.

**William S. Barney** did postdoctoral work in the Cass group from 1999–2001 after receiving a Ph.D. degree in chemistry from UC Irvine. While in the group, Dr. Barney spent most of his time conducting experiments at Aerodyne Research, Inc., in Massachusetts. His research focused on heterogenous reactions between ozone and organic aerosols. He currently works at the TIAX corporation in Cambridge, Massachusetts.

**Ann M. Dillner** joined the Cass group at Georgia Tech after completing her Ph.D. in environmental engineering at UIUC in 2000. As a postdoc, she conducted field measurement campaigns in Houston, Beijing, and southern California, aimed at characterizing the chemical composition of atmospheric ultrafine particles. In 2001, Dr. Dillner joined the faculty of Arizona State University, where she is currently an assistant professor. Her research group studies various aspects of air pollution aerosols with a focus on ambient field measurements.

**Mei Zheng** received her Ph.D. degree in oceanography from the University of Rhode Island before joining the Cass group in 2000. She spent the first part of her postdoctoral appointment working at the University of Wisconsin with Jamie Schauer and the latter portion at Georgia Tech. As a postdoc, Dr. Zheng conducted applied receptor-oriented models to determine the contributions of different emissions sources to $PM_{2.5}$ concentrations in the southeastern United States and Beijing, China. She is currently a research scientist at Georgia Tech.

### A.2.3 Research Staff

Dr. Cass employed a considerable number of staff scientists to ensure long-term continuity of the group's efforts. This continuity and constant staff support enabled his graduate students and postdoctoral researchers to conduct world-class research while maintaining a high rate of productivity.

**Kenneth F. McCue** joined the Cass group in 1983 with a Ph.D. degree in social sciences from Caltech. He brought a strong statistics background to the group, and helped analyze data from the 1982 and 1984 field studies. Primarily, he was responsible for administering the group's computer hardware and extensive air pollution data bases. While working for Glen, Dr. McCue founded Pactech Data and Research Incorporated, and split his time between both responsibilities until July 2002. He is currently a staff scientist in the applied and computational mathematics department at Caltech.

**Shohreh Gharib** volunteered her time in the Cass group in the early 1980's and worked as a staff scientist in the early 1990's. She developed an ammonia emission inventory for the southern California area and assisted with the 1982 and 1993 field studies. She has retired from her professional career.

**Theresa Fall** joined the Cass research group in 1984, after working as a draftsperson in Caltech's Environmental Quality Laboratory. She played significant roles during the 1986 basinwide field study and the southern California museum studies in 1987–1988. Theresa left the group in 1988 and is currently working in the Energy and Geoscience Institute at the University of Utah, Salt Lake City.

**Lynn G. Salmon** joined the Cass group in September 1986 after earning a bachelors degree from MIT and a masters degree from UCLA. Lynn either participated in or analyzed samples from nearly every atmospheric field campaign, source characterization study, and indoor air quality experiment conducted by the research group between 1986–2002. She coordinated the global ozone passive monitoring project in March and August 1999, in which ozone concentrations were determined at more than 400 locations worldwide. In addition, Lynn was primarily responsible for operation

and maintenance of all laboratory equipment in the Cass research group. She continues to collect air pollution samples and conduct chemical analyses as a staff scientist in the Hoffman research group at Caltech.

**Ann G. Miguel** received a Ph.D. degree in biophysics from the Federal University of Rio de Janeiro in 1981. She was an associate professor at the University of Rio de Janeiro and the University of Sao Paulo before joining the Cass group in April 1994. From 1994–2002, Dr. Miguel characterized the allergens in airborne particulate matter and investigated their relationship with asthma incidences. She continues to study these subjects as a staff scientist in the Flagan research group at Caltech.

**Paul R. Mayo** worked in the Cass group from 1997–2002. During that time, he participated in several field studies and helped prepare and analyze air pollution samples. Paul is currently a scientist at UCLA in the Southern California Particle Center and Supersite.

**Julie Saxton** worked on the global ozone passive monitoring project while in the Cass group from 1999–2000. She is currently pursuing graduate studies in England.

### A.2.4 Other Contributors

In addition to the investigators mentioned above, a very large number of undergraduate students contributed to research efforts in the Cass group. An exhaustive record of these individuals is not readily available, so only those who authored or were acknowledged in published work are listed here. Mari Peterson and Barbara Turpin assisted with the 1982 field study. Philip Lin, Barbara Turpin, and Frank Vasquez, helped with the 1984 summer visibility studies. Cynthia Shaver Atherton, C. Pamela De Moor, Kaitlin Drisko, Nathan Frei, Heather Mason, Cynthia Whitman, and Christine Tiller, contributed to the research on artwork deterioration. Betsy Andrews, Sandra Blumhorst, David Cole, Nancy Drehwing, Doug Gray, Michael Jones, Philip Lin, Harvey Liu, and Frank Vasquez helped with the 1986 field study. Christopher Hance analyzed data from the 1986 field study. Michael Jones helped with source characterization experiments in the 1980's. Mark Adams, Michael Jones, Har-

vey Liu, and Timothy Ma, assisted with museum sampling campaigns. Heather and Michael Masonjones (previously, Heather Mason and Michael Jones) collected measurements in August 1989 at the Grand Canyon and managed the high resolution gas chromatography data base. Nathan Frei and Timothy Gerk helped with the 1991 Yungang Grottoes experiments. Chen Yuan, John King, and Nathan Frei made significant contributions to aerosol sampler construction. Claudine Butcher prepared samples for the 1993 southern California field experiment. Robert Johnson helped with the 1996 trajectory study and conducted extensive analyses of the allergens found in ambient aerosols. Megha Deshpande assisted with an Atlanta field study in 2001.

Martha Conklin, Susan Hunts, Luiz Palma, Yun Ye, Steve Dutton, Brian King, and Kimberly Mertz, were graduate research assistants in the group, but did not complete doctoral degrees under Glen's supervision for a variety of reasons. Leon Bellan authored an artwork deterioration study as a high school student at the Polytechnic School.

Although not contributing directly to scientific research, several administrative assistants provided invaluable support for the Cass group. These include Pat Houseworth, Christina Conti, Dixie Fiedler, Shirley Anderson, and Laurel Martin at Caltech, and Rita Bryan and Susan Ryan at Georgia Tech. Pat Rankin, Fran Matzen, and Laura Cederquist helped manage Glen's research accounts.

## A.3 Miscellaneous Notes

Figure A.1 shows the number of Cass group researchers between 1979–2003, excluding the contributors listed in section A.2.4. The number of staff scientists grew steadily from 1982–2000, while the number of Ph.D. students fluctuated between four and eight, with an average of 5.75. Postdoctoral researchers were in the group during only two isolated time periods.

Dr. Cass expected his group members to conduct high quality research and encouraged his students to pursue fairly ambitious projects. Under these conditions

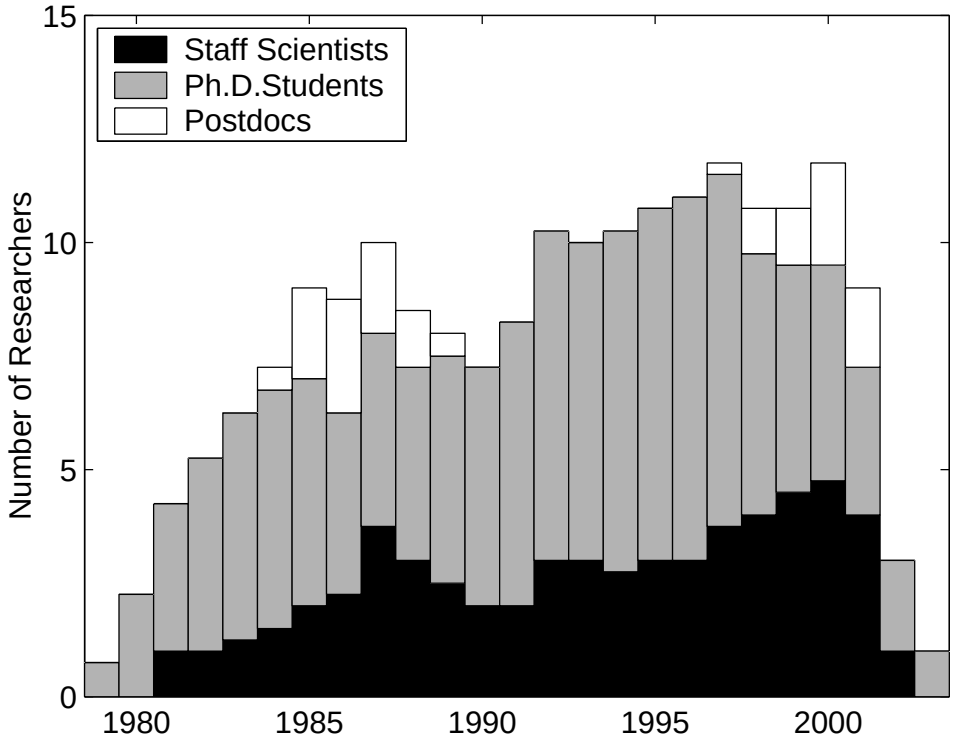


Figure A.1: Temporal distribution of the size of the Cass research group.

Glen's students, on average, managed to finish their graduate work in less time than the Caltech average. The frequency distribution of the time required to complete a Ph.D. degree in the Cass research group is shown in Figure A.2. The mean and median of this distribution are 6.1 years. On average, students whose research work was primarily computational (Russell, Nazaroff, Harley, Eldering, Winner, Kleeman, and Bhave) finished in 5.5 years ($\sigma = 1.5$), whereas the remaining students, whose research work included a substantial experimental component, required 6.4 years on average ($\sigma = 0.9$).

Dr. Cass supported his students unconditionally in their search for employment as they neared completion of their doctoral work. This support helped launch all of his Ph.D. students into successful careers in either academic, governmental, or industrial sectors. Figure A.3 displays the distribution of careers that Glen's Ph.D. students pursued after graduating from Caltech. The numbers in parentheses indicate the number of students who pursued a career in the indicated sector. Dr. Gray did

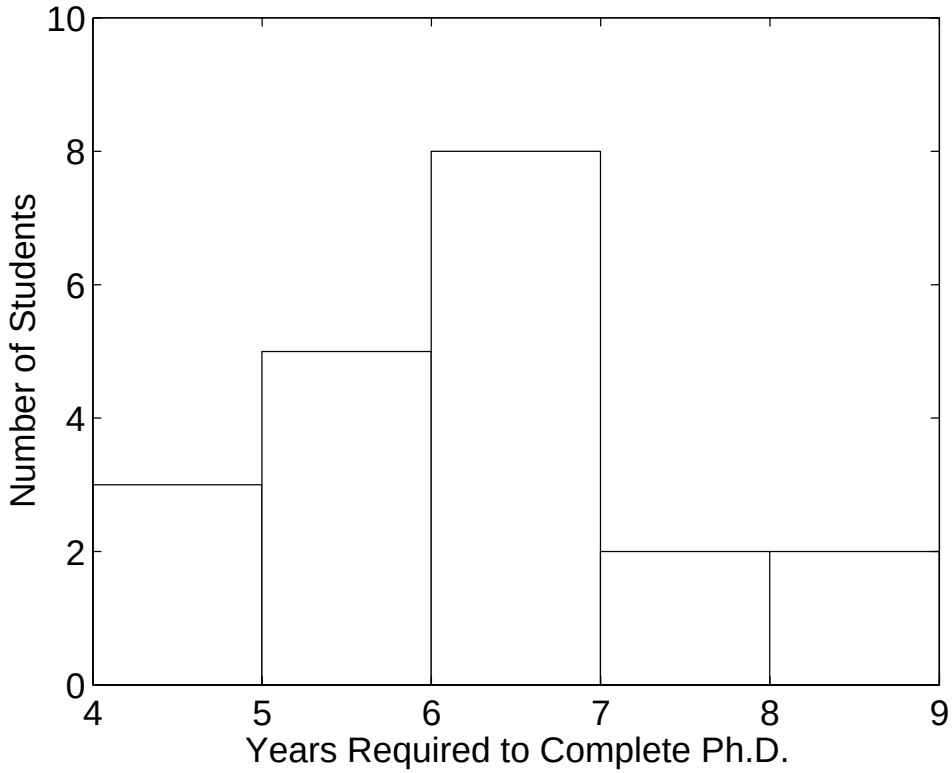


Figure A.2: Frequency distribution of time required to complete a Ph.D. degree in the Cass research group.

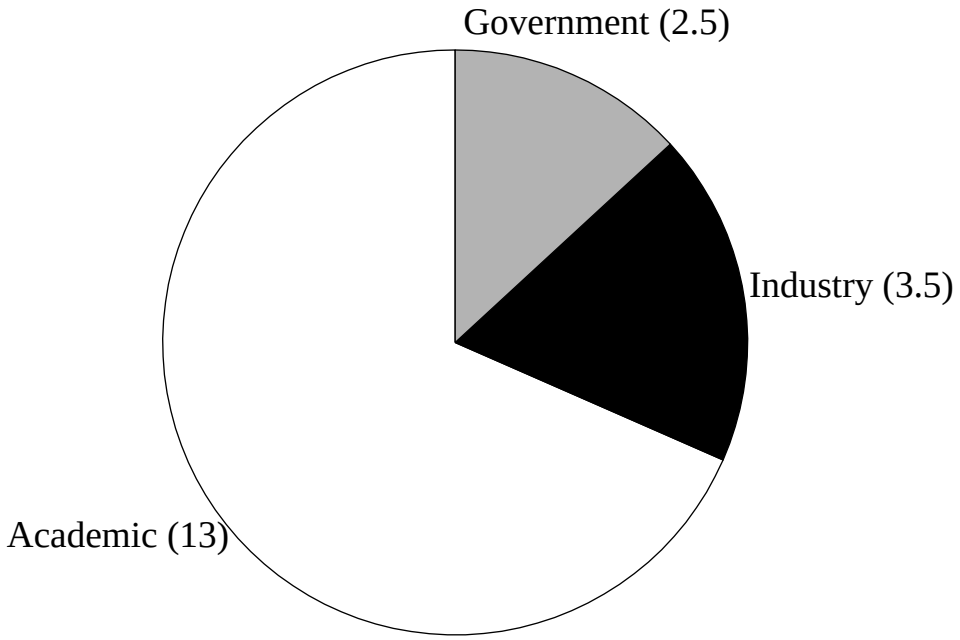


Figure A.3: Careers pursued by former Ph.D. students in the Cass research group.

substantial work in governmental and industrial sectors, so a half unit is attributed to both categories. The career path of Zohir Chowdhury is uncertain and, therefore, is excluded from Figure A.3.

The majority of Ph.D. students from the Cass group are pursuing careers in academia. Among them, ten are currently advising graduate students in universities across the United States. Five of Glen's former doctoral students have already supervised graduate-level researchers to the completion of Ph.D. degrees. A number of these "second generation Cass students" are now professors at reputed universities including Arizona State University (Ann Dillner), Clarkson University (Andrea Ferro), the National University of Singapore (Liya Yu), California State University at Hayward (Karina Garbesi), National Cheng-Kung University in Taiwan (Tsair-Fuh Lin), the University of Colorado at Boulder (Shelly Miller), University of Missouri-Rolla (Glenn Morrison), and Virginia Tech (Linsey Marr). Figure A.4 depicts the first and second generation doctoral "descendants" of Professor Cass. Several aspects of Glen's very successful method of advising as well as his style of scientific writing have undoubtedly been passed on to these individuals, and will likely be carried on

for generations to come.

## A.4 Conclusion

During his twenty-two year academic career at Caltech and Georgia Tech, Dr. Cass shaped the careers of many students and scientists. His good nature and significant contributions to this world will have long-lasting effects.

Lynn Salmon, Ken McCue, and Linda Scott are acknowledged for their help in piecing together historical information contained in this appendix.

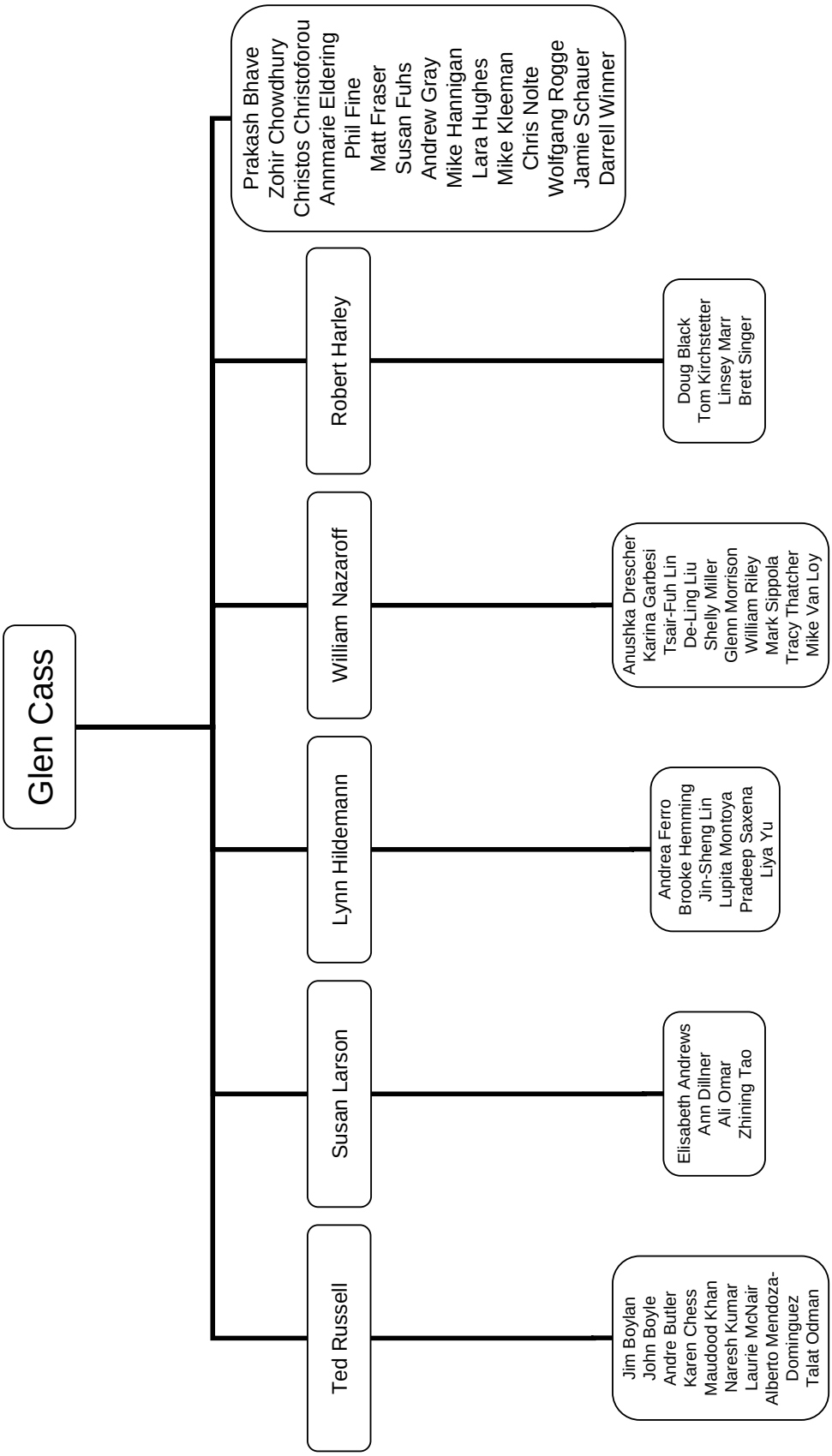


Figure A.4: Ph.D. "descendants" of Dr. Cass.

# References

[1] Yu, C. P. Exact analysis of aerosol deposition during steady breathing. Powder Technology, 21:55–62, 1978.

[2] Harrison, R. M. and J. Yin. Particulate matter in the atmosphere: Which particle properties are important for its effects on health? Sci. Total Environ., 249:85–101, 2000.

[3] National Research Council. *Protecting Visibility in National Parks and Wilderness Areas*. National Academy Press, Washington, DC, 1993.

[4] Charlson, R. J., S. E. Schwartz, J. M. Hales, R. D. Cess, J. A. Coakley, J. E. Hansen, and D. J. Hofmann. Climate forcing by anthropogenic aerosols. Science, 255:423–430, 1992.

[5] Dockery, D. W., C. A. Pope, X. Xu, J. D. Spengler, J. H. Ware, M. E. Fay, B. G. Ferris, and F. E. Speizer. An association between air pollution and mortality in six United States cities. New England Journal of Medicine, 329:1753–1759, 1993.

[6] Roberts, O. F. T. The theoretical scattering of smoke in a turbulent atmosphere. Proc. Royal Soc., A, 104:640–654, 1923.

[7] Sutton, O. G. A theory of eddy diffusion in the atmosphere. Proc. Royal Soc., A, 135:143–165, 1932.

[8] Meetham, A. R. Natural removal of pollution from the atmosphere. Quart. J. of Royal Met. Soc., 76:359–371, 1950.

[9] Roberts, P. T. *Gas-to-particle conversion: Sulfur dioxide in a photochemically reactive system.* Ph.D. thesis, California Institute of Technology, 1975.

[10] Russell, A. G., G. J. McRae, and G. R. Cass. Mathematical modeling of the formation and transport of ammonium nitrate aerosol. Atmos. Environ., 17:949–964, 1983.

[11] Russell, A. G. and G. R. Cass. Verification of a mathematical model for aerosol nitrate and nitric acid formation and its use for control measure evaluation. Atmos. Environ., 20:2011–2025, 1986.

[12] Pandis, S. N., R. A. Harley, G. R. Cass, and J. H. Seinfeld. Secondary organic aerosol formation and transport. Atmos. Environ., 26A:2269–2282, 1992.

[13] Suck, S. H. and J. R. Brock. Evolution of atmospheric aerosol particle size distributions via Brownian coagulation: Numerical simulation. J. Aerosol Sci., 10:581–590, 1979.

[14] Gelbard, F. and J. H. Seinfeld. Simulation of multicomponent aerosol dynamics. J. Colloid and Interface Sci., 78:485–501, 1980.

[15] Whitby, K. T. Determination of aerosol growth rates in the atmosphere using lumped aerosol dynamics. J. Aerosol Sci., 12:174–178, 1981.

[16] Pilinis, C., J. H. Seinfeld, and C. Seigneur. Mathematical modeling of the dynamics of multicomponent aerosols. Atmos. Environ., 21:943–955, 1987.

[17] Pilinis, C. and J. H. Seinfeld. Continued development of a general equilibrium model for inorganic multicomponent atmospheric aerosols. Atmos. Environ., 21:2453–2466, 1987.

[18] Wexler, A. S., F. W. Lurmann, and J. H. Seinfeld. Modeling urban and regional aerosols – I. Model development. Atmos. Environ., 28:531–546, 1994.

[19] Binkowski, F. S. and U. Shankar. The regional particulate matter model 1. model description and preliminary results. J. Geophys. Res., 100:26191–26209, 1995.

[20] Eldering, A. and G. R. Cass. Source-oriented model for air pollutant effects on visibility. J. Geophys. Res., 101:19343–19369, 1996.

[21] Lurmann, F. W., A. S. Wexler, S. N. Pandis, S. Musarra, N. Kumar, and J. H. Seinfeld. Modeling urban and regional aerosols – II. Application to California's South Coast Air Basin. Atmos. Environ., 31:2695–2715, 1997.

[22] Middleton, P. DAQM-simulated spatial and temporal differences among visibility, PM, and other air quality concerns under realistic emission change scenarios. J. Air and Waste Management Assoc., 47:302–316, 1997.

[23] Jacobson, M. Z. Development and application of a new air pollution modeling system. 2. Aerosol module structure and design. Atmos. Environ., 31:131–144, 1997.

[24] Sun, Q. and A. S. Wexler. Modeling urban and regional aerosols near acid neutrality – Application to the 24-25 June SCAQS episode. Atmos. Environ., 32:3533–3545, 1998.

[25] Meng, Z., D. Dabdub, and J. H. Seinfeld. Size-resolved and chemically resolved model of atmospheric aerosol dynamics. J. Geophys. Res., 103:3419–3435, 1998.

[26] Ackermann, I. J., H. Hass, M. Memmesheimer, A. Ebel, F. S. Binkowski, and U. Shankar. Modal aerosol dynamics model for Europe: Development and first applications. Atmos. Environ., 32:2981–2999, 1998.

[27] Pai, P., K. Vijayaraghavan, and C. Seigneur. Particulate matter modeling in the Los Angeles basin using SAQM-AERO. J. Air and Waste Management Assoc., 50:32–42, 2000.

[28] Kleeman, M. J., G. R. Cass, and A. Eldering. Modeling the airborne particle complex as a source-oriented external mixture. J. Geophys. Res., 102:21355–21372, 1997.

[29] Jacobson, M. Z. Strong radiative heating due to the mixing state of black carbon in atmospheric aerosols. Nature, 409:695–697, 2001.

[30] Kleeman, M. J. and G. R. Cass. A 3D Eulerian source-oriented model for an externally mixed aerosol. Environ. Sci. Technol., 35:4834–4848, 2001.

[31] Casuccio, G. S., P. B. Janocko, R. J. Lee, J. F. Kelly, S. L. Dattner, and J. S. Mgebroff. The use of computer controlled scanning electron microscopy in environmental studies. J. Air Pollut. Control Assoc., 33:937–943, 1983.

[32] Bruynseels, F. and R. Van Grieken. Direct detection of sulfate and nitrate layers on sampled marine aerosols by laser microprobe mass analysis. Atmos. Environ., 19:1969–1970, 1985.

[33] Van Malderen, R., R. Van Grieken, N. V. Bufetov, and K. P. Koutzenogii. Chemical characterization of individual aerosol particles in Central Siberia. Environ. Sci. Technol., 30:312–321, 1996.

[34] Malderen, H. V., R. V. Grieken, T. Khodzher, V. Obolkin, and V. Potemkin. Composition of individual aerosol particles above Lake Baikal, Siberia. Atmos. Environ., 30:1453–1465, 1996.

[35] Dahneke, B. Aerosol beam spectrometry. Nature, 244:54–55, 1973.

[36] Suess, D. T. and K. A. Prather. Mass spectrometry of aerosols. Chem. Rev., 99:3007–3035, 1999.

[37] Noble, C. A. and K. A. Prather. Real-time single-particle mass spectrometry: A historical review of a quarter century of the chemical analysis of aerosols. Mass Spec. Rev., 19:248–274, 2000.

[38] Hinz, K.-P., R. Kauffman, and B. Spengler. Laser-induced mass analysis of single particles in the airborne state. Anal. Chem., 66:2071–2076, 1994.

[39] Carson, P. G., K. R. Neubauer, M. V. Johnston, and A. S. Wexler. Online chemical analysis of aerosols by rapid singe particle mass spectrometry. J. Aerosol Sci., 26:535–545, 1995.

[40] Murphy, D. M. and D. S. Thomson. Laser ionization mass spectroscopy of single aerosol particles. Aerosol Sci. Technol., 22:237–249, 1995.

[41] Prather, K. A., T. Nordmeyer, and K. Salt. Real-time characterization of individual aerosol particles using time of flight mass spectrometry. Anal. Chem., 66:1403–1407, 1994.

[42] Weiss, M., P. J. T. Verheijen, J. C. M. Marijnissen, and B. Scarlett. On the performance of an on-line time-of-flight mass spectrometer for aerosols. J. Aerosol Sci., 28:159–171, 1997.

[43] Mallina, R. V., A. S. Wexler, K. P. Rhoads, and M. V. Johnston. High speed particle beam generation: A dynamic focusing mechanism for selecting ultrafine particles. Aerosol Sci. Technol., 33:87–104, 2000.

[44] Murphy, D. M. and D. S. Thomson. Chemical composition of single aerosol particles at Idaho Hill: Positive ion measurements. J. Geophys. Res., 102:6341–6352, 1997.

[45] Murphy, D. M. and D. S. Thomson. Chemical composition of single aerosol particles at Idaho Hill: Negative ion measurements. J. Geophys. Res., 102:6353–6368, 1997.

[46] Noble, C. A. and K. A. Prather. Real-time measurement of correlated size and composition profiles of individual atmospheric aerosol particles. Environ. Sci. Technol., 30:2667–2680, 1996.

[47] Liu, D.-Y., D. Rutherford, M. Kinsey, and K. A. Prather. Real-time monitoring of pyrotechnically derived aerosol particles in the troposphere. Anal. Chem., 69:1808–1814, 1997.

[48] Salt, K., C. A. Noble, and K. A. Prather. Aerodynamic particle sizing versus light scattering intensity measurement as methods for real time particle sizing coupled with time-of-flight mass spectrometry. Anal. Chem., 68:230–234, 1996.

[49] Tan, P. V., G. J. Evans, J. Tsai, S. Owega, M. S. Fila, and O. Malpica. On-line analysis of urban particulate matter focusing on elevated wintertime aerosol concentrations. Environ. Sci. Technol., 36:3512–3518, 2002.

[50] Trimborn, A., K.-P. Hinz, and B. Spengler. Online analysis of atmospheric particles with a transportable laser mass spectrometer. Aerosol Sci. Technol., 33:191–201, 2000.

[51] Johnston, M. V. and A. S. Wexler. On the cover - MS of individual particles. Anal. Chem., 67:721A–726A, 1995.

[52] Rhoads, K. P., D. J. Phares, A. S. Wexler, and M. V. Johnston. Size-resolved ultrafine particle composition analysis 1. Atlanta. J. Geophys. Res., 108, doi:10.1029/2001JD001211, 2003.

[53] Phares, D. J., K. P. Rhoads, M. V. Johnston, and A. S. Wexler. Size-resolved ultrafine particle composition analysis 2. Houston. J. Geophys. Res., 108, doi:10.1029/2001JD001212, 2003.

[54] Hughes, L. S., J. O. Allen, M. J. Kleeman, R. J. Johnson, G. R. Cass, D. S. Gross, E. E. Gard, M. E. Gälli, B. D. Morrical, D. P. Fergenson, T. Dienes, C. A. Noble, D.-Y. Liu, P. J. Silva, and K. A. Prather. Size and composition distribution of atmospheric particles in Southern California. Environ. Sci. Technol., 33:3506–3515, 1999.

[55] Kleeman, M. J., L. S. Hughes, J. O. Allen, and G. R. Cass. Source contributions to the size and composition distribution of atmospheric particles: Southern California in September 1996. Environ. Sci. Technol., 33:4331–4341, 1999.

[56] Hughes, L. S., J. O. Allen, L. G. Salmon, P. R. Mayo, R. J. Johnson, and G. R. Cass. Evolution of nitrogen species air pollutants along trajectories crossing the Los Angeles area. Environ. Sci. Technol., 36:3928–3935, 2002.

[57] Potukuchi, S. and A. S. Wexler. Predicting vapor pressures using neural networks. Atmos. Environ., 31:741–753, 1997.

[58] Binkowski, F. S. and S. J. Roselle. Models-3 community multiscale air quality (CMAQ) model aerosol component 1. Model description. J. Geophys. Res., In press.

[59] McMurry, P. H. and M. R. Stolzenburg. On the sensitivity of particle size to relative humidity for Los Angeles aerosols. Atmos. Environ., 23:497–507, 1989.

[60] Zhang, X. Q., P. H. McMurry, S. V. Hering, and G. S. Casuccio. Mixing characteristics and water content of submicron aerosols measured in Los Angeles and at the Grand Canyon. Atmos. Environ., 27A:1593–1607, 1993.

[61] Kleeman, M. J. and G. R. Cass. Identifying the effect of individual emission sources on particulate air quality within a photochemical aerosol processes trajectory model. Atmos. Environ., 33:4597–4613, 1999.

[62] Kleeman, M. J. and G. R. Cass. Effect of emissions control strategies on the size and composition distribution of urban particulate air pollution. Environ. Sci. Technol., 33:177–189, 1999.

[63] Kleeman, M. J., A. Eldering, J. R. Hall, and G. R. Cass. Effect of emissions control programs on visibility in Southern California. Environ. Sci. Technol., 35:4668–4674, 2001.

[64] Kleeman, M. J. and G. R. Cass. Source contributions to the size and composition distribution of urban particulate air pollution. Atmos. Environ., 32:2803–2816, 1998.

[65] Kleeman, M. J., J. J. Schauer, and G. R. Cass. Size and composition distribution of fine particulate matter emitted from wood burning, meat charbroiling, and cigarettes. Environ. Sci. Technol., 33:3516–3523, 1999.

[66] Kleeman, M. J., J. J. Schauer, and G. R. Cass. Size and composition distribution of fine particulate matter emitted from motor vehicles. Environ. Sci. Technol., 34:1132–1142, 2000.

[67] Bhave, P. V., D. P. Fergenson, K. A. Prather, and G. R. Cass. Source apportionment of fine particulate matter by clustering single-particle data: Tests of receptor model accuracy. Environ. Sci. Technol., 35:2060–2072, 2001.

[68] Goodin, W. R., G. J. McRae, and J. H. Seinfeld. A comparison of interpolation methods for sparse data: Application to wind and concentration fields. J. Applied Meteor., 18:761–771, 1979.

[69] Wexler, A. S. and J. H. Seinfeld. Second-generation inorganic aerosol model. Atmos. Environ., 25A:2731–2748, 1991.

[70] Odum, J. R., T. P. W. Jungkamp, R. J. Griffin, R. C. Flagan, and J. H. Seinfeld. The atmospheric aerosol-forming potential of whole gasoline vapor. Science, 276:96–99, 1997.

[71] Odum, J. R., T. P. W. Jungkamp, H. J. L. Griffin, R. J. Forstner, R. C. Flagan, and J. H. Seinfeld. Aromatics, reformulated gasoline, and atmospheric organic aerosol formation. Environ. Sci. Technol., 31:1890–1897, 1997.

[72] Jacob, D. J. Chemistry of OH in remote clouds and its role in the production of formic acid and peroxymonosulfate. J. Geophys. Res., 91:9807–9826, 1986.

[73] Jacob, D. J., E. W. Gottlieb, and M. J. Prather. Chemistry of a polluted boundary layer. J. Geophys. Res., 94:12975–13002, 1989.

[74] Harley, R. A., A. G. Russell, G. J. McRae, G. R. Cass, and J. H. Seinfeld. Photochemical modeling of the Southern California Air Quality Study. Environ. Sci. Technol., 27:378–388, 1993.

[75] Gard, E., J. E. Mayer, B. D. Morrical, T. Dienes, D. P. Fergenson, and K. A. Prather. Real-time analysis of individual atmospheric aerosol particles: Design and performance of a portable ATOFMS. Anal. Chem., 69:4083–4091, 1997.

[76] Guazzotti, S. A., J. R. Whiteaker, D. T. Suess, K. R. Coffee, and K. A. Prather. Real-time measurements of the chemical composition of size-resolved particles during a Santa Ana wind episode, California USA. Atmos. Environ., 35:3229–3240, 2001.

[77] Guazzotti, S. A., K. R. Coffee, and K. A. Prather. Continuous measurements of size-resolved particle chemistry during INDOEX-Intensive Field Phase 99. J. Geophys. Res., 106:28607–28627, 2001.

[78] Whiteaker, J. R., D. T. Suess, and K. A. Prather. Effects of meteorological conditions on aerosol composition and mixing state in Bakersfield, CA. Environ. Sci. Technol., 36:2345–2353, 2002.

[79] Pastor, S. H., J. O. Allen, L. S. Hughes, P. V. Bhave, G. R. Cass, and K. A. Prather. Ambient single particle analysis in Riverside, CA by aerosol time-of-flight mass spectrometry during the Southern California Ozone Study. Atmos. Environ., In press.

[80] Liu, D.-Y., R. J. Wenzel, and K. A. Prather. Aerosol time-of-flight mass spectrometry during the Atlanta Supersite experiment: Part 1 Measurements. J. Geophys. Res., In press.

[81] Sodeman, D. A., A. Dillner, K. R. Coffee, R. J. Wenzel, and K. A. Prather. Trends in aerosol composition at La Porte, Texas during TexAQS 2000. J. Geophys. Res., In preparation.

[82] Allen, J. O., D. P. Fergenson, E. E. Gard, L. S. Hughes, B. D. Morrical, M. J. Kleeman, D. S. Gross, M. E. Gälli, K. A. Prather, and G. R. Cass. Particle detection efficiencies of aerosol time of flight mass spectrometers under ambient sampling conditions. Environ. Sci. Technol., 34:211–217, 2000.

[83] Fergenson, D. P., D.-Y. Liu, P. J. Silva, and K. A. Prather. SpectraSort: A data analysis program for real-time aerosol analysis by aerosol time-of-flight mass spectrometry. Chemom. Intell. Lab., 37:197–203, 1997.

[84] Allen, J. O. YAADA reference manual. Software toolkit to analyze single-particle mass spectral data. http://www.yaada.org, Arizona State University, 2001.

[85] Hughes, L. S., J. O. Allen, P. V. Bhave, M. J. Kleeman, G. R. Cass, D.-Y. Liu, D. P. Fergenson, B. D. Morrical, and K. A. Prather. Evolution of atmospheric particles along trajectories crossing the Los Angeles basin. Environ. Sci. Technol., 34:3058–3068, 2000.

[86] Silva, P. J., R. A. Carlin, and K. A. Prather. Single particle analysis of suspended soil dust from Southern California. Atmos. Environ., 34:1811–1820, 2000.

[87] Gross, D. S., M. E. Gälli, P. J. Silva, and K. A. Prather. Relative sensitivity factors for alkali metal and ammonium cations in single-particle aerosol time-of-flight mass spectra. Anal. Chem., 72:416–422, 2000.

[88] Silva, P. J. personal communication, 1999.

[89] Fergenson, D. P., X.-H. Song, Z. Ramadan, J. O. Allen, L. S. Hughes, G. R. Cass, P. K. Hopke, and K. A. Prather. Quantification of ATOFMS data by multivariate methods. Anal. Chem., 73:3535–3541, 2001.

[90] Liu, D.-Y., K. A. Prather, and S. V. Hering. Variations in the size and chemical composition of nitrate-containing particles in Riverside, CA. Aerosol Sci. Technol., 33:71–86, 2000.

[91] Bhave, P. V., J. O. Allen, B. D. Morrical, D. P. Fergenson, G. R. Cass, and K. A. Prather. A field-based approach for determining ATOFMS instrument sensitivities to ammonium and nitrate. Environ. Sci. Technol., 36:4868–4879, 2002.

[92] Houck, J. E., J. C. Chow, J. G. Watson, C. A. Simons, L. C. Pritchett, J. M. Goulet, and C. A. Frazier. Determination of particle size distribution and chemical composition of particulate matter from selected sources in Southern California. Final report to California Air Resources Board - contract A6-175-32, OMNI Environmental Services, Inc. and Desert Research Institute, Beaverton, OR, 1989.

[93] Middlebrook, A. M., D. M. Murphy, and D. S. Thomson. Observations of organic material in individual marine particles at Cape Grim during the first Aerosol Characterization Experiment (ACE 1). J. Geophys. Res., 103:16475–16483, 1998.

[94] Silva, P. J. and K. A. Prather. On-line characterization of individual particles from automobile emissions. Environ. Sci. Technol., 31:3074–3080, 1997.

[95] Silva, P. J., D.-Y. Liu, C. A. Noble, and K. A. Prather. Size and chemical characterization of individual particles resulting from biomass burning of local Southern California species. Environ. Sci. Technol., 33:3068–3076, 1999.

[96] Silva, P. J. *Source Profiling and Apportionment of Airborne Particles: A New Approach Using Aerosol Time-of-Flight Mass Spectrometry.* Ph.D. thesis, University of California, Riverside, 2000.

[97] Suess, D. T. *Single Particle Mass Spectrometry Combustion Source Characteri-*

*zation and Atmospheric Apportionment of Vehicular, Coal and Biofuel Exhaust Emission.* Ph.D. thesis, University of California, Riverside, 2002.

[98] McMurry, P. H. A review of atmospheric aerosol measurements. Atmos. Environ., 34:1959–1999, 2000.

[99] Johnston, M. V. Sampling and analysis of individual particles by aerosol mass spectrometry. J. Mass Spectrom., 35:585–595, 2000.

[100] Mansoori, B. A., M. V. Johnston, and A. S. Wexler. Quantitation of ionic species in single microdroplets by on-line laser desorption/ionization. Anal. Chem., 66:3681–3687, 1994.

[101] Rose, H. A. and D. F. DuBois. Statistical propoperties of laser hot-spots produced by a random phase plate. Physics of Fluids B, 5:590–596, 1993.

[102] Reents, W. D. and M. J. Schabel. Measurement of individual particle atomic composition by aerosol mass spectrometry. Anal. Chem., 73:5403–5414, 2001.

[103] Ge, Z., A. S. Wexler, and M. V. Johnston. Laser desorption/ionization of single ultrafine multicomponent aerosols. Environ. Sci. Technol., 32:3218–3223, 1998.

[104] Woods, E., G. D. Smith, Y. Dessiaterik, T. Baer, and R. E. Miller. Quantitative detection of aromatic compounds in single aerosol particle mass spectrometry. Anal. Chem., 73:2317–2322, 2001.

[105] Carson, P. G., M. V. Johnston, and A. S. Wexler. Laser desorption/ionization of ultrafine aerosol particles. Rapid Commun. Mass Spectrom., 11:993–996, 1997.

[106] Reilly, P. T. A., A. C. Lazar, R. A. Gieray, W. B. Whitten, and J. M. Ramsey. The elucidation of charge-transfer induced matrix effects in environmental aerosols via real-time aerosol mass spectral analysis of individual airborne particles. Aerosol Sci. Technol., 33:135–152, 2000.

[107] Neubauer, K. R., M. V. Johnston, and A. S. Wexler. Humidity effects on the mass spectra of single aerosol particles. Atmos. Environ., 32:2521–2529, 1998.

[108] Kane, D. B. and M. V. Johnston. Size and composition biases on the detection of individual ultrafine particles by aerosol mass spectrometry. Environ. Sci. Technol., 34:4887–4893, 2000.

[109] Stolzenburg, M. R. and S. V. Hering. Method for the automated measurement of fine particle nitrate in the atmosphere. Environ. Sci. Technol., 34:907–914, 2000.

[110] Allen, J. O., L. S. Hughes, L. G. Salmon, P. R. Mayo, R. J. Johnson, and G. R. Cass. Characterization and evolution of primary and secondary aerosols during PM(2.5) and PM(10) episodes in the South Coast Air Basin. Final Report to Coordinating Research Council A-22, California Institute of Technology, 2000.

[111] Allen, J. O., L. Hughes, L. G. Salmon, P. R. Mayo, R. J. Johnson, and G. R. Cass. Size-resolved aerosol composition during transport and transformation downwind of central Los Angeles. Atmos. Environ., Submitted for publication.

[112] Nordmeyer, T. and K. A. Prather. Real time measurement capabilities using aerosol time of flight mass spectrometry. Anal. Chem., 66:3540–3542, 1994.

[113] Marple, V. A., K. L. Rubow, and S. M. Behm. A microorifice uniform deposit impactor (MOUDI): Description, calibration, and use. Aerosol Sci. Technol., 14:434–446, 1991.

[114] Wall, S. M., W. John, and J. L. Ondo. Measurement of aerosol size distributions for nitrate and major ionic species. Atmos. Environ., 22:1649–1656, 1988.

[115] Mulik, J., R. Puckett, D. Willims, and E. Sawicki. Ion chromatographic analysis of sulfate and nitrate in ambient aerosols. Anal. Letters, 9:653–663, 1976.

[116] Bolleter, W. T., C. T. Bushman, and P. W. Tidwell. Spectrophotometric determinations of ammonium as indophenol. Anal. Chem., 33:592–594, 1961.

[117] Silva, P. J. and K. A. Prather. Interpretation of mass spectra from organic compounds in aerosol time-of-flight mass spectrometry. Anal. Chem., 72:3553–3562, 2000.

[118] Angelino, S., D. T. Suess, and K. A. Prather. Formation of aerosol particles from reactions of secondary and tertiary alkylamines: Characterization by aerosol time-of-flight mass spectrometry. Environ. Sci. Technol., 35:3130–3138, 2001.

[119] Reents, W. D., S. W. Downey, A. B. Emerson, A. M. Mujsce, A. J. Muller, D. J. Siconolfi, J. D. Sinclair, and A. G. Swanson. Real-time compositional analysis of submicrometre particles. Plasma Sources Sci. Technol., 3:369–372, 1994.

[120] Morrical, B. D. *The Design and Application of a Field Transportable Time-of-Flight Mass Spectrometer (ATOFMS) and the Use of Two Step Laser Desorption/Ionization (L2MS) to Determine PAH in Single Particles.* Ph.D. thesis, University of California, Riverside, 1999.

[121] Carson, P. G., M. V. Johnston, and A. S. Wexler. Real-time monitoring of the surface and total composition of aerosol particles. Aerosol Sci. Technol., 26:291–300, 1997.

[122] Otten, P., F. J. Bruynseels, and R. V. Grieken. Study of inorganic ammonium-compounds in individual marine aerosol-particles by laser microprobe mass-spectrometry. Anal. Chim. Acta, 195:117–124, 1987.

[123] Stelson, A. W. and J. H. Seinfeld. Relative humidity and temperature dependence of the ammonium nitrate dissociation constant. Atmos. Environ., 16:983–992, 1982.

[124] Wang, H. C. and W. John. Characteristics of the Berner impactor for sampling inorganic ions. Aerosol Sci. Technol., 8:157–172, 1988.

[125] Larsen, R. J. and M. L. Marx. *Statistics and Its Applications.* Prentice-Hall, Englewood Cliffs, NJ, 1981.

[126] Hinz, K.-P., M. Greweling, F. Drews, and B. Spengler. Data processing in on-line laser mass spectrometry of inorganic, organic, and biological airborne particles. J. Am. Soc. Mass Spectrom., 10:648–660, 1999.

[127] Song, X.-H., P. K. Hopke, D. P. Fergenson, and K. A. Prather. Classification of single particles analyzed by ATOFMS using an artificial neural network, ART-2a. Anal. Chem., 71:860–865, 1999.

[128] Phares, D. J., K. P. Rhoads, A. S. Wexler, and M. V. Johnston. Application of the ART-2a algorithm to laser ablation aerosol mass spectrometry particle standards. Anal. Chem., 73:2338–2344, 2001.

[129] Tan, P. V., O. Malpica, G. J. Evans, S. Owega, and M. S. Fila. Chemically-assigned classification of aerosol mass spectra. J. Am. Soc. Mass Spectrom., 13:826–838, 2002.

[130] Murphy, D. M., A. M. Middlebrook, and M. Warshawsky. Cluster analysis of data from the Particle Analysis by Laser Mass Spectrometry (PALMS) instrument. Aerosol Sci. Technol., 37:382–391, 2003.

[131] Murphy, D. M., D. S. Thomson, and A. M. Middlebrook. Bromine, iodine, and chlorine in single aerosol particles at Cape Grim. Geophysical Research Letters, 24:3197–3200, 1997.

[132] Murphy, D. M., D. S. Thomson, A. M. Middlebrook, and M. E. Schein. In situ single-particle characterization at Cape Grim. J. Geophys. Res., 103:16485–16491, 1998.

[133] Murphy, D. M., D. S. Thomson, and M. Mahoney. In situ measurements of organics, meteoric material, mercury, and other elements in aerosols at 5 and 19 kilometers. Science, 282:1664–1669, 1998.

[134] Lee, S.-H., D. M. Murphy, D. S. Thomson, and A. M. Middlebrook. Chemical components of single particles measured with Particle Analysis by Laser

Mass Spectrometry (PALMS) during the Atlanta Supersite project: Focus on organic/sulfate, lead, soot, and mineral particles. J. Geophys. Res., 107, doi:10.1029/2000JD000011, 2002.

[135] Lee, S.-H., D. M. Murphy, D. S. Thomson, and A. M. Middlebrook. Nitrate and oxidized organic ions in single particle mass spectra during the 1999 Atlanta Supersite project. J. Geophys. Res., 108, doi:10.1029/2001JD001455, 2003.

[136] Bhave, P. V., M. J. Kleeman, J. O. Allen, L. S. Hughes, G. R. Cass, and K. A. Prather. Evaluation of an air quality model for the size and composition of source-oriented particle classes. Environ. Sci. Technol., 36:2154–2163, 2002.

[137] Liu, D.-Y. *Using Aerosol Time-of-Flight Mass Spectrometry (ATOFMS) Data to Gain New Insight into the Temporal Profiles, Composition and Evolution of Individual Particles in the Troposphere.* Ph.D. thesis, University of California, Riverside, 2000.

[138] Gard, E. E., M. J. Kleeman, D. S. Gross, L. S. Hughes, J. O. Allen, B. D. Morrical, D. P. Fergenson, T. Dienes, M. E. Gälli, R. J. Johnson, G. R. Cass, and K. A. Prather. Direct observation of heterogeneous chemistry in the atmosphere. Science, 279:1184–1187, 1998.

[139] Carpenter, G. A., S. Grossberg, and D. B. Rosen. ART 2-A: An adaptive resonance algorithm for rapid category learning and recognition. Neural Networks, 4:493–504, 1991.

[140] Pilinis, C. and J. H. Seinfeld. Development and evaluation of an Eulerian photochemical gas-aerosol model. Atmos. Environ., 22:1985–2001, 1988.

[141] Lawson, D. R. The Southern California Air Quality Study. J. Air and Waste Management Assoc., 40:156–165, 1990.

[142] Jacobson, M. Z. Development and application of a new air pollution modeling system. 3. Aerosol phase simulations. Atmos. Environ., 31:587–608, 1997.

[143] Song, C. H. and G. R. Carmichael. A three-dimensional modeling investigation of the evolution processes of dust and sea-salt particles in East Asia. J. Geophys. Res., 106:18131–18154, 2001.

[144] Boylan, J. W., M. T. Odman, J. G. Wilkinson, A. G. Russell, K. G. Doty, W. B. Norris, and R. T. McNider. Development of a comprehensive, multiscale "one-atmosphere" modeling system: Application to the Southern Appalachian Mountains. Atmos. Environ., 36:3721–3734, 2002.

[145] Mebust, M. R., B. K. Eder, F. S. Binkowski, and S. J. Roselle. Models-3 community multiscale air quality (CMAQ) model aerosol component 2. Model evaluation. J. Geophys. Res., In press.

[146] Meng, Z. and J. H. Seinfeld. Time scales to achieve atmospheric gas-aerosol equilibrium for volatile species. Atmos. Environ., 30:2889–2900, 1996.

[147] Chang, M. C., C. Sioutas, S. Kim, H. Gong, and W. S. Linn. Reduction in nitrate losses from filter and impactor samplers by means of concentration enrichment. Atmos. Environ., 34:85–98, 2000.

[148] Jayne, J. T., D. C. Leard, X. F. Zhang, P. Davidovits, K. A. Smith, C. E. Kolb, and D. R. Worsnop. Development of an aerosol mass spectrometer for size and composition analysis of submicrometer particles. Aerosol Sci. Technol., 33:49–70, 2000.

[149] Phares, D. J., K. P. Rhoads, and A. S. Wexler. Performance of a single ultrafine particle mass spectrometer. Aerosol Sci. Technol., 36:583–592, 2002.

[150] Atkinson, S. E. and D. H. Lewis. A cost-effective analysis of alternative air quality control strategies. J. Environ. Econ. Manage., 1:237–250, 1973.

[151] Harley, R. A., S. E. Hunts, and G. R. Cass. Strategies for the control of particulate air quality: Least-cost solutions based on receptor oriented models. Environ. Sci. Technol., 23:107–1014, 1989.

[152] Gordon, G. E. Receptor models. Environ. Sci. Technol., 14:792–800, 1980.

[153] Watson, J. G., R. C. Henry, J. A. Cooper, and E. S. Macias. The state of the art of receptor models relating ambient suspended particulate matter to sources. In E. S. Macias and P. K. Hopke, eds., *Atmospheric Aerosol: Source/Air Quality Relationships*, pages 89–106. American Chemical Society, Washington, D. C., 1981.

[154] Henry, R. C., C. W. Lewis, P. K. Hopke, and H. J. Williamson. Review of receptor model fundamentals. Atmos. Environ., 18:1507–1515, 1984.

[155] Watson, J. G. Overview of receptor model principles. J. Air Pollut. Control Assoc., 34:619–623, 1984.

[156] Gordon, G. E. Receptor models. Environ. Sci. Technol., 22:1132–1142, 1988.

[157] Henry, R. C. History and fundamentals of multivariate air quality receptor models. Chemom. Intell. Lab., 37:37–42, 1997.

[158] Blifford, I. H. and G. O. Meeker. A factor analysis model of large scale pollution. Atmos. Environ., 1:147–157, 1967.

[159] Henry, R. C. Current factor analysis receptor models are ill-posed. Atmos. Environ., 21:1815–1820, 1987.

[160] Friedlander, S. K. Chemical element balances and identification of air pollution sources. Environ. Sci. Technol., 7:235–240, 1973.

[161] Schauer, J. J., W. F. Rogge, L. M. Hildemann, M. A. Mazurek, G. R. Cass, and B. R. T. Simoneit. Source apportionment of airborne particulate matter using organic compounds as tracers. Atmos. Environ., 30:3837–3855, 1996.

[162] Schauer, J. J. and G. R. Cass. Source apportionment of wintertime gas-phase and particle-phase air polutants using organic compounds as tracers. Environ. Sci. Technol., 34:1821–1832, 2000.

[163] Xie, Y., P. K. Hopke, and D. Wienke. Airborne particle classification with a combination of chemical composition and shape index utilizing an adaptive resonance artificial neural network. Environ. Sci. Technol., 28:1921–1928, 1994.

[164] Stevens, R. K. and T. G. Pace. Overview of the mathematical and empirical receptor models workshop (Quail Roost II). Atmos. Environ., 18:1499–1506, 1982.

[165] Taback, H. J., A. R. Brienza, J. Macko, and N. Brunetz. Fine particle emissions from stationary and miscellaneous sources in the South Coast Air Basin. Final report to California Air Resources Board - contract A6-191-30, KVB, Inc., Research Cottrell, Tustin, CA, 1979.

[166] Cooper, J. A., D. C. Redline, J. R. Sherman, L. M. Valdovinos, L. C. Scavone, and C. Badgett-West. Final appendix V-G, PM10 source composition library for the South Coast Air Basin. Final report to South Coast Air Quality Management District, NEA, Inc., Beaverton, OR, 1987.

[167] Hildemann, L. M., G. R. Markowski, and G. R. Cass. Chemical composition of emissions from urban sources of fine organic aerosol. Environ. Sci. Technol., 25:744–759, 1991.

[168] Schauer, J. J. *Source Contributions to Atmospheric Organic Compound Concentrations: Emissions Measurements and Model Predictions.* Ph.D. thesis, California Institute of Technology, 1998.

[169] Grossberg, S. Adaptive pattern classification and universal recoding: I. Parallel development and coding of neural feature detectors. Biol. Cybernetics, 23:121–134, 1976.

[170] Grossberg, S. Adaptive pattern classification and universal recoding: II. Feedback, expectation olfaction, illusions. Biol. Cybernetics, 23:187–202, 1976.

[171] Wienke, D. and L. Buydens. Adaptive resonance theory based neural network for supervised chemical pattern recognition (fuzzyARTMAP) Part 1: Theory and network properties. Chemom. Intell. Lab., 32:151–164, 1996.

[172] Gan, K. W. and K. T. Lua. Chinese character classification using an adaptive resonance network. Pattern Recognition, 25:877–882, 1992.

[173] Wienke, D. and G. Kateman. Adaptive resonance theory based artificial neural networks for treatment of open-category problems in chemical pattern recognition - Application to UV-Vis and IR spectroscopy. Chemom. Intell. Lab., 23:309–329, 1994.

[174] Wienke, D., Y. Xie, and P. K. Hopke. An adaptive resonance theory based artificial neural network (ART-2a) for rapid identification of airborne particle shapes from the scanning electron microscopy images. Chemom. Intell. Lab., 25:367–387, 1994.

[175] Hopke, P. K. and X.-H. Song. Classification of single particles by neural networks based on the computer-controlled scanning electron microscopy data. Anal. Chim. Acta, 348:375–388, 1997.

[176] Song, X.-H., L. Hadjiiski, P. K. Hopke, L. L. Ashbaugh, O. Carvacho, G. S. Casuccio, and S. Schlaegle. Source apportionment of soil samples by the combination of two neural networks based on computer-controlled scanning electron microscopy. J. Air and Waste Management Assoc., 49:773–783, 1999.

[177] Bhave, P. V., J. O. Allen, J. R. Whiteaker, M. J. Kleeman, and K. A. Prather. A field-based approach for determining ATOFMS instrument sensitivities to aerosol-phase ionic species. Presented at the 21st Annual Meeting of the American Association for Aerosol Research, Charlotte, NC, Oct. 7–11, 2002.

[178] Kaye, P. H. Spatial light-scattering analysis as a means of characterizing and classifying non-spherical particles. Meas. Sci. Technol., 9:141–149, 1998.

[179] Seigneur, C., A. B. Hudischewskyj, J. H. Seinfeld, K. T. Whitby, E. R. Whitby, J. R. Brock, and H. M. Barnes. Simulation of aerosol dynamics: A comparative review of mathematical models. Aerosol Sci. Technol., 5:205–222, 1986.

[180] Zhang, Y., C. Seigneur, J. H. Seinfeld, M. Z. Jacobson, and F. S. Binkowski. Simulation of aerosol dynamics: A comparative review of algorithms used in air quality models. Aerosol Sci. Technol., 31:487–514, 1999.

[181] Betts, K. S. Air pollution expert dies. Environ. Sci. Technol., 35:399A–400A, 2001. Obituary.

[182] Glen R. Cass 1947–2001. Engineering & Science, 64(2):42, 2001. Obituary.

[183] Glen Cass 1947–2001. Caltech News, 35(2/3):31, 2001. Obituary.

[184] Russell, T. Glen Rowan Cass: 1947–2001. Aerosol Sci. Technol., 36:367–368, 2002. Obituary.

[185] Hemming, B. L. Glen R. Cass 1947–2001. Atmos. Environ., 36:2271–2273, 2002. Obituary.